DISSERTATION DER FAKULTÄT FÜR GEOWISSENSCHAFTEN
DER LUDWIG-MAXIMILIANS-UNIVERSITÄT MÜNCHEN

FLOOD MODELLING IN THE AMMER WATERSHED USING COUPLED METEOROLOGICAL AND HYDROLOGICAL MODELS

Vorgelegt von:

STEFAN TASCHNER

Eingereicht: *15. September 2003*

"It will be rain tonight." "Let it come down."
- *Macbeth* -

Table of contents

List of figures

List of tables

List of abbreviations

AFORISM	A Comprehensive Forecasting System for Flood Risk Mitigation and Control
AVHRR	Advanced Very High Resolution Radiometer
CN	Curve Number
CSA	Critical Source Area
CST	Convective-Stratiform Technique
DEM	Digital Elevation Model
DLR	Deutsches Zentrum für Luft- und Raumfahrt: German Aerospace Centre
DWD	Deutscher Wetterdienst: German Weather Service
ECMWF	European Centre for Medium-Range Weather Forecasts
ECST	Enhanced CST Technique
EM	Europa-Modell
ENPOC	ENvironmental POssibility Classifier
ESCIMO	Energy Snow Cover GIS Integrated Model
FAP	Flächen Analyse Programme
HHQ	highest runoff ever measured
HQ1	Flood flow with an annuality of 1 year
HQ2	Flood flow with an annuality of 2 years
HQ5	Flood flow with an annuality of 5 years
HQ10	Flood flow with an annuality of 10 years
HQ20	Flood flow with an annuality of 20 years
HQ50	Flood flow with an annuality of 50 years
HQ100	Flood flow with an annuality of 100 years
GIS	Geographical Information System
GPI	GOES Precipitation Index
IR	Infrared
LAI	Leaf Area Index
LAM	Limited Area Model
MAP	Mesoscale Alpine Program
Meso-NH	Mesoscale Nonhydrostatic Model
MHQ	Mean flood flow

MNQ	Mean low water flow
MOS	Model Output Statistic
MQ	Mean runoff
MSCL	Minimum Source Channel Length
MSM	Combined METEOSAT - Station Measurement technique
NNQ	Lowest runoff ever measured
NWP	Numerical Weather Prediction
PAR	Photosynthetically Active Radiation
PDUS	Primary Data User Station
PP	Perfect Prog
PROMET	PRocess Oriented Multiscale EvapoTranspiration model
PROMET-D	PRocess Oriented Multiscale EvapoTranspiration model - Discharge
RAPHAEL	Runoff and Atmospheric Processes for flood HAzard forEcasting and controL
SCS	Soil Conservation Service
SM	Swiss Model
SM-d	Swiss Model result disaggregated applying the duplication method
SM-i	Swiss Model result disaggregated applying a bilinear interpolation
SM-id	Swiss Model result disaggregated applying a quadratic inverse distance algorithm
SOP	Special Observation Period
SRZ	Soil root zone
SRMAX	Maximum storage in the upper soil layer
SUZ	Unsaturated zone
SVAT	Soil-Vegetation-Atmosphere-Transfer
TOPAZ	TOpographic PArameteriZation
TOPMODEL	TOPographic MODEL
USDA	United Sates Department of Agriculture
UTM	Universal Transversal Mercator

Preface

In recent years the number of devastating flood events has enormously increased in large parts of Europe. New stream gauge records were established at many rivers recently. A most impressive example herefore is the large flood at the river Elbe in the year 2002, where large parts of Eastern Germany were flooded. Major damages on private and public property has not only a negative economic effect but also forces the need for an appropriate flood forecasting system that takes into account a changing environment. Since most operative flood forecasting systems have failed to predict the major floodings of the near past, a strong need in developing new flood forecasting systems was initialised by the European Union. The coupling of meteorological forecasts and hydrological runoff modelling seems to be a promising approach. Herefore the co-operation of meteorologist and hydrologist is essential. The EU-funded project RAPHAEL (Runoff and Atmospheric Processes for flood HAzard forEcasting and controL) was intended to evaluate this issue in a mountainous region.

The presented work is integrated into this project and composed at the Department of Earth and Environmental Sciences, Section Geography, University of Munich. It can be seen as a first step to bring the two branches of sciences, hydrology and meteorology, together in order to develop a flood forecasting system for the Alpine region that can be applied by local authorities to forecast and manage flood events in the future. For the financial support the European Union is gratefully acknowledged.

First of all, I would like to thank very much my supervisor and doctor father Prof. Mauser, who had decisive influence on the successful outcome of my work under many different aspects. His help, comments, and constructive criticism have been invaluable during my scientific work at his chair. He gave me not only the opportunity to work in an interesting and exciting field of science but also gave me an understanding of the main aspects in hydrological modelling. He supplied me with his model PROMET as well as an excellent equipped workplace, which was fundamental for the successful realisation of my work. Moreover, he encouraged me to be free to develop own ideas and cope with a large part of the project RAPHAEL (together with Dr. Ludwig). For the trust in me I would like to say thank-you.

As one of my partners within the project RAPHAEL I would like to thank Dr. Ludwig for the excellent project collaboration. I enjoyed not only the everyday working with him but also the

Zusammenfassung

In den letzten Jahren hat die Zahl der Extremhochwasser deutlich zugenommen. An vielen Flußpegeln wurden dabei neue Rekordmarken erreicht. Schäden an privatem und öffentlichem Eigentum haben nicht nur negative wirtschaftliche Folgen, sondern führen auch zu einer verstärkten Nachfrage nach neuen und verbesserten Hochwasservorwarnsystemen. Eine der Hauptaufgaben hydrologischer Forschung ist deshalb, die jüngsten Erkenntnisse und Errungenschaften im Bereich der meteorologischen und hydrologischen Modellierung miteinander zu verbinden, um eine verbesserte Hochwasservorhersage zu ermöglichen.

Ziel des von der EU geförderten Projektes RAPHAEL (Runoff and Atmospheric Processes for flood HAzard forEcasting and controL) war hierbei die Entwicklung von Methoden zur synergetischen Nutzung von meteorologischen Niederschlagsvorhersagen und hydrologischen Abflußmodellen zur Hochwasservorhersage. Der Schwerpunkt lag dabei auf Einzugsgebiete in den Alpen.

Die vorliegende Arbeit ist Teil dieses Projektes.

Als eines der Testgebiete des Projektes wurde das Einzugsgebiet der Ammer ausgewählt, das sich am Nordrand der Alpen, 50 km südwestlich von München befindet. Das Ammereinzugsgebiet (709 km²) weist sowohl alpinen Charakter als auch voralpine Züge auf und ist hinsichtlich Relief, Böden und Klima heterogen.

Die Ammer, die in den Ammergauer Alpen (2200 m ü. NN) entspringt, fließt anschließend durch die Ammergauer Flyschberge und die Jungmoränenlandschaft, bevor sie schließlich nördlich der Ortschaft Fischen in den Ammersee mündet (533 m ü. NN). Der langjährige mittlere Abfluß der Ammer beträgt 16.6 m³/s am Pegel Fischen. Das Abflußregime ist nach PARDE (1960) pluvio-nival und weist ein Abflußmaximum auf, das aus Schneeschmelze und sommerlichem Niederschlagsmaximum resultiert. Meteorologische Messungen belegen einen deutlichen Nord-Süd Gradienten. Der mittlere Jahresniederschlag beträgt 1200 mm und reicht von 900 mm im Norden bis zu über 1800 mm im Süden. Das Gebiet wird auch landwirtschaftlich genützt. Dabei spielt die Weidewirtschaft die dominante Rolle, während der Ackerbau nur im Norden von Bedeutung ist. Etwa die Hälfte des Einzugsgebietes ist bewaldet.

Zur Modellierung zweier ausgewählter Hochwasserereignisse wurde das Modell PROMET-D (PRocess Oriented Multiscale EvapoTranspiration model - Discharge) verwendet. Es handelt sich hierbei um eine Kombination aus dem physikalisch basierten SVAT-Modell PROMET

(MAUSER und SCHÄDLICH 1998) und einem GIS basierten Abflußmodell, das auf dem TOPMODEL- Ansatz beruht (BEVEN und KIRKBY 1979; LUDWIG 2000).

PROMET basiert auf der Penman-Monteith Formel (MONTEITH 1978), welche die aktuelle Verdunstung als Funktion der Wasserverfügbarkeit, der Strahlungsbilanz und der physiologischen Regulationsmechanismen von verschiedenen Pflanzenarten berechnet. Die Bodenfeuchte wird nach einem Ansatz von EAGLESON (1978 a-g) als Funktion von Infiltration, Exfiltration und kapillarem Aufstieg modelliert. Dabei wird eine vereinfachte Richards Gleichung verwendet. Die Verteilung des Schneewasseräquivalents und der Schneeschmelze wird mit einem Schneemodell nach dem Energie- und Massenbilanzansatz berechnet (TODINI 1996; TASCHNER et al. 1998).

Die so modellierte räumliche Verteilung von Verdunstung, Bodenfeuchte und Schneewasseräquivalent werden dem Abflußmodell zur Wasserhaushaltsbilanzierung zur Verfügung gestellt.

Das Abflußmodell wurde von LUDWIG (2000) entwickelt und basiert auf dem TOPMODEL-Ansatz von BEVEN und KIRKBY (1979). Mit ihm wird zum einen das räumlich-zeitlich variable Verteilungsmuster der Abflußbildung und zum anderen der Abflußgang in stündlicher Auflösung modelliert. Die prinzipiellen, der Modellvorstellung von TOPMODEL zu Grunde liegenden Annahmen wurden von LUDWIG (2000) übernommen und erweitert.

Die Berechnung der Abflußbildung erfolgt dabei für jeden Punkt. So werden kleinräumige Variabilitäten der Meteorologie, der Verdunstung, der Schneedecke, der Bodenart und der Landnutzung berücksichtigt. Hierbei findet die mit PROMET modellierte Verdunstung als auch die flächenverteilte Zwischenspeicherung und verzögerte Abgabe des Niederschlagswassers aus der Schneedecke Verwendung. Zur Bilanzierung des Wurzelzonenspeichers am Punkt werden sowohl die aus der Landnutzung abgeleitete Durchwurzelungstiefe als auch die bodenartspezifische nutzbare Feldkapazität herangezogen. Die Berechnung des Infiltrationsüberschußes erfolgt ebenfalls für jeden Punkt nach dem Modell von GREEN und AMPT (1911).

Als wesentlichste Neuerung wurde von LUDWIG (2000) der verdunstungs-boden-topographische Index eingeführt. Dieser neue Index basiert auf der Annahme, daß verdunstende Oberflächen eine jahreszeitliche Dynamik der Separation in ober- und unterirdische Bestandteile aufweisen. Deshalb wurde der ursprüngliche boden-topographische Index um einen Verdunstungsquotienten erweitert, der aus langjährigen Verdunstungsdaten (berechnet mit PROMET) gebildet wird und der in Form eines Verdunstungsregimes die Wahrscheinlichkeit zur Ausprägung gesättigter Bedingungen an einem Ort mitbestimmt.

Zur Ermittlung der Konzentrationszeit wird das Verfahren des SOIL CONVERSATION SERVICE (1983) angewandt. Die Abschätzung der mittleren Fließgeschwindigkeit im Vorfluter erfolgt nach der Manning-Strickler-Gleichung.

PROMET-D wird im Ammereinzugsgebiet mit einer räumlichen Auflösung von 100 m betrieben. Die zeitliche Auflösung beträgt eine Stunde. Zur Modellierung der ausgewählten Hochwasserereignisse wurde keine spezielle Kalibrierung vorgenommen. Alle nötigen Parameter stammen aus LUDWIG (2000).

Der zur Berechnung der Abflußbildung und des Abflußganges benötigte Niederschlag wird dem Modell als räumlich verteilte Niederschlagsfelder zur Verfügung gestellt.

Zur Modellierung der Hochwasserereignisse an der Ammer standen verschiedene Niederschlagsfelder unterschiedlichster Herkunft zur Verfügung.

PROMET verwendet standardmäßig Messungen von Klimastationen des Deutschen Wetterdienstes (DWD), die temperatur- und windabhängig korrigiert werden (SCHULLA 1997). Die drei mal täglich erhobenen Meßdaten werden räumlich und zeitlich innerhalb PROMETs zu meteorologischen Feldern interpoliert. So erhaltene Niederschlagsfelder wurden auch für die Hochwassermodellierung verwendet.

Ebenfalls als punktueller Meßwert wurden Daten von DWD-Niederschlagsschreibern herangezogen. Diese mußten zunächst zeitlich aggregiert und anschließend räumlich interpoliert werden. Beide DWD-Datensätze dienten zur Überprüfung der Güte der Abflußmodellierung.

Als Niederschlagsvorhersage standen Ergebnisse von vier verschiedenen meteorologischen Modellen (NWP) - namentlich BOLAM, MC2, Meso-NH und Swiss Model - zur Verfügung. Die Berechnung des Niederschlags erfolgte in stündlicher Auflösung entweder im „Analysis Mode" oder im „Forecast Mode". Der „Analysis Mode" unterscheidet sich hierbei vom „Forecast Mode" insofern, daß in einem Abstand von sechs Stunden jeweils neue Randbedingungen (boundary conditions) in die Modellierung einfließen. Die räumliche Auflösung der Modelle, die in dieser Arbeit verwendet wurden, beträgt 10 bzw. 14 km in der Standardeinstellung.

Bevor diese Modellergebnisse jedoch zur Hochwassermodellierung herangezogen werden konnten, mußten sie erst auf die räumliche Auflösung des hydrologischen Modells von 100 m disaggregiert werden.

Hierfür kamen drei verschiedene Methoden zum Einsatz. Zum einen die gleichmäßige Unterteilung einer 10- bzw. 14 km-Zelle in 100 m Zellen, die jeweils alle den gleichen Niederschlagswert zugewiesen bekamen (Vervielfachung). Zum anderen wurde ein Ansatz gewählt, der den modellierten Wert einer Vorhersagemodellzelle dem Zentrum dieser zuweist. Diese so erhaltenen Punktdaten wurden anschließend räumlich interpoliert. Hierbei wurde einerseits eine einfache lineare Interpolation und andererseits ein abstandsgewichteter Ansatz verwendet.

Neben den NWP-Daten standen für eines der Hochwasserereignisse noch Datensätze des DWD-Wetterradars Fürholzen und aus METEOSAT abgeleiteter Niederschlag zur Verfügung. Da auch hier, im Vergleich zu PROMET-D die räumliche Auflösung niedriger ist (1 km für den Wetterradar und 5 km für den aus METEOSAT abgeleiteten Niederschlag), mußten diese Daten ebenfalls disaggregiert werden. Dabei wurde die Methode der Vervielfachung angewandt.

Für die hydrologische Modellierung wurden für diese Arbeit zwei Hochwasserereignisse ausgewählt. Das erste Hochwasser ereignete sich vom 17.-20. Juli 1997 und ist meteorologisch gesehen im Zusammenhang mit dem Oderhochwasser 1997 in Verbindung zu bringen. Das zweite Testhochwasser, das sogenannte Pfingsthochwasser, ereignete sich vom 20.-23. Mai 1999 und führte an der Ammer zu einem 200-jährlichen Hochwasser, das größere Überflutungen und beträchtliche Schäden zur Folge hatte.

Die beiden Hochwasserereignisse unterscheiden sich sowohl in ihrer Quantität als auch in ihrem Ursprung. Sie eignen sich deshalb, um die Anwendbarkeit der verwendeten Modellsynergie zur Hochwasservorhersage zu untersuchen.

Für die Modellierung des Hochwassers von 1997 standen neben den meteorologischen Feldern aus Messungen der DWD-Klimastationen bzw. DWD-Niederschlagsmessern auch Niederschlagsvorhersagen von den vier meteorologischen Modellen im „Analysis Mode" als auch im „Forecast Mode" zur Verfügung. Die Disaggregation der NWP-Ergebnisse erfolgte nach dem Prinzip der Vervielfachung.

Die besten Abflußergebnisse am Pegel Fischen wurden mit den Datensätzen der DWD-Messungen modelliert (R^2=0.65 bei Verwendung des Datensatzes der DWD-Niederschlagsschreiber).

Die modellierten Hochwasserganglinien weisen eine deutliche Ähnlichkeit mit der gemessenen auf. Das Hochwasservolumen wird um bis zu 10.8% unterschätzt, das Volumen

des Hochwasserscheitels um bis 4.5%. Lediglich bei der Verwendung des Datensatzes der DWD-Klimastationsmessungen weist die Abflußganglinie eine negative zeitliche Verschiebung von neun Stunden auf. Dies könnte wohl auf Fehler in der zeitlichen Interpolation zurückgeführt werden.

Bei der Anwendung der NWP-Ergebnisse ergab sich hingegen ein sehr uneinheitliches Bild für den modellierten Abfluß. Dies gilt für den „Analysis Mode" wie für den „Forecast Mode". Das Hochwasservolumen wird hierbei sowohl unter- als auch überschätzt (+10.2% bis – 24.5%). Gleiches gilt für das Volumen des Hochwasserscheitels (+16.1% bis 68.6%). Hier ist die Überschätzung mit bis zu 68.6% noch deutlicher. Die Eintrittszeit des Hochwasserscheitels ist im Allgemeinen zu früh (bis zu 5 Stunden). Ausnahme bildet lediglich das Ergebnis, das unter Verwendung des Swiss Model Datensatzes im „Analysis Mode" modelliert wurde. Hier ist die Eintrittszeit des Hochwasserscheitels vier Stunden verspätet.

Beim Vergleich zwischen den Abflußergebnissen, die mit Daten im „Analysis Mode" und denen, die im „Forecast Mode" berechnet wurden, zeigen die Ergebnisse von BOLAM und Meso-NH kaum eine Veränderung hinsichtlich des Verlaufes der modellierten Hochwasserganglinie. Dagegen weisen die Ergebnisse, die mit Datensätzen von MC2 und Swiss Model im „Forecast Mode" berechnet wurden, eine Verbesserung hinsichtlich der Angleichung an die gemessene Hochwasserganglinie auf.

Räumlich hochauflösende Datensätze standen zusätzlich für die ersten 36 Stunden des Hochwasserereignisses von BOLAM (3.5 km) und Meso-NH (2 km) zur Verfügung. Meso-NH lieferte hierfür zwei Datensätze: einen mit Berücksichtigung der Eisphase, den anderen ohne. Das Ergebnis, das unter Verwendung des BOLAM Datensatzes berechnet wurde, weist eine deutlich Verbesserung auf, während dies lediglich nur für die Anwendung des Meso-NH Eisphasen-Datensatzes gilt.

Eine Sensitivitätsanalyse wurde hinsichtlich der Lagegenauigkeit der modellierten Niederschlagsfelder durchgeführt. Hierbei wurden Niederschlagsfelder im „Analysis Mode" jeweils um eine NWP Zelle räumlich in acht Himmelsrichtungen verschoben. Die so erhaltenen Abflußganglinien zeigen ebenfalls ein sehr uneinheitliches Bild. Die größten Unterschiede ergaben sich bei Verwendung der Datensätze von MC2 und Swiss Model.

Für die Modellierung des Pfingsthochwassers standen zur Verfügung:
-    Niederschlagsfelder aus DWD Niederschlagschreibern,
-    Swiss Model Ergebnisse im „Forecast Mode",

- ein vom deutschen Luft- und Raumfahrtzentrum (DLR) korrigierter Datensatz des DWD-Wetterradars Fürholzen,

- aus METEOSAT abgeleiteter Niederschlag.

Die Disaggregation der Swiss Model Ergebnisse wurde hierbei nach den drei beschriebenen Methoden durchgeführt.

Ein gutes Abflußergebnis wurde für das Hochwasserereignis unter Verwendung des Datensatzes der Niederschlagsschreiber modelliert (R² = 0.91). Das berechnete Hochwasservolumen wird um 9% unterschätzt, das Volumen des Hochwasserscheitels ist 13% zu niedrig. Die Hochwasserganglinie weist jedoch zwei Scheitel auf, wobei der erste 5 Stunden zu früh und der zweite 6 Stunden zu spät eintritt.

Die Ergebnisse, die unter Verwendung der verschieden disaggregierten Swiss Model Ergebnisse erzielt wurden, weisen sowohl eine Überschätzung des Hochwasservolumens (15 - 46%) als auch des Volumens des Hochwasserscheitels (30 - 67%) auf. Die Eintrittszeit des Hochwasserscheitels ist bis zu drei Stunden zu früh. Die Überschätzung des modellierten Abflußes läßt sich im Zusammenhang mit einer Überschätzung des Niederschlages durch Swiss Model am Beginn des Hochwasserereignisses bringen. Dies führt zu einer zu raschen Abnahme des Sättigungsdefizits.

Der zeitlich verspätete (4 Stunden) und im Volumen deutlich überschätzte (59%) Hochwasserscheitel der mit dem Datensatz des Wetterradars Fürholzen modelliert wurde, läßt sich auf einen unrealistisch hohen Niederschlag in den Alpen zurückführen.

Ähnlich gute Ergebnisse wie unter Verwendung des DWD-Niederschlagsschreiber-Datensatzes wurden bei der Anwendung von Niederschlagsfeldern aus METEOSAT-Daten unter Berücksichtigung von Niederschlagsmessungen erzielt. Dagegen führte die Verwendung des mittels ECST Algorithmus (BENDIX et al. 2000) aus METEOSAT abgeleiteten Niederschlags zu einer mehrgipfligen Abflußganglinie mit einem zu frühen (9 Stunden) und im Volumen überschätzten (39%) Hochwasserscheitel.

Zwei Sensitivitätsanalysen wurden für das Pfingsthochwasser durchgeführt.

Zum einen wurden die ersten 24 Stunden der Swiss Model Vorhersage durch Niederschlagsfelder aus DWD-Niederschlagsschreiberdaten ersetzt. Da nun die Überschätzung des Niederschlags durch Swiss Model am Beginn des Hochwasserereignisses nicht mehr vorhanden ist, ergeben sich verbesserte Resultate.

Zum anderen wurde die räumliche Verschiebung der Niederschlagsfelder um eine NWP Zelle in acht Himmelsrichtung vorgenommen. Daraus ergibt sich eine Reihe von möglichen

Ergebnissen, die erzielt werden, wenn man von einer Lageungenauigkeit des NWP-Modell-Ergebnisses von einer Zelle ausgeht.

Insgesamt hat die Studie gezeigt, daß zum derzeitigen Zeitpunkt eine Hochwasservorhersage im Ammereinzugsgebiet nur bedingt möglich ist. Abflußergebnisse, die unter Verwendung von modellierten Niederschlagsvorhersagen berechnet wurden, zeigen eine zu hohe Variabilität hinsichtlich Abflußganglinie, Abflußvolumen und Hochwasserscheitel auf. Lediglich für das Pfingsthochwasser 1999 ließen sich gute Ergebnisse erzielen. PROMET-D hat jedoch seine grundsätzlich Fähigkeit zur Hochwassermodellierung mit Niederschlagsmeßdaten demonstriert.

1. Introduction

1.1 Aspects of hydrological research

In recent years hydrology as the science of water in all its different phases (fluid, solid and gaseous) and occurrence on and beneath the earth's surface, has gained increasing consideration in public opinion. This is induced by the need to solve socially relevant problems linked to water, like e.g. fresh water supply, avalanche and flood prevention.

However hydrology from the scientific point of view has also developed from the descriptive approach, based mainly only on parameter measurements, to a fully natural science. The understanding of the interactive processes, including the biosphere, pedosphere and atmosphere is the central topic of actual research. Frequently these processes are described by physically based approaches and are often realised in different kinds of models, like e.g. SVAT (Soil-Vegetation-Atmosphere-Transfer) models. This new approach in hydrological science has become a useful tool in the decision process of hydrological water authorities.

For successful co-operation of science and end-users of the scientific work, like e.g. water authorities, hydrological research has to be newly oriented. Due to LUDWIG (2000) these main aspects of hydrological research can be summarised as follows:

- Water cycle research under consideration of physical, chemical and biological relevant matter and energy fluxes
- Water balance modelling on a global, regional and local scale in order to describe the temporal and spatial distribution of the water cycle components
- Determination of available water resources for fresh water supply and irrigation
- Process oriented studies under particular consideration of soil-vegetation-atmosphere processes for the coupling with regional and global circulation models
- Hydrological prediction of floods and low water flow in order to improve project planing and water management.

Moreover, hydrology has developed important interfaces to their neighbour sciences. One of the major tasks in hydrology is to link recent progress in atmospheric and hydrological sciences to improve the understanding of the atmosphere – land surface processes as a whole system. This is also induced by increasing natural hazard events.

Especially the coupling of hydrological models with regional and global circulation models for flood hazard forecasting has become more and more important.

The problem of flooding is as old as time. However, while natural flooding of large areas did not create situations more dangerous than others in a prehistoric world, the expansion of human activity and the aggregation of people in larger urbanised areas has made the prevention of damages caused by flooding as well as the control and management of flood waters a problem of vital necessity (TODINI 1997). In addition the increase of flood events in the last years has lead to a strong social and economic need to improve the prediction of disastrous flood events (BERZ 1999). Long or short time flood prevention measures by hydraulic engineers can be based on hydrologic-meteorological model forecasts and simulations. The possibilities of hazardous event control can be increased by means of hydrology and meteorology as natural sciences.

1.2 The study objectives and structure

Recent years have seen booming population and indiscriminate urbanisation creating extremely dangerous situations, with floodplain areas that are inhabited, or with houses built at the foot of dikes, where the safety of life and economic goods tends to vanish during prolonged periods of flooding. One of the major tasks in hydrology is therefore to link recent progress in atmospheric and hydrological sciences to improve real time flood forecasting. The precondition for such a venture was given by the atmospheric science as well as by hydrology. Numerical weather prediction (NWP) models improved not only in the reliability of the modelled precipitation. Also the model resolution gap between the atmospheric science and hydrology has become narrower. NWP models can provide their forecast within a resolution of ten kilometres or higher. Hydrological models have proven their ability to model flood events with a reasonable accuracy in terms of discharge volume, flood peak and flood peak occurrence time. The possibility of exchanging data between weather forecast models and hydrological models opens new perspectives for the two scientific disciplines that are strongly coupled.

Therefore, a multidisciplinary approach is needed, especially for dealing with fast evolving phenomena, such as flood episodes, to be predicted with high accuracy and fine temporal and spatial resolution. The EU funded project RAPHAEL (Runoff and Atmospheric Processes for flood HAzard forEcasting and controL) was designed on the base of this cognition. It was the first interdisciplinary project of that kind in the Alpine region.

In this study several data sources are employed to identify their applicability for flood modelling in a prealpine watershed. Precipitation fields derived from different kind of

meteorological models and surface observation data are used as hourly input for the hydrological simulation of two selected flood events.

The study is performed in the Ammer catchment, which is located south-west of Munich in the Bavarian Alps and prealpine foreland covering an area of 709 km². It is characterised by a strong climatic and physiographic heterogeneity in terms of geology, pedology, and landuse (Chapter 2). The applied hydrological model structure PROMET-D (PRocess Oriented Multiscale EvapoTranspiration model - Discharge) establishes a link between PROMET (MAUSER and SCHÄDLICH 1998) and an enhanced distributed GIS-version of the TOPMODEL (LUDWIG 2000; BEVEN and KIRKBY 1979). The hydrological calculations are performed in the Ammer watershed with a spatial resolution of 100 m. The spatial distribution of actual evapotranspiration, soil moisture and snow water equivalent is calculated using PROMET, to define the boundary conditions advancing the flood event. An enhanced distributed GIS-version of TOPMODEL is linked to PROMET in order to enable runoff formation and stream discharge modelling (LUDWIG and MAUSER 2000) (Chapter 3).

For the Ammer watershed two flood events were selected to be modelled. The Christopherus Flood in mid July 1997 and the Whitsun Flood that occurred in May 1999 as a bicentennial flood hazard. Both floods are briefly described in Chapter 4.

Four different meteorological input sources were applied:

a)   surface observation data: (1) DWD (Deutscher Wetterdienst: German Weather Service) climatological stations with 3 measurements a day (Christopherus Flood), (2) DWD rain gauge data sampled to an hourly resolution

b)   radar observations of precipitation provided by the DWD rain radar in Fürholzen in a grid resolution of 1km by 1 km (sampled to a 1-hour time step), for the Whitsun Flood

c)   precipitation fields derived from METEOSAT data (spatial resolution: 5 km) using two different retrieval algorithms: an indexing based approach combined with rain gauge measurements (MAUSER and BACH 1994) and the ECST approach (BENDIX 1997) (both schemes are applied for the Whitsun Flood) and

d)   simulated data of the following numerical weather prediction models using forecast mode and analysis mode: Swiss Model, MESO-NH, BOLAM, and MC2. The data were provided at a 14 km resolution for the Swiss Model and at a 10 km resolution for the other models over a time duration of up to 96 hours (time step: 1 hour). Additionally for the Christopherus Flood, MESO-NH and BOLAM provided information at a higher spatial resolution (2.5 and 3km respectively), however for a shorter time period.

The differences in grid resolution of the input data (NWP model 10 res. 14 km, METEOSAT 5 km, rain radar 1 km and PROMET-D 0.1 km) require a specific focus on the scale issue. Therefore different spatial disaggregation and temporal aggregation schemes of mesoscale meteorological data have to be applied. The influence of different disaggregation and interpolation methods on the model results is presented in Chapter 5. The model results are compared to gauged data and show good agreement for several input data sets (Chapter 6). A high uncertainty retains depending on the chosen set of inputs. Different error sources of both meteorological data sets and hydrological modelling are addressed and quantified. Sensitivity analysis of PROMET-D was carried out to evaluate the hydrological model reaction on shifted precipitation fields of the NWP models output in the Ammer basin. A short summary of the studies basic results as well as a conclusion and an outlook discussion of future perspectives finalise the study.

1.3 The project RAPHAEL

The basic objective of the EU funded RAPHAEL project, as indicated by its acronym is to develop, implement and demonstrate the use of coupled meteorological and hydrological models at the regional scale in order to improve flood forecasting and management in complex mountain watersheds (RANZI 1997). Therefore simulation experiments with hydrological-meteorological models were implemented in two basins represented in the figure 1.1: the Ammer watershed (709 km²) in the Bavarian Alps and the watershed upstream the Lago Maggiore at its outlet (6599 km²) called Ticino-Toce. To achieve the project's goals 11 partners contributed their scientific expertise to a multidisciplinary expert network.

The involved partners are:

1. Università di Brescia, Dipartimento di Ingegneria Civile, Brescia - I.
2. CNRS, Université Paul Sabatier, Laboratoire d'Aérologie, Toulouse - F.
3. University of Munich, Department of Earth and Environmental Sciences, Section Geography, Chair of Geography and Geographical Remote Sensing, München - D.
4. Politecnico di Milano, Dipartimento di Ingegneria Idraulica, Ambientale e del Rilevamento, Milano - I.
5. FISBAT-CNR, Bologna - I.
6. VISTA - Remote Sensing Applications in Geosciences, München - D.
7. DLR-Institut für Physik der Atmosphäre, Oberpfaffenhofen - D.
8. Swiss Meteorological Institute, Zürich - CH.

9.   Institute of Geography, ETH, Zürich - CH.

10.   Atmospheric Environment Service-Environment Canada, Dorval - Canada.

11.   University of Waterloo, Department of Civil Engineering, Waterloo - Canada.

The application of coupled meteorological and hydrological models was carried out in a multi-scenario modelling experiment to show the potential use of advanced flood forecasts in view of the reservoir regulations during hazardous flood events. Further major objectives of the project were defined as:

- to investigate the benefits achievable in atmospheric models by introducing hydrological feedback with detailed land-surface schemes, including snow and ice dynamics;

- to validate meteorological data generated by Numerical Weather Prediction models and meteorological observations by means of runoff measurements and distributed hydrologic water balance calculations;

- to improve techniques and tools for scale-adaptation of observed and simulated variables, with particular reference to the areal distribution of rainfall, snow cover, and land-surface-atmosphere fluxes.
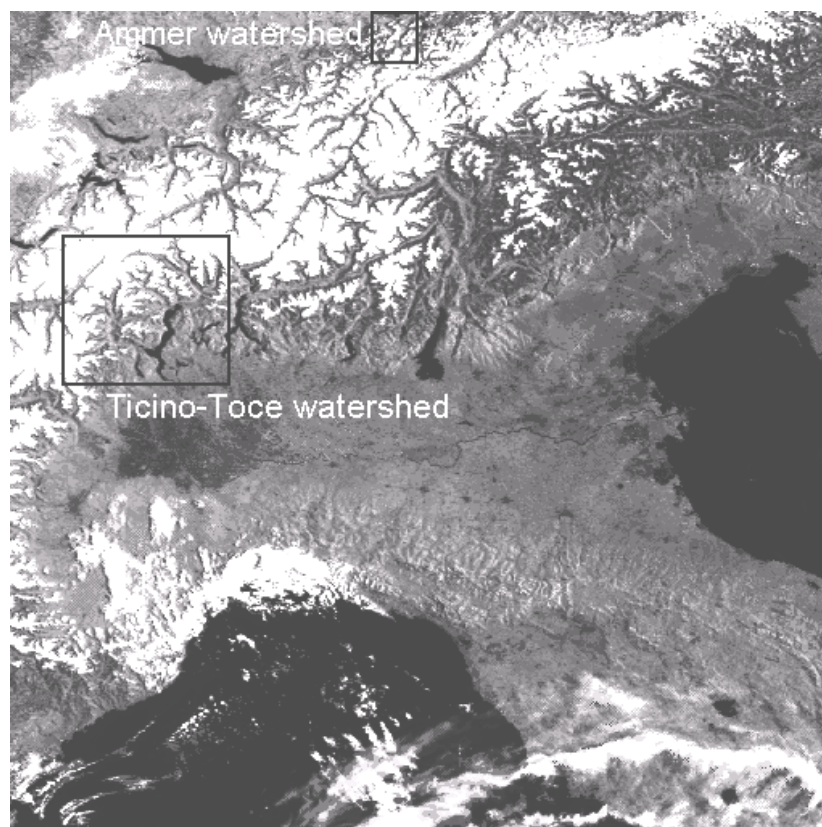
Fig. 1.1: The location of the Ticino-Toce and of the Ammer watershed areas, as depicted by a NOAA-AVHRR image recorded on 22nd May 1992

1.4 The state of art and research capability

1.4.1 Meteorological models

For the derivation of spatially distributed meteorological parameters different kinds of meteorological models can be applied. These models can be categorised into three different major classes, namely numerical weather prediction models, weather radar and satellite derived meteorological parameters like e.g. METEOSAT.

Weather radar data and METEOSAT imagery have to be processed to derive meteorological information like e.g. precipitation intensities. Climatic station data on the other hand have to be spatially and temporally interpolated to obtain meteorological fields. Both kinds of data sources are some kind of measurements and are available with a certain time offset after the weather situation has occurred. Numerical Weather Prediction Models on the other hand can supply spatially distributed meteorological parameters as a forecast, i.e. before the weather situation will occur and are therefore of special interest for flood forecasting.

Numerical weather prediction models

Numerical Weather Prediction Models are presently applied in everyday operational short-range (24-48 h) forecast, having horizontal spatial resolution approaching 10 km, and in some cases even higher (GYAKUM et al. 1996).

With the presently available computer resources, such a high resolution can only be achieved on a regional scale, by integrating over a limited domain of the earth's surface. For this reason, the NWP models applied to short-range forecasts are known as Limited Area Models (LAMs), Regional Models, or Mesoscale Models. The latter case emphasises that they are capable of describing atmospheric processes pertaining to a mesoscale range. The benefits of these high resolution models are expected in areas of complex terrain, where strong surface heterogeneity in height, slope, vegetation, soil moisture, albedo, snow cover etc. not only induce local variations in atmosphere-soil exchanges of energy, humidity and momentum, but also favour atmospheric processes on the entire mesoscale range (1-100 km) that largely control precipitation (VOLKERT et al. 1996).

Within the last few years, a new generation of NWP research models have emerged. These models resolve the full non-hydrostatic system of equations, meaning the same model can be used over a very broad range of scales (from a few thousand of kilometres to a few hundred of meters). Moreover, these models have the capability of being self-nested. It is possible to

have several models with differences in resolution of a factor 5 to 10 running simultaneously and interacting smoothly on their boundaries (BOUGEAULT et al. 1998).

In the Alpine region, several of these limited area NWP models provide short range forecasts with a spatial resolution approaching 10 km. The models have demonstrated their capability to reasonably model and predict the mesoscale features of the Alpine meteorology (e.g. lee cyclogenesis, hydrostatic mountain wave and related phenomena) (BUZZI et al. 1994). An intercomparison of daily accumulated precipitation calculated by different NWP models in the western Alps shows in general good agreement with measured ground truth data (RICHARD et al. 1998).

However in the Alpine region, as in other mountainous areas, individual mountain elements possess intrinsic scales of a few kilometres or less. Therefore even a 10 km scale is generally inadequate to describe them: only relatively large massifs and valleys can be marginally captured (GEORGELIN et al. 1994). A resolution approaching 1 km is therefore necessary to adequately incorporate terrain properties in such rough areas (BENOIT and DESGAGNE 1996). New investigations have already improved the model resolution ranging from two (MC2, Meso-NH) to three kilometres (BOLAM, Lokalmodell) and will be operationally applied in the future.

Weather radar

An indirect precipitation measurement system is the weather radar system, which importance has grown in the last decade, particularly after the introduction of the dual polarisation systems and the Doppler radars. Weather radars are active remote sensing systems and can provide images of instantaneous rainfall intensity distribution over large areas. There are three major benefits in using radars: the first one is a finer spatial description of the precipitation pattern (usually 1 km spatial resolution) than NWP, the second one is the high temporal resolution of up to five minutes that make radar systems interesting for several hydrological problems and the third one is the possibility of observing approaching storms before arriving over the area of interest. In this meaning weather radar can also be seen as a resource that provides short pre-event forecasts.

However, several factors also limit the use of radar for quantitative work especially in an Alpine region. A major disadvantage lies in the need for recalibration of parameters used for converting reflectivity to rain intensities, which generally also requires the installation of a conventional ground based rain gauge network. The precision needed for quantitative radar

measurements in hydrology - especially for flood modelling - is far more demanding than a qualitative use of radar (JOSS et al. 1997).

The rain rate is estimated from the measured radar reflectivity using empirical relationships (e.g. ANIOL et al.1980). This reflectivity is influenced by a number of error sources. Errors arise because the reflectivity is not a direct measure of rainfall rate, but depends on type, size and concentration of particles, all depending on the meteorological conditions, ground clutter, shadowing by mountain ridges, attenuation and parameters of the instrument itself (JOSS and WALDVOGEL 1990). Several studies deal with correction algorithms counteracting these error sources (GABELLA et al. 2000; HAGEN 1997). However as shown by FABRY et al. (1994), a proper sampling in space and time by the radar measurements for a given catchment area needs to be applied in order to minimise measurement errors.

In general three different kind of radar systems can be distinguished:

- conventional radar,
- doppler radar and
- polarimetric doppler radar.

Conventional radar can have difficulties identifying ground clutter and anomalous propagation. Polarisation parameters can be used to identify them unambiguously (SAUVAGEOT 1992). Doppler radars are characterised by the ability to measure the motion of the targets (rain drops) and permit the estimation of their velocity in radial direction. However conventional radar and doppler radar achieve an accuracy of high temporal resolution precipitation of only 30 %. Polarimetric doppler radar can improve this accuracy up to the expected range of about 15% as it only responds to the backscatter of raindrops (MEISCHNER et al. 1991). This kind of radar measure the specific differential phase shift that is not influenced by the most errors affecting conventional or doppler radar (SACHIDANANDA and ZRNIC 1987). In heavy rainfall, attenuation at polarimetric C-band doppler radar occurs and correction procedures need to be applied properly. Such problems can be at least partially overcome by using multiparameter techniques, although at present, these are only available for research purposes. Possible errors induced by the vertical profiles of the raining cloud system must also be considered too (HAGEN et al. 1998).

Precipitation intensities derived from METEOSAT

Another remote sensing technique to determine precipitation intensities can be carried out by exploiting geostationary satellite data. For the derivation of precipitation intensities from METEOSAT the use of the infrared (IR) band is widespread because of the day and night time availability. However the visible band is also applied in several studies to improve IR information (e.g. GRIFFITH et al. 1978, NEGRI and ADLER 1987a-b, LOVEJOY and AUSTIN 1979).

The algorithms are based on the assumption that the precipitation falling from the bottom of a cloud is related to the radiation reflected and emitted from the top of the considered cloud. All precipitation-estimations schemes are thus necessarily indirect and are valid only on a regional scale and for a specific time step. Algorithms developed for tropic thunder storms may not perform in the mid latitudes (KIDDER and VANDER HAAR 1995).

First approaches of precipitation-estimation were developed by BARRETT (1970) using the cloud indexing method. The algorithm is based on the identification of cloud types. Each of these types can be related to a rain rate. Whereas BARRETT (1970) wanted to improve rainfall information over Australia in a monthly resolution, several familiar approaches deal with different spatial and temporal resolutions. FOLLANSBEE (1973) derived daily precipitation over mesoscale areas, KILONSKY and RAMAGE (1976) estimated precipitation over tropical oceans and e.g. ARKIN and MEISNER (1987) developed the GPI (GOES Precipitation Index) for climatological purposes over the tropics. Another technique is based on the assumption that the rain rate of a cloud is a function of the stage in its life cycle. This approach is particular valid for convective clouds. A widely applied method is known as the Grifith-Woodley technique (GRIFITH et al. 1978, WOODLEY et al. 1980). It has been applied to a wide range of tropical and mid-latitude convective situations. The bispectral method attempts to combine the rules that clouds have a high possibility to precipitate if they are both cold and bright (LETHBRIDGE 1967). Cloud temperature can be derived from the IR bands, brightness from the visible band. One approach, also applied in the midlatitudes, is the TSONIS and ISAAC (1985) algorithm and is based on cluster analysis. To improve precipitation estimation techniques based only on satellite data it is of advantage to include the physics of the cloud into the retrieval process. One way of performance is the use of cloud models (KIDDER and VONDER HAAR 1995). Some of the earliest approaches date from GRUBER (1973) and WYLIE (1979). A widespread method is the Convective-Stratiform Technique (CST), developed by ADLER and NEGRI (1988). Good results can be achieved regarding tropical and subtropical convective precipitation (BENDIX 1997, NEGRI et al.

1995). New investigations showed also that, with an improved parameterisation developed by BENDIX (1997), this approach can be applied also for rainfall estimations in Germany. The accuracy of this precipitation-estimation is in the range comparable to the weather radar measurements of the DWD (REUDENBACH et al. 2001).

1.4.2 Hydrological models

A catchment can be considered as a dynamical system where the independent variable precipitation is transferred to the dependent variables evapotranspiration and discharge. Between model input and output many processes are involved like e.g. soil saturation processes. Not all of these processes can even be measured on the field scale and the measurement of spatially distributed water cycle parameters is impossible. Hence all relevant processes of the water cycle in a catchment can not be recorded. System oriented, mathematical models are therefore applied to simulate reality. The system is thereby a self contained entity of physical parameters that relate the input and output to a certain time increment (DYCK and PESCHKE 1995). Input and output are linked by system operations that can be described by models. The complexity of these models depends on the purpose of the model application, the character of the modelled system, the considered hydrological process or the degree of the causality of different variables (LUDWIG 2000).

Hydrological models have developed from those of purely statistical, lumped or distributed conceptual type, through models to the latest generation of physically-based distributed models (TODINI 1997). Predicted or measured rainfall can be used as input to drive these kind of hydrological models.

In a wider sense hydrological models can be distinguished in deterministic and stochastic ones. A deterministic model is one in which a given input of rain must produce a fixed output of runoff in a certain physical environment (JONES 1997). The causality is described by cause and impact. It calculates several depended variables (impact) from a data base of given independent variables (cause) (WILHELM 1997). However a deterministic model may ignore natural stochastic variations in occurring reality. In contrast, the output from stochastic model is subject to change. The deterministic model is not necessarily superior to a stochastic model (JONES 1997). BECKER and SERBAN (1990) defined coupled deterministic-stochastic models because hydrological processes always include deterministic and stochastic elements. A stochastic model might be used to generate rainfall input to a deterministic runoff model (Fig. 1.2).
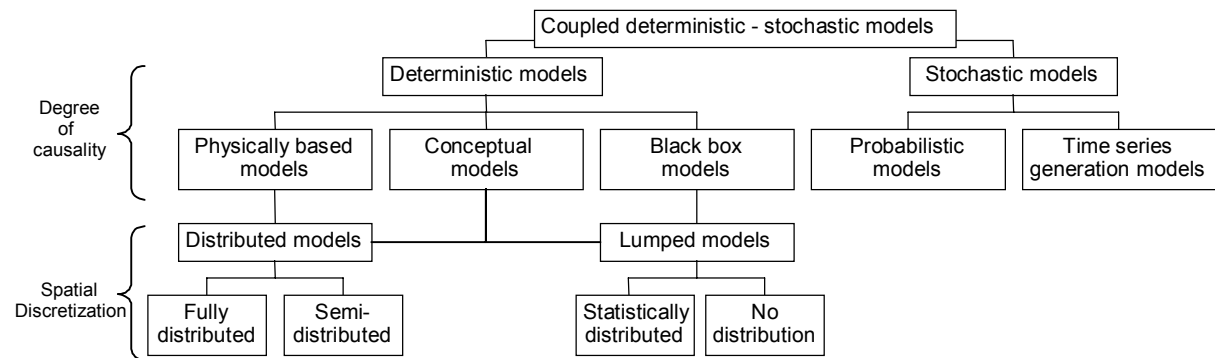
Fig. 1.2: Classification of hydrological models (based on BECKER and SERBAN 1990)

Deterministic models can be further distinguished by their degree of causality.

Simple, empirical or black box model are derived from the input-output analysis of data. They consider only the input and output without regarding the physics. System processes are not described in detail but by empirical assumptions based on experiences. The first approach was the unit hydrograph method introduced by SHERMAN (1932). The discharge models of the United States Soil Conservation Service (SCS) TR-20 and TR-55 (SOIL CONSERVATION SERVICE 1975, 1983, 1985) are based on that idea. The SCS method is widely used in the United States and all over the world for estimating floods on small to medium-sized ungauged drainage basins (PILGRIM and CORDERY 1993). It has been adopted as the required procedure in many municipal and regional authorities and has become also applicable in juristic proceedings (MAUSER 1985).

Conceptual models are based on a theoretic concept in which processes are represented in a simplified manner. They describe the physics by assumptions whereby they use empirical methods (grey box models). These model approaches are widespread. The first model becoming international known is the STANFORD-IV model (CRAWFORD and LINSLEY 1966). Further representations of this kind of models are the hydrological model HBV (BERGSTRÖM 1976), the basin models ARNO (TODINI 1996) and EGMO (BECKER 1975), the network models HEC-1 (US ARMY CORPS OF ENGINEERS 1981) and RORB (LAURENSEN and MEIN 1988), the rainfall-runoff models DRM3 (ALLEY and SMITH 1982) and PRMS (LEAVESLEY et al. 1983). All of these models have in common that the physical description of several processes is implemented but the conceptional approach still dominates. This can be particular found in the water balance simulation model WASIM-ETH (SCHULLA 1997).

Also of that type is the famous and widespread TOPMODEL. It can be described as a physically-conceived semi-distributed hydrological model, in which topographic structure is

considered as the main driving force (BEVEN et al. 1994). Many model extensions were developed in recent years like the TOPOG (VERTESSY et al. 1994) or the TOPKAPI (CIARAPICA and TODINI 2002)

Physically based models on the other hand are based on the fundamental laws of physics and are called white box models. All hydrological processes are described on a physical basis. A large number of model parameters is therefore required. This limits the use of this kind of models for operational purposes. They are mostly found in the field of scientific work. However these models can provide physical descriptions of several processes that can be implemented in the distributed conceptual models like the infiltration model by GREEN and AMPT (1911). Yet complex physically based models are also established. Famous is the SHE (Système Hydrologique Européen) water flow modelling system (ABBOTT et al. 1986a, 1986b). Also well known are the WATFLOOD model (KOUWEN and SOULIS 1990), the LISFLOOD model (DE ROO et al. 2000), the Object Watershed Link Simulation Model OWLS (CHEN 1996) and the SHETRAN model (EWEN 1995) which has been developed by upgrading the SHE model. Of exceptional position in these kind of models are the SVAT (Soil Vegetation Atmosphere Transfer) models. They describe the water fluxes through the soil, the plant stands and the atmosphere as a sequence of several different resistances. An overview of several SVAT models is given by GEYER and JARVIS (1991). A linkage of the SVAT model PROMET (MAUSER and SCHÄDLICH 1998) and an enhanced TOPMODEL (LUDWIG 2000) will be presented in this study.

A criticism of physically-based models like SHE or physically-conceived models such as TOPMODEL is that similar model results, in terms of prediction of discharge at the catchment outlet, may be obtained by the use of a number of different parameter combinations (e.g. BEVEN 1989). This indicates that hydrological processes within the catchment may not be represented correctly, or have been parameterised incorrectly, even if the overall effect is reproduced. However in order to consider changed environmental conditions, models must have the capability to reproduce hydrological processes within a basin. This requires that the models have a physical basis, rather than relying on empirical or statistical relationships.

Besides the degree of causality, deterministic models can be further distinguished by their spatial discretization. They can be distributed in a full sense or in a semi distributed way or be lumped models without any distribution. An overview is given by BECKER and SERBAN (1990).

Especially in flood modelling, the time sampling interval is of importance. From a hydrological point of view the time increment depends on the catchment size and ranges from the 5 – 15 minutes needed in urban or steep mountain catchments, to 1h for a wide variety of catchments ranging from 200 to 1.000 km^2 (or sub-units into which larger catchments may be sub-divided), to 3h for very large catchments (20.000-30.000 km^2 or more). It is not advisable to operate on larger time steps because of the high non-linearities in the soil response to precipitation. The time sampling interval must in fact be substantially smaller than the time required to fill the soil and reach saturation and it is a function of both rain intensity and soil moisture capacity (TODINI 1997). Hydrological models must have the capability to cope with this requirement.

This aspect however shows one of the major gaps between meteorologists and hydrologists. Traditionally, meteorologists sample precipitation at daily intervals or at most every 6 hours. Unfortunately the sampling interval of 6 hours is rarely adequate for real time flood forecasting.

1.4.3 Coupled hydro-meteorological models

Coupled hydro-meteorological models are applied in several studies. Different climatic regions as well as the use of different precipitation sources and hydrological models are represented in a number of projects. Several of these projects deal in particular with flood forecasting and streamflow simulation.

The forecasting of floods in the watershed of the Reno river (4000 km^2), draining the eastern slopes of the Appenines, near Bologna, to the Adriatic Sea, was studied recently within the EU-funded project AFORISM (A Comprehensive Forecasting System for Flood Risk Mitigation and Control) (TODINI 1995). A system was set up involving one mesoscale meteorological model with a 10 x 10 km mesh width and two hydrological models: the ARNO model and the TOPMODEL. Radar and other classical observation were also used to bridge the resolution gap between the mesoscale meteorological model resolution and the small size of the sub-catchments (such as 70 km², less than one grid cell of the meteorological model). However the context of the application is rather different from that of the project RAPHAEL, since the complexity of the Alpine environment that includes snowmelt processes, reservoir regulation and a steep topography that also influences the microphysics of the atmosphere was absent in the AFORISM project application.

The EU funded Project TELEFLOOD deals with forecasting of floods in urban areas downstream of steep catchments (GOLLVIK 1997). The studies objectives were to develop

and evaluate the components of a modelling system to forecast floods in rivers draining steep mountainous catchments into flat plains where large urban areas are flooded. The proposed system consisted of a high-resolution limited area meteorological model (HIRLAM) together with a hydrological catchment model (HBV) and a hydraulic channel network model. The study was carried out in an Irish, Swedish and Italian catchment.

During the large-scale field campaign SOP (Special Observation Period) of the Mesoscale Alpine Program (MAP), which is an international research initiative devoted to the study of atmospheric and hydrological processes over the Alps (BOUGEAULT et al. 1998), the NWP models BOLAM and MC2 were linked to the hydrological WATFLOOD model in order to evaluate the possibilities of flood forecasting in real practice. Runoff modelling in the Ticino-Toce basin was carried out continuously during the SOP. The results range from good agreement to considerable over- and underestimation. However during SOP no real flood event occurred (RANZI et al. 2001). The model schemes and settings for this study were based on the results of the RAPHAEL project.

A study in the Pacific Northwest of the United States (Oregon and Washington) deals also with real time streamflow forecasting. The scarcity of real time rain gauge network, poor radar coverage for precipitation estimation and strong orographically induced precipitation gradients complicates precipitation monitoring in this region. Therefore the use of the mesoscale atmospheric model MM5 overcomes this problem for an area of 15 000 km². The MM5 model is used to simulate the dynamics of the atmosphere fluxes of energy and precipitation to the land surface on spatial resolution scale of 4 km. A linkage with the distributed hydrological soil vegetation model DHSVM is set up to compute the streamflow for a series of watersheds. Results for the winter season 1998/99 were only mild and moderate flood events occurred showed reasonable streamflow simulations (WESTRICK et al. 2000).

In North America, the forecasting of the combined effect of the spring snowmelt and heavy orographic rain on the management of water for hydroelectric power generation has been under examination since 1993 (KOUWEN et al. 1996). The calculations are computed over the Columbia River basin (50000 km^2) in the Rocky Mountains. Three mesoscale meteorological models are coupled to two hydrologic models on the temporal scale of individual storm events (e.g. 3 days) and on seasonal time series of model produced precipitation fields, and even on multi-year series. Resolutions range from 2 to 15 km squared.

Since 1988, the hydrologic model used at the Ohio region River Forecast Center (National Weather Service) receives as input sub-basin-averaged quantitative precipitation forecasts

prepared from the Forecast Office in Pittsburgh, Pennsylvania. There are eight sub-basins ranging from 2000 to 10000 km², for a total of 60000 km²; they drain the western slopes of the Appalachians into Lake Erie. The system is being evaluated for an operational use since 1990 (KRZYSZTOFOWICZ et al. 1993). Here the meteorological model resolution is about 30 km.

1.5 Flood generation in the Bavarian Alps and prealpine foreland

Floods are in general the result of many meteorological and hydrological processes interacting in a complex way. Sometimes also geological and geophysical processes like e.g. earthquakes can trigger floods.

The term flood is understood to mean the temporary rise of the water level of surface waters or an increased discharge in a river channel. Hereby a distinct threshold value is reached or exceeded. Floods occur frequently and often without causing any damage.

The temporary inundation, either partial or complete, of normally dry land with water, suspended matter and/or rubble is called flooding.

Floods that occur in the Bavarian Alps and prealpine foreland can be distinguished in different major types (SWISS RE 1998).

Most common are floods that result from prolonged rainfall lasting days or even weeks. Consequence of which is that soils get saturated. Any further precipitation is then transformed to surface runoff. Frozen soils can prevent infiltration leading to a reinforced surface runoff. Water flows straight or delayed into the watercourses. Tributaries lead the mass of water into the main river channel which can become incapable of handling the water inflow. If the inflow of water exceeds the capacity of the channel or if the flood protection fails for other reasons, the result is flooding.

Another type of floods is the flash flood. A flash flood is set off by high-intensity local precipitation that may continue for several hours. A large portion of the rain cannot be absorbed by the ground and runs along the surface directly and fast to the next watercourse causing a flood event.

Both types of floods described above are mainly linked to heavy and/or ongoing precipitation. But also snowmelt can contribute to flood generation. Decisive for the course of the flood event is besides other parameters (described later) the percentile coverage of the watershed with rainfall at the same time. Short-duration thunderstorms with a small extent can cause

flash floods in a small mountain creek while the streamflow of a larger river will not be affected by this storm event. Floods in major rivers occur mainly after long-during precipitation mostly combined with almost saturated soils (BRONDSTERT 1996).

Less frequent in the Bavarian Alps and prealpine foreland are flood events linked to river ice. Border ice and ground ice that can be found at watercourses in winter can develop to drift ice. An ice barrier can result where drift ice get caught up on obstacles such as bridges. This greatly reduces the cross section of the watercourse and dams the water upstream. If the ice barrier breaks up in consequence of increased water pressure or rising temperatures floods can occur in the lower course of the river. Flooding in Bavaria caused by ice jams are reported in several chronicles but nowadays occur seldom because of river warming and river regulations (BAYERISCHES LANDESAMT FÜR WASSERWIRTSCHAFT 1998).

Another source of floods results from dam bursts or failure of levee systems. However these types of floods occur seldom but often cause damage.

Flood generation is a result of a specific combination of different influencing factors that leads to a unique flood event. Several of these factors can be determinate and addressed to a specific region like e.g. the Bavarian Alps and prealpine foreland.

Besides heavy precipitation also event specific and basin specific parameters are decisive for flood generation (ULENBROOK et al. 2001). Event specific parameters are understood to mean the condition of the catchment preceding the flood event. These parameters are variable in time and space and unique for every flood event. Basin specific parameters result from the physiogeographic characteristics of the catchment and can be seen as time constant.

Referring to the Bavarian Alps and prealpine foreland these factors are discussed in the following.

Severe flood events in general are always linked to heavy precipitation. In the Bavarian Alps and prealpine foreland the precipitation maximum is measured in summer with a meridional increase of the precipitation sum towards the Alps. The maximum is recorded around 2000 mm/year.

The Alps act as a topographic barrier to airflow. In consequence of its spatial east-west orientation the effect of air mass blocking is, strictly speaking, only existent regarding the general weather situation North or Northwest. The frequency maximum of this general weather situation lasts in Mid-Europe from late spring to summer. Since synoptic precipitation is linked to this general weather situation the highest precipitation sum has to be

expected in this period. Furthermore in the Alpine region the frequency maximum of convective storms is recorded in the summer months (LIEDTKE and MARCINEK 1995). Also in winter the northern Alpine region receives a considerable amount of precipitation. This precipitation is often linked to general weather situations with a western component. Hereby the general weather situation West-cyclonal often leads to heavy precipitation. This can cause also flood events especially in late winter and at the begin of spring when snowmelt is forced by rainfall (ULENBROOK et al. 2001). As reported in several studies (e.g. BARDOSSY and CASPARY 1990; CASPARY 1996) the frequency of this general weather situation has increased in the last years which can lead to an increase in winter flood events. However due to low temperatures in the Alpine region and its foreland the precipitation is often recorded as snowfall in winter.

Additionally it should be mentioned that Alpine valleys can show considerable differences in the precipitation sum. East-west oriented, inner Alpine valleys often receive less precipitation due to lee effects. The summer precipitation maximum is there mainly caused by convective thunderstorms. North oriented, funnel-shaped valleys that are opened towards the prealpine foreland, show in general higher precipitation sums. This might be caused by a cross section reduction toward the Alps in combination with blocking effects (LIEDTKE and MARCINEK 1995).

Special attention should be drawn the so-called Vb weather situation that can lead to flood events. A Vb weather situation occurs mostly in late spring and summer. Warm moisture air masses are transported over the Adriatic Sea, passing the eastern side of the Alps towards Mid-Europe where they slide on cold North-Atlantic air masses. The huge amount of moisture air and the cooling over Mid-Europe leads to intensive precipitation. A stationary of the weather situation and the ongoing supply of warm moisture air can result in precipitation that lasts for several days (BISMUTH et al. 1998). Especially in late spring this weather situation can enforce snowmelt in the Bavarian Alps and prealpine foreland and cause flood events.

Especially in the Bavarian Alps and prealpine foreland the snow cover is of importance. In winter almost all precipitation is recorded as snowfall. However in spring snow melt runoff can contribute to flood generation. A thin snow cover can hereby melt much faster while a thick one can store a considerable amount of rainwater. In general the snow melt in the Bavarian Alps and prealpine foreland is ruled by altitude. While in lower reaches the melting period starts around April, the higher reaches of the Alps can still accumulate snow (BAYERISCHES LANDESAMT FÜR WASSERWIRTSCHAFT 1998).

Flood events in general are linked to the local maximum of the precipitation regime. In the Bavarian Alps and prealpine foreland floods occur in late spring and summer (BAYERISCHES LANDESAMT FÜR WASSERWIRTSCHAFT 1998). Recordings of the stream gauge Peissenberg (1962–2001), located in the Ammer watershed in the prealpine foreland prove this fact (WASSERWIRTSCHAFTSAMT WEILHEIM 2001). All flood events with an annuality of two years or higher were recorded in the months May, June, July and August. No flood event was ever measured in January, March and April (for details see appendix D).

Similar results are reported in a study dealing with the seasonality of flood processes in Austria (MERZ et al. 1999).

Severe flood events in Mid-Europe result from a combination of heavy, spatially distributed precipitation and a catchment that has already a tendency to generate flood runoff. This tendency results from event specific parameters like frozen soils, rapidly melting snow, interaction of rainfall and snowmelt and/or almost saturated soils (GRÜNEWALD 1996). Especially in the Bavarian Alps and prealpine foreland, where flood events occur generally in summer the soils are often almost saturated preceding the flood event in consequence of rainfall within a few days before.

The main basin specific parameters that have an influence on flood generation are soil texture, vegetation, topography, shape and areal extent of the catchment.

The soil texture of a catchment is of importance since, if the soil is not frozen, it decides how much water can be stored in the ground. Decisive are hereby the infiltration capacity and the pore size distribution (GRÜNEWALD 1996).

Also vegetation can store rainwater. Interception reduces the amount of water that reaches the ground. Hereby deciduous forests can store the highest quantity. During precipitation breaks transpiration can increase the soil water deficit. However the seasonal variability of plant activity by means of evapotranspiration, rooting and surface roughness leads to a seasonal influence of vegetation on flood generation. In general it can be stated that small flood events can be attenuated by dense vegetation, larger ones not (GRÜNEWALD 1996).

The catchment area, its topography and shape also influence flood generation. All three factors are parameters of the time of concentration.

In general it could be stated that the smaller a basin the shorter the flow pass and the shorter the time of concentration.

In steep terrain water flows much faster than in plains. It also favours subsurface runoff in consequence of saturation surplus while in depressions water is stored and contributes delayed to the runoff.

A circular shaped catchment has a shorter time of concentration compared to a longish one of the same area. Assuming an equal spatially distributed precipitation the hydrograph course is much steeper and shows a higher flood peak in circular shaped watershed (BAUMGARTNER and LIEBSCHER 1990).

Referring the basin specific parameters to the Bavarian Alps and prealpine foreland shows that there are flood favouring as well as reducing factors.

The pedogenesis in the Bavarian Alps and prealpine foreland is characterised by an early or initial stage. It started in general after the ice recession in the postglacial. Soils are therefore mostly shallow and tend to saturate rapidly. However on behalf of the relief soil types have to be distinguished on small scales. (FETZER 1986). The main landuse in the Bavarian Alps and prealpine foreland is pasture and especially in the Alps, forest. Forest has hereby the most reducing influence of all landuse on flood generation (ULENBROOK et al. 2001). However forest is mainly found on the slopes of mountains which counteract the effect of steep terrain on flood generation. The topography of the Bavarian Alps and prealpine foreland is heterogeneous. The steep slopes in the Alps are followed northerly by a smoothly reliefed foreland in consequence of Pleistocene deposits (LIEDTKE and MARCINEK 1995).

The relation of the influence of heavy precipitation and basin specific parameters on flood generation was investigated by WOOD et al. (1990). The study shows that for heavy precipitation with an annuality of up to five years the basin specific parameters are dominant. Whereas precipitation events with an annuality of 20 years and more can result in a flood independently from the basin specific parameters. However the result of this study is not generally valid for every catchment but can serve as a clue.

2. The testsite

In the frame of the project RAPHAEL two major testsites have been selected for the simulation experiments: the Ticino-Toce and the Ammer watershed, that are both located in the Alps, a region with an extraordinary history of flood hazards.

The Ticino-Toce watershed (6599 km^2 at the Miorina dam gauging station) located on the south side of the Alps is of particular interest in the context of MAP as a European wide key research area. The watershed is strongly exposed to extreme precipitation events which occur quite frequently, caused by the particular topographic conditions at the southern part of the Alps, when moist air masses are transported towards these mountain barriers. Many serious flood events, some of them of catastrophic nature, have been experienced.

The second target area for testing the coupled atmospheric-hydrologic modelling experiment is the catchment of the Ammer (709 km^2 at the Fischen gauging station) located on the northern side of the Alps. It is also of particular interest due to its strong morphological, pedological and climatological heterogeneity. Especially precipitation shows a strong north-south gradient caused by the blocking effects of the Alps. As a mountainous catchment of a smaller size, the Ammer emphasises the importance of a correct monitoring and simulation of convective and advective rainfall events, providing a crucial test for the actual predictive capabilities of coupled hydro-meteorological models.

The Ammer is also the major testsite of several research projects performed at the Chair of Geography and Geographical Remote Sensing, Department of Earth and Environmental Sciences, Section Geography at the University of Munich. Referring to topography, landuse and water balance modelling this catchment is well studied (BACH et al. 1998, STOLZ 1998, SCHÄDLICH 1998, STRASSER 1998, LUDWIG 2000). Additionally the watershed is well equipped with meteorological and hydrological measuring instruments.

The presented study focuses on the Ammer catchment which is briefly described in the following.

2.1 The Ammer catchment

The Ammer catchment is located in the Bavarian prealpine foreland, 50 km south-west of the city of Munich with a catchment area of 709 km² referred to the gauge Fischen (Fig. 2.1). It's north south extension is approximately 50 km, east west about 30 km. The Ammer basin is

bordered by the Loisach catchment in the south-east and by the Lech catchment in the west. At it's north end the Ammer mouths into Lake Ammer.

The watershed boundary between the Ammer and the Loisach basin follows from the steep mountains of the Ammergauer Alps south of the valley of the Linder including the highest elevation, the Kreuzspitze (2185 m) up to the flysch mountain area with the top of the Hörnle (1584 m). At Bad Kohlgrub the syncline boundary of the Murnauer Mulde at the east side of the Riegsee and further on the lateral moraines west of the Osterseen up to the southern shore of Lake Ammer builds up the basin boundary. The watershed between the Ammer catchment and the Lech basin is built up by the northern spurs of the Ammergauer Alps including the Hochplatte (2081 m) up to the flysch mountains valley of the Halbammer including the Hoher Tauchberg (1527 m) along the Wildsteig to the Ammer Knee and further on to the Hohenpeissenberg (988 m). North of the village of Polling the catchment of the Rott, a former Ammer tributary is separated by ground moraine. At the village of Wielenbach a dyke dams up the river Ammer which flows along this dyke into Lake Ammer at an elevation of 533 m. The relief energy amounts 1652 m.
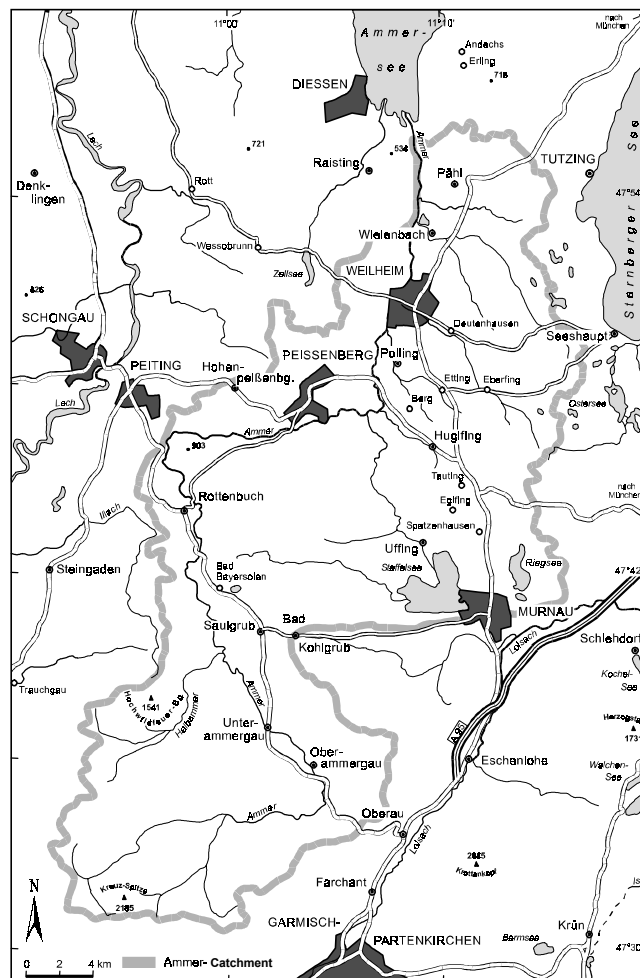
Fig. 2.1: Location of the Ammer catchment (Cartography: V. Falck)

2.2. Landscape units

The zoning of a landscape in different units can be carried out under many different aspects. The study of WITTMANN (1991) is herefore essential. His work emphasises the results of MEYEN et al. (1962) and subdivides the landscape from ecological viewpoints. A landscape unit is defined if the unit of source rock, climate, relief and soil is homogenous or can be assumed to be ecologically comparable. The method is oriented on a grading system based on suitability for agriculture and forestry but also on the relationships between landscape potential of soils, climate and geomorphology (STOLZ 1998). The methodology selects the following criteria:

- Source rock

- Climatological criteria (annual precipitation, annual mean temperature)

- Phenological criteria (begin of spring, vegetation duration)

- Soil criteria (soil type, dispersal of loess)

This approach is suited for hydrological problems and especially for flood modelling because the most relevant control parameters of the water balance and runoff process are considered by this scheme. Besides the meteorological input, the parameters of evapotranspiration and runoff formation are likewise taken into account.

The application of these criteria leads to a hierarchical differentiation of landscape units. First large regions are described (MEYEN et al. 1962) that can be further subdivided into subunits of different order. While large regions are defined by geological-geomorphologic aspects, subunits of the first order are characterised by soil properties. On the level of the second order climatological characteristics are decisive. For the natural region of the Ammer catchment the application of this methodology leads to four different second order landscape units (Fig. 2.2) (STOLZ 1998). From North to South these are:

- Northern young moraine area

- Southern young moraine area

- Ammergau flysch mountains

- Ammer mountains
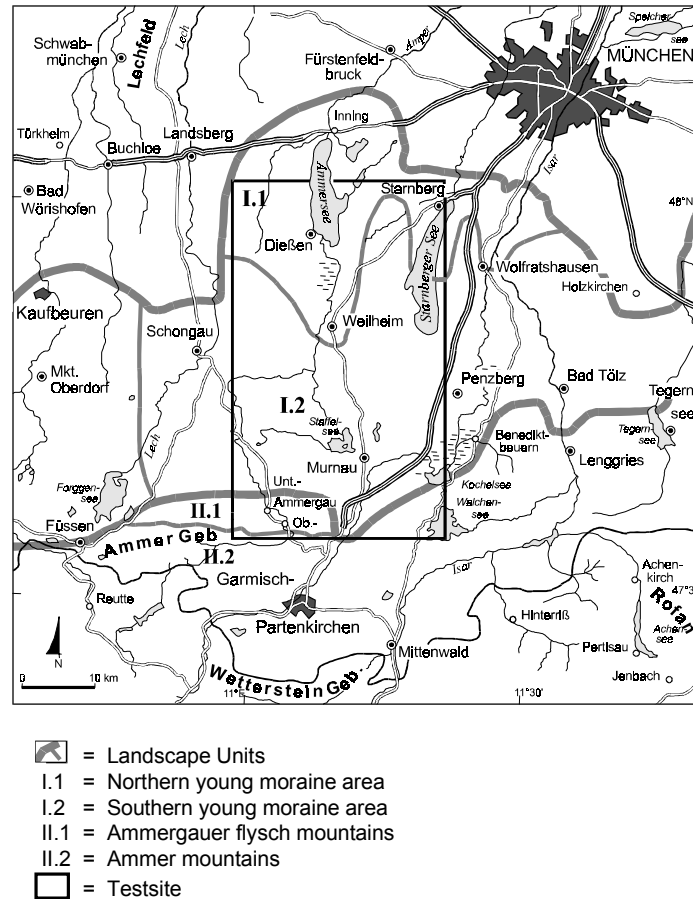
Fig. 2.2: Natural landscape units of the Ammer catchment (based on STOLZ 1998, Cartography: V. Falck)

In this study the terms of the landscape units defined by STOLZ (1998) are used:

- *"Valley of the Ammer"*: the northern young moraine area from the south shore of Lake Ammer up to the Guggenberg molasse dam. This includes the ground moraine area demarcated by the Ammer in the west and the rise of the end moraine in the east including the drumlin field in the surrounding of the village Eberfing

- the southern young moraine area and the outlier formed by molasse are called *"Molasse and Moraines"*. This area includes the steep moraines at the boundaries of the catchment followed southerly by folded molasse, covered with Pleistocene sediments, and further on to the tectonical border of the Alps.

- the alpine landscape units of the flysch mountains and the mountains built up by limestone are geologically demarcated and are called the *"Flysch mountains"* res. *"Ammergauer Alps"*.

2.3 Geography of the Ammer catchment

To carry out flood modelling in the Ammer catchment, the geography of the basin has to be considered in detail. Many parameters that are dominant for the runoff formation and especially for flood modelling vary not only within a temporal but also in a spatial distribution. These parameters are a function of the local geography and have a direct influence on spatial and temporal runoff formation.

2.3.1 Geomorphology and geology

For a geomorphologic and geological characterisation, the Ammer catchment has to be distinguished under geological viewpoints. Due to their sediment genesis and the influence of orogeny, four geological units from north to south can be separated (Fig. 2.3) (JERZ 1993a, 1993b, MEYEN et al. 1962, DOBEN and FRANK 1983, MÖBUS 1997):
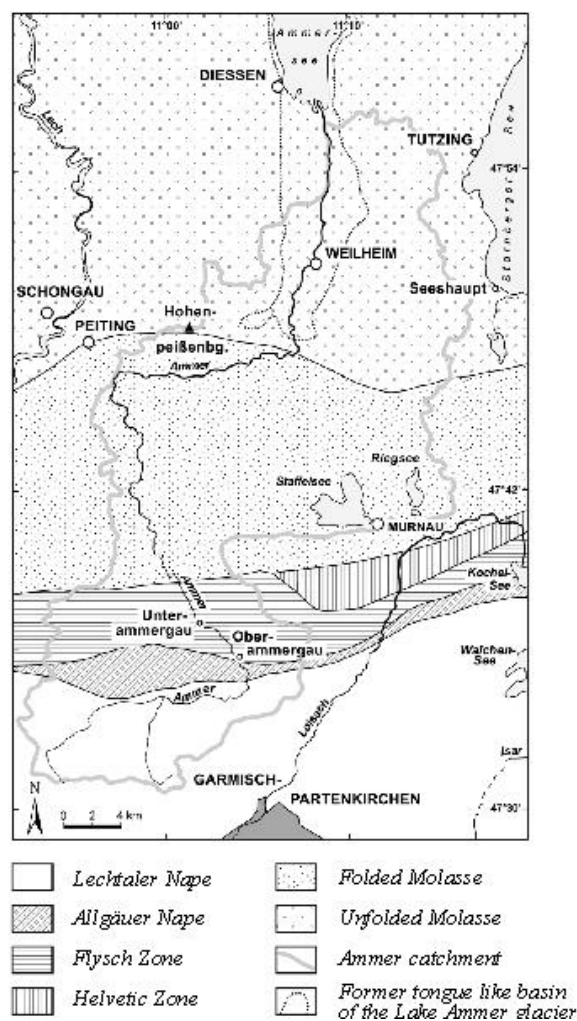
Fig. 2.3: Geomorphologic and geological characterisation of the Ammer (based on KUHNERT 1967, Cartography: V. Falck)

Kalkalpine zone (Region of the Alps formed mainly by limestone)

The most southern region of the catchment is characterised by nappe structures of the Lechtaler Decke and the Allgäuer Decke. The Allgäuer Decke is already allocated to the marginal zone of this geological unit. The thickness of the nappes, built up by shallow water sediments amounts up to 1000m. Peaks are formed by Wettersteinkalk (limestone) in the western part and in the eastern part by Hauptdolomit (dolomite). Both are characterised by karstification (KUHNERT 1967).

Flysch zone

North of the Kalkalpine Zone the flysch zone appears as a small band. Flysch, as a marine sedimentary facies, consists of marl and sandstone. Morphologically flysch mountains are dominated by round forested tops or ridges. In addition, drainage networks carry lots of debris and form huge alluvial cones.

Folded molasse

Further north the molasse, still being affected by the alpine orogeny, is called the folded molasse. Evidence is given by parallel east-west directed synclines (Murnauer Mulde, Rottenbucher Mulde and Guggenberger Mulde). The syncline flanks, partly reaching the surface, can be dated back to the Oligocene. Particular in the region of the Murnauer Mulde, nagelfluh and sandstone build up long hard ridges. At the north end of the folded molasse the peak of the Hohenpeissenberg is located. It is formed by molasse-banked conglomerate rocks and rises up to an elevation of 988 m.

Unfolded molasse

North of the Hohenpeissenberg the tectonical border of the Alps separates folded from unfolded molasse, which has not been affected by the alpine orogeny. In this region Quaternary deposits dominate. Only at few locations the upper fresh-water molasse is exposed.

The whole catchment area is characterised by Pleistocene deposits and forms. In most parts the forms are built up by the Isar-Loisach glacier that scooped out Lake Ammer. The Ammer glacier, supplied from a subsidiary branch of the Isar-Loisach glacier and from ice masses coming out from the Linder valley formed the Ammergau. North exposed cirque and vestiges

of exaration can be found in the mountainous region. The valleys of the flysch mountains are filled with terraced gravel deposits (MEYEN et al. 1962).

Selective glacial erosion causes the exposition of the geological synclines and the exaration of the Staffel- and Riegsee basin. North of the Murnauer Mulde a huge gravel deposit, called the Murnauer Vorstoßschotter can be found which is sporadically covered by ground moraine. The thickness of this deposit reaches 120 m (BAYERISCHES GEOLOGISCHES LANDESAMT 1976) and is characterised by a missing surface drainage system and a constant spring supply at its boundaries. As a ground water reservoir it is of importance for regional fresh-water supply.

Another distinctive elements of the glacial forming is the large drumlin field in the region of Eberfing at the north end of the catchment. The drumlins, built up by ground moraine and orientated with their major axis in north-west south-east, enable the reconstruction of the flow direction of the glacier. The moraines of the Ammer glacier surround today's Ammer valley. Different stages of the last ice age, the Würm ice age, can be distinguished. Referring to FELDMANN (1990) the crest elevation decreases northwards from 850 m in the south to 620 m north. Thereby they surmount Lake Ammer by up to 150 m in the east and 250 m in the west.

The basin of Lake Ammer expands from the north of the Guggenberger molasse dam up to the end moraine north of Lake Ammer near Grafrath. Today Lake Ammer covers an area of 47,6 km² and has a maximum depth of 82 m. The southern silting zone is filled with gravel and lacustrine clay moraine deposits (JERZ 1993b).

2.3.2 Soils

Pedogenesis started in general after the ice recession in the postglacial and is therefore at an early or initial stage.

In the alpine region the soil development is characterised by periglacial mud and talus deposits as a result of the high relief intensity and associated landslide tendency. On the calcic source rock mould and moder rendzina can be found sporadically (RIEKEL 1983). In the flysch mountains podzolized brown earth, pelosol and, in zones of damming wetness, gley dominates as a result of the clayish-marly source substrate.

The index soil of the Molasse and Moraines region is the para-brown earth which only developed to average thickness on the gravel fan of the Ammer Valley and on the Murnauer Vorstoßschotter (DOBEN and FRANK 1983). On behalf of the relief soil types have to be distinguished on small scales (FETZER 1986). Along the steep slopes of the young moraines

rendzina and para rendzina are well developed. Because of accumulation of fine grain sediments in depressions, damming wetness leads to the pedogenesis of similigley. In coniferous forest, forms of podzolation can be detected.

In the Ammer Valley and in the depressions between the molasse dams soil formation is characterised by a high ground water level. Flood plain rendzina, similigley and moor gley as well as marshy soil dominates in this regions (FETZER 1986). Ancient lake mire and swampy moors have a thickness up to more than 10 m. Close by the actual and ancient river these soils are covered with flood plain sediments.

2.3.3 Climate

Due to the KLIMA-ATLAS VON BAYERN, the Ammer catchment is located in the Upper Bavarian prealps and the Alps (BAYERISCHER KLIMAFORSCHUNGSVERBUND 1996). The climate can be characterised in general as temperate cool and humid with a summerly precipitation maximum. All climatic parameters show a distinctive gradient caused by topography and latitude. The reason therefore can be seen in the close location to the Alps, which is also reflected in the spatial distribution of temperature and precipitation.

The long term annual mean temperature is 7 – 8 °C (BAYERISCHER KLIMAFORSCHUNGSVERBUND 1996). Particularly in summer the temperature distribution is highly correlated with the altitude and has a referring elevation gradient of approximately 0.6 – 0.65 K per 100m. In winter the frequency of inversion weather conditions has an influence on this gradient which then amounts to only 0.4 – 0.5 K per 100m (RAPP and SCHÖNWIESE 1995). Southward, the mean annual temperature decreases. While in the Ammer Valley the temperature is about 7.5 – 8 °C, in the Molasse and Moraine region 6 – 7.5 °C and in the Ammergauer Alps only 6 – 6.5 °C is recorded. In the mountain range the annual mean temperature is measured at around 4.5°C.

The long term annual mean regional precipitation is given by the German Weather Service with 1380 mm. The precipitation amount decreases with an increase of distance towards the Alps so that the latitude can be assumed as the dominating descriptive parameter. This effect becomes obvious by comparing the measurements of selected climatic weather stations, located in the Ammer catchment but also in the near surrounding (Fig. 2.4). Moist air masses from the west and north west are frequently transported towards the alpine ridges, causing a strong gradient of precipitation amount on a very short distance from the prealps (1000 m) up to the alpine valleys (1500 mm).
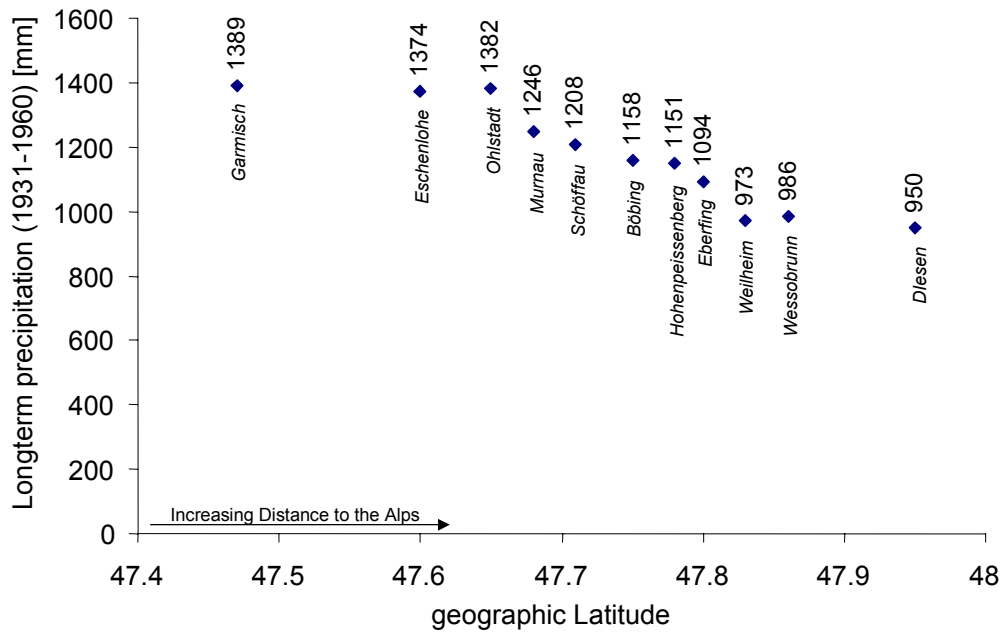
Fig. 2.4: Long annual precipitation (1931 – 1960) depending on the distance towards the Alps (LUDWIG 2000)

The ratio of summer precipitation to winter precipitation is also strongly influenced by the Alps. In the prealps the ratio is 1.7:1 with a rainfall maximum of 140 – 160 mm in June. In the mountainous area this ratio increases to more than 2:1 caused by numerous convective rainfall events in summer, resulting in a mean monthly precipitation maximum in July with more than 200 mm.

Of climatic and especially of hydrological importance is the temporal and spatial distribution of snow. As a direct consequence of the temporal and spatial distribution of temperature and precipitation the number of days with snow cover increases towards the Alps and higher altitudes. The major synoptic climatic station Hohenpeissenberg (977 m), operated by the German Weather Service and located in the Molasse and Moraine area, records a long annual mean of 127 days of snow cover, whereby 87 days of more than 10 cm snow cover are observed. The KLIMA-ATLAS VON BAYERN specify about 78 days of snowfall in average for the whole catchment (BAYERISCHER KLIMAFORSCHUNGSVERBUND 1996).

For the whole testsite the short-wave radiation input can be assumed as being constant. Referring to the KLIMA-ATLAS VON BAYERN the annual amount is about 1000 – 1150 kWh/m², in summit altitudes up to 1200 kWh/m² (BAYERISCHER KLIMAFORSCHUNGSVERBUND 1996).

An overview of the mean annual values of major climatic parameters in relation to their landscape unit in the Ammer catchment is given in table 2.1 based on STOLZ (1998).

	Valley of the Ammer	Molasse and Moraine	Flysch Mountains /Ammergauer Alps
T [°C]	7.5 - 8	6 – 7.5	< 4.5 – 6.5
N [mm]	1100 - 1300	1300 – 1500	1500 – 2000
N_{sommer}/N_{winter}	1.7	1.7	>2
Days of frost	110 – 120	120 – 140	140 – 160
Moisture index based on DE MARTONNE	52 - 82	60 – 100	> 100

Tab. 2.1: Major climatic elements due to the landscape units of the Ammer catchment (based on STOLZ 1998)

2.3.4 Landuse

The landuse of the Ammer catchment is largely influenced by the heterogenity of climate, relief and soil properties. Although the Bodengütekarte (Soil quality map) of Bavaria shows only low yield expectation, the whole area is dominated by an intense agricultural and forestry use. The landuse characteristics of the catchment however change towards the Alps.

Fifty percent of the total non-urbanised (agricultural) acreage is covered by forest. Coniferous forest is predominant while mixed forest (beech and fir) can only be found in the higher altitudes of the Ammergauer Alps. The percentage of the landuse class forest differs within the landscape units defined earlier (Tab. 2.2). In the mountainous region, forest is the predominant landuse (61%). This can be traced back to the changing climatic situation, the shallow thickness of soils and the steeper relief. Forest sites are mainly found in areas with damming wetness, steep relief and on soils with a low water storage capacity (FETZER et al. 1986).

Agricultural landuse has to be distinguished into pasture and arable land. As a consequence of lower temperature and increasing precipitation, the ratio of pasture and arable land is shifted towards pasture approaching the Alps. In the Ammer Valley the fraction of arable land is 17.5% while in the Molasse and Moraine area only 1.2% to 6 % of the land is cultivated and none can be found in the flysch mountains and the Ammergauer Alps (BAYERISCHES LANDESAMT FÜR STATISTIK UND DATENVERARBEITUNG 1995). Hence farming can only be carried out on mid and upper Pleistocene gravel deposits or alluvial soils (STOLZ 1998).

The possibility of cultivation is therefore limited not only by climate but also by soil conditions. While in the Ammer Valley wheat farming is widespread, southwards, due to

lower pretension on the habitats, oats and barley dominate. The overall percentage of corn cultivation in arable land decreases from 52% in the north to 39% in the south (BAYERISCHES LANDESAMT FÜR STATISTIK UND DATENVERARBEITUNG 1995). Because of the higher tolerance to more precipitation maize is the preferred landuse in the Molasses and Moraine area. Like the cultivation of trefoil and lucerne, maize is produced for intense livestock raising. Other cultivation products like rape seeds or row crop are of no particular importance and are produced only for subsistence requirements (STOLZ 1998). In the moors of the Ammer Valley some areas are still used for peat digging.

Landscape Unit	Forest	Agriculture Landuse	Use of the Agriculture Acreage [%]		Use of the Agriculture [%]		
			Pasture	Arable Land	Corn	Maize	Forage crop
the Ammer Valley	37.8	56.0	82.5	17.5	52	28.6	14.0
Molasse - Moraine a) East b) West	34.4 23.0	52.0 68.2	94.0 98.8	6 1.2	39 47	43.5 34.5	17.2 9.6
Flysch Mountains and Ammergauer Alps	60.9	12.6	100				

Tab. 2.2: Agricultural landuse in the Ammer catchment (based on BAYERISCHES LANDESAMT FÜR STATISTIK UND DATENVERARBEITUNG 1991)

2.3.5 Hydrology

The river Ammer belongs to the Danubian river network (Fig. 2.5). It mouths into Lake Ammer and drains further north through the Amper and the Isar towards the Danube. The GEWÄSSER-ATLAS VON BAYERN classifies the Ammer as a 4th order catchment (BAYERISCHES LANDESAMT FÜR WASSERWIRTSCHAFT 1978).
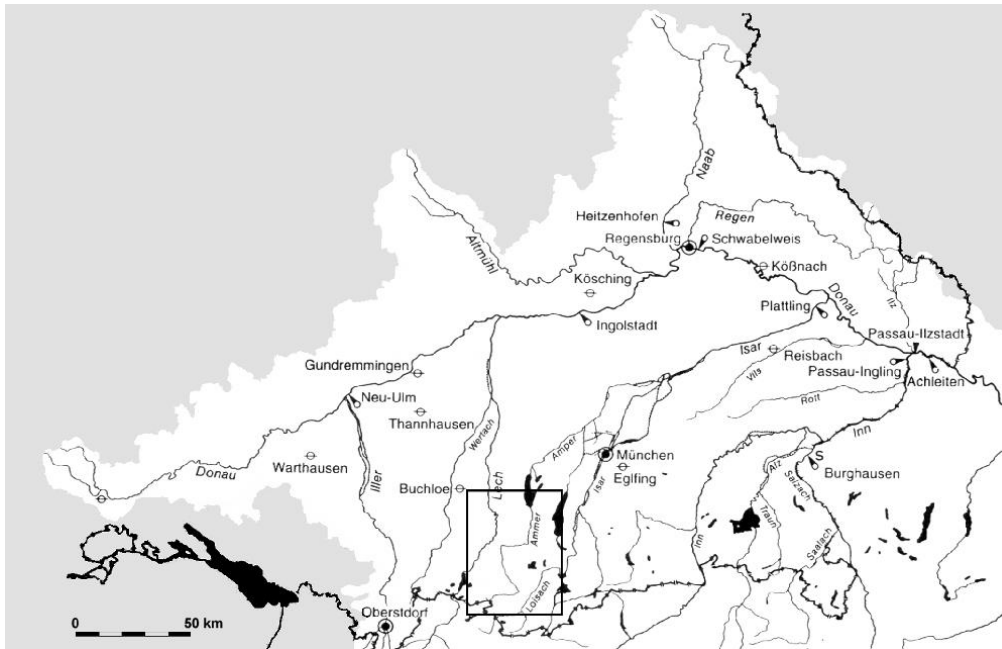
Fig. 2.5: Location of the Ammer catchment in the Danubian river network (BAYERISCHES LANDESAMT FÜR WASSERWIRTSCHAFT 1997)

Since 1941 runoff is recorded continuously at the stream gauge in Fischen, a small village close to the southern shore of Lake Ammer. Upstream the Ammer three other gauges record the water level, namely in Weilheim, Peissenberg and Oberammergau. Additional major tributaries are also gauged like the Ach in Oberhausen and Obernach, the Halbammer in Unternogg and the Linder in Linderhof and Graswang. A summary is given in table 2.3. From a hydrological point of view the Ammer is well equipped with measuring instruments.

Gauge	River	Altitude [m asl]	Area [km²]	Longitude [UTM 32]	Latitude [UTM 32]	Records since
Fischen	Ammer	533	709	443623	531035	1941
Weilheim	Ammer	550	601	443532	530144	1926
Peissenberg	Ammer	592	294	442950	529380	1958
Oberammergau	Ammer	831	114	443016	527284	1921
Obernach	Ach	652	41.5	443422	528420	1954
Oberhausen	Ach	585	117	443434	529256	1951
Graswang	Linder	865	71	442708	527084	1976
Linderhof	Dreisäulerbach	964	2.3	442124	527100	1984
Unternogg	Halbammer	849	43.5	442238	527892	1975

Tab. 2.3: Stream gauges in the Ammer catchment (BAYERISCHES LANDESAMTES FÜR WASSERWIRTSCHAFT 1997)

Statistical primary values can be used to evaluate the dimension of runoff. These are published annually in the GEWÄSSERKUNDLICHEN JAHRBÜCHERN (e.g. BAYERISCHES LANDESAMT FÜR WASSERWIRTSCHAFT 1997), which refer to the German DIN 4049, and provide general records and observations of the respective hydrological year as well as long term annual mean values. Table 2.4 shows for the Ammer gauges the longterm average of annual primary values (NNQ: lowest runoff ever measured; MNQ: mean low water flow; MQ: mean runoff; MHQ: mean flood flow; HHQ: highest runoff ever measured).

Gauge	Period	NNQ	MNQ	MQ	MHQ	HHQ
Fischen	1941 – 1990	3.0	6.16	16.6	199	376
Weilheim	1926 – 1990	2.6	5.83	15.5	157	461
Peissenberg	1958 – 1990	1.32	2.85	8.79	113	286
Oberammergau	1921 – 1990	0.44	1.18	3.73	53.6	135

Tab. 2.4: Statistical primary values for the stream gauges in the Ammer catchment [m³/s]

The primary values render the derivation of runoff regimes referring to PARDE (1960). They can be applied to describe the runoff behaviour during the hydrological year as a function of relief, climate, soil and vegetation (WILHELM 1997). The course of the runoff hydrograph is shown as a dimensionless ratio of the long term monthly discharge and the mean annual runoff. The coefficients of fluctuation a1 and a2 result from the ratio of the mean extreme discharges MHQ res. MNQ to the mean runoff MQ. The amplitude of fluctuation a3 is the ratio of mean extreme discharges (MHQ/MNQ) (Fig. 2.6).
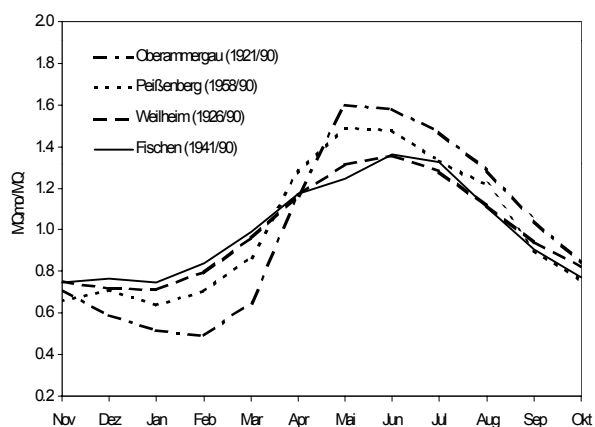
Gauge	a_1	a_2	a_3
Oberammergau	14.4	0.32	45
Peissenberg	13	0.32	40
Weilheim	10	0.37	27
Fischen	12	0.37	32

Fig. 2.6: Runoff regimes along the Ammer and the coefficients res. amplitudes of fluctuations referring to PARDE (1960)

The complexity of the runoff regime in the Ammer catchment is not obvious at first sight. Analysis shows that the regime is influenced by two dominating factors: primarily the precipitation maximum in the summer, but also the snow melt period during late spring. The temporal sequence shows, as a result a temporal transition of snowmelt and precipitation maximum, a single peak distribution with a low maximum. With increasing distance from the mountains, the peak defers to the summer months. The run of the regime curve flattens with increasing catchment area and decreasing slope while the amplitude of fluctuation is getting smaller. The heterogeneity of the catchment, referring to geology and pedology, is also reflected in the varying distribution of drainage density. The area of the Murnauer Schotterfeld shows no surface drainage while the ground moraine covered molasse region is characterised by a high river density (BAYERISCHES LANDESVERMESSUNGSAMT 1997). The huge ground water reservoirs in the gravel covered Molasse and Moraine area in the north east of the catchment have an additional diminishing influence on the runoff behaviour. The valley of the Linder located in the kalkalpine zone shows several forms of karst like e.g. small dolines. The influence on the surface runoff is evident. Due to KUHNERT (1967) it can be assumed that one of the two ground water flows out of the valley of the Linder drains into the eastward catchment of the Loisach. For this study this aspect is neglected, since the influence of the karst is seen as a minor error source in flood event modelling.

3. Model concept

3.1 Synergetic use of meteorological and hydrological models

The main objective of the project RAPHAEL was the synergetic application of hydrological models and meteorological models to improve flood forecasting. In the Ammer catchment, the combination of mesoscale meteorological and microscale hydrologic models is investigated with a special focus on the scale issue resulting from the resolution gap of the two model families. The mesoscale is defined in this sense as a domain that includes several geographical units which show a strong heterogenity to each other, like e.g. the Alps. The microscale on the other hand can be defined as a regional scale where the subunits vary only on a minor level.

The study also targets in particular on the evaluation of different meteorological data sources in order to assess their applicability and reliability for flood modelling. Apart from conventional rain gauge and climatic station data, the information of the NWP models, namely MC-2, BOLAM, MESO-NH and SWISS MODEL, radar interpreted precipitation taken from the DWD rain radar Fürholzen and precipitation fields retrieved from METEOSAT has been available. The resulting hourly precipitation fields are applied for the hydrological simulations as input parameter fields.

The hydrological model structure PROMET-D establishes a link between the physically based SVAT-model PROMET (MAUSER and SCHÄDLICH 1989) and an enhanced distributed GIS-version of the TOPMODEL (LUDWIG 2000). The TOPMODEL-PROMET interface is generated by assessing the outputs of PROMET (evapotranspiration, snowmelt, soil moisture to initialise the flood event) to hourly update the water balance terms of the runoff model in a distributed sense.

To reach the scientific goal of the project, a raster-GIS-based model structure has been set up that easily enables the integration of the meteorological model results as the driving variable for the hydrological model. The application of different disaggregation schemes has to be carried out on the meteorological model output to overcome the resolution gap. An overview of the model structure is given in figure 3.1.

In the following the different models and their components are briefly described.
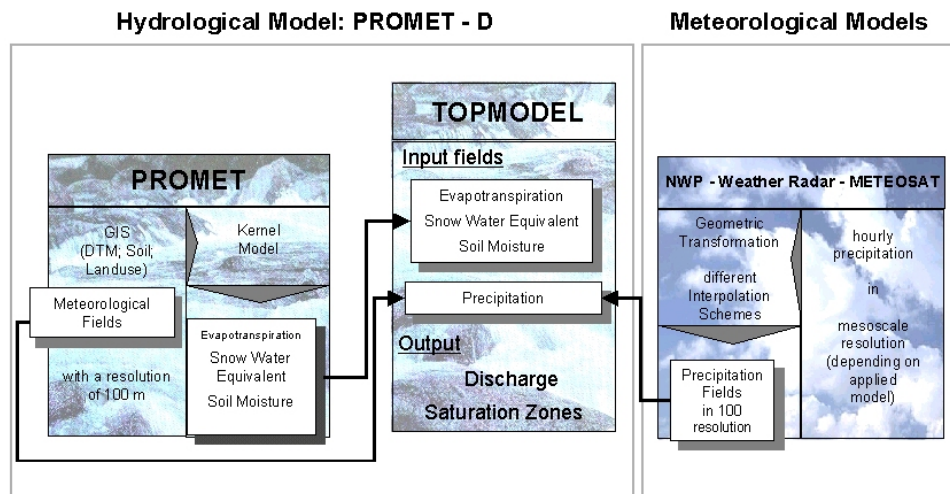
Fig. 3.1: Synergetic hydrologic and meteorological model structure

3.2 Hydrological model PROMET-D

3.2.1 PROMET

PROMET is a physically based SVAT (Soil Vegetation Atmosphere Transfer) model developed by MAUSER at the Department of Earth and Environmental Sciences, Section Geography of the University of Munich (MAUSER and SCHÄDLICH 1998). It calculates the actual evapotranspiration based on the Penman-Monteith equation (MONTEITH 1965) as a function of water availability, energy budget, physical soil characteristics and the physiological regulation mechanisms of heterogeneous plant stands. The spatial modeller of PROMET organises the following interdependent model components:

- a **soil water submodel** (EAGLESON 1978 a-g) for soil-moisture calculation as a function of in- and exfiltration, percolation and capillary rise
- a **vegetation submodel** (BALDOCCHI et al. 1987) computing the water transport through plant stands as a function of stomata conductance mechanisms,
- an **aerodynamical component** (MONTEITH 1978) modelling the transport of water vapour from the plant stands into the atmosphere
- a **radiance model** (MAUSER 1989) calculating the energy budget of each location depending on geographical co-ordinates, the sun zenith angle and the cloud coverage
- a **snow submodel** based on an energy balance approach (TODINI 1996) calculating snow accumulation, snow depletion and the snow melt.

PROMET is embedded within a raster GIS-structure to allow the integration of spatial distributed data fields like e.g. remotely sensed data.

The model requires a set of parameters referring to relief, soil, landuse and meteorology. These information are either provided as spatial data sets or in tabular format. Terrain height, slope, aspect and soil type information are considered as time independent parameter fields. Soil physical parameters are stored in tabular format and are assigned to the spatial soil type data set. The landuse is also provided as spatially distributed information and is assumed to be constant. The dynamic development of the different landuse types over the year is also taken into account. Plant height, albedo and LAI (leaf area index) are provided in tabular format for each landuse type and daily increment. Meteorology is highly variable in time and space. PROMET usually applies DWD climatic station measurements. In order to generate the meteorological input parameter fields for hourly modelling, these measurements have to be temporally and spatially interpolated. This is also performed within the spatial modeller of PROMET. An overview of the model structure is given in figure 3.2.
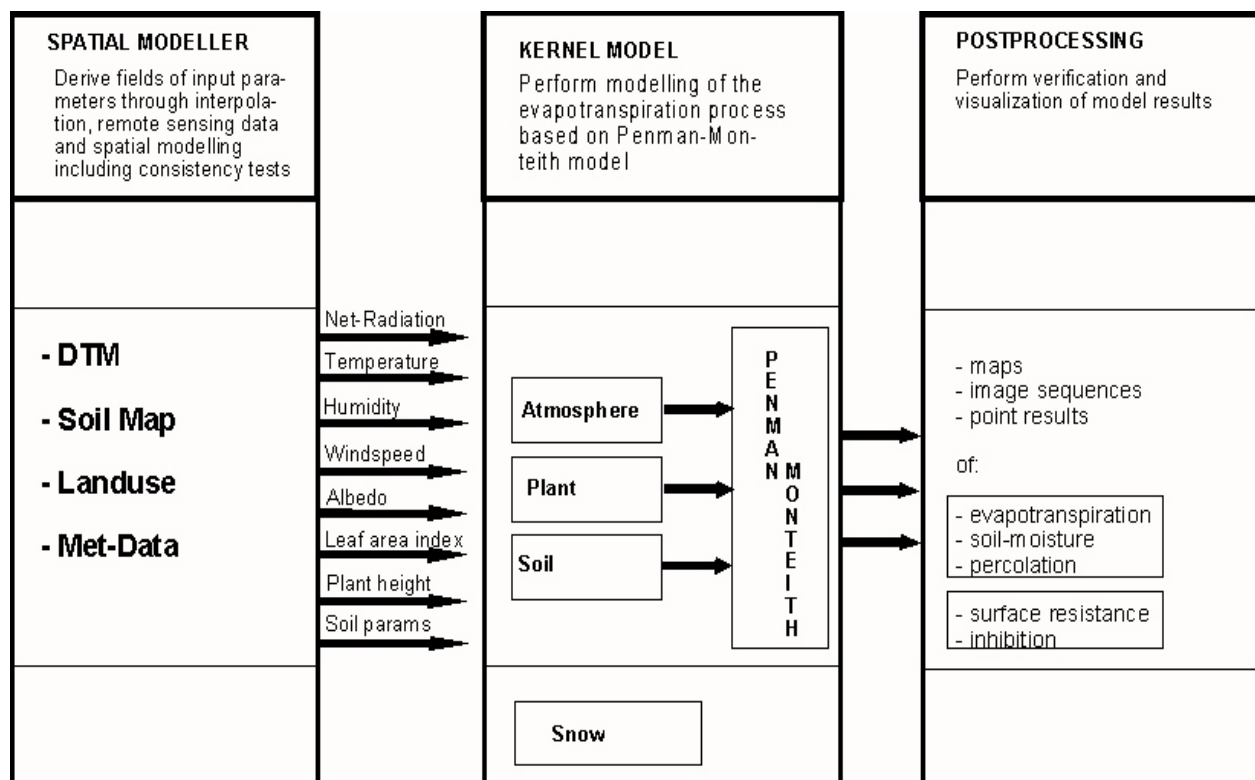
Fig. 3.2: Schematic structure of PROMET (BACH et al. 2000)

The actual evapotranspiration is computed in the kernel model of PROMET by the Penman Monteith equation:

(Eq. 3.1)

$$E_v = \frac{\Delta\,(Q-B) + \rho \cdot c_P \cdot \dfrac{D}{r_a}}{\Delta + \gamma \cdot \dfrac{1+r_s}{r_a}}$$

with:

E_v	=	actual evapotranspiration
Δ	=	gradient of saturated vapour pressure
Q	=	energy budget
B	=	ground heat
ρ	=	density of air
c_p	=	specific heat of moisture air
D	=	vapour pressure deficit
γ	=	psychometric constant
r_a	=	aerodynamical resistance
r_s	=	surface resistance

All required parameters to solve Eq. 3.1 are provided by the different submodels.

This formulation of the Penman-Monteith equation also considers the ground heat flux that is computed by an empirical algorithm taking into account the LAI and the energy budget (SCHÄDLICH 1998):

(Eq. 3.2) $B = (0.2 - 0.03 \cdot LAI)\, Q$

Besides the actual evapotranspiration, PROMET also calculates several other water balance terms like e.g. soil moisture or snowmelt. The computed results can be visualised as maps, image sequences or tabular point data.

PROMET has been successfully applied on different scales, ranging from point modelling, to microscale and mesoscale catchment modelling in different natural environments (SCHÄDLICH 1998; STRASSER 1998; LUDWIG 2000; BACH et al. 2000).

3.2.1.1 The soil water submodel

The soil water submodel is based on an approach by EAGLESON (1978 a-g) and computes the volumetric soil moisture and the matrix potential of the rooting zone of a vertically homogeneous soil layer. The simulated processes of infiltration, exfiltration, percolation and capillary rise determine the water availability depending on the matrix potential and hence regulate transpiration of plant stands or evaporation of bare soil. Therefore the model distinguishes wet from dry periods. During rainfall, infiltration is generated depending on rainfall intensity and infiltration capacity. The actual infiltration capacity is thereby calculated as a function of soil moisture. Surface runoff occurs when rainfall intensity exceeds the actual infiltration capacity. During periods of no rain the actual exfiltration capacity is calculated based on soil moisture (MAUSER and SCHÄDLICH 1998). Infiltration and capillary rise increase the soil moisture of the unsaturated zone while percolation and exfiltration in times of no-rain decrease it. During arid periods only capillary rise is calculated.

The change in soil moisture and therefore the change in water availability for plants can be described for homogeneous soils by the one dimensional Philip equation (PHILIP 1960):

(Eq. 3.3)

$$\frac{\delta\,\Theta}{\delta\,t} = \frac{\delta}{\delta\,z}\left[D(\Theta)\frac{\delta\,\Theta}{\delta\,z}\right] - \frac{\delta\,K(\Theta)}{\delta\,z}$$

with t as the time, z as the soil depth, K(Θ) as the hydraulic conductivity and D(Θ) as the diffusion in m²/s:

(Eq. 3.4)

$$D(\Theta) = K(\Theta)\cdot\frac{\delta\,\Psi(\Theta)}{\delta\,\Theta}$$

with Ψ as the matrix potential at a volumetric water content Θ.

The equation developed by PHILIP (1960) describes an analytic approximated solution of the RICHARDS equation (RICHARDS 1931). It is valid for a one-dimensional vertical infiltration in a semi-infinite, homogeneous soil compartment. The RICHARDS equation is derived from a combination of the continuity equation and Darcy's law. The application of Darcy's law under unsaturated conditions leads to the conclusion that the conductivity is no longer only a constant of the substratum but also a function of saturation. Thereby the hydraulic gradient is the sum of the gradient of matrix and gravity potential (STRASSER 1998).

The PHILIP equation can only be solved analytically considering the following simplified assumptions:

- soil and liquid characteristics have to be considered separately

- the soil water transport has to be separated in infiltration, exfiltration, percolation and capillary rise

- for any of these processes a solution of the PHILIP equation has to be found by means of simplified boundary and initial conditions

- to simulate independent processes the separate solutions of the PHILIP equation have to be linearly superimposed.

The analytic solution of the PHILIP equation with simplified boundary conditions leads to equations for the infiltration and exfiltration capacity which only depend on time and initial saturation.

Under the assumption of a homogeneous soil compartment, approximation functions for the matrix potential and the hydraulic conductivity can be derived utilising physical soil parameters. However, these parameters have to be time independent. Considering the functional relation of the matrix potential and the soil saturation by BROOKS and COREY (1964), EAGLESON (1978 a-g) formulates the following approximation function for the matrix potential Ψ:

(Eq. 3.5)

$$\Psi(s) = \Psi(1) \cdot s^{-1/m}$$

$$\Psi(1) = \frac{\sigma_\omega}{\tau_\omega} \sqrt{\frac{n}{k(1) \cdot \Phi(m)}}$$

with:

s	=	degree of saturation
n	=	porosity
m	=	pore size distribution index
σ_ω	=	surface tension
τ_ω	=	density of water
$k(1)$	=	normalised hydraulic conductivity at complete saturation
Φ	=	pore shape parameter

The normalised saturated hydraulic conductivity can be written as:

(Eq. 3.6) $k(1) = \mu \, K(1) / \, \tau_\omega$

with:

    μ = dynamic viscosity

    $K(1)$ = hydraulic conductivity at complete saturation

The dependency of the pore shape parameter on the pore size distribution index is derived from empirical investigations of CARMAN (1937). The matrix potential at field capacity is substituted by the bubbling pressure head. The bubbling pressure head describes the soil suction value recorded when air is sucked for the first time while draining the soil.

All required parameters can be derived from literature and are linked to the spatially distributed soil type information layer. For the calculation of percolation and capillary rise following assumptions are made:

- in deeper layers, close to the ground water, the soil moisture can be assumed as constant throughout the year. Percolation therefore equals the hydraulic conductivity at this moisture.

- The ground water level is much deeper then the capillary fringe of the soil. Capillary rise can be then computed in analogy to ex- and infiltration.

3.2.1.2 The vegetation submodel

The vegetation submodel is based on an approach of BALDOCCHI et al. (1987) and simulates the water transport through the plant considering the physical and physiological influences on the evapotranspiration process. Net canopy resistance is computed as the sum of the individual stomata resistance. Besides the radiate transfer in the canopy the influence of air temperature, soil suction and leaf water potential is taken into account.

The water flow through the plant and hence its transpiration is regulated by active and passive control mechanism. In analogy of Ohm's law, water transport can be compared to an electric flow that is inhibited by several resistances. Thereby the water tension between soil and atmosphere Ψ refers to the electric potential difference and the resistance between soil and atmosphere to R the electric resistance. The evapotranspiration flow V can be formulated as:

(Eq. 3.7)

$$V = \frac{\Psi}{R}$$

The exchange of water and carbon dioxide with the atmosphere is controlled by the plant through several mechanisms. Leaf and root growth are generally in equilibrium. Otherwise the stomata are closed to prevent high leaf water potential. Besides these active mechanisms, there are limiting factors that have an influence on the transpiration of the plant. Especially the water and energy availability is of importance. If there is a lack of water the plant reduces the transpiration and hence fixation of carbon in the plant. When water supply is sufficient the available energy regulates the transpiration and thus the carbon fixing.

Several actual evapotranspiration models modify the potential evapotranspiration by a reduction term describing all of these mechanisms. In PROMET the vegetation submodel describes these processes in more detail.

The following environmental factors are considered:

- the influence of the leaf area index on the Photosynthetically Active Radiation (PAR),
- the influence of the sun's zenith angle on the fraction of shaded and sunlit leaf area,
- the influence of air temperature on stomatal resistance,
- the influence of leaf water potential on stomatal resistance and
- the influence of potential difference between soil and atmosphere on the water transport.

LAI is used in a 10-layer radiative transfer model (NORMAN 1979) to convert the incoming PAR into fractions of shaded and sunlit leafs depending on the sun elevation angle and assuming spherical leaf orientation. The fraction of shaded and sunlit leaf area is also used to convert stomatal conductance into canopy conductance. PAR is thereby computed by an approach based on LANGHOLZ and HÄCKEL (1985), taking into account the global radiation Q_g.

(Eq. 3.8)

$$PAR = \frac{Q_g}{2.05}$$

The stomatal resistance is determined in dependence of PAR and the inhibition g:

(Eq. 3.9)

$$r_s(PAR) = \left[r_s(\min) + b_{rs} \cdot \frac{r_s(\min)}{PAR} \right] \cdot \frac{1}{g}$$

with:

   $r_s(\min)$ =   minimal stomatal resistance

   b_{rs} =   increase of stomatal resistance with PAR

The parameter $r_s(min)$ is assumed to be constant for a plant species and neglectably differs due to climate, leaf age and nutrient absorption (e.g. KÖRNER et al. 1979).

Temperature (g(T)), leaf water potential (g(Ψ)) and soil-moisture (g(Psi)) inhibition functions are furtherly introduced as limiting factors for the stomatal resistance in the form of an environmental influence function:

(Eq. 3.10)   g = g(T) g(Ψ) g(Psi)

The function ranges from zero (total inhibition, stomatal resistance approaches infinity) to one (no inhibition). Its product is the net inhibition influencing the stomatal resistance.

Stomatal resistance decreases with increasing temperature until a threshold is reached, after which it increases. Assuming equal leaf and air temperature the following function based on JARVIS (1976) determines:

(Eq. 3.11)

$$g(T) = \frac{T - T_{min}}{T_o - T_{min}} \cdot \frac{(T_{max} - T)^b}{(T_{max} - T_o)^b}$$

with:

T	=	air temperature
T_{min}	=	minimum air temperature for stomatal resistance
T_{max}	=	maximum air temperature for stomatal resistance
T_o	=	optimum air temperature for stomatal resistance
b	=	$(T_{max} - T_o)/(T_{max} - T_{min})$

The referring temperatures are taken from literature for each plant type (e.g. KÖRNER et al. 1979).

Water stress can be quantified in terms of leaf water potential Ψ. Stomatal resistance is relatively independent of the leaf water potential until it drops below a threshold value Ψ_0, after which the stomata close rapidly. The inhibition function can be computed by literature available parameters (e.g. POSPISILOVA and SOLAROVA 1980) and is expressed as:

(Eq. 3.12)   g(Ψ) = 1   if $\Psi > \Psi_0$

and as:

g(Ψ) = aΨ + b_w if $\Psi \leq \Psi_0$

with:

a	=	slope of the increase of stomatal resistance with soil suction beyond the value at which stomata close
b_w	=	soil suction at which stomatal closure starts

The parameters a and b_w are assumed constant for each plant species (BALDOCCHI et al. 1987).

Stomatal resistance also depends on root potential. A study of BISCOE et al. (1976) showed that transpiration linearly increases with potential difference between soil and plant. It is shown that the potential difference is not zero even if no water fluxes occur. Therefore a constant plant specific soil potential is assumed.

In summery, the following parameters are required for the vegetation submodel.

- minimal stomatal resistance

- increase of stomatal resistance with PAR

- minimum, optimum and maximum air temperature for stomatal resistance

- leaf water potential threshold value

- slope of the increase of stomatal resistance with soil suction beyond the point, at which stomata close

- soil suction at which stomatal closure starts

- plant specific soil potential

These are provided as either statistical or dynamical plant parameters in separate files, referring to the categories of the spatially distributed landuse. In the model plant growth is represented through the temporal evolution of green leaf area index, plant height and albedo. These values, taken from field measurements or literature, are provided in a daily increment.

3.2.1.3 The aerodynamical component

After the water proceeds its way from the soil through the plant, as described in the preceding submodels, water vapour emits into the atmosphere. Therefore PROMET incorporates an aerodynamical component that distinguishes two resistances (MONTEITH 1978):

- R_b as the boundary resistance of the plant stand that regulates the diffusion of water vapour into the surrounding air

- R_a as the aerodynamical resistance of the atmosphere describing the transport of water vapour from the boundary layer into the atmosphere

The original version of the PENMAN-MONTEITH equation formulates an overall aerodynamical resistance that includes R_b. However the reason to separately describe the two processes lies in the fact that the substance and energy fluxes at the boundary layer between the leaf and the atmosphere depend on the molecular diffusion of the involved media. The

logarithmic wind profile assumed for the derivation of R_a cannot be seen as valid for this process. Therefore R_b has to be introduced (MAUSER 1989).

Taken from investigations by BRUDSAERT (1982), the following function is valid for meadows, maize and forest:

(Eq. 3.13)

$$R_b = \frac{2}{k \cdot u*}$$

with:

u*   =   sheer stress velocity

k   =   Karman constant

In PROMET this algorithm is assumed to be valid also for all other vegetation types.

The aerodynamical resistance R_a is determined by the height z and the displacement height d. The displacement height describes the height in the plant stand where the exponential wind speed profile is equal to zero. Assuming a logarithmic wind profile under neutral layering conditions R_a is modelled as (MONTEITH 1978):

(Eq. 3.14)

$$R_a = \frac{1}{k^2 \cdot u(z)} \cdot \ln^2 \left(\frac{z - d}{z_0} \right)$$

with:

u(z) =   wind speed at the height z

d   =   displacement height

z_0 =   roughness length

3.2.1.4 The radiation model

The driving engine of the evapotranspiration process and thus the water cycle is the available energy. In PROMET this is computed by a radiation model, introduced by MAUSER (1989). For each location the energy budget is modelled depending on geographical co-ordinates, sun zenith angle and cloud coverage. The radiation balance is formulated as:

(Eq. 3.15) $Q = (1 - a) \cdot Q_s + Q_l$

with:

a   =   albedo

Q_s =   short-wave radiation

Q_l =   long-wave radiation

The albedo of the surface is thereby taken from literature and is assigned to the respective plant species.

The short-wave radiation has to be distinguished in a direct and diffusive component. In a first step, the potential total radiation Q_{pot} is calculated applying a standard clear sky model using a visibility range of 23 km. From the terrain parameters height, slope and aspect and the astronomic parameters local time, sunrise and sun set, azimuth and zenith angle, distance sun-earth and the solar constant, the potential total radiation is determined for each location and each modelling time step (MCCLATCHEY 1972). The total transmissivity of a standard atmosphere is computed by an approach based on HOTTEL (1976). The seasonal conditions of the mid-latitude atmosphere in winter and summer is taken into account as well as the terrain height. The relation of direct and diffusive transmissivity is derived from LIU and JORDAN (1960):

(Eq. 3.16) $T_{A,dif} = 0.271 - 0.2939 \cdot T_{A,dir}$

with:

$T_{A,dif}$ = diffusive transmissivity of the atmosphere

$T_{A,dir}$ = direct transmissivity of the atmosphere

The direct radiation Q_{dir} is then computed as:

(Eq. 3.17) $Q_{dir} = T_{A,dir} \cdot Q_{pot}$

The diffusive radiation Q_{diff} furthermore considers the view factor VF which depends on the slope β and is derived by $(1+\cos\beta)/2$. This is carried out in order to correct the radiation on inclined terrain.

(Eq. 3.18) $Q_{diff} = T_{A,dif} \cdot Q_{pot} \cdot VF$

The short-wave radiation, as the sum of direct and diffusive radiation, is modified with a factor derived from actual cloud coverage C (MÖSER and RASCHKE 1983):

(Eq. 3.19) $Q_s = (Q_{dir} + Q_{diff}) (0.321 + 1.364 \cdot C - 0.691 \cdot C^2)$

The long-wave radiation Q_l as the sum of the emission of the surface Q_E and the atmospheric counter radiation Q_A, can be described as:

(Eq. 3.20) $$Q_l = - Q_E + Q_A = -\varepsilon \cdot \sigma \cdot T_s^4 + \varepsilon_{eff} \cdot \sigma \cdot T^4$$

with:

> ε =   emissivity of the surface
>
> σ =   Stefan-Boltzmann constant
>
> T_s =   soil temperature
>
> ε_{eff} =   effective emissivity of the atmosphere
>
> T =   air temperature

If cloud coverage is not zero, the atmospheric counter radiation is modified with an algorithm by BOLZ (1949a,b):

(Eq. 3.21) $$Q_A = 0.99 \, (\varepsilon_{eff} \cdot \sigma \cdot T^4) \cdot (1 + 0.243 \cdot C^{2.5})$$

The radiation model was successfully verified with measurements at the DWD station Hohenpeissenberg (LUDWIG 2000) and spatially validated in the Weser catchment (STRASSER 1998).

3.2.1.5 The snow submodel ESCIMO

With regard to the temporal dynamic of the water cycle, the temporal storage of water in a snowpack is of importance. PROMET therefore incorporates a snow submodel called ESCIMO (Energy Snow Cover GIS Integrated Model). It is a physically based submodel for the hourly calculation of the snow water accumulation and melt with regards to the energy and mass balance. The model concept was originally developed by TODINI (1996). It was implemented in the PROMET shell by STRASSER (1998) and extended by TASCHNER et al. (1998).

ESCIMO models the following energy terms:

- The energy input combines the short wave radiation, the long wave reflected radiation, sensible heat flux, advective energy (rain or snow fall) and ground heat flux,
- the energy output contains the reflected short wave radiation and the long wave emission (Fig. 3.3).

Internal energy and mass fluxes as well as advective energy fluxes by lateral air mass movements are not considered.
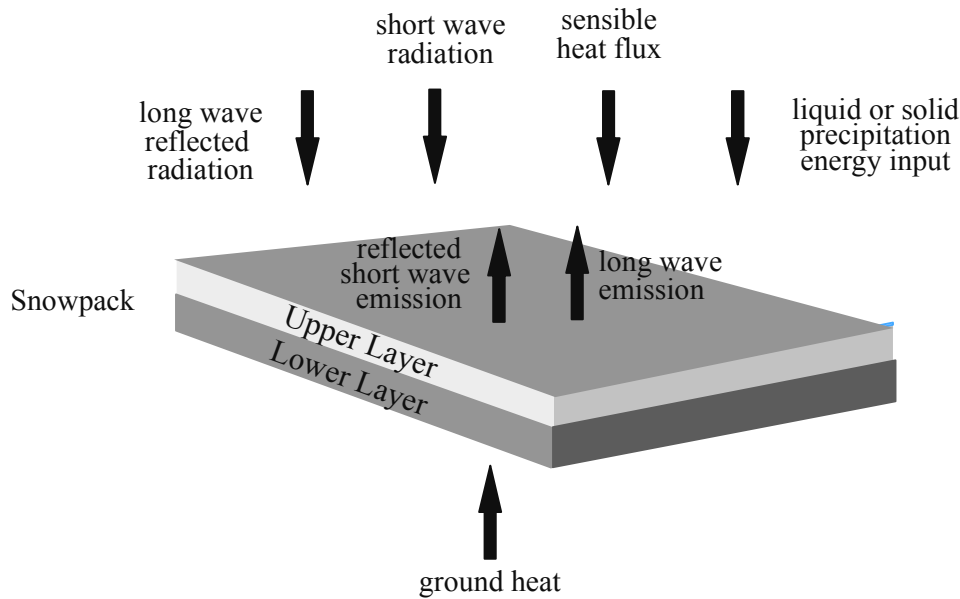
Fig. 3.3: Energy fluxes in a snow pack

The ground heat flux is assumed to be constant. The energy input by liquid and solid precipitation is based on an approach by TODINI (1996). The air temperature of phase transition from rain to snow is set to 273.16 °K.

According to the energy balance approach the sum of radiation, sensible heat flux, advective energy (rain or snowfall), ground heat flux and the change in the internal energy of the snowpack has to be zero. The fluxes into and out of the snowpack are expressed by its internal change of energy.

The snowpack is stratified in two dynamic isothermal snow layers. After more than nine days without considerable precipitation the snowpack is assumed to developed a boundary layer. With the next considerable snowfall the snowpack is isolated as the lower layer and the upper layer is generated. The internal energy of the lower layer is conserved. Only the ground heat is added at each time step. All other energy fluxes are now affecting only the upper layer. After the upper layer is completely melted the lower layer is activated again.

The basic extensions to the original version (STRASSER 1998) are, besides the two layer approach, a more sophisticated albedo function and the introduction of sleet as a form of precipitation. These new aspects are described in the following.

The short wave radiation is modified by the albedo. The derivation of the albedo A is based on ROHRER (1992) and considers the effect of the ageing snow cover and the landuse:

(Eq. 3.22a) $$A = A_0 + Ke^{-nk}$$

with:

A_0 = lowest possible albedo of snow

K = constant (added to A_0 to maintain the initial albedo of snow)

k = factor that depends on whether the air temperature is below or above 273.16 °K

n = number of days after the last snowfall of more than 0.5 mm per hour

After each snowfall of more than 0.5 mm per hour the albedo function is reset to n = 0. The variable landuse influence is taken into account by the application of adapted albedo functions (Fig. 3.4), regarding that in coniferous forests the snow accumulation is less compared to the open field while the snow cover period is almost the same (RAKHMANOV 1958). This effect is mainly caused by the shadow influence and by wind drifted snow from open field to the coniferous forest (catch).

The chosen albedo functions are :

(Eq. 3.22b,c)   in coniferous forest: $A = 0.40 + 0.20 \cdot e^{(-n\,k)}$;

in open land: $A = 0.40 + 0.54 \cdot e^{(-n\,k)}$

with T_a as the air temperature and k = 0.12 when $T_a > 273.16$ °K or 0.05 when ($T_a \leq 273.16$ °K)
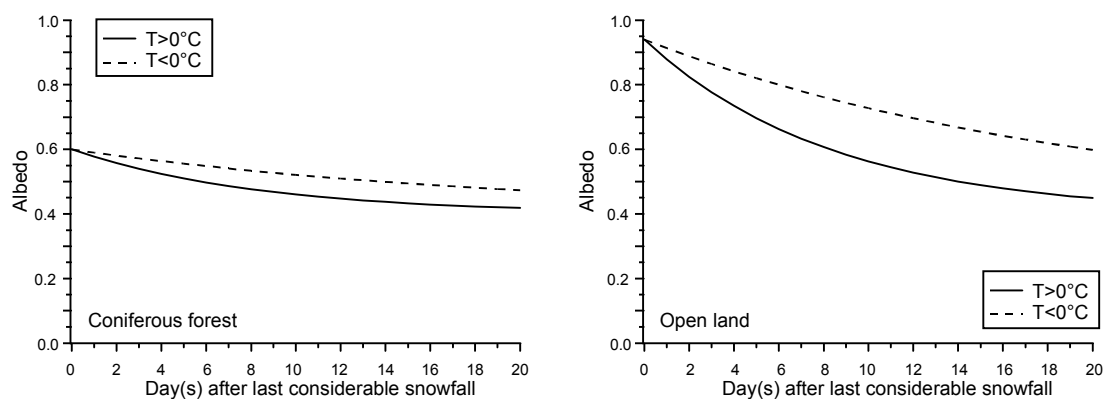
Fig. 3.4: Landuse-dependent albedo ageing functions for snow

For the estimation of the energy balance it is necessary to make an assumption about the status of the precipitation (snow or rainfall). In this approach the decision whether the

precipitation is solid or liquid depends on the air temperature and is distinguished in rain-, snowfall and sleet depending on the actual air temperature (SCHULLA 1997). Pure snowfall occurs at a temperature below 272.16 K, pure rainfall above 274.16 K and sleet in the interval from 272.16 K to 274.16 K (Fig. 3.5). Each precipitation is then discriminated energetically regarding its percentage fraction.
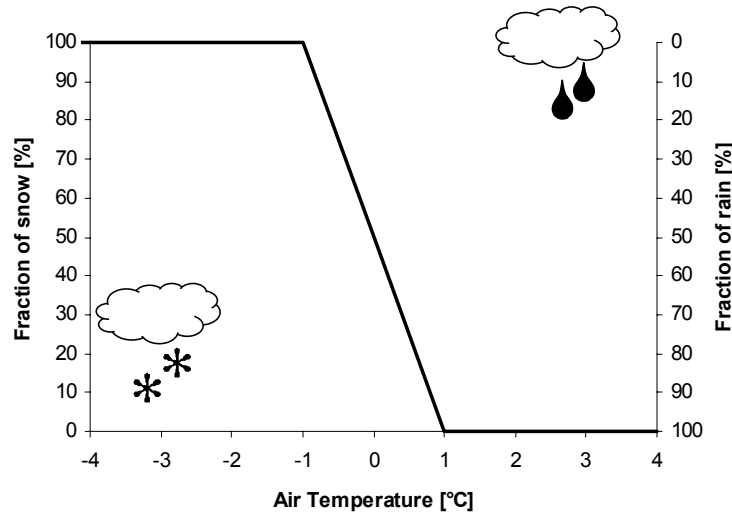
Fig. 3.5: Distinction of precipitation in rain-, snowfall and sleet

The total amount of energy is the sum of all energy fluxes:

(Eq. 3.23) $Q = Q_s - Q_{rs} - Q_{lwe} + Q_{lw} + Q_{sh} + Q_g + Q_{liquid} + Q_{solid} + Q_i$

with:

Q_{rs} = reflected short-wave radiation

Q_{lwe} = long wave emission

Q_{lw} = long wave reflected radiation

Q_{sh} = sensible heat flux

Q_g = ground heat

Q_{liquid} = liquid precipitation energy input

Q_{solid} = solid precipitation energy input

Q_i = internal energy of the snow pack calculated in the previous time step

For each time step the total available energy Q is compared with the internal energy of the snow pack at 273.16 °K. Therefore melting only occurs in the model if the snowpack is isothermal at or above 273.16 °K (GRAY and PROWSE 1993):

(Eq. 3.24) $Q \geq 273.16 \cdot c_{ice} \cdot Z$

with:

    Z = snow water equivalent of the snowpack

    c_{ice} = specific heat of ice

otherwise $Q_i = Q$

and $Z = Z + P$

with P as the precipitation.

If the total available amount of energy is sufficient for melting snow, melt M is calculated as

(Eq. 3.25) $M = [Q - (273.16 \cdot c_{ice} \cdot Z)] / c_f$

with c_f as the heat of fusion of water.

The new mass is

(Eq. 3.26) $Z = Z - M$

and the new energy

(Eq. 3.27) $Q_i = Q - (273.16 \cdot c_{ice} + c_f) \cdot M$

ESCIMO was developed originally for an application in the Weser catchment. Verification and validation were carried out by STRASSER (1998), showing good results. The successful transfer of the model approach to the Ammer catchment will be shown in Chapter 6.2.1.

3.2.2 The enhanced TOPMODEL

In this study an extended version of the original TOPMODEL, developed by LUDWIG (2000) is linked to the raster GIS-structure of PROMET. It utilises spatially distributed information on evapotranspiration, soil moisture and snowmelt calculated by PROMET. The PROMET derived soil moisture pattern and quantities are used to initialise the soil storage for the TOPMODEL application. Evapotranspiration and snowmelt are applied for its balancing.

As the original TOPMODEL, introduced by BEVEN and KIRKBY (1979) the enhanced TOPMODEL is also a conceptual modular model with a more sophisticated physical background. The basic idea is thereby the dynamic time and space calculation of surface and subsurface areas, contributing to the channel runoff. This approach is called the concept of variable source areas (BEVEN et al. 1994). The number of parameters that have to be calibrated should be minimised, but they still have to be physically interpretable.

The model version contains three soil storages:

- a soil root zone (SRZ)

- an unsaturated zone (SUZ) and

- a saturated zone,

which govern the distribution of water in the soil and therefore the partition of runoff in a surface and a subsurface component.

Nevertheless many assumptions have to be made to model stream runoff with the TOPMODEL approach. The three basic ones (BEVEN et al. 1995, FRANCHINI et al. 1996) can be summarised as:

- the dynamics of the saturated zone are approximated by successive steady states

- the hydraulic gradient of the saturated zone is approximated by the local surface slope

- the distribution of hydraulic conductivity K with depth z is an exponential function of storage deficit S, with m being the recession parameter, written as

(Eq. 3.28) $K(z) = K_S e^{-S/m}$

with:

K_s =   saturated hydraulic conductivity

Many assertions are based on the adoption of hydrologically similar units, in which model calculations are performed for classes believed to have hydrological similarity through belonging to a specific class of the topographic index. In contrast, in the enhanced TOPMODEL the local water-balance is computed for each pixel in the catchment. It is assumed that the consideration of distributed soil and land use information as well as spatial rainfall and evapotranspiration patterns (OBLED et al. 1994) is indispensable for the understanding of the physical processes involved in runoff formation and hence for accurate hydrological modelling.

One of the major extensions of the enhanced TOPMODEL is the introduction of the evapotranspiration-soil-topographic-index α_{ET} developed by LUDWIG (2000).

The available spatial distribution of evapotranspiration has been implemented into the theory of the topographic index in order to account for the presently underrated importance of land cover and its hydrological activity in TOPMODEL. Using PROMET, the actual evapotranspiration for each pixel in the Ammer watershed is calculated on an hourly basis over the hydrological year. The monthly mean of daily evapotranspiration is evaluated and divided

by the annual mean of daily evapotranspiration for each month in order to achieve a spatially distributed "seasonal evapotranspiration regime" for each pixel.

The resulting coefficients (ET_{coeff}) are used to create an evapotranspiration-soil-topographic-index, considering seasonal deviations in runoff partition over the year. Thus, knowing the upslope area A and slope β for each pixel from the digital terrain analysis, and using the evapotranspiration coefficient and the saturated hydraulic conductivity K_s, taken from the digital soil map, an evapotranspiration-soil-topographic index α_{ET} for each element in the catchment can be calculated. This development consequently leads to a more dynamic description of runoff formation, allowing not only for temporal changes in the location of the variable source-areas contributing to surface runoff, but also creating an overall change in the separation of runoff components. The formerly used static distribution of index-values is replaced by a dynamic course of index distributions representing the annual course of saturation excess runoff potential in the catchment. Taking into account the mean value of α_{ET}, the shape of the α_{ET} distribution is of great importance in predicting soil moisture patterns, thus longer high tails of its distribution imply a greater saturated area and hence a greater likelihood of saturation excess overland flow (BEVEN and WOOD 1983).

(Eq. 3.29)
$$\alpha_{ET} = \ln\left(\frac{A}{ET_{coeff} \cdot K_S \cdot \tan \beta} \right)$$

It must be emphasised that α_{ET} is not only a land use dependent coefficient, but can be interpreted as an integration over all influencing physiogeographic characteristics of any point in the catchment, because all specific local characteristics of each pixel are taken into account. Besides the radiation balance influencing factors (terrain height, slope and aspect) also the landuse characteristics linked with the soil properties are considered in this approach. The spatial distribution of the original soil topographic index values is so extended by the unique temporal and local characteristic of each pixel in the basin (LUDWIG 2000).

3.2.2.1 Runoff modelling

Flood runoff has often been considered to consist of surface runoff produced at the ground surface when rainfall intensity exceeds the infiltration capacity. However this process, known as Hortonian overland flow, is just one of several processes involved in storm runoff processes (MAIDMENT 1993). To calculate the accurate flood runoff, all of these processes have to be taken into account.

Runoff in general can be separated into a surface runoff and a subsurface runoff component. Surface runoff consists of runoff resulting from infiltration surplus or from saturation excess or from the combination of both. On the other hand the subsurface runoff is represented by the base flow and/or by the interflow, which is produced by water that infiltrates into the soil, percolates rapidly and then moves laterally in a temporally saturated zone (MAIDMENT 1993). However the interflow is not considered in the TOPMODEL concept. The computing of the other processes as illustrated in figure 3.6 is described further below.
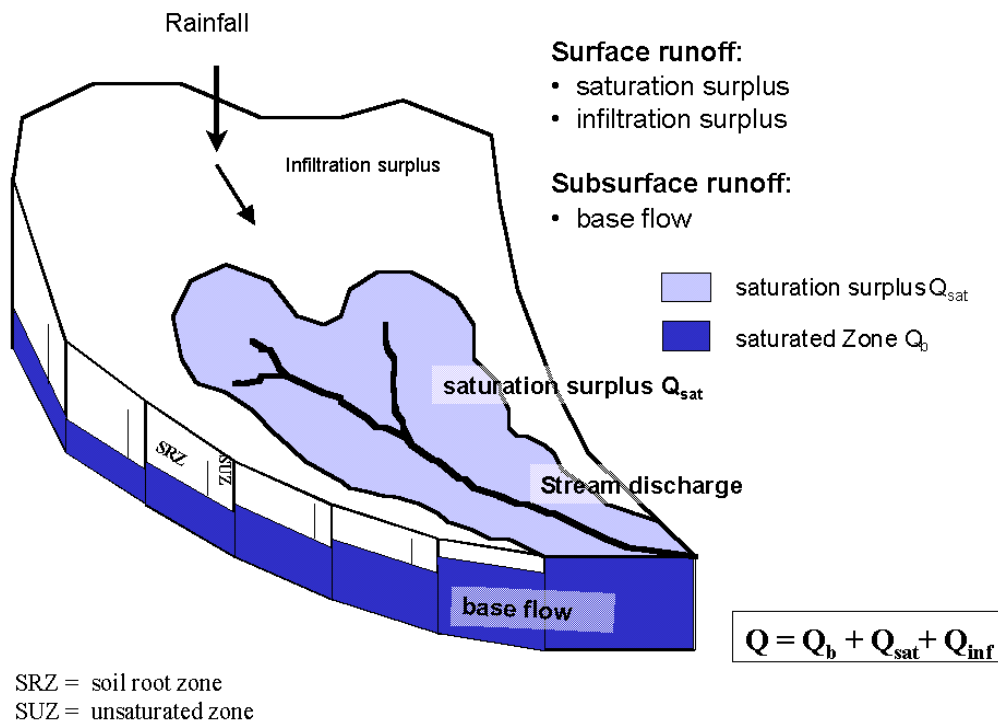
Fig. 3.6: Schematic illustration of the runoff formation (LUDWIG 2000)

Once runoff is produced it has to be routed to the catchment outlet. Overland flow and channel routing has to be conducted. Therefore it is necessary to derive the time of concentration and flow velocity as well as the temporal distribution of the runoff process. The concentration time is modelled in the present approach by applying a SCS Algorithm (SOIL CONSERVATION SERVICE 1985) while for the channel routing the constant wave velocity algorithm for quasi uniform flow conditions is used (BEVEN and WOOD 1993). A brief description of the related processes can be found further below.

Runoff processes operating in a watershed vary in time and location. Large variations in hydrologic characteristics, and therefore in runoff processes, also occur over small, apparently homogeneous areas to the extent that the variety of runoff processes discussed above may occur during a single storm event (PILGRIM et al. 1978).

Surface runoff

For the generation of surface runoff the enhanced TOPMODEL approach takes two different processes into account. On the one hand saturation excess is produced if the soil is saturated and any further precipitation is transferred directly into runoff (Q_{sat}). The chance of a pixel to be saturated is thereby highly influenced by the spatial and temporal distribution of the evapotranspiration-soil-topographic-index. The deviation of the local index value from the catchment mean determines the possibility of saturation since this is decisive for the local saturation deficit and so for the separation in surface and subsurface flow. In general it can be stated that during the summer months according to higher evapotranspiration rates the possibility is reduced while in winter more pixels tend to be saturated. The second possibility allows surface runoff to be generated from infiltration surplus (Q_{inf}). This process occurs if the precipitation intensity exceeds the infiltration capacity. The total surface runoff Q_{sur} can generally be calculated as:

(Eq. 3.30) $$Q_{sur} = Q_{sat} + Q_{inf}$$

Infiltration surplus

When modelling at a daily timestep the process of infiltration excess is a seldom found phenomena in the Ammer catchment (LUDWIG 2000). However, during extreme flood events when a much higher temporal resolution is required this process may occur since huge precipitation intensities can be reached and the infiltration rate varies largely with time (VIESSMAN et al. 1989).

In the enhanced TOPMODEL the process of infiltration excess has to be additionally computed since this component is transferred into direct runoff and is then drained with regard to the local slope. Many approaches deal with this problem. The complex representation of this process by the RICHARDS equation requires a huge amount of parameters, which makes it inapplicable for a spatially distributed model over larger domains. A more simple model, but still physically based is the infiltration model developed by GREEN and AMPT (1911). This approach is applied in the enhanced TOPMODEL.

The Green-Ampt model is an approximate model solution based on Darcy's law and the mass balance law. The original model was developed for ponded infiltration into a deep homogeneous soil with a uniform water content and an undefined depth. Water is assumed to infiltrate into the soil as piston flow resulting in a sharply defined wetting front which separates the wetted and unwetted zone. Neglecting the depth of the ponding surface, the Green-Ampt rate can be written as:

(Eq. 3.31)
$$f = K \left[1 + \left((\Phi - \theta_i) \cdot \frac{S_f}{F} \right) \right]$$

with f being the infiltration rate, the porosity Φ, the effective soil suction S_f, the initial water content θ_i and the accumulated infiltration amount F.

The initial water content is provided by PROMET while the porosity and the hydraulic conductivity K is made available by the GIS data set. The effective soil suction for several soil textures is taken from literature (e.g. MAIDMENT 1993).

Saturation surplus and baseflow

Saturated overland flow occurs when the surface horizon of the soil becomes saturated as a result of either the building-up of a saturated zone above a soil horizon or the rise of a shallow water table to the surface. While this usually occurs in valley bottoms or naturally wet region, e.g. moors, in some regions saturated areas first occur on ridges where the surface soil horizon is thin (MAIDMENT 1993).

This modelling of saturation surplus, as the second possibility of surface runoff generation, is performed by calculating the balance of different soil storages. Therefore water transport from the surface to the saturated zone is realised by introducing different soil storages that are linked to each others (Fig. 3.7). The three soil storages are a soil root zone, an unsaturated zone and a saturated zone. In contrast to the original version the interception/infiltration storage is replaced by a soil root storage. The unsaturated zone storage deficit is calculated by a non-linear approach, while the other two are computed linearly.
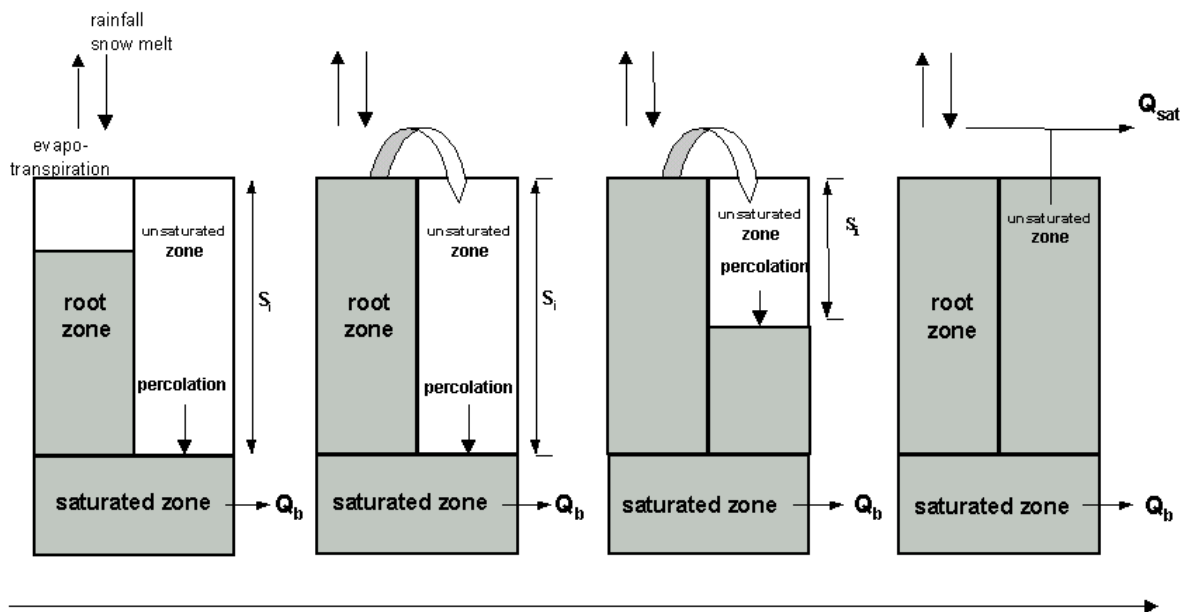
Fig. 3.7: Saturation runoff generation (LUDWIG 2000)

For each pixel in the catchment and timestep t the water availability in the soil root zone can be calculated by balancing the water content at t-1, the system input (rain, snowmelt) and the output (evapotranspiration) from the SRZ. Since the evapotranspiration is already balanced by PROMET, the parameter SRMAX from the original version, formerly used as the parameter for maximum storage in the upper soil layer to control the calculation of actual evapotranspiration (BRUNEAU et al. 1995, BEVEN et al. 1995) can be neglected.

Once the soil specific field capacity is reached, water is transferred from the SRZ to the unsaturated zone, where the local storage deficit S_i can then be computed as a function of the mean storage deficit in the catchment S_m and the deviation of the local α_{ET} to its areal mean γ, scaled by the recession parameter m.

(Eq. 3.32)

$$S_i = S_m - m\left(\ln \frac{A}{ET_{coeff} \cdot K_S \cdot \tan \beta_i} - \gamma \right)$$

The individual master recession curves for each gauging station and thus the specific recession parameter m were derived by LUDWIG (2000) through an analysis of numerous baseflow recession curves. Therefore several spring and autumn events of 1992 were analysed to exclude snowmelt impact and minimise evapotranspiration influence. By applying a 1/Q transformation, a linear regression can be carried out. The inverse rise of this regression defines the event specific recession parameter m for the considered gauging station. By averaging several individual event derived parameters a catchment specific value can be found.

The recharge rate q_v into the saturated zone (BEVEN and WOOD 1983) is calculated as

(Eq. 3.33)

$$q_v = \frac{S_{UZ}}{S_i \cdot t_d}$$

where S_{UZ} is the storage capacity of the unsaturated zone and t_d is a soil specific time delay parameter. The baseflow volume Q_b of each subwatershed at each timestep results as a function of integrated storage deficit S_m (OBLED et al. 1994, BEVEN et al. 1995), initial baseflow Q_0, and the recession parameter m over the basin and can therefore be written as:

(Eq. 3.34)

$$Q_b = Q_0 \cdot e^{-S_m / m}$$

Once the local storage deficit has reached a value of zero, the soil is saturated to the top and saturation excess can occur.

Runoff concentration

The generated surface runoff (direct runoff) has to be transformed into a hydrograph at a potential catchment outlet. However, overland flow and stream discharge has to be explicitly modelled to interpret the catchment specific flood flow behaviour.

Time of concentration

As the first step the time of concentration of surface runoff for each catchment has to be determined. Saturated areas nearest to the basin outlet contribute runoff immediately to the catchment mouth. Runoff generated at upstream points arrive at later times until surface flow eventually has been transported from all saturated points of the watershed, concentrating at the outlet. Because time of concentration is conceptually the time required for 100% of the watershed to contribute, it is often defined as the time from the end of rainfall to the inflection point on the hydrograph recession (VIESSMAN et al. 1989).

For the calculation of the time of concentration no separate consideration of saturation and infiltration surplus has to be made.

Several approaches for computing the time of concentration are reported in literature, like e.g. SNYDER (1938). Most of them take into account topographic and runoff delaying parameters. In the enhanced TOPMODEL the time of concentration T_c, and hence the overland flow velocity as its derivative, is calculated by employing the SCS-method (SOIL CONSERVATION SERVICE 1983) as applied in the rainfall runoff model TR20. This method has been selected since all necessary parameters are already provided from the GIS (overland retention from land-cover-soil complex S [inch]) and the digital terrain analysis (hydraulic length λ [feet] and mean catchment slope γ [%]). However special attendance has to be drawn to the application of American units used in the formula that is written as:

(Eq. 3.35) $$T_c = \frac{1,67 \cdot \lambda^{0.8} \cdot (S - 1)}{1900 \cdot \sqrt{\gamma}}$$

The parameter *overland retention from land-cover-soil complex* is a TR20 specific parameter, which is represented by the Curve Number (CN). It describes the runoff potential of a region and is derived by a combination of soil type and landuse. Values are taken from literature

(e.g. MAIDMENT 1993) and are assigned to the model GIS. When the catchment areal mean of CN is calculated, the parameters can be interpreted as an approximation of surface roughness (HAAN et al. 1994).

Overland flow algorithm

Through the derivation of the time of concentration, the period of temporal runoff translation is defined. However the temporal distribution in separate time increments is still not defined. Therefore an overland flow algorithm has to be applied. In the enhanced TOPMODEL the application of time-area functions, derived individually for each subwatershed from digital terrain analysis is therefore realised. This approach has been widely used in hydrologic applications and was original developed by CLARK (1945), recognising that discharge at any point in time is a function of translation and the storage characteristics of the catchment. The translation is obtained by estimating the overland and channel travel time of runoff, which is then combined with an estimate of the delay caused by the storage effects of a watershed.

The translation of rainfall excess from its point of impact to the watershed outlet is accomplished using the individual time-area curve for each subcatchment, which described a histogram of incremental runoff versus time, constructed as shown in figure 3.8. The indicated isochrones are lines of equal runoff travel time. The major isochrones represent each model time step, defining the amount of water available for runoff and contributing to the basin outlet for the considered time increment (VIESSMAN et al. 1989). The method however assumes that there is no temporary storage of water on the surface in the drainage area and that in the whole (sub)catchment surface runoff is produced all over. The applied approach is just a rough approximate of reality but nevertheless it has been successfully applied in several studies, like e.g. SCHULLA (1997).
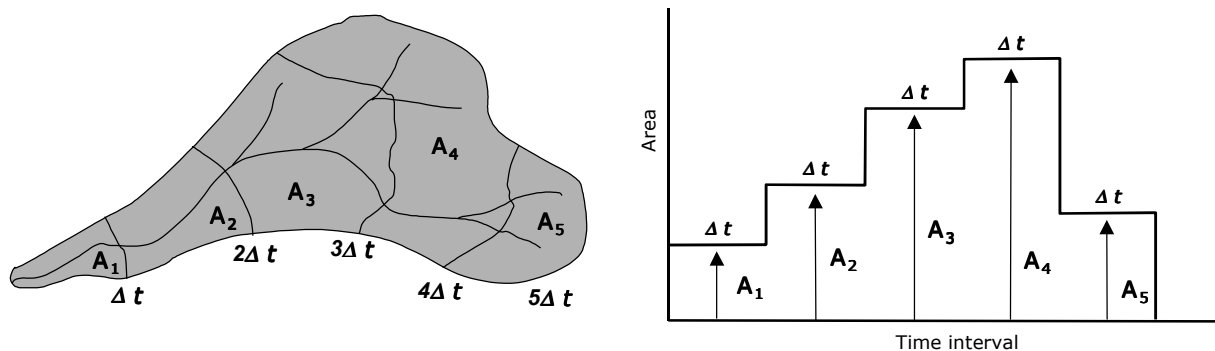
Fig. 3.8: Development of time-area histogram: isochrones spaced time steps apart (left) and resulting time-area histogram (VIESSMAN et al. 1989)

Channel routing

The surface runoff water collected in the river channels has to be transported to the watershed outlet assuming a specific flow velocity. Several approaches have been developed for this purpose. For quasi uniform flow conditions the flow velocity in the channel may be described by one of the equations that take the bed slope roughness and the hydraulic radius into account (BEVEN and WOOD 1993). Well known equations are the Darcy-Weisbach or the Manning-Strickler equation which is used in the model and can be written as:

(Eq. 3.36)
$$v = \frac{R^{2/3} \cdot J^{1/2}}{n}$$

where v is the calculated flow velocity resulting from the hydraulic radius R and the bed slope J and n as the Manning's roughness coefficient. The hydraulic radius is defined as the flow cross-sectional area divided by the wetted perimeter.

Of particular interest is the Manning's roughness coefficient that parameterises the flow friction. The value can be determined from field measurements at various cross sections and flow discharges, but it can also be estimated for gravel river beds applying the equation of JARRETT (1984):

(Eq. 3.37)
$$n = 0.32 \, J^{0.38} \, R^{-0.16}$$

Values of n can be found in literature for several river bed types, like e.g. BARNES (1967). The values for the hydraulic radius and the roughness coefficient used in this study are taken from LUDWIG (2000). Based on several field measurements at selected cross sections, these values are then individually assigned according to the order of STRAHLER (1957). The values are assumed as constant for all model timesteps. This is also an approximation of actual conditions since the roughness varies with the magnitude of flow. As flow increases and more portions of the bank and the overbank become inundated, the roughness can increase as well as decrease (MAIDMANET 1993). However a more detailed description of the process would significantly increase the required number of parameters. This would make this approach quite more difficult to handle in terms of a real time flood forecasting model. Easy applicability and regionalisation for watersheds would no longer be possible.

A detailed description of the enhanced TOPMODEL can be found in LUDWIG (2000).

3.2.3 Data requirements

The data sets required to drive PROMET-D are stored in GIS raster respectively in tables that are assigned to a specific GIS layer. It consists of terrain, landuse, soil and meteorological information. All GIS-layers are projected to an UTM-grid with an upper left corner co-ordinate of 5313.720 N / 639.150 E (zone 32) and a 100 meter resolution. A summary of the statistical physiogeographic catchment characteristics is given in table 3.1.

EXPOSITION [°]		Percentage [%]	SLOPE [%]	Percentage [%]	ALTITUDE [m a.s.l.]	Percentage [%]
315 – 360	N	14.99	0 - 20	73.81	500 - 750	55.68
0 – 45	N	14.94	21 - 40	11.67	750 - 1000	21.53
45 – 90	E	10.09	41 - 60	8.35	1000 - 1250	10.51
90 – 135	E	3.63	61 - 80	4.48	1250 - 1500	7.23
135 – 180	S	11.46	81 -100	1.40	1500 -1750	3.88
180 – 225	S	15.03	> 100	0.29	1750 -2000	1.13
225 – 270	W	9.48	mean [%]	14.8	2000-2250	0.04
270 – 315	W	20.37	max [%]	174.0	mean [m a.s.l.]	841.3
					min [m a.s.l.]	533.0
LANDUSE		Percentage [%]	SOIL TYPES	Percentage [%]	max [m a.s.l.]	2129.0
Water		1.6	loamy sand (LS)	4.36		
Coniferous forest		25.8	sandy loam (SL)	0.04		
Deciduous forest		13.6	loam (L)	39.67		
Birch wood		2.24	clay (C)	2.61		
Moor		3.83	moor (M)	25.56		
Peat		0.29	rock (R)	26.11		
Settlement		2.43	Water	1.66		
Rape seed		0.0				
Corn		0.9				
Crop		1.2				
Barley		0.8				
Meadow		44.49				
Rock		2.75				

Tab. 3.1: Catchment characteristics of the Ammer basin (percentage of catchment area)

3.2.3.1 Digital terrain model

The digital elevation model, also used to derive terrain slope and aspect (Fig. 3.9) was provided by the German military geodetic survey. It is derived from digitised topographic maps. The original resolution of 30 m was resampled to a resolution of 100 m. Slope and aspect are calculated from the elevation data using the image processing software FAP (Flächen Analyse Programme) (MAUSER and BACH 1993).
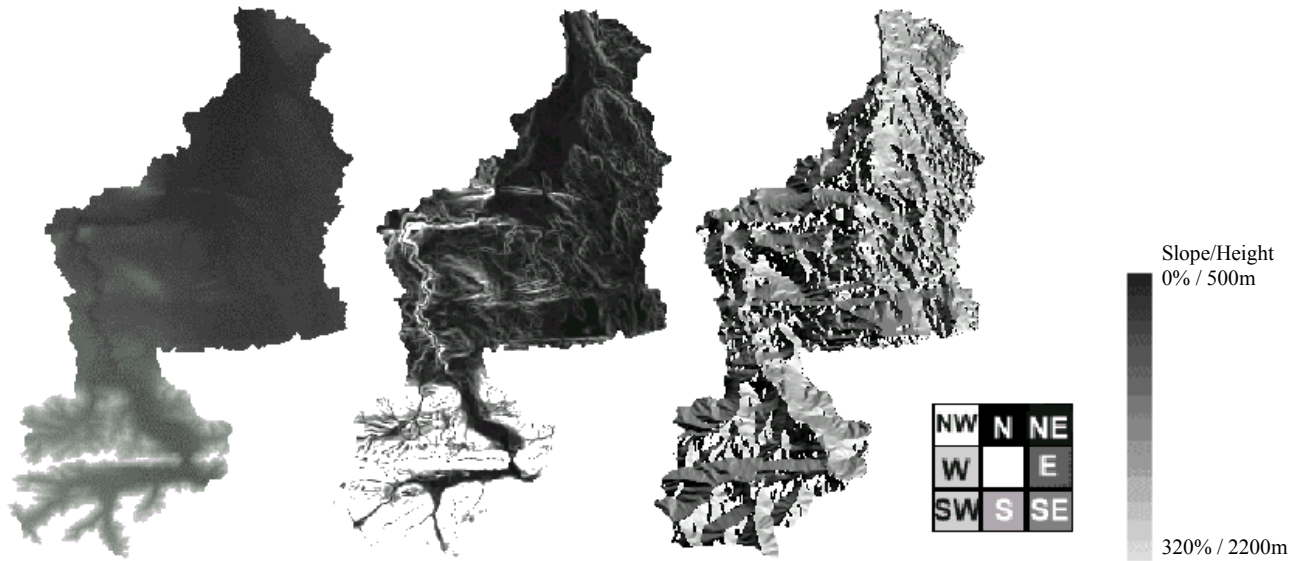
Fig. 3.9: Digital Terrain Model of the Ammer watershed (height, slope, aspect, from left to right)

The catchment boundaries as well as the subwatersheds referring to each stream gauge are calculated from the terrain height layer applying the digital terrain analysis program TOPAZ (TOpographic PArameteriZation) (Fig. 3.10) (GARBRECHT and MARTZ 1993).
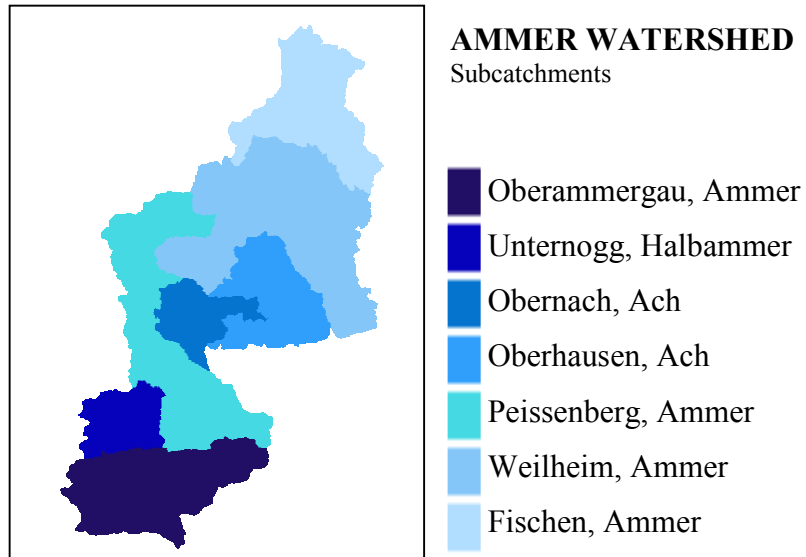
Fig. 3.10: The Ammer watershed and the subcatchments referring to the stream gauges calculated by TOPAZ

3.2.3.2 Landuse

Spatial information about landuse was derived from remote sensing data using the result of a fuzzy logic classification of LANDSAT-TM imagery dating from May 28th 1992 (STOLZ 1998).

This approach takes into account additional spatial information in the form of fuzzy factors. These fuzzy factors can comprise various GIS information layers such as e.g. terrain height, slope, soil characteristics or climatic elements. The idea of this approach is that the possibility for a specific land cover type varies with the fuzzy factors. Each fuzzy factor determines a spatially distributed possibility for a certain land use, like e.g. that maize can only be cultivated up to a certain terrain height (resulting from climatic reasons). Thus, these possibilities, combined with the spectral Maximum Likelihood results can improve the classification result, that sometimes misclassify due to uncertain spectral information. ENPOC (ENvironmental POssibility Classifier) was introduced by STOLZ (1998), where a detailed description can be found.

A common problem of optical remote sensing is cloud coverage. Especially in mountainous areas this is an often found phenomenon. The used LANDSAT scene is also partly cloud covered in the southern part of the watershed, where the classification result is largely dominated by the fuzzy factors as shown in figure 3.11.
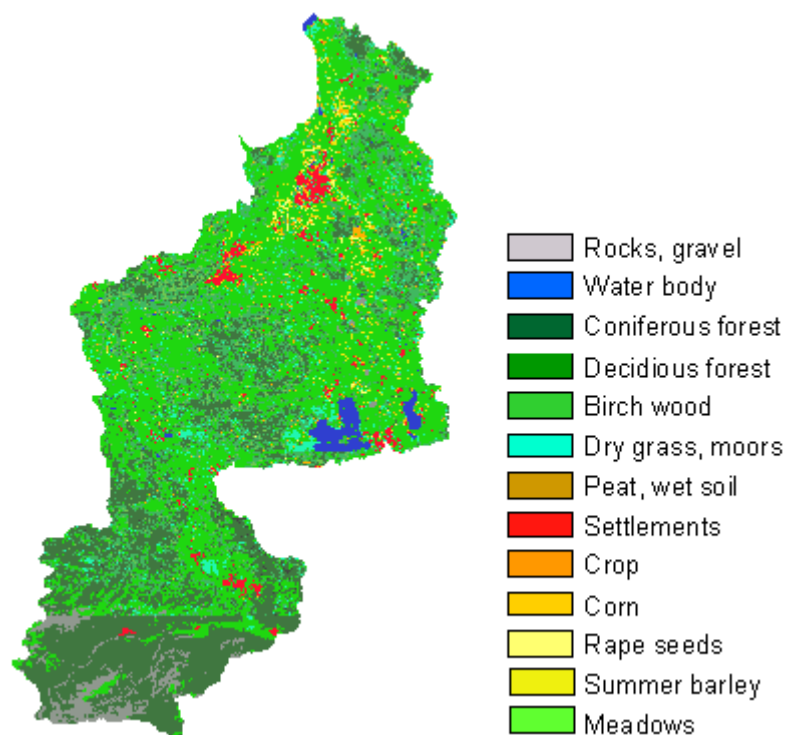
Fig. 3.11: Fuzzy logic LANDSAT-TM classification 28.5.1992 (STOLZ 1989)

3.2.3.3 Soil

Information about the distribution of soil parameters in the Ammer watershed (Fig. 3.12) was derived from the Bavarian Bodengütekarte (soil quality map) 1:100000. The digitised soil classes are:

– clay

– loam

– sandy loam

– loamy sand

– moor

– mountainous soil
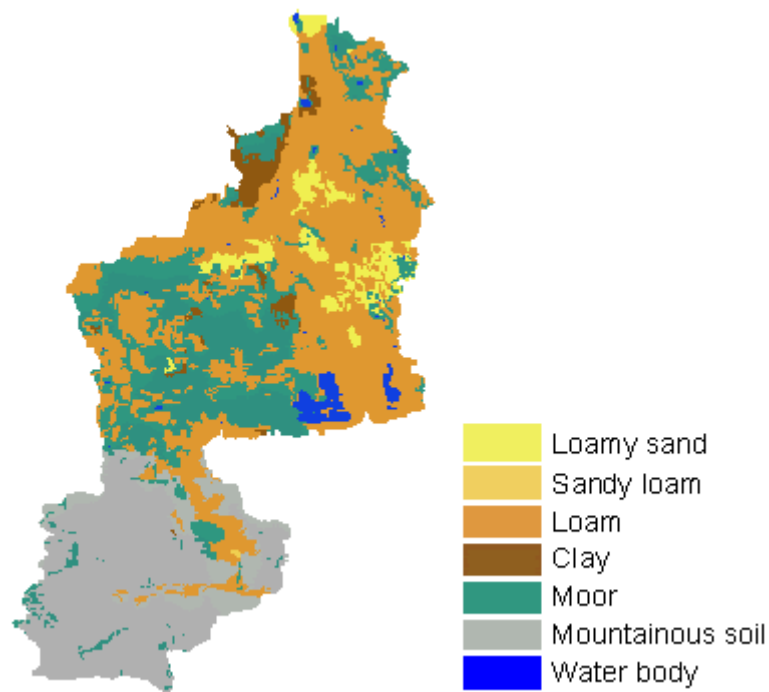
Fig. 3.12: Soil classes derived from the Bavarian Bodengütekarte (soil quality map) 1:100000 (BUDYNCUK 1996)

Soil parameters are taken from literature (RAWLS et al. 1993) and are accordingly assigned to the soil classes. The values are shown in table 3.2.

	Pore Size Distribution Index	Porosity	Bubbling Pressure Head [cm]	Saturated hydraulic conductivity [m/sec]
Clay	0.165	0.475	37.30	0.00000017
Loam	0.252	0.463	11.15	0.00000367
Sandy loam	0.378	0.453	14.66	0.00000606
Loamy sand	0.553	0.437	8.69	0.000017
Silty clay loam	0.177	0.471	32.56	0.00000056

Tab. 3.2: Physical soil parameters (RAWLS et al. 1993)

Because of lacking parameter information for the soil class „moor", the parameters for sandy loam are assigned. Organic soils contain substantial amounts of organic matter with a minimum amount of 30%, while in general clay, silt and sand share in the same portion (BELL 1983). In addition the organic material is a highly porous media (DYCK and PESCHKE 1995). Therefore it is assumed that the hydrological behaviour of moors can be sufficiently described by the sandy loam parameter set. For mountainous soil (in the Ammer watershed mostly soil type rendzina), the physical parameters are considered to equal silty clay loam. Rendzina is a shallow soil over calcareous material and is characterised by fine textured loam of residual origin especially in karst regions (SCOTT 2000).

3.2.3.4 Meteorology

In its standard mode PROMET is driven by spatially and temporally interpolated climatic station measurements of the DWD.

The DWD climatic station measurements are recorded three times a day (7:30, 14:30, 21:30 Central European Time (UTC +01)) and publicly available. In order to generate the meteorological input parameter fields for spatially distributed hourly modelling, these measurements have to be temporally and spatially interpolated. This is performed within the spatial modeller of PROMET.

The measured precipitation data are corrected individually to account for the typical recording losses due to the influence of wind turbulence, evapotranspiration and moistening, employing a temperature and wind speed dependent method (SCHULLA 1997). The temporal interpolation is performed using a spline function. Since precipitation is not continuous, a special algorithm is applied to interpolate the measured rain for the timestep between the last two measurements.

The algorithm for the spatial interpolation takes into account the terrain elevation-dependency of meteorological parameters. For each time step a regression function with terrain elevation is calculated for all measurements, resulting in a specific trend level over the basin. The station residuals are determined and interpolated using inverse cubic weighting of the station distance. The result of this interpolation layer is then added to the regression trend level, guaranteeing a reproduction of the originally measured value at each station. A detailed description is given in chapter 5.1.1.

PROMET requires spatially distributed hourly information of precipitation, air temperature, wind speed, humidity and radiation. An example of the interpolated meteorological fields is given in figure 3.13.

increasing	increasing	increasing	increasing	increasing
Precipitation	Temperature	Wind Speed	Humidity	Direct Radiation
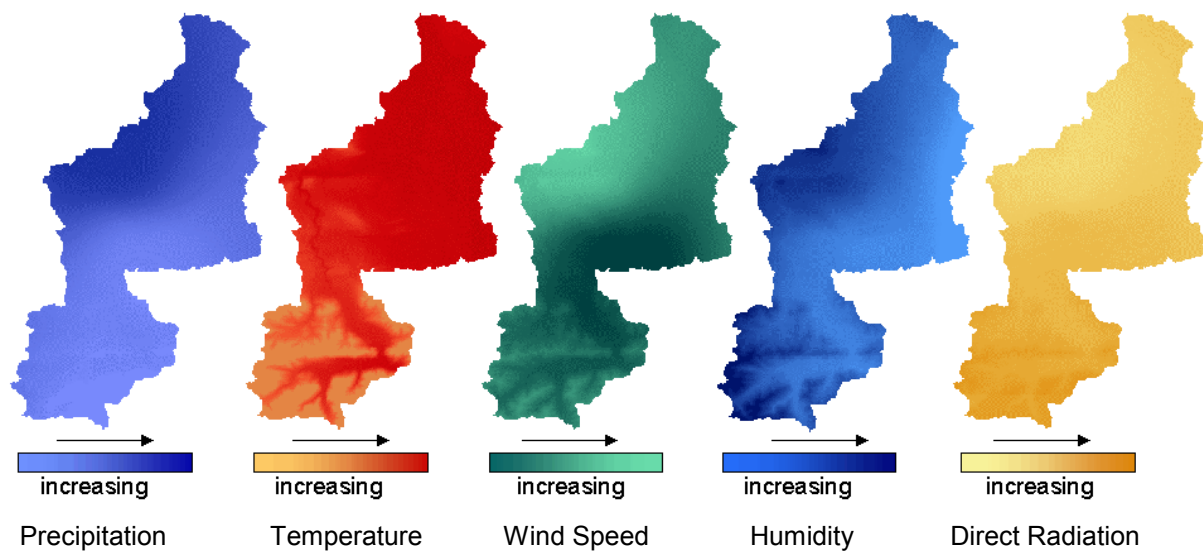
Fig. 3.13: Spatial distributed meteorological information as provided for PROMET (Example from 20.5.1999; 11:00 UTC except the rainfall field that dates from 21.5.99; 8:00 UTC)

*3.2.3.5 Digital terrain analys*is

Additional to the standard GIS data set that PROMET requires (see Fig. 3.2), several topographic parameters have to be added to the GIS data base in order to run the enhanced TOPMODEL. Parameters like e.g. catchment segmentation, drainage network and channel length can be derived from the terrain height distribution applying methods of digital terrain analysis.

For the digital processing of the terrain model used in this study (as described in chapter 3.2.3.1) the model package TOPAZ was applied. TOPAZ is provided by the United Sates Department of Agriculture (USDA) and is developed and distributed by Dr. Garbrecht at the Granzinglands Research Laboratory (GARBRECHT and MARTZ 1993). The public domain

software is available via Internet (http://grl.ars.usda.gov/topaz/TOPAZ1.HTM) where a detailed description can be found. However for the use in PROMET the program has been slightly extended and modified to fit the requirements of the image processing program FAP developed by MAUSER and BACH (1993).

The DEM processing in TOPAZ is based on three fundamental concepts: the D8 method, the downslope flow routing concept, and the critical source area (CSA) concept.

The D8 method defines landscape properties for each individual raster cell by the evaluation of itself and its 8 immediately adjacent cells. The downslope flow routing scheme calculates the drainage and flow direction on the landscape surface as the steepest downslope path from the cell of interest to one of its 8 adjacent cells. The CSA approach computes the channels draining the landscape as those raster cells that have an upstream drainage area greater than a threshold drainage area, called the critical source area. A minimum drainage area below which a permanent channel is so defined by the CSA value. The CSA concept controls the watershed segmentation and all resulting spatial and topologic drainage network and subcatchment characteristics. Additionally the Minimum Source Channel Length (MSCL) is introduced to truncate unwanted short riverlets in order to prevent an over parameterization of the river network. The MSCL defines the minimal possible headwater stream length.

Within this general framework, the digital elevation data is processed in TOPAZ by a system of interdependent computational programs. The analytical operations performed by these programs achieve three broad functions: elevation data pre-processing, hydrographic segmentation and topographic parameterization:

- TOPAZ pre-processes the input DEM to rectify unwanted features like e.g. depressions and flat surfaces most of which are artefacts of the horizontal and vertical DEM resolution, DEM generation method or elevation noise. Corrections made during DEM pre-processing are strictly limited to cells of depressions and flat surfaces so as to minimise the impact on the overall information content of the elevation data.

- Hydrographic segmentation identifies the channel network, the upstream and lateral subcatchments contributing flow to each channel link in that network and corresponding drainage divides. Once the channel network has been fully defined, it is further processed to determine the Strahler order of each channel link and to assign an identification number to each network node and channel link. Also, subcatchment identification numbers based on network node and channel link identification numbers are assigned to provide the topological relationship between network nodes, channel links and subcatchments.

- The topographic parameterization involves measuring a variety of properties and parameters of the DEM raster and of the derived channel network, channel links and subcatchments. Spatial parameters, such as rectified elevations, landscape slope and aspect, drainage pattern, channel network and subcatchment boundaries, are stored in raster format while parameters that describe specific features of the landscape, such as the geometry of a channel link or subcatchment, are stored in tabular format.

The major output results from TOPAZ can be summarised as following:

- For each pixel information is given on uparea and channel length,
- for each riverlet on the routing sequence, degree of STRAHLER order, in- and outlet point, length and bed slope,
- and for each subcatchment on the position, area, hydraulic length and mean slope.

For the digital terrain analysis of the Ammer catchment the CSA res. the MSCL values are derived from LUDWIG (2000) where also a detailed description due to the application of TOPAZ in the Ammer catchment can be found.

The results of the TOPAZ analysis show good accordance with values published by the BAYERISCHES LANDESAMT FÜR WASSERWIRTSCHAFT (1978). The modelled river network was compared to one, digitised from the topographic map. Since only minor deviations can be found it is proved that the river network in the Ammer catchment, modelled by TOPAZ, is represented with a sufficient accuracy by the applied digital terrain model as described above.

3.3 Meteorological models

Different meteorological model outputs were available for the investigation of the synergetic use of hydrological and meteorological models for flood modelling. Besides four NWP models, weather radar data and METEOSAT derived precipitation were applied.

NWP models simulate the precipitation process. Since they calculate the atmospheric physics they are able to provide forecasts. Weather radar and METEOSAT derived precipitation are both hindcast methods. Since these methods do not perform direct measurements of precipitation several algorithms have to be applied to derive precipitation fields from the

remote sensing data. However they provide spatially distributed patterns of precipitation fields over large domains.

3.3.1 NWP models

NWP models are physical-mathematical models that calculate the temporal and spatial state of the atmosphere. Precipitation is, among other parameters like temperature, wind speed or air pressure computed for each time step and each pixel. The models are based on the physical laws of conservation of mass, energy and momentum. These are reflected in the equation of motion, the continuity equation and the thermodynamical equation.

Mathematically these models consist of several non-linear partial differential equations. After an initialisation using start and boundary conditions the temporal course of the meteorological parameters is approximated by prognostic and diagnostic coupled equations. NWP models compute meteorological fields and are able to provide forecasts up to four days in advance (WMO 1996).

Important characteristics of NWP models are:

- Number of vertical layers

- Spatial resolution

- Temporal integration algorithm

- Integration time step

- consideration of terrestrial features, like orography or land use.

Depending on their respective spatial resolution the models can be distinguished in global models, regional models or local models.

However even nowadays these models are limited mostly on the available computer capacity.

3.3.1.1 Applied models

Four different NWP models are employed in this study. Namely these are MC-2, BOLAM, Meso-NH and SWISS MODEL. All of them are new-generation mesoscale models that have been at least in part originally developed by the NWP groups of the RAPHAEL project. The models are to some extent complementary to each other, since they differ not only in terms of dynamical and numerical aspects (grid, resolution, approximations of basic equations etc.), but also in terms of parameterisation of the physical processes and their effects related to subgrid variability, regarding in particular those processes that are relevant for the formation and release of precipitation. All models contain a surface-atmosphere transfer scheme responsible for describing the evolution of the soil state and providing the latent and sensible

heat fluxes from the surface into the planetary boundary layer. Also all models include some explicit microphysical representation at different degrees of complexity and different parameterisation of moist convection. Both aspects are crucial in quantitative precipitation forecasting at high spatial resolution (BACCHI and RANZI 2000).

Moreover, the models are different also in terms of operational use. Two of them, MC2 and SWISS MODEL are in fact, at present, operational in different countries and hence have a multi-year record of everyday short-range forecasting. The other two (BOLAM and MESO-NH) are essentially research oriented models (BENOIT et al. 2000). An overview of the applied models is given in table 3.3.

NWP model	Spatial resolution (available for hydrological simulation)	Number of vertical layers	Boundary conditions derived from	Nestings at spatial resolutions of
MC2	10 km	15	analysis mode: ECMWF analysis forecast mode: Swiss Model	50 and 10km
Swiss Model	14 km	20	Europa-Modell of DWD analysis/ forecast	14 km
BOLAM	10 res. 3.5 km	30	ECMWF analysis/ forecast	35, 10 and 3.5 km
MESO-NH	10 res. 2 km	Not fixed (depends on application)	ECMWF analysis/ forecast	50, 10 and 2km

Tab. 3.3: Characteristics of applied NWP models

MC2

The MC2 model is a semi operational model that has been developed by the Atmospheric Environment Service (Environment Canada, Dorval). It is a non-hydrostatic compressible limited-area model which allows to simulate all scales ranging from turbulent large eddies to the synoptic scale (BENOIT et al. 1997). The numerical simulations carried out in the framework of RAPHAEL were performed by applying successive one way nesting at resolutions of 50 km and 10 km. MC2 has been extensively tested at very high resolution (with respect to operational mode) as a part of a flood forecasting model ensemble. Since 1993, MC2 is used in an ongoing study of orographic precipitation over the Canadian Rockies, involving spring-time floods due to rain and snow-melt. It has been used extensively with one-way coupling to the hydrologic model WATFLOOD (KOUWEN et al. 1996).

SWISS MODEL

The SWISS MODEL is the full operational model for short range weather prediction at the Swiss Meteorological Institute. It is a hydrostatic limited-area model with 145x145 grid

points horizontally and 20 vertical layers. It uses a rotated longitude/latitude grid with a resolution of 0.125 degrees (ca. 14 km). The five prognostic variables of the SWISS MODEL are surface pressure, total heat, total water content, and the two components of horizontal wind. All other output values are derived diagnostically from these variables at specified intervals (WMO 1996). For the RAPHAEL project, two sub-domains of the SWISS MODEL domain were defined, one for the Ticino-Toce area the other for the Ammer area. The output domain for the Ammer area contained 5 x 7 grid points and covered 70 km x 98 km = 6693 km^2.

BOLAM

The BOLAM model is a hydrostatic research model. It has been preliminarily tested in a series of simulation exercises in the limited area model intercomparison project known as COMPARE (GYAKUM et al. 1996). The results have been very encouraging in simulating an extra-tropical cyclone (COMPARE 1), a mesoscale lee vortex (COMPARE 2) and a typhoon (COMPARE 3). The latter case, in which the BOLAM model reproduced a realistic intensity of the tropical cyclone, especially at the 10 km resolution, is closely dependent on the simulation of the moist processes and of surface fluxes over the sea, and in this sense the results are relevant to the simulation of heavy precipitation. BOLAM has a complex microphysical representation, suitable for calculations up to resolutions of a few kilometres. BOLAM also includes a simplified scheme based on a 3-layer soil model, capable of predicting surface fluxes, boundary layer fluxes, snow accumulation and melting (CARDINALI et al. 1998).

Meso-NH

The Meso-NH model is a research model that has been recently developed by Laboratoire d'Aérologie (Toulouse) in co-operation with Météo-France. It is a non-hydrostatic limited-area model which allows to simulate all scales ranging from turbulent large eddies to the synoptic scale. The cloud model of Meso-NH includes very sophisticated microphysics suitable to describe explicitly cumulus-scale conversion processes (ASENCIO et al. 1994). The numerical simulations carried out in the framework of RAPHAEL were performed by applying successive one way nesting at resolutions of 50 km, 10 km and 2km. Initial conditions and boundary conditions of the coarser domain were provided by ECMWF analysis (or forecasts) available every 6 hours. The boundary conditions of the 10 km res. 2

km simulations were obtained from the 50 km res.10 km Meso-NH simulations interpolated in time every 3 hours res. 1 hour.

3.3.1.2 Model strategy

When using NWP models, it is crucial to clarify two important aspects:

- Sequence of meshwidths (nesting) adopted to refine the solutions to the final resolution;

- Type (forecast or analysis) and time sampling of the boundary conditions.

To obtain the NWP model output at the desired resolution it might be necessary to nest the model. Model nesting involves placing a model with a smaller domain and higher spatial resolutions within the bigger domain of a model with a coarser spatial resolutions in order to zoom in the coarse mesh simulation results (BENOIT et al. 1997). In this study a successive one way nesting was applied for all models, i.e. information will go from the coarse mesh model to the fine-mesh model only. The coarse-grid model provides initial and boundary data to the fine-grid model. (BENOIT et al. 2000). The nesting strategy however depends on the respective NWP model (see. Tab. 3.3).

As an example figure 3.14 shows the computational domains of MC2 used for the nesting procedure to refine the spatial resolution to 10km.
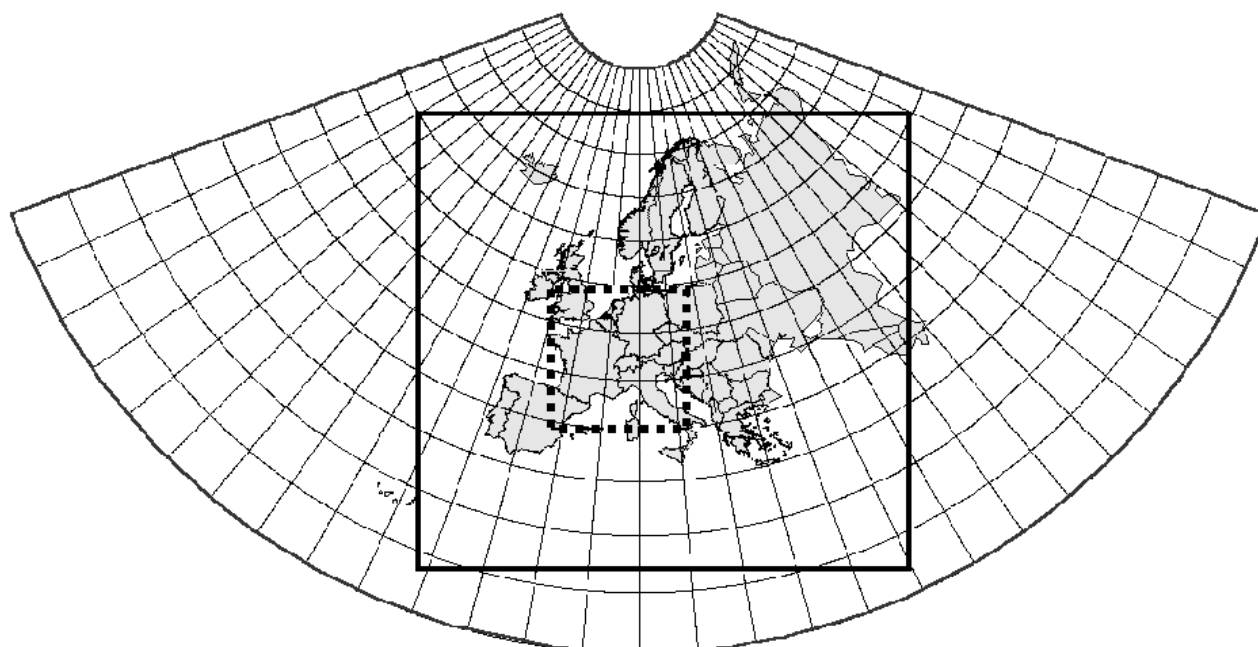
Fig. 3.14: Computational domains of MC2: the Polar-stereographic projection represents the ECMWF analysis domain, the black line the MC2 50 km grid mesh domain and the dotted line the MC2 10 km grid mesh domain (based on BENOIT et al. 2000)

NWP simulations can be computed in two modes: the forecast and the analysis mode.

The two types differ in the application of the driving lateral boundary values, which are provided by the ECMWF, the Europa-Modell (EM) or the Swiss Model (referring to the applied NWP model, see. Tab.3.3) running in the corresponding forecast or analysis mode. However the initial conditions are in both cases taken from the analysis mode of the ECMWF or the EM at initial time. Figure 3.15 shows an example for the Swiss Model.

In the forecast mode (Fig. 3.15a) the boundary conditions are provided hourly by the operational EM forecast which is itself initialised only once by the EM analysis. In the analysis mode of the Swiss Model (Fig. 3.15b), the boundary conditions for the simulation are provided in six-hourly intervals by the newly initialised EM analysis (BENOIT et al. 2000).
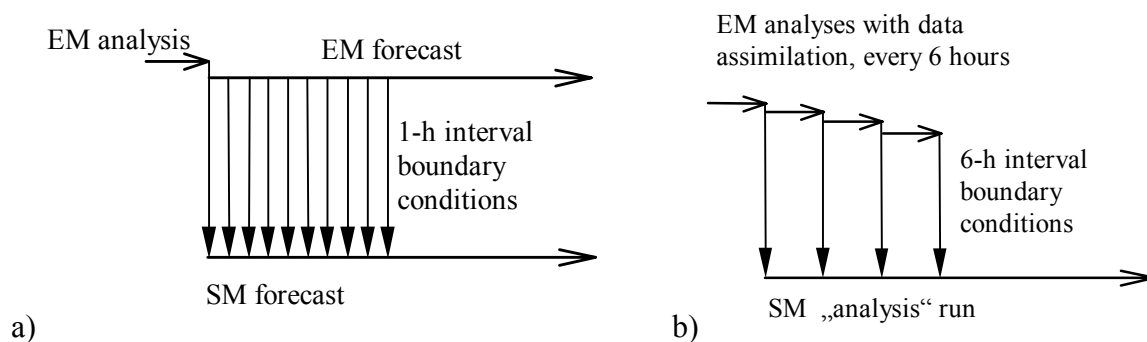
Fig. 3.15: a) Swiss Model forecast driven by hourly EM forecast. b) Swiss Model analysis mode driven by 6-hourly EM analyses (BENOIT et al. 2000)

3.3.2. Remote sensing methods of precipitation derivation

In recent years several operational algorithms of precipitation derivation from remote sensing sources – namely weather radars and satellites - have been developed. The disadvantage of this method is that there is no direct measurement of rainfall. However, these sources provide spatially distributed precipitation fields in almost real time.

Satellite algorithms are mainly passive methods of precipitation derivation, based on cloud temperature measurements and their relation to rainfall intensities. Weather radar on the other hand is based on the measured reflectivity of the emitted radar signal and is therefore an active method.

3.3.2.1 Weather radar

The use of weather radar is a common method to derive precipitation fields in real time. The area covered by a weather radar is a circle of some tens kilometres around the radar location.

By combining different weather radars, called radar composites also a larger area can be observed and a sort of weather forecast can be carried out.

Weather radar in the Ammer catchment

The Ammer catchment is well covered by three weather radars: the DLR polarimetric Doppler-radar POLDIRAD at Oberpfaffenhofen, the DWD Doppler-radar at Hohenpeissenberg and the DWD non-Doppler radar at Fürholzen. Figure 3.16 shows the location of the three radars around the Ammer catchment.
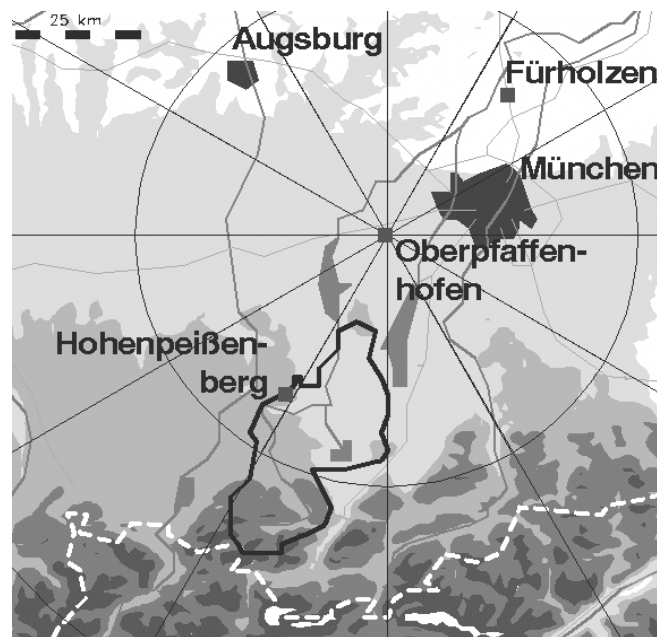
Fig. 3.16: Map of the Ammer catchment and the location of the weather radar at Hohenpeissenberg, Oberpfaffenhofen and Fürholzen (HAGEN and MEISCHNER 2000)

However POLDIRAD and the DWD radar data at Hohenpeissenberg are in operation only for selected time periods and therefore the data availability is limited. None of these periods include the selected flood events discussed in this study.

The DWD non Doppler-radar at Fürholzen is located north of Munich about 50 km north-north-east from the northern shore of the Ammer catchment. A large number of products is available from this DWD radar, but most of them are not archived. However for the 1999 Whitsun flood precipitation data are available from this radar at Fürholzen.

Data processing

As described in chapter 1.4.1, weather radar data consist of several error sources and have therefore to be further processed. Data processing was carried out by the German Aerospace Centre (DLR), also partner in the RAPHAEL project.

Two major products were available from the radar Fürholzen: the PL-product as the standard surveillance product and the DH-product, a special product for rain-rate estimation.

An inspection of the PL-product showed, that those data are not suited for the anticipated use within the RAPHAEL project. First, the coarse reflectivity steps do not allow an exact estimation of the rain rate from individual data sets. For example, one level (37 - 46 dBZ) represents rain rates between 8.1 and 34 mm/h. Second, radar beams from the Fürholzen radar are partially blocked by a nearby hill. In consequence the measured reflectivity is too low above the Ammer catchment. A correction is not possible due to the data processing of the complete volume scan. This is completely different for the DH-product. The DH-product is a special product for rain-rate estimation. Low level scans are performed every 5 minutes with high resolution. The retrieved rain rates are then integrated to hourly rain sums. The data are recorded in 0.1 mm steps at a spatial resolution of 1 x 1 km. The high resolution of this data allows a more exact estimation of the rain rate. Since the data for the DH-product result from a single elevation scan, beam blockage by nearby obstacles can be corrected more easily. A detailed description of the data correction carried out by the DLR can be found at HAGEN and MEISCHNER (2000).

As the final product of the weather radar data processing, spatially distributed precipitation at a temporal resolution of one hour was available for a raster of 1 km ground resolution. The overall temporal coverage of the Whitsun flood is 96 hours.

3.3.2.2 METEOSAT

For the derivation of precipitation fields also satellite data can be utilised. Like shown in chapter 1.4.1, literature reports several approaches for the determination of spatially distributed precipitation fields from geostationary satellite (e.g. BARRETT 1970, ARKIN 1979, ADLER and NEGRI 1988). Two of them, developed for the application in the mid-latitudes, are presented in this study and are used to compute the 1999 Whitsun flood event.

Combined METEOSAT - Station Measurement technique (MSM)

A technique developed by MAUSER and BACH (1994) was used to combine METEOSAT imagery with stationary measurements of DWD rain gauges. This algorithm is based on following assumptions:

- There is a linkage between precipitation intensity and cloud surface temperature. This coherence depends on the specific cloud physics at the respective location and time and is

considered as being linear. In general it can be assumed that lower cloud surface temperature is linked to higher precipitation intensity probabilities.

- A distinct cloud surface temperature can be identified leading to the demarcation of precipitation and non precipitation areas. This critical temperature (T_C) has to be determined for each METEOSAT imagery.

- A rainfall efficiency (RE) can then be calculated for all rain gauge locations and all time steps through the ratio of measured precipitation intensity at the rain gauge and the difference of cloud surface temperature (T_{CS}) and the critical temperature derived from METEOSAT (Eq. 3.38)

$$RE = P / (T_{CS} - T_C) \quad \text{for } T_{CS} > T_C$$

- The spatially interpolated rainfall efficiency is multiplied with the difference of cloud surface temperature and the critical temperature derived from METEOSAT to derive rainfall intensities. This method ensures that station measurements are reproduced.

The first step of METEOSAT image processing is radiometric calibration. The grey values of the METEOSAT raw data are transformed into temperature. This procedure is carried out for the infrared band. The geometric processing projects the image to a UTM grid. In the following, the contrast is calculated applying an algorithm introduced by WU et al. (1985). Contrast information provides information on the local variations of temperatures. It can be used for the distinction of different cloud types. In general, cumulus clouds show higher temperature contrasts then cirrus or alto stratus clouds. These three processing steps are part of the standard processing procedure at the PDUS receiving station implemented by the Chair of Geography and Geographical Remote Sensing, Department of Earth and Environmental Sciences, Section Geography at the University of Munich.

The critical temperature for the demarcation of precipitation and non precipitation areas is a very sensitive parameter and has to be determined with care. For the 1999 Whitsun Flood event a further simplification had to be introduced to cope with the lack of available station measurements. Based on the eight gauging stations the statistical sample is to small to calculate the critical temperature for each time step (Fig. 3.17). Therefore all measurements are summarised in one data set to determine one critical temperature, which is assumed to be constant during the whole event.
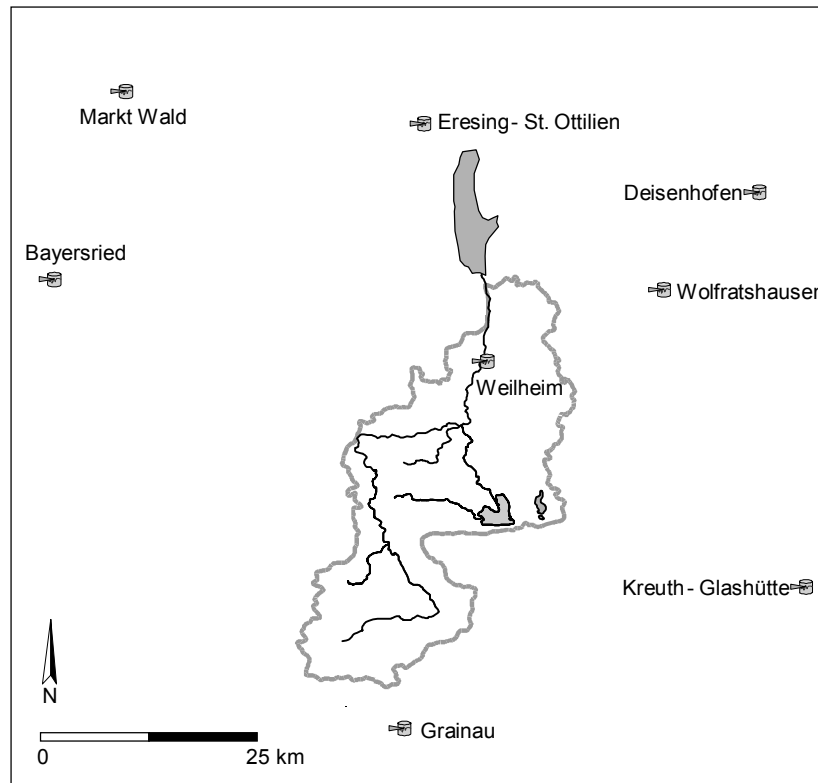
Fig. 3.17: Rain gauges available for the derivation of precipitation fields from METEOSAT (Cartography: V. Falck)

The rain gauge data are corrected using a wind- and temperature dependent algorithm (SCHULLA 1997). These data were correlated to the cloud surface temperature of the corresponding pixel of the infrared band illustrated in Fig. 3.18. The solid line in figure 3.18 indicates the maximum precipitation intensity referring to the respective cloud surface temperature. This maximum is calculated according to an approach developed by MAUSER and BACH (1995):

(Eq. 3.39)

$$F(x) = 55* e^{-0.2* P} + T_{offset} \qquad \text{with } P = \text{Precipitation intensity}$$
$$T_{offset} = \text{Offset temperature}$$

The offset temperature was chosen in a way that only 2% of the values are excluded of the integral underneath the maximum line, according to fact that 98% of the precipitation measurements are considered to be in a valid range (MAUSER and BACH 1994). The identified offset temperature for the 1999 Whitsun Flood METEOSAT data was therefore set to 225 K.

For the derivation of the critical temperature only precipitation intensity measurements exceeding 0.5 mm/h are taken into account(MAUSER and BACH 1994). Considering this the warmest cloud surface temperature in the valid range is found to be 263.5 K (blue arrow in Fig. 3.18) and taken as the critical temperature.
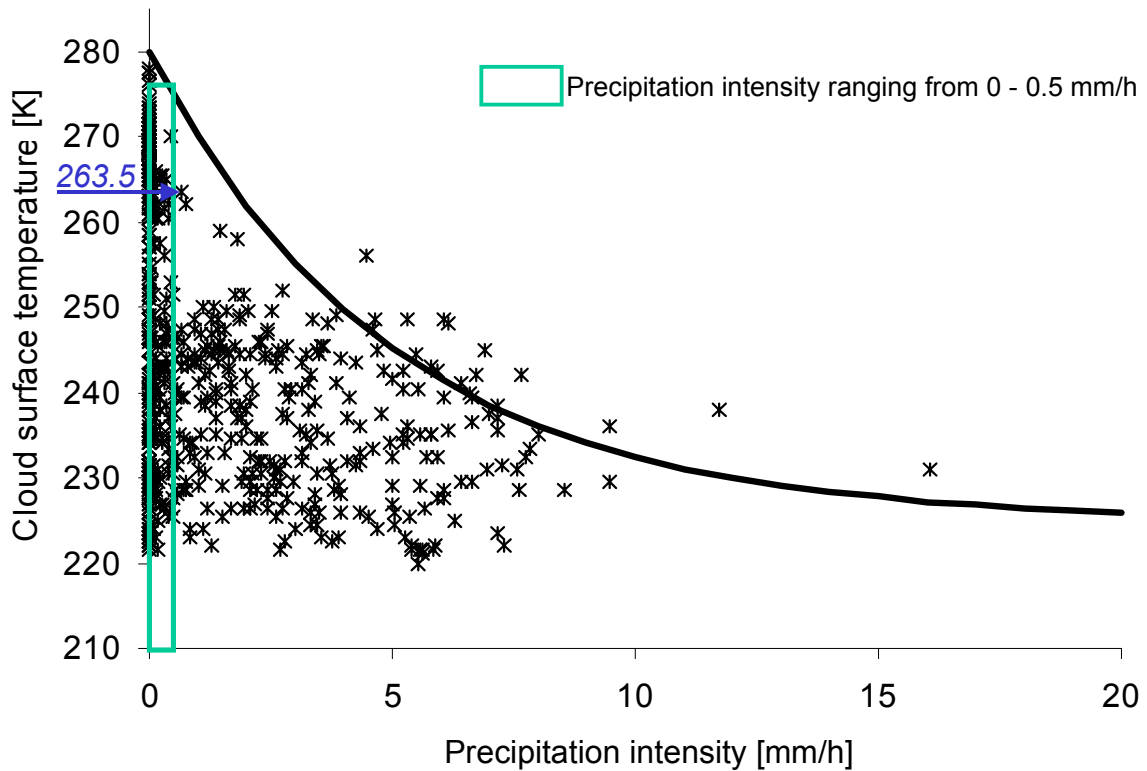
Fig. 3.18: Cloud surface temperature related to rain gauge measurements

After the determination of the critical temperature the rainfall efficiency can be calculated for all rain gauge locations and all time steps. The local rainfall efficiency values are interpolated applying an inverse distance algorithm with linear weighting. The critical temperature is subtracted from the cloud surface temperature of the METEOSAT IR channel. Negative values are set equal to zero. Precipitation is calculated for each hour by multiplying the temperature difference image with the respective rainfall efficiency field. This algorithm ensure that measured rainfall values are reproduced.

Enhanced CST technique (ECST)

The second approach of precipitation derivation from METEOSAT imagery used in this study is the Enhanced CST Technique (ECST) developed by BENDIX (1997).

The original CST method of ADLER and NEGRI (1988) for estimating convective and stratiform precipitation rates from infrared geostationary satellite data over the subtropics and

the tropics was improved with respect to regional adjustments to mid-latitude situations. One new feature is the use of the water vapour channel of METEOSAT to detect mid-latitude convective clouds. Numerical model data (1D cloud model and mesoscale model) are used for a better adjustment to the actual atmospheric situation.

The calculation of the precipitation fields for the Whitsun flood 1999 was carried out by the research group of Prof. Bendix at the University of Bonn res. University of Marburg and was made available for the hydrological computation in the frame of this study. A detailed description of the model and the adjustment to the Whitsun flood weather situation can be found in BENDIX et al. (2000).

4. Selected flood events

Two flood events, the 1999 Whitsun flood and the 1997 Christopherus flood, have been selected within the RAPHAEL project for being simulated in the Ammer catchment by meteorological models of different sources to be coupled with hydrological models. While the 1999 Whitsun flood is of an outstanding extent in the Ammer catchment, the Christopherus flood was less hazardous in Bavaria, though the referring weather situation led to the 1997 Oder flooding in East Germany and Poland. These two events represent very different storms, both in terms of quantities and origin and are therefore considered as suitable examples to interpret the effectiveness of the meteo-hydro model synergy.

4.1 The Whitsun flood 1999

One of the selected case studies investigates the 1999 Whitsun flood that occurred from 20.05. to the 23.05.1999. An unusually steady advective rainband across Southern Germany caused a 48-hour period of excessive rainfall north of the Alps, resulting in the highest rainfall intensity ever recorded. This and several other factors led to hazardous floods in Southern Bavaria causing extensive damage (Fig. 4.1 and Fig. 4.5). The recorded stages along the Ammer correspond to a bicentennial flood. An animation of this event is presented in the film meteosat.avi that illustrated the meteorological situation by METEOSAT images (see appendix E).

Fig. 4.1: Pictures from the upper course of the Ammer taken on the 22.05.1999 (Photos: W. Mauser)

Preceding the flood event outstanding high precipitation was recorded in February (Fig. 4.2), which led to high snow accumulation in the whole Alpine region. For instance the snow depth increased by 160 cm within seven days at the Zugspitze. The precipitation in March was average while in April above average rainfall was measured. This resulted in almost saturated soils during the whole winter that in addition to the high water equivalent stored as snow led to favourable initial conditions for flood occurrence (FUCHS et al. 1999).
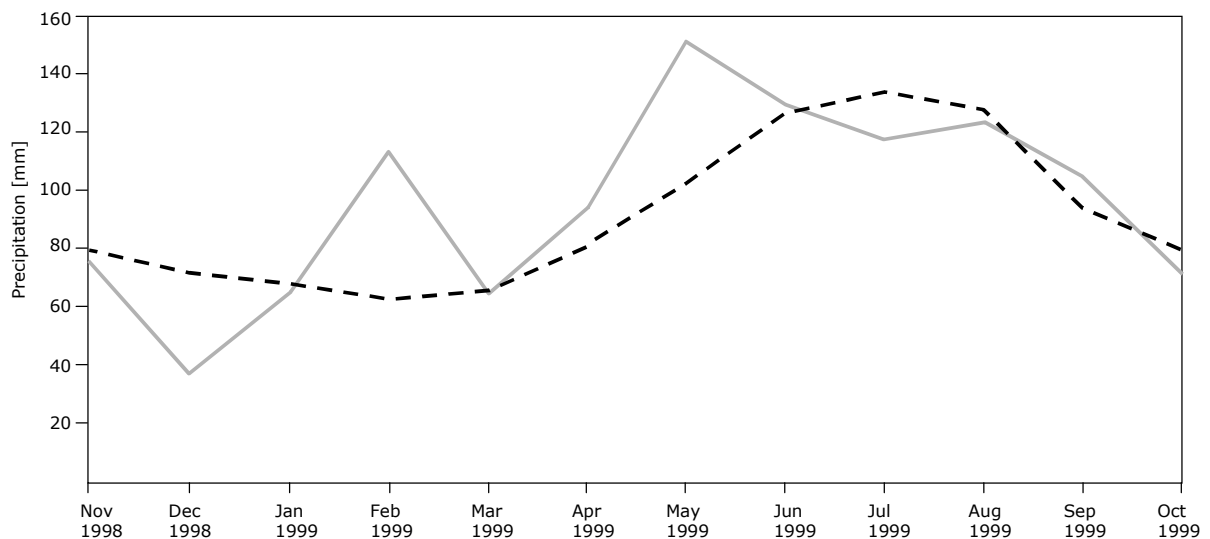
Fig. 4.2: Mean spatial precipitation in the Danube Catchment for the period from Nov. 1998 to Oct. 1999 (grey line) and the longterm mean spatial precipitation (1961 – 1990) for the corresponding months (dotted line) (FUCHS et al. 1999)

One week prior to the 1999 Whitsun flood several floods of smaller extent occurred in Southern Bavaria. These Pre-Whitsun floods are linked to extreme floods in Switzerland. The precipitation field was relative steady and resulted in a distinct rainfall maximum over northern Switzerland in the Region of St. Gallen. High temperatures led to snow ablation in the Swiss Alps up to altitudes of 2300 m asl. As a consequence of this weather situation snow melt and soil saturation also occurred in the Ammer catchment (Fig. 4.4).

Finally at the end of May, during Whitsun, the Danube catchment and several of its subcatchments experienced an extraordinary flood event caused by a typical Vb weather situation. A Vb weather situation occurs mostly in late spring and summer and is generally characterised by a north-south oriented frontal zone resulting from hot air masses over Russia and cold air masses over Western Europe. At the southern part of this frontal zone cyclones are generated moving northward. Over the Adriatic Sea these air masses moisture with water vapour and consequently lead to heavy precipitation in the east Alpine region (LILJEQUIST

and CEHAK 1994). In particular the meteorological situation of the Whitsun flood in the Ammer catchment can be described as a flow convergence of cool-moist air masses from the Atlantic and warm-moist air masses from the Balkan that in the blocking effect of the Alps caused two days of high precipitation (BENDIX et al. 2000).

The spatial distribution of precipitation in the Danube catchment shows a basin wide total rainfall coverage with a three day minimum of 50 mm and an distinct core with over 150 mm over the catchments of Lech, Loisach and Ammer (Fig. 4.3). The maximum was recorded at the Zugspitze with 207 mm. In Garmisch-Partenkirchen the highest rainfall ever measured was newly established with 135 mm. The mean monthly rainfall amount for May in Garmisch-Partenkirchen is 131 mm. The precipitation in the Ammer catchment was also outstanding. At the rain gauge Hohenpeissenberg 138 mm were recorded within 24 hours at the 21.5. 1999. The 72 hours rainfall amount of 186 mm at this site corresponds to a centennial event.
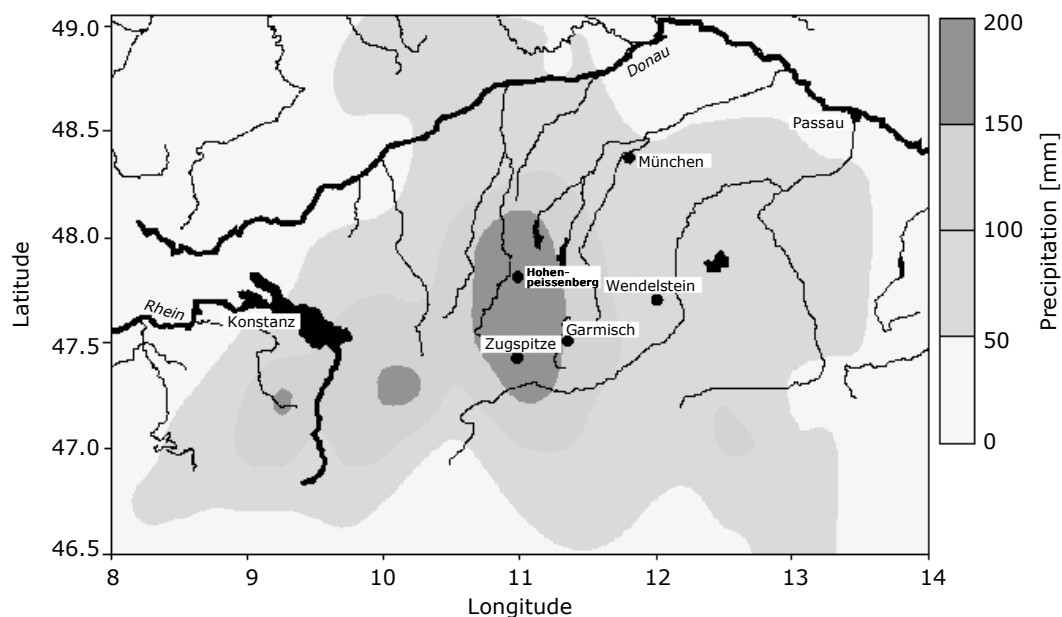
Fig. 4.3: Spatial distribution of interpolated measured precipitation from the 20.05. – 22.05.1999 (FUCHS et al. 1999)

The rainfall during the event enforced snow melt up to regions of altitudes around 1800 m asl. However the impact of this snowmelt can be seen as minor since most snow was already melted before Whitsun. In higher altitudes however precipitation was observed as snowfall. The snow depth at the Zugspitze increased from 470 cm to 610 cm (Fig. 4.4).
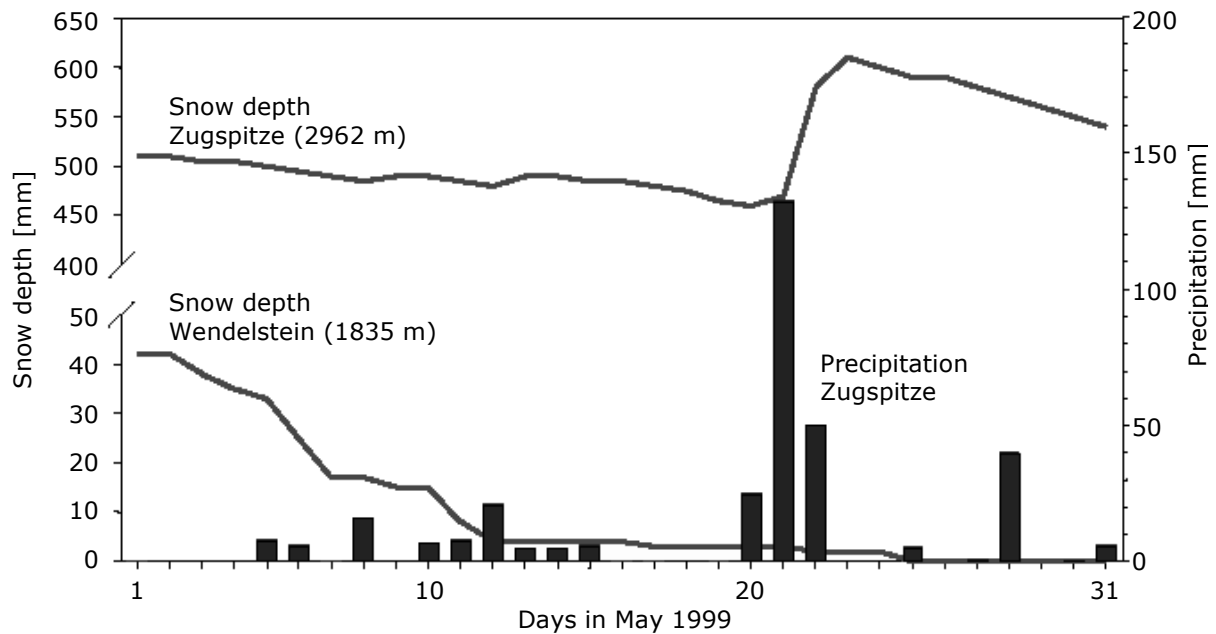
Fig. 4.4: Daily snow depth recorded at the Zugspitze and at the Wendelstein and daily precipitation sum measured at the Zugspitze in May 1999 (FUCHS et al. 1999)

On account of preceding precipitation and snowmelt, soils were rapidly saturated and so almost all precipitation and melt water was transformed to direct runoff, leading so to the Whitsun flood event in the Ammer basin.

The floods in May caused extensive damage. In the Ammer catchment, several levees broke particularly in the upper course. Also infrastructure facilities like bridges or riverside roads were damaged or destroyed. Most affected was the area around the villages of Peissenberg and Polling. However flooding of major settlements did not take place. The economic loss of the Swiss and Southern Bavaria floods in May was 710 million US$. Only 300 Mio. US$ was covered by insurance (MUNICH RE 1999).

Fig. 4.5: Pictures of damages caused by the Whitsun flood in the Ammer catchment

4.2 The Christopherus flood 1997

Less spectacular and of a much lower extent compared to the 1999 Whitsun flood is the Christopherus flood that occurred from 17.07. to 20.07.1997 prior to Christopherus day (Fig. 4.6). It is less well documented in the Alpine region, while in East Germany and Poland this weather situation caused the Oder flooding that was present in press coverage for several weeks.

Alike before the Whitsun flood, prior to the Christopherus flood a pre-flood event of almost the same extent occurred. This flood can be linked to the first flood period at the river Oder. In the first week of July 1997 a period of intense precipitation was observed. On the front side of a high altitude trough extending from Southern France to Poland an area of intense rise led to thunderstorms. Although the maximum was recorded in the Sudetenland and the Bescides, in the region of the towns of Brno, Wrocław and Katowice, also Lower and Upper Austria and the Bavarian Alps were affected by this precipitation field.

Therefore the soil water content was still high when two weeks later the second period of high rainfall took place. The maximum was again observed in the area of the Sudetenland and Southern Poland. A low from Italy moved north to Bohemia leading to a similar weather

situation like two weeks earlier (MALITZ and SCHMIDT 1998). The corresponding precipitation caused the second Oder flooding with hazardous levee breaks along the Oder. The Christopherus flood in the Ammer catchment can be assigned to this weather situation. The overall analysis of the precipitation in July 1997 show that 50% more rainfall was recorded in the southern Isar-Loisach area compared to its long annual mean (FUCHS and RAPP 1997).

However in contrast to the lower course of the Oder, in the Ammer catchment no major flood damage was recorded and no settlements were flooded.

(a)

(b)

Fig. 4.6: Pictures of the 1997 Christopherus Flood taken at the gauge in Oberammergau (a) and at the gauge Fischen (b) (Photos: R. Ludwig)

5. Assimilation of precipitation data

The available precipitation data sets need to be furtherly processed to meet input requirements of the hydrological model operated on a spatial resolution of 100 m. Two different types of data have to be considered: point measurements and meteorological model output data.

Point measurements have to be transformed to spatially distributed data within a 100 m grid of the hydrological model. Precipitation data computed by meteorological models are already spatially distributed. However rain radar data, NWP outputs as well as METEOSAT derived precipitation have all a much coarser horizontal resolution than the resolution of the hydrological model. The difficulties in scaling these meteorological data for hydrological application require a specific focus. Different scaling schemes are described in the following chapter.

5.1 Spatial distribution of measured precipitation data

The two different sources of measured precipitation available for the flood modelling within this study are:

- Measurements of the DWD climatic stations, taken three times a day, which enforce both, spatial and temporal interpolation and

- DWD rain gauge data which as continuous records have to be aggregated to hourly values before a spatial interpolation algorithm is carried out.

The locations of the climatic stations and the rain gauges are illustrated in figure 5.2.

5.1.1 DWD Climatic station measurements

Climatic station measurements, available at a 7-hour interval, are spatially and temporally interpolated by the spatial modeller of PROMET to meet the resolution of the hydrological model (as described in chapter 3.2.3.4).

However precipitation in particular can not easily be temporally disaggregated since it is a discrete phenomenon. Therefore PROMET distinguishes two different types of precipitation. Shower events are assumed when only an isolated rainfall event is observed, i.e. no precipitation was measured in the time interval preceding and following the measurement under consideration. In this case, a Gaussian distribution of the precipitation intensity is assumed for the considered interval. On the other hand there are so called long term events with a minimum of at least two consecutive recordings. Therefore the measured precipitation

sum is distributed into equal hourly intensities.

However due to specific errors in the measurements of precipitation the data first has to be corrected. This is carried out applying a temperature and wind-speed dependent algorithm (SCHULLA 1997).

After the derivation of hourly data, the spatial interpolation of processed station data is performed using a trend analysis with elevation, made available by the GIS (MAUSER 1989). A linear regression trend analysis with elevation is performed, creating two timestep-specific trend coefficients. The residuals are interpolated using a squared inverse distance function and are added to the formerly calculated trend level in order to reproduce the measured values. The inverse distance weighted method is based on the assumption that the interpolating surface should be influenced most by the nearby point and less by the more distant point. The interpolating surface is a weighted average of the scatter points. The weight assigned to each scatter point decreases as the distance from the interpolation point to the scatter point increases (FISHER et al. 1987). The method is schematically illustrated in figure 5.1.

For the computation of the meteorological fields 12 climatic stations, located at different altitudes, are available in and around the Ammer watershed (Fig. 5.2 and Tab. 5.1).
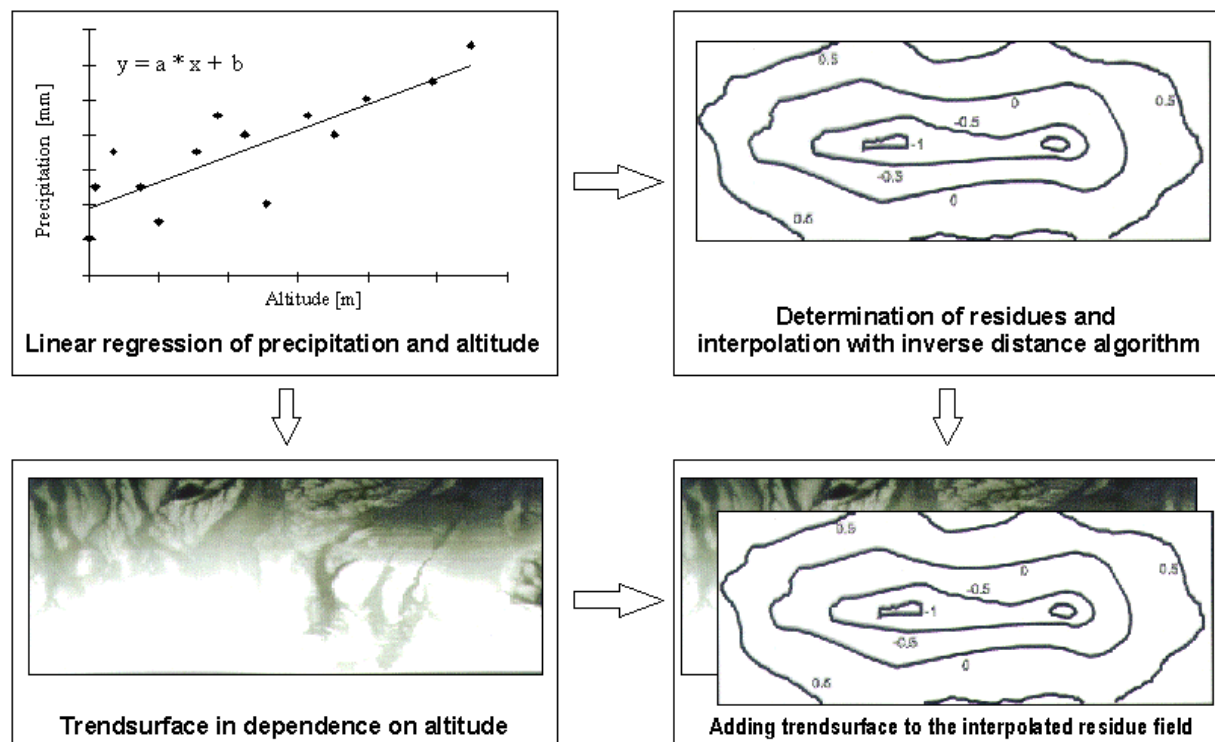
Fig. 5.1:Schematic illustration of the meteorological parameter interpolation carried out in the spatial modeller of PROMET (MAUSER 1999)
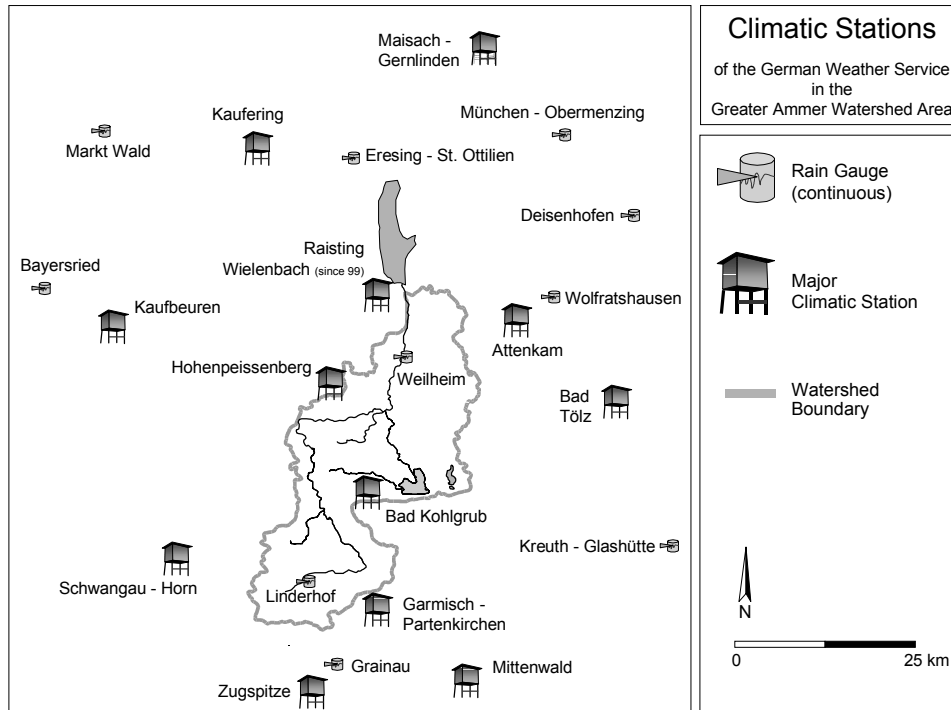
Fig. 5.2: Location of DWD climatic stations and DWD rain gauges within the greater Ammer catchment domain (Cartography: V. Falck)

Station name	UTM-E (32N)	UTM-N (32N)	Altitude [m asl.]
Attenkam	676871	5305493	655
Garmisch	658269	5261108	719
Hohenpeissenberg	650689	5296226	977
Kaufbeuren	619845	5302708	716
Kaufering	638597	5327945	585
Kohlgrub Bad	656401	5281312	734
Maisach	670575	5343033	509
Mittenwald	671107	5256559	920
Raisting	657485	5308402	553
Wielenbach	660745	5305674	541
Schwangau-Horn	628946	5287483	796
Toelz Bad	690551	5294921	640
Zugspitze	649853	5254018	2960
Bayersried	610112	5305450	710
Deisenhofen	692172	5323732	585
Grainau	652146	5259584	760
Kreuth-Glashütte	698937	5276563	895
Ettal-Linderhof	648548	5270613	940
Markt Wald	617704	5332731	633
München-Obermenzing	682199	5336980	522
Eresing (St. Ottilien)	652271	5328986	590
Weilheim	661166	5301311	568
Wolfratshausen	681597	5311262	570

Tab. 5.1: Location and altitude of the DWD climatic stations and DWD rain gauges (in italics)

5.1.2 DWD rain gauge measurements

For computing the 1999 Whitsun Flood also data from ten continuously recording gauges of the German Weather Service were collected. The location of the rain gauges is illustrated in figure 5.2, geographical information is given in table 5.1. The continuous records, available as analogue measurement sheets, were digitised and aggregated to hourly rainfall intensities. Also these data are corrected by using an algorithm introduced by SCHULLA (1997). The spatial interpolation is carried out the same way as for the DWD climatic station measurements and is described above.

5.2 Assimilation of modelled spatially distributed precipitation

The meteorological models and the hydrological model in the presented coupled forecasting scheme, do not operate on a common space mesh. In particular, due to the high computational costs of 3D mesoscale models, the NWP models have a much coarser resolution, of the order of some kilometres, than the hydrological model PROMET-D. The available data from the rain radar Fürholzen has a minimum spatial resolution of one kilometre while the METEOSAT resolution is five kilometres.

Because of the non-linearity of the runoff response to a precipitation forcing, the runoff production following a precipitation input uniformly distributed over the meteorological model's computational cell is expected to be different from that resulting from a non-homogeneous precipitation field, with the same rainfall volume, as it can be observed, for instance, by meteorological radars (RANZI 2000). The problem in linking the meteorological data of a coarse resolution with a hydrologic model running on a finer space mesh requires specific investigations.

5.2.1 NWP models

A comparison of precipitation output of the different NWP models in use for this study shows that over a large domain, like e.g. the eastern central part of the Alps, similarities in the spatial distribution and daily precipitation volume can be identified. In the presented example (figure 5.3, over 24 hours accumulated rainfall during the Christopherus Flood) two major precipitation cores can be identified in each NWP model result: one over central Switzerland and one over western Austria. Also relative high precipitation is shown by each model over southern Bavaria. The deviations in the NWP model results are caused on the one hand by the

unique model algorithm and on the other hand by the applied boundary conditions provided by either DWDs Europa Modell or the ECMWF (see also table 3.3)
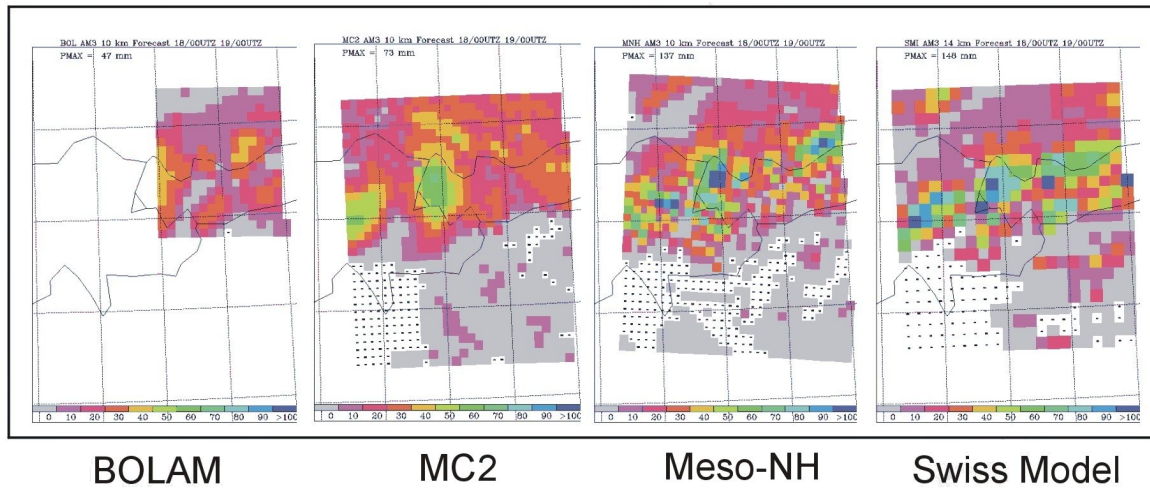
Fig. 5.3: Comparison of 24 hours accumulated NWP precipitation model output for the East-Central-Alps domain, referring to the Christopherus Flood

A study dealing with several of those simulations proved the principle capacity of the NWP models in use to accurately describe meteorological patterns for accumulated periods and long term investigations (RICHARD et al. 1998). For a daily time step and a mesoscale spatial domain the NWP model results can be directly applied for further processing steps, like e.g. model input for macroscale terrestrial models.

On a regional catchment scale like the Ammer watershed however this is no longer possible. Not only the differences in the NWP model results become drastically visible as shown in figure 5.4. Due to the coarse spatial resolution (10 res. 14 km pixel spacing), even minor deviations in NWP results are crucial for flood modelling. They largely affect the basin wide available effective rainfall, which consequently leads to major deviations in the flood simulation. Furthermore it becomes obvious that the NWP output data have to be processed to be applicable for hydrological simulations on a regional catchment scale. Investigations are therefore focused on the spatial disaggregation of NWP data to meet the scale requirements of the hydrological model.
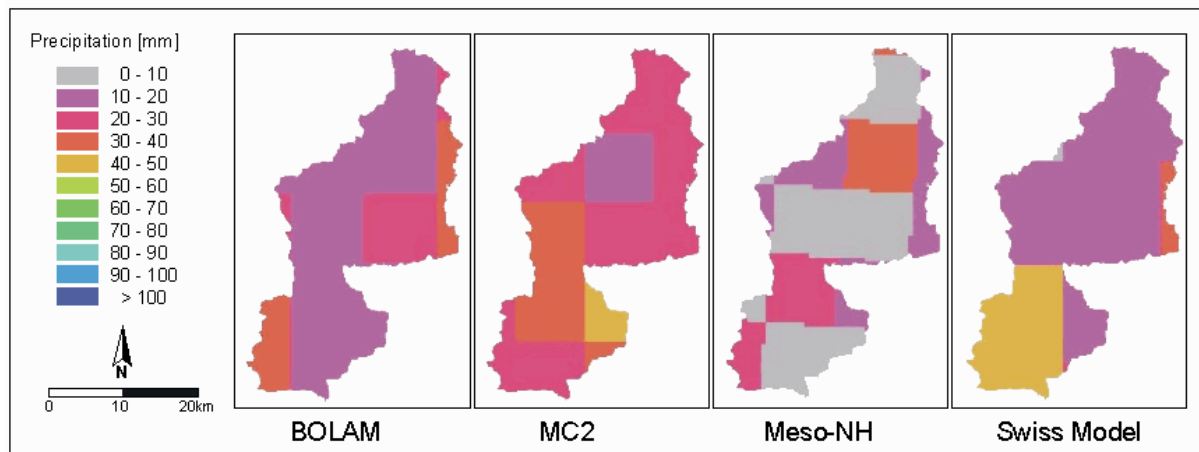
Fig. 5.4: Comparison of 24 hours accumulated NWP precipitation model output for the Ammer catchment, referring to the Christopherus Flood

In literature several studies can be found that reports methods to counteract this resolution mismatch. Two approaches for example, in use by the DWD are the Perfect Prog (PP, KLEIN et al. 1959) and the Model Output Statistic (MOS, GLAHN and LOWRY 1972). Both models are based on a statistical reprocessing of rainfall data made available by NWP models. By calculating a trend analysis surface from a historic database, the computed rainfall data can be distributed according to different terrain altitudes located within a NWP model cell. However both methods require a long term database of meteorological measured data, from which the trend analysis is calculated.

The DWD applied the MOS algorithm for a long time as a standard procedure for the distribution of modelled precipitation on a smaller scale (KUSCH et al. 1985). The MOS algorithm was also applied in a study carried out in the Leine catchment, in northern Germany. However encouraging results were obtained only in winter months while major deviations were observed during summer due to the convective character of rainfall (FRANKE 1987).

Another method dealing with this problem was introduced by RANZI (1994). It is a multiscale disaggregation scheme based on the use of an inverse wavelet transformation, with parameters derived from radar observations.

However all of these methods require quite a huge set of additional data and time intensive reanalysis. Since the major goal of this study is to test coupled real time flood forecasting none of these methods were therefore applied.

Several simple and time extensive disaggregation methods were tested to investigate the sensitivity of the hydrological model response to the applied scheme.

The NWP model outputs are in general spatially distributed raster grids of precipitation data. Each value of the grid represents the mean areal rainfall over an area of squared pixel spacing (WMO 1993).

For each modelled time step of 1 hour the data sets were downscaled to the required model grid of 100 m using the following different interpolation and disaggregation procedures:

- simple disaggregation, i.e. duplicating the data up to the required resolution

- bilinear interpolation between pixel centres

- a quadratic inverse distance algorithm.

A schematic overview of the three different disaggregation algorithms applied in this study is given in figure 5.5.
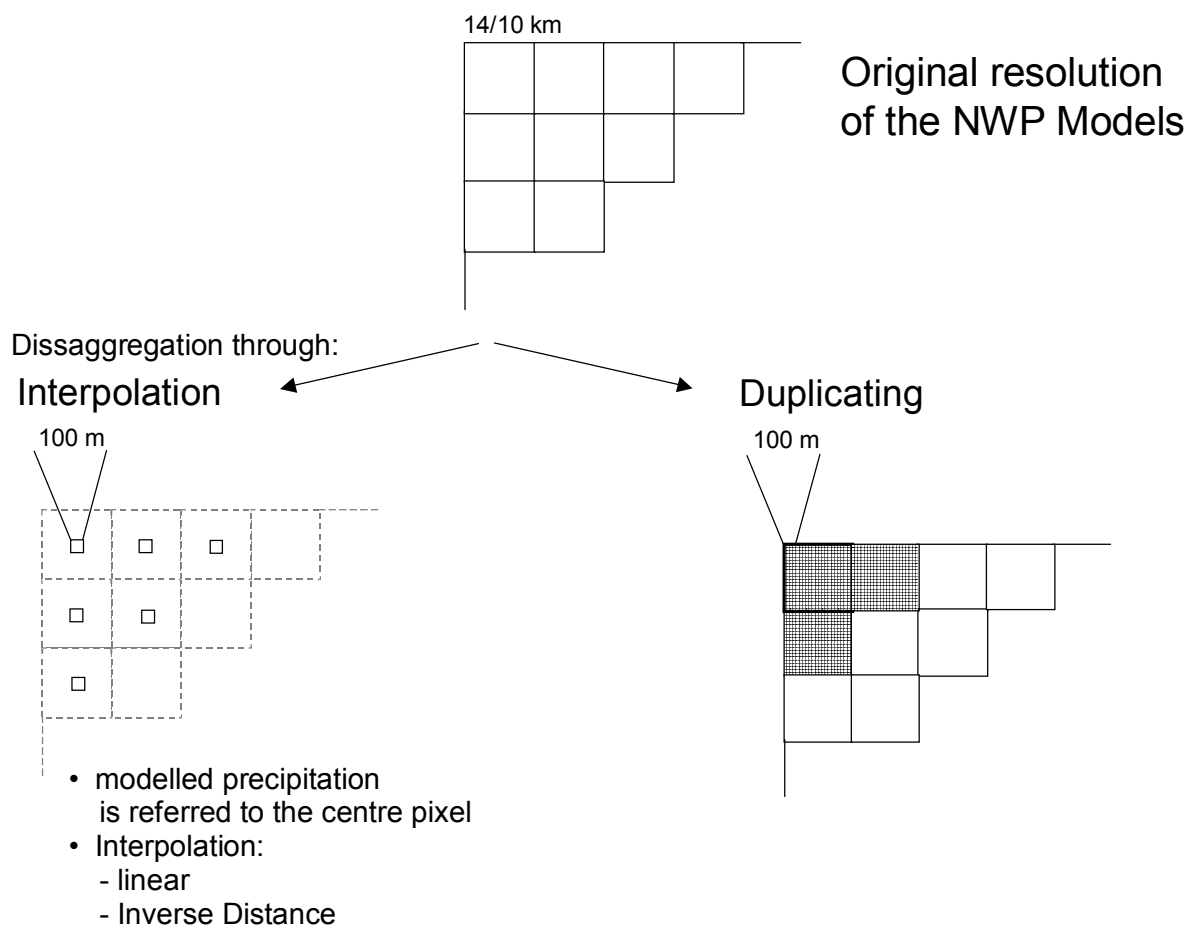
Fig. 5.5: Principles of the applied disaggregation algorithms used in this study

The simplest disaggregation method just duplicates the original cell into equal subcells. Each subcell is labelled with the value of the origin. For example, the 10 km resolution cell of BOLAM with the rainfall value x is subdivided into 10.000 cells containing the value x. The result, illustrated in figure 5.6 a, maintains the original information which being applicable to

the 100 m resolution of the hydrological model. Although precipitation is a continuous spatial phenomenon without quadratic boundaries, the procedure was proposed by the project's meteorologists as the one that least affects the calculated rainfall. Therefore it was defined as the standard disaggregation mode for the project (BACCHI and RANZI 2000).

Two other disaggregation algorithms were applied to estimate the influence of different assimilated precipitation data sets on runoff response, calculated by the hydrological model.

Both schemes are based on the assumption that the value of the NWP cell represents only the cell centre. More commonly noted, the hourly precipitation field is determined by a symmetrical distribution of rain gauges, located at the cell centre. From a meteorologist point of view this method is considered a valid downscaling procedure (KAUFMANN 1999).

Again, different interpolation algorithms are now applied to gain spatial coverage from the distributed point data. The simplest method is a bilinear interpolation between the value points. A more sophisticated method is the inverse distance algorithm that is also applied to the station measurements, as described above. Both methods were also used to scale the NWP model result to the hydrological model resolution. Examples for assimilated rainfall by these interpolation methods can be seen in figure 5.6 b and 5.6 c.

(a)   (b)   (c)
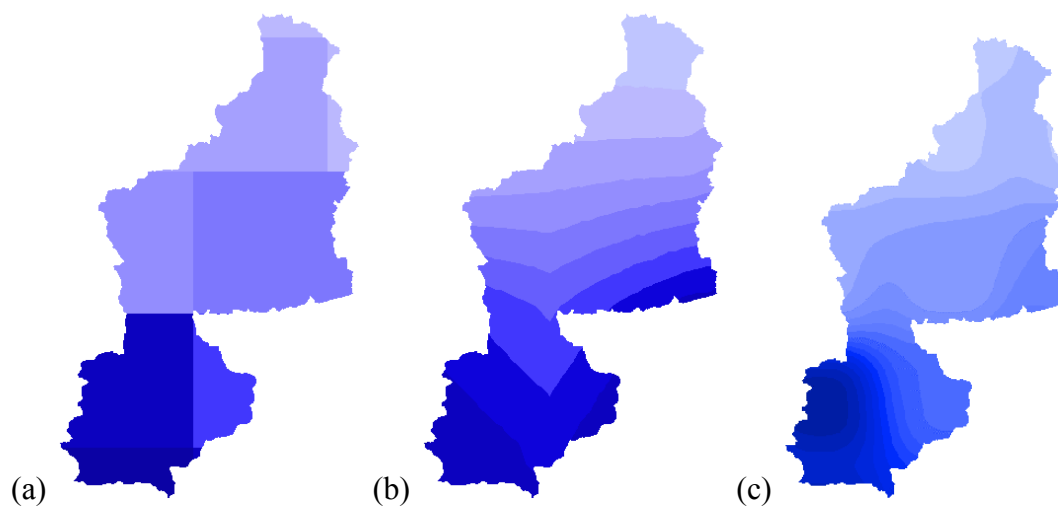
Fig. 5.6: Examples for the different spatially distributed rainfall patterns resulting from the different disaggregation methods; (a) duplicated, (b) bilinear interpolation, (c) inverse distance

5.2.2 Rain radar and METEOSAT derived precipitation

The corrected, temporally aggregated and to UTM transformed rain radar data as well as the METEOSAT derived rainfall data have also a much coarser spatial resolution than the resolution of PROMET-D (1 km for the rain radar and 5 km for the METEOSAT).

For the disaggregation of these data sets the simple disaggregation algorithm was applied by duplicating each grid value to a 100m grid. The preference of this algorithm is forced by an agreement within the RAPHAEL community to maintain the original accuracy and to provide a common procedure for comparing the performance of the different hydrological models involved. It should not be mistaken to be the best suited method for any meteorological situation.

Aside from the problem of disaggregating the meteorological input, the question arose to determine the critical hydrological model resolution at which the hydrological process can no longer be properly be interpreted. Any disaggregation of modelled precipitation with a coarser mesh space than the hydrological model, should only be carried out to the maximum resolution at which the hydrological model can still be reliably driven. So the most efficient scale or grid resolution that allows the synergetic use of the two model components has to be found.

A critical characteristic in flood modelling is the catchment topography, which will generally have a major control over flow pathways for surface and near surface flow processes. An accurate distributed digital elevation model must reflect not only the proper flow pathway for a water particle falling on any point in the catchment, but also the spatial and temporal variations in flow velocity taken by that particle on its route to the catchment outlet (QUINN et al. 1993).

For the Ammer basin a respective analysis was undertaken by averaging the digital elevation model from 100 m to a 500 m resolution. This resolution is considered the first upscaling step converging towards the meteorological models' grid resolution.

However, applying the digital terrain analysis with TOPAZ apparently showed that the hydrological situation in the Ammer catchment is no longer properly represented on a 500 m resolution. Most obviously is this fact illustrated by the calculated channel network as shown in figure 5.7. The river network shows that the river Ammer heading north from the Ammergauer Moos is now deflected towards the Ach (red arrow in figure 5.7). This has a tremendous influence on the parameters, like e.g. the realisation of subcatchments or a considerable change in channel length, that are crucial for the enhanced TOPMODEL.
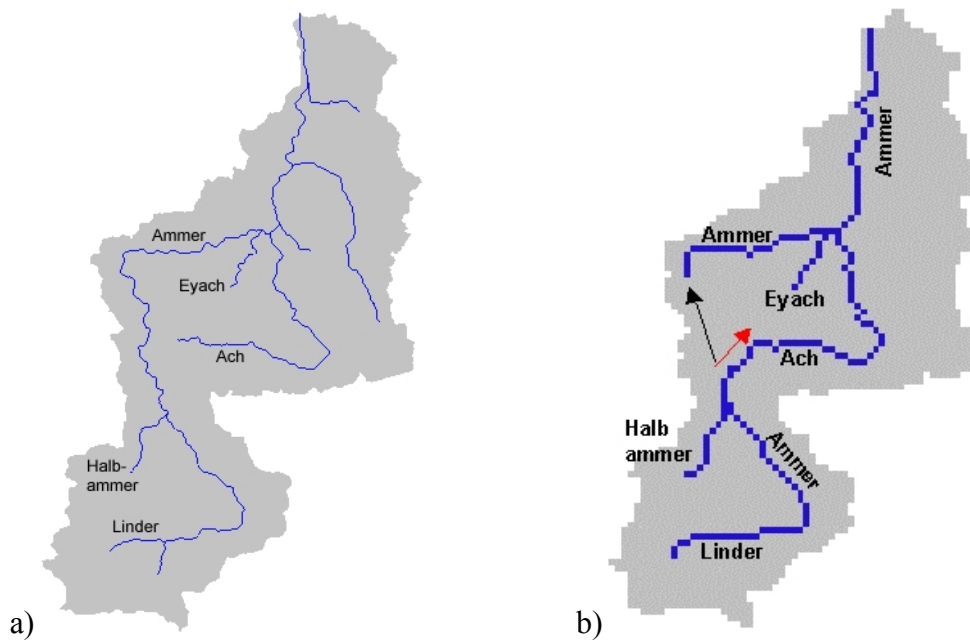
Fig. 5.7: Catchment area and channel network calculated by TOPAZ for the Ammer basin when using a) 100m resolution and b) 500m resolution DEM. The red arrow in (b) indicates the deflection of the Ammer towards the Ach instead of heading northward (black arrow)

As shown by QUINN et al. (1993), in the TOPMODEL approach the routing algorithm and the flow path algorithm have an enormous effect on the model and, in particular, the pattern of prediction in space.

Also the hillslope computation is affected by the DEM upscaling. As shown by the river network calculation, the hillslope calculated from the 500 m DEM of the Ammer no longer represents in some parts of the watershed (especially in the area of the Ammer deflection towards the Ach) properly the approved slope of the 100 m DEM. However this affects the topographic index distribution (see Eq. 3.29) which controls the separation in surface and subsurface flow in the TOPMODEL approach. An appropriate topographic index distribution is, due to QUINN et al. (1993), essential for a realistic application of the TOPMODEL in order to compute properly the changing patterns of water table and soil moisture status.

Aside from the TOPMODEL restrictions due to LUDWIG (2000) the influences caused by generalisation of the geographical information are considered to be still minor up to a spatial resolution of 100m. The study of LUDWIG (2000) showed also the successful application of the PROMET-TOPMODEL interface in the Ammer watershed computed at this mesh width for the hydrological year 1992. Therefore the 100 m scale is assumed as the coarsest resolution for the Ammer basin on which a hydrological flood model can be realistically driven.

6. Model Results

6.1. Christopherus Flood 1997

The so called Christopherus Flood (17.-20.7.1997), is a summer flood event, characterised by one distinct maximum in runoff ($\sim$ 150 m³/s) following a rather moderate filling of soil storages, and a second peak displaying a lower peak discharge ($\sim$ 110 m³/s) 18 hours later (Fig.6.1). A more detailed description of the flood event and the meteorological situation can be found in chapter 4.2.
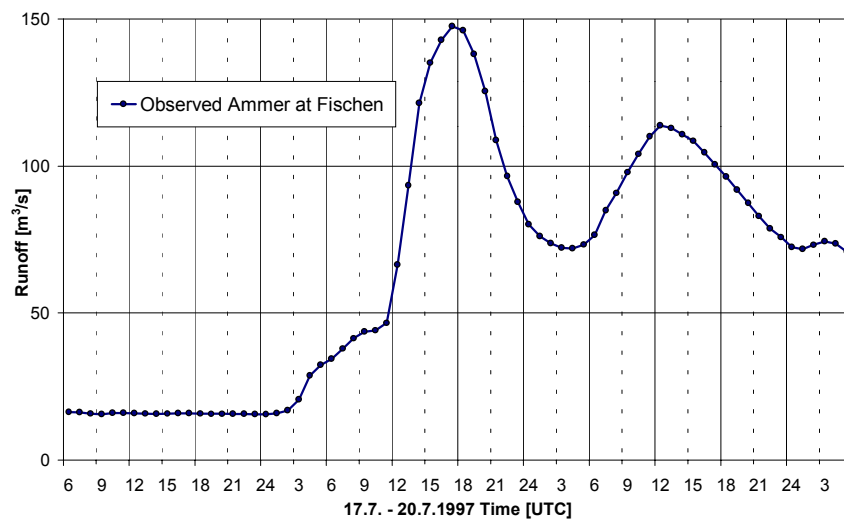
Fig. 6.1: Discharge hydrograph of the Christopherus Flood measured at the gauge Fischen

6.1.1. Runoff calculation

The Christopherus flood has been selected as the flood event to compare the hydrological model results as a function of different NWP forecasts.

Therefore model results of four different NWP models, namely BOLAM (10 km resolution), MC2 (10 km resolution), Meso-NH (10 km resolution) and Swiss Model (14 km resolution), were consecutively applied. All runs were carried out in two different modes: analysis mode and forecast mode (see chapter 3.3.1.2). Additionally, BOLAM and Meso-NH provided rainfall data with a high spatial resolution however for a shortened time period (3.5 km and 2 km respectively). The NWP results were disaggregated applying the duplication scheme as described in chapter 5.2.1.

For the validation and quality control of the modelled runoff using the input from the meteorological models, continuous records of DWDs rain gauge measurements as well as temporally interpolated climatic station measurements of the DWD were applied.

From the application of radar data, available from the DWD Radar Fürholzen was refrained since this data did not undergo a correction procedure. However according to ground clutter and beam blockage, postprocessing is essential in order to compute a precise correction especially in mountainous regions where rainfall intensities are highly affected by these effects. This correction procedure was not carried out for the Christopherus flood by the data provider. Corrections calculated by the data provider for the DWD Radar Fürholzen and the Whitsun flood 1999 (see chapter 6.2) show an underestimation of the radar data in the range of 1.6 (HAGEN and MEISCHNER 2000). However since this is an event specific factor it can not generally be applied on other flood events. But it demonstrates that it is necessary to carry out data reprocessing in order to derive correct precipitation intensities.

No further hydrological model calibration was carried out for this flood event. All necessary parameters were taken from LUDWIG (2000). All specific values of the different model runs are summarised in appendix A and in appendix B. Percentage values referring to the measured runoff at the gauge Fischen are summarised at the end of chapter 6.1.1.2 in table 6.1.

6.1.1.1. Analysis mode

Before discussing the modelled discharge hydrographs resulting from the application of the various precipitation input data in the analysis mode, the spatial distribution of the aggregated rainfall over the flood event period is shown. The accumulated modelled rainfall for the Christopherus Flood period, shows the wide variety in the spatial distribution of precipitation by the meteorological models (Fig. 6.2).
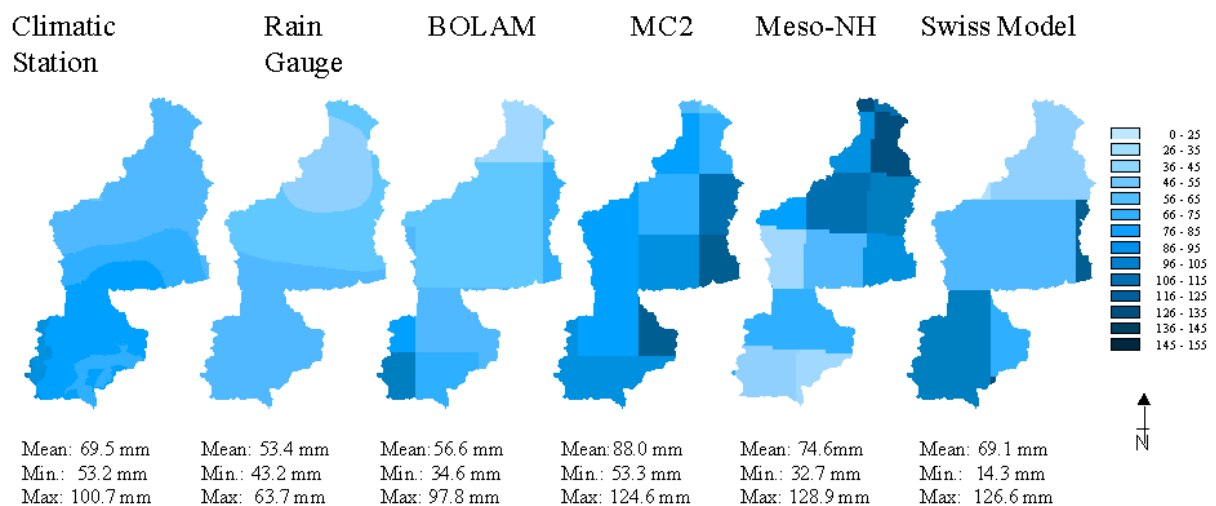
Fig.6.2: The spatial distribution of accumulated rainfall for the Christopherus Flood in the analysis mode

BOLAM and Swiss Model show increasing precipitation towards the Alps, Meso-NH models a relative maximum in the north of the watershed, while MC2 illustrates a differentiated rainfall distribution with no significant maximum. However all four meteorological models show a relative maximum east of the watershed. The spatially interpolated measured data sets (rain gauges and DWD climatic stations) also show an increasing precipitation towards the Alps but only with a slight gradient. The rain gauge data set has the lowest variance, while BOLAM and the climatic station data set are quite similar. The three other NWP models significantly overestimate the maximum. Additionally BOLAM as well as Meso-NH and Swiss Model even underestimates the minimum.

However, as shown in chapter 5.2.1 the accuracy of NWP modelled precipitation over a catchment, like the Ammer depends on the accuracy of the location of the rainfall computed for the whole NWP model domain (like the western-central Alps in this study) where in general the basin is only a part of (see also Fig. 5.3 and Fig. 5.4). Keeping also in mind that the Ammer catchment is covered by only 24 pixels of a NWP model with a spatial resolution of 10 km, a location error of the precipitation field of one pixel has an enormous influence on the hydrological model results (as shown later in the sensitivity analysis).

According to BENOIT et al. (2000) the smallest area that can be properly computed by a NWP model with a mesh width of 10 km is 1600 km². The error in calculated precipitation due to positioning errors grows with decreasing size of the catchment.

Applying the different precipitation input data for the hydrological computation the rain gauge data set leads to the most accurate hydrograph representation (Fig. 6.3.e). Besides a negative time shift of 3 hours and a slight underestimation of the second peak the result is fairly satisfying. With a difference of −1.5 % in the peak volume and an overall discharge volume underestimation of −10.8 %. The resulting coefficient of determination reaches 0.65 which can be seen as a quite good representation of the measured runoff. This proves that on the one hand the applied correction algorithm for rain gauge measurements and the interpolation algorithm for the spatial distribution of precipitation are within a good accuracy range. On the other hand it is also shown that the specific parameters needed for the enhanced TOPMODEL (see chapter 3.2.2), like e.g. the recession parameter are chosen correctly. This enables to introduce this simulation as the reference results for the comparison with other precipitation input data sets.

a) BOLAM
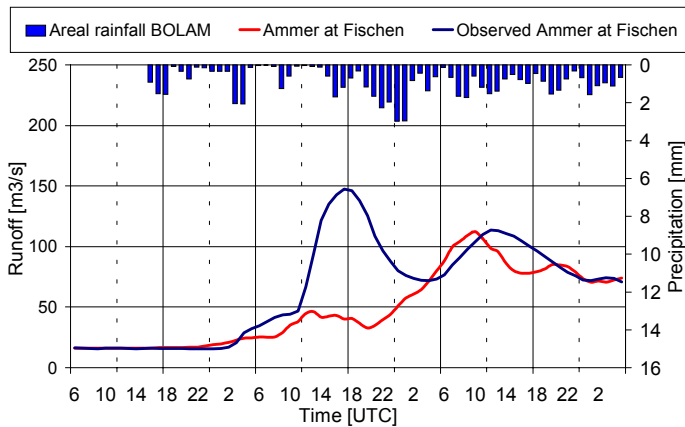
b) MC2
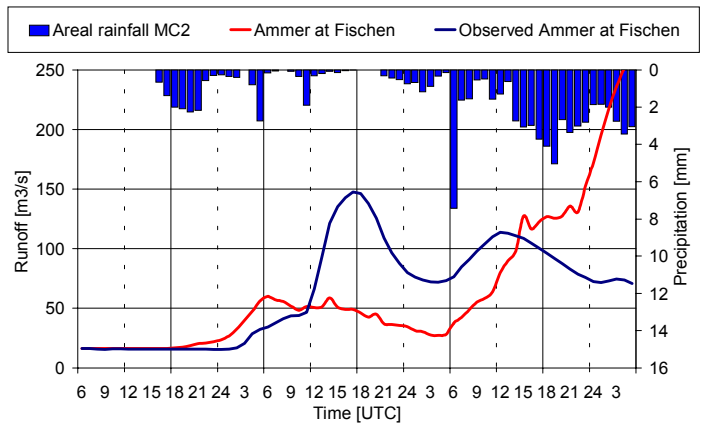
c) Meso-NH
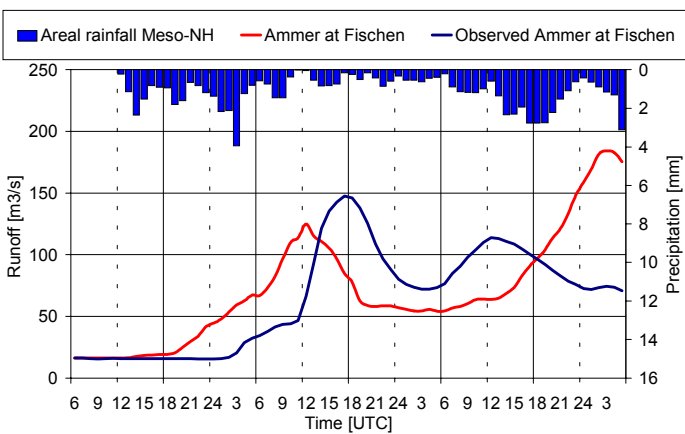
d) Swiss Model
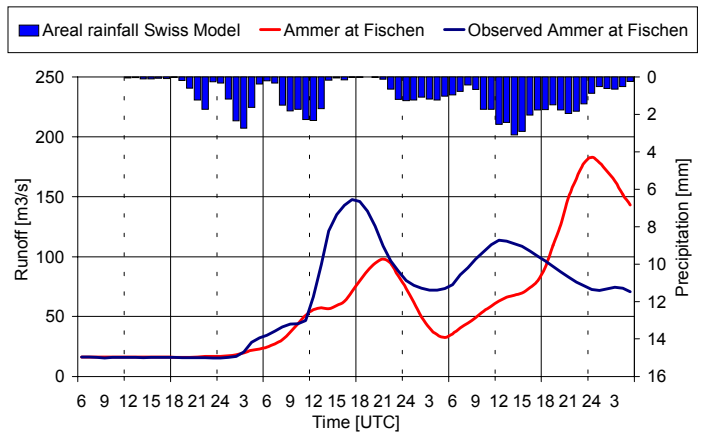
e) DWD Rain Gauges
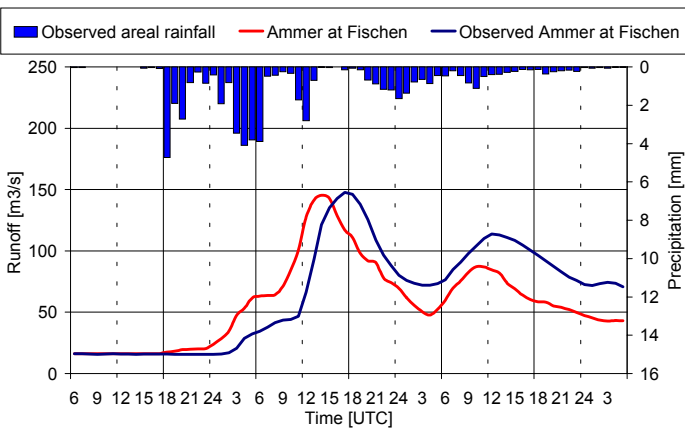
f) DWD Climatic Stations
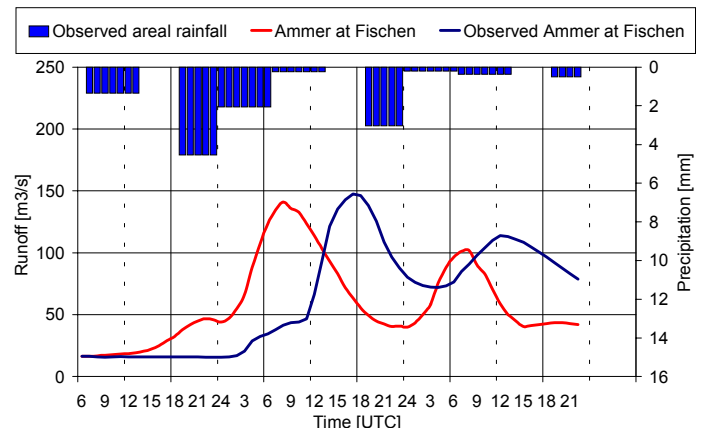
Fig. 6.3.a-f: The hydrological model results of the Christopherus Flood starting on 17 July 1997 at 06:00 UTC – analysis mode. In red are shown the hourly modelled runoff hydrograph applying the referring precipitation input data set (a) BOLAM; b) MC2; c) Meso-NH; d) Swiss Model; e) DWD rain gauge measurements; f) DWD climatic station measurements) and in blue the hourly measured runoff at the stream gauge in Fischen. Also included in every diagram is the hourly areal rainfall for the Ammer catchment calculated with the referring precipitation data set

The model calculation using the climatic station data set leads to similar results in the course of the hydrograph (Fig. 6.3.f). Besides a negative time shift of 9 hours, the shape of the hydrograph is closely approximated. Clearly identifiable is a two peak hydrograph with the first one higher than the second. The overall discharge volume is undervalued by 7.1 %. The first peak underrates the measured maximum by 4.5 %.

Two possible error sources need to be addressed in terms of the modelled time shift. Since both results show the same trend, a connection to an incorrect temporal interpolation of precipitation data may be assumed for the "climatic stations" case (only 3 recordings per day are available). Conducting a 9-hour time postponement of the climatic stations data results in a coefficient of determination improved to 0.91. The other possibility refers to a malfunctional selection of routing parameters in the time-area-histograms of the runoff model. However this seems to be more unlike since the time difference between the first and the second peak is almost the same (19 hours in the simulation and 20 hours in stream gauge measurements). Further sensitivity analysis of model parameters is not performed at this point.

The results applying the meteorological data in the analysis mode of all meteorological models are widespread, with a general incapability to accurately represent the first measured peak. Comparing the precipitation data of the different sources explains this phenomenon in terms of a wrong temporal rainfall distribution.

BOLAM misses the first precipitation peak (resulting in an anticipation of 4 hours and –68.6 % discharge difference in the simulated peak) but calculates the second one quite well (2 hours too early) (Fig. 6.3.a). The concentration and recession of this modelled hydrograph is in good agreement to the measured runoff. While the precipitation sum is closely approximated (6 %), the coefficient of determination is only 0.44, resulting from an incorrect spatial and temporal distribution of rainfall patterns.

MC2 data provides comparable results to BOLAM (Fig. 6.3.b). The first peak is not generated due to a lack in precipitation at the beginning of the event. The peak discharge is underestimated by 60.2 %. At the end of the event high precipitation is predicted by MC2, leading to a strong rise of the hydrograph with an indicated high flood peak beyond the RAPHAEL flood time window. Comparing the runoff volumes within the RAPHAEL time-frame, leads to a deviation of only –0.6 %, but according to the reasons mentioned above the coefficient of determination is only 0.12.

Meso-NH results are different from BOLAM and MC2 (Fig. 6.3.c). The first peak is determined well with a peak discharge difference of only –15.4 %. But the peak arrives 5 hours early, whereas the second peak has a time delay of 15 hours. The second flood wave is

grossly overestimated, which is a result of ongoing simulated precipitation at the end of the event. The overall flood discharge volume is nevertheless miscalculated by only 10.2 %. The coefficient of determination of measured and modelled hydrographs is 0.21.

The result of the Swiss Model input is similar to that of Meso-NH (Fig. 6.3.d). While the starting point of surface runoff is accurately met, the first peak is underestimated by 33.7% along with a time displacement of 4 hours. As in Meso-NH and MC2, the second peak is much higher with a time shift of 12 hours. The overall discharge volume is underestimated by -7.5 %, with a R^2 of only 0.29.

However the similarity of Swiss Model and Meso-NH results can not be traced back to the initial boundary conditions. Instead of ECMWF fields, that are applied by Meso-NH, the Swiss Model uses analysis and forecast fields of the DWDs Europa Modell as the driving boundary conditions. Besides Meso-NH also MC2 incorporates the ECMWF analysis fields as well as BOLAM that however needs to perform a set up in order to prepare the suitable fields for the limited area numerical simulations. For this event the obvious influence of the initial boundary conditions on the result of the NWP models with the same initialisation is not evident although they are reinitialised by the same boundary conditions every six hours.

The discrepancy in the runoff model results may be related to the way the models represent topography. MC2 and BOLAM used a more strongly filtered orography than Swiss Model and Meso-NH. Depending upon the properties of the filtering, the final orographies and therefore the resulting orographic forcing may differ substantially from one model to the other eventhough they use the same resolution. However precipitation linked to orography is common in mountain areas like the Alps. An increase of precipitation can be monitored on windward slopes due to forced lifting of air over the mountains. Concomitant with this effect is the decrease on lee areas (WMO 1986). So the different representation of the orography in the different NWP models might have also an influence on the amount of simulated precipitation.

Significant is also the fact that all meteorological models provide precipitation data in order to compute a higher second runoff peak. Since NWP simulations are not only sensitive to the rainfield location but also to the temporal precipitation distribution, the effective rainfall may be calculated several hours later and is therefore not included in the time window that was chosen for the meteorological modelling. However, the short time period of NWP data availability makes a sensitivity study due to time shifts impossible. Nevertheless this fact seems to be more unlike for the analysis mode since the NWP model run is updated every six hours with newly derived boundary conditions.

6.1.1.2. Forecast mode

Only slight deviations become obvious in the comparison of the accumulated rainfall of the analysis model run and the forecast model run (Fig 6.4).
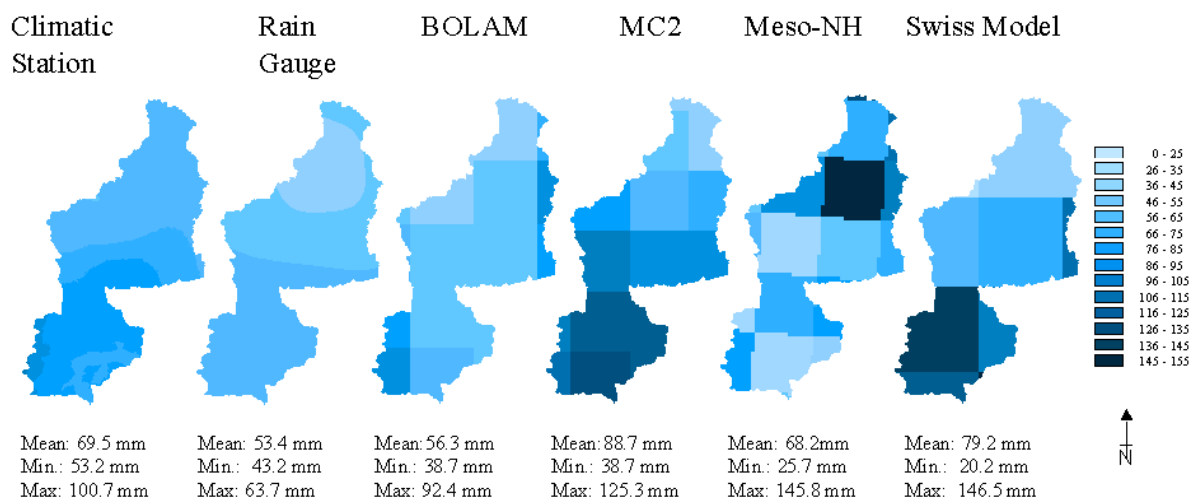
Fig.6.4: The spatial distribution of aggregated rainfall for the Christopherus Flood in the forecast mode

The gradient of increasing precipitation towards the Alps still remains with BOLAM and Swiss Model data. But in contrast to the analysis mode also MC2 shows this distinct gradient with a precipitation maximum in the Alpine region. Swiss model computes a higher precipitation in the south of the catchment that is also reflected by the calculated maximum of 146.5 mm (compared to 126.6 mm in the analysis mode). The Meso-NH forecast run indicates no specific gradient. Pixels with high precipitation especially the significant precipitation maximum in the centre of the basin is surrounded by low precipitation cells. The maximum precipitation of the Meso-NH forecast run has increased compared to the analysis mode from 128.9 mm to 145.8 mm while the basin minimum precipitation has decreased from 32.7 mm to 25.7 mm. The statistical values of minimum, maximum and mean areal precipitation, indicated in figure 6.4 however show in general only minor deviations from the analysis mode results.

But it has to be kept in mind that the Ammer basin is very small compared to the grid size of the NWP models. A relatively small spatial shift in the rainfall field can lead to large deviations in the average precipitation. The Ammer basin is at the lower end of the scale of basin sizes, for which NWP forecast with a resolution of 10 res. 14 km can be sensibly used.

Remarkable deviations however occur in comparing the hydrological model results calculated applying the analysis and the forecast mode. Except for BOLAM, all meteorological models surprisingly show a considerable improvement (Fig. 6.5).

a) BOLAM
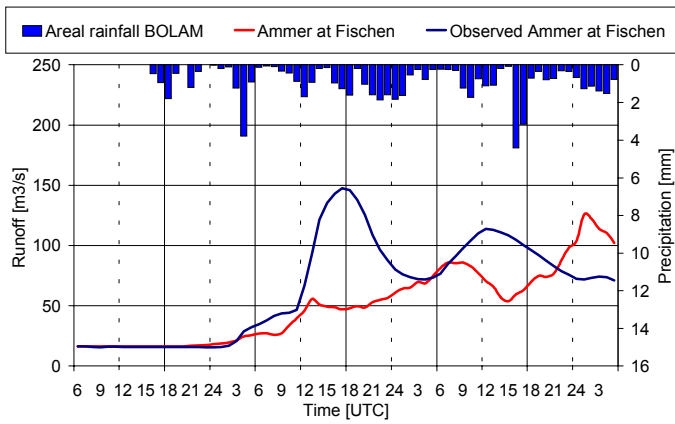
b) MC2
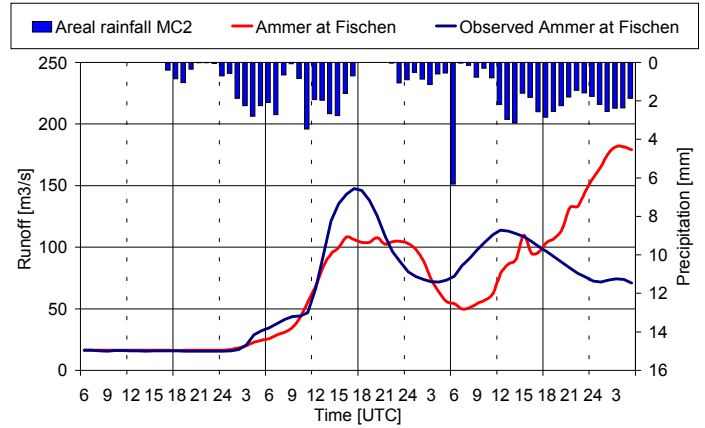
c) Meso-NH
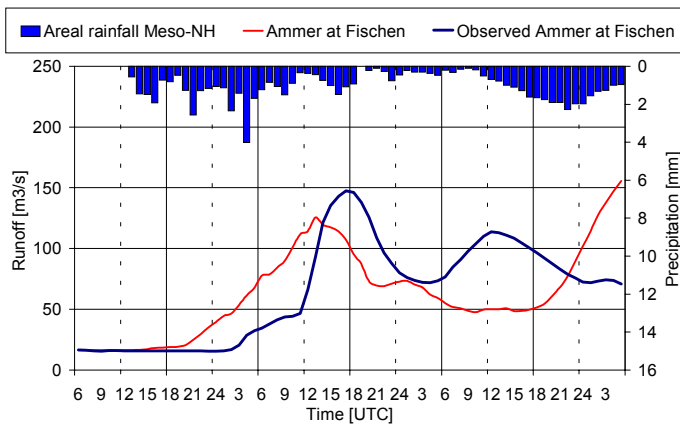
d) Swiss Model
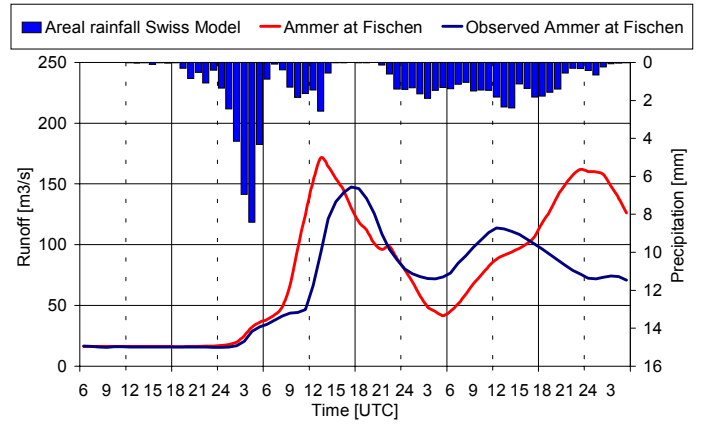
e) DWD Rain Gauges
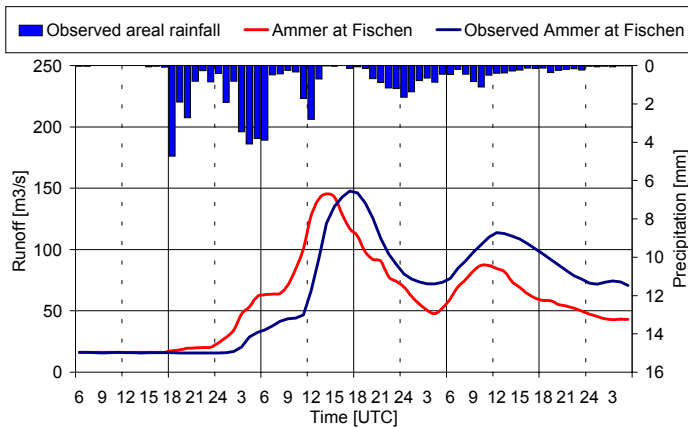
f) DWD Climatic Stations
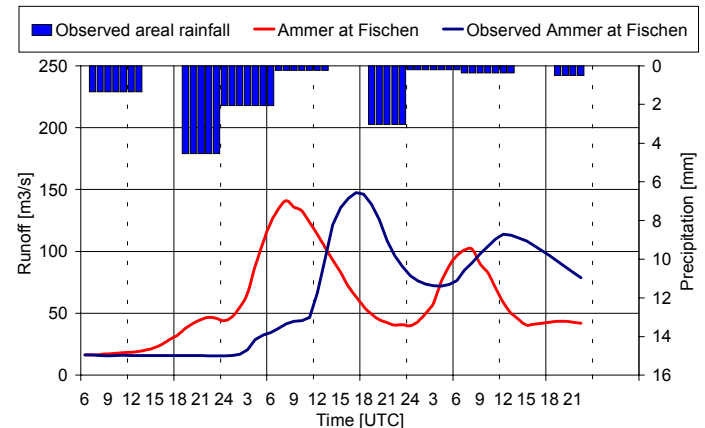
Fig. 6.5.a-f: The hydrological model results of the Christopherus Flood starting on 17 July 1997 at 06:00 UTC – forecast mode. In red are shown the hourly modelled runoff hydrograph applying the referring precipitation input data set (a) BOLAM; b) MC2; c) Meso-NH; d) Swiss Model; e) DWD rain gauge measurements; f) DWD climatic station measurements) and in blue the hourly measured runoff at the stream gauge in Fischen. Also included in every diagram is the hourly areal rainfall for the Ammer catchment calculated with the referring precipitation data set

In general the analysis mode data are more precise, since there are continuously updated with newly derived boundary conditions. However there are also other cases reported where the operational forecast is more accurate (BENOIT et al. 2000).

BOLAM results in the forecast mode are almost the same as in the analysis mode. Peak discharge, overall discharge volume and predicted rainfall as well as the associated time delays are in a comparable range. The second peak is modelled less accurately. Due to a considerable change in areal rainfall distribution, there is an overemphasised relative runoff minimum and a delayed, overestimated second peak. The coefficient of determination is therefore only 0.39.

MC2 shows a distinct first peak with a time shift of only minus one hour and a volume underestimation of 26.7 %. The second peak is lower than in the analysis mode but still delayed and exceeded. The overall discharge volume has a 5.9 % surplus.

The modelled hydrograph using the Meso-NH data in forecast mode is only marginally deviating from the analysis mode results due to the peak runoff volume. The overall flood discharge volume is now miscalculated by -2.6 %, with an additional decrease of peak time delay.

The most significant difference between analysis mode and forecast mode is detected applying the Swiss model data set. The rise of the hydrograph is calculated fairly accurate, while a first distinct peak is modelled four hours early with an overestimation of 16.1 %. The deviation from the analysis mode according to the first peak can be traced back to a distinct precipitation maximum after 27 hours that does not appear in the analysis mode. The second peak however is in a comparable range to the analysis mode. It still arrives late and is overestimated in volume. However, in comparison to the analysis mode, the second peak is reduced, which is also apparent for the MC2 data set.

Among all meteorological model data sets, the best coefficient of determination ($R^2 = 0.56$) for the Christopherus Flood is calculated using the Swiss model forecast mode.

Besides the above mentioned error sources, an additional error can be addressed for the forecast mode. An accurate wind field modelling is crucial, since the location of the rainfall depends on it. The wind field is heavily influenced by the boundary values. With a single initialisation at the beginning of the model run this error source is more likely in the forecast mode than in the analysis mode.

The following table summarises the main statistical values of the hydrological modelling applying the input data sets of the NWP forecast and the analysis mode as well as the rainfall fields of derived from DWD climatic stations and rain gauges measurements. All values are referred to the measured runoff at the gauge Fischen. Absolute values can be found in appendix A and appendix B.

Precipitation data set	Volume [%]	Peak volume [%]	Peak entry time [h]	R^2
BOLAM analysis	-24.5	-68.6	-4	0.44
BOLAM forecast	-22.3	-62.3	-4	0.39
MC2 analysis	-0.6	-60.2	-3	0.12
MC2 forecast	5.9	-26.7	-1	0.48
Meso-NH analysis	10.2	-15.4	-5	0.21
Meso-NH forecast	-2.6	-14.9	-4	0.30
Swiss Model analysis	-7.5	-33.7	4	0.29
Swiss Model forecast	-16.1	16.1	-4	0.56
DWD climatic stations	-7.1	-4.5	-9	0.04
DWD rain gauges	-10.8	-1.5	-3	0.65

Tab. 6.1: Statistical values of the hydrological modelling applying the indicated precipitation data sets. All values are referred to the stream gauge measurements at Fischen

6.1.1.3. High Resolution NWP data

Applying high resolution NWP model runs can improve the accuracy of precipitation fields. The higher resolution allows e.g. to apply an improved orographic representation, with respect to the 10 km resolution. It permits to take into account the morphology of the major Alpine valleys. With the increase in resolution, fine scale structures in the precipitation fields can be computed which is essential in a basin like the Ammer where the model gap between NWP mesh width and hydrological model resolution is considerable.

High resolution NWP model data were made available from BOLAM and Meso-NH, with Meso-NH additionally providing a data set descending from a model run implementing an ice-phase algorithm. BOLAM precipitation fields are computed with 3.5 km spatial resolution while the Meso-NH data set is calculated with 2 km mesh width. Due to computing time and capacity the high resolution NWP data however cover only the starting hours of the Christopherus Flood, but nevertheless give an impression about the modelled accuracy of the

initial conditions for the flood event. Results of the application of the high resolution NWP model runs are shown in figure 6.6 and figure 6.7.

a) DWD rain gauges

$\sum = 35.8$
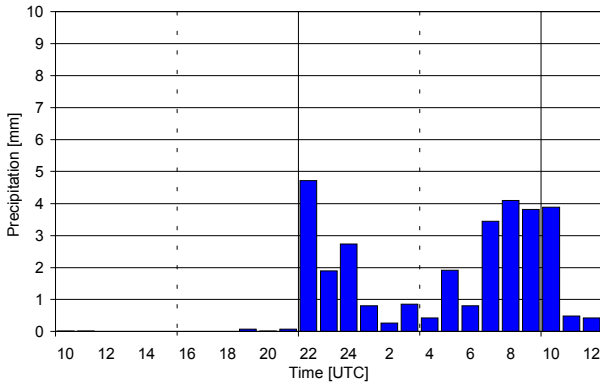
b) Meso-NH forecast 10 km resolution

$\sum = 31.6$ mm
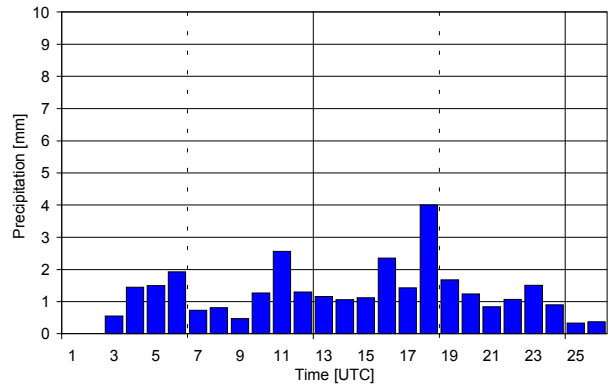
c) Meso-NH forecast 2 km resolution

$\sum = 31.2$ mm
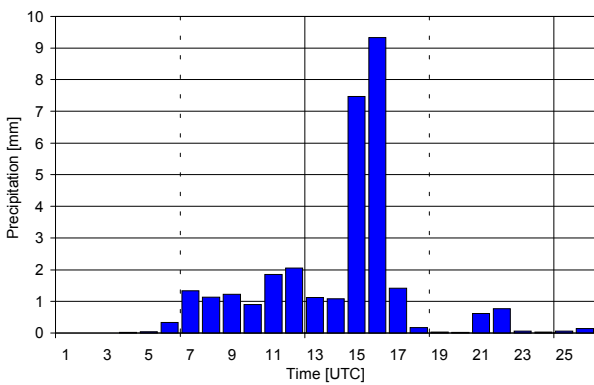
d) Meso-NH forecast 2 km resolution ice phase

$\sum = 23.7$ mm
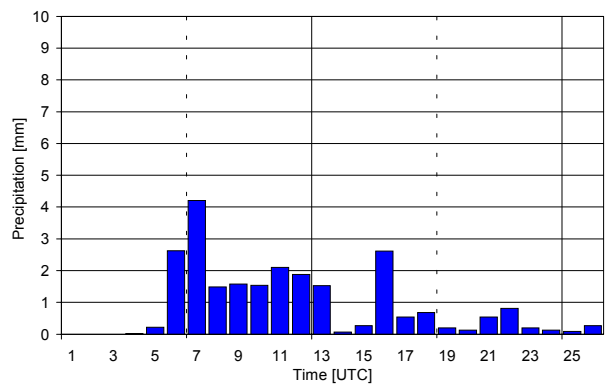
e) BOLAM forecast 10 km resolution

$\sum = 15.9$ mm
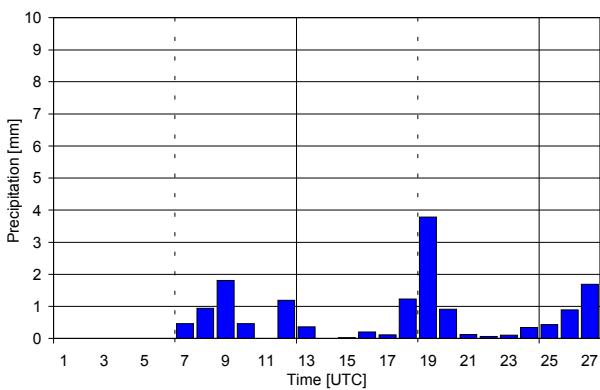
f) BOLAM forecast 3.5 km resolution

$\sum = 24.6$ mm
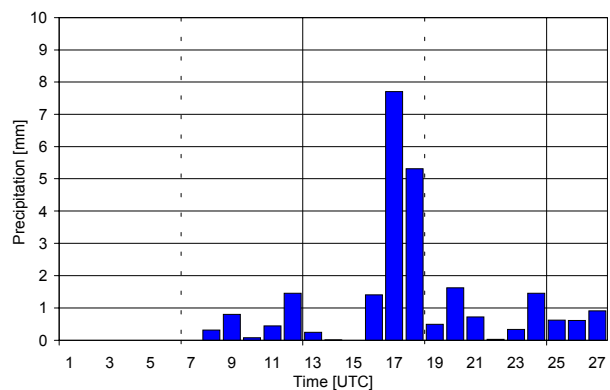
Fig. 6.6.a-f: Comparison of the precipitation distribution of the indicated data sets for the Christopherus Flood starting on 17 July 1997 at 10:00 respectively 11:00 UTC – forecast mode

a) DWD Rain Gauges
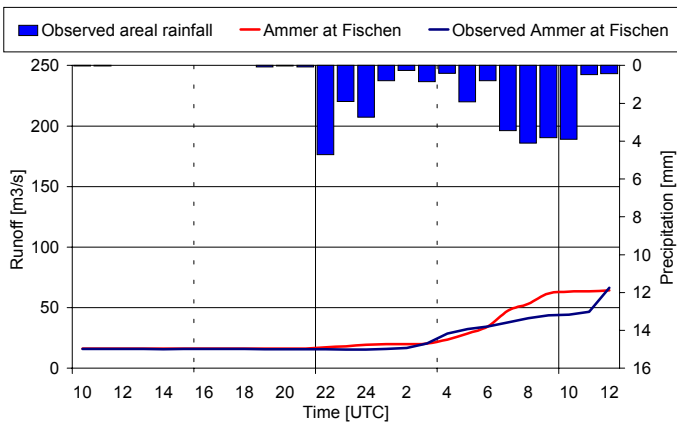
b) BOLAM forecast high resolution
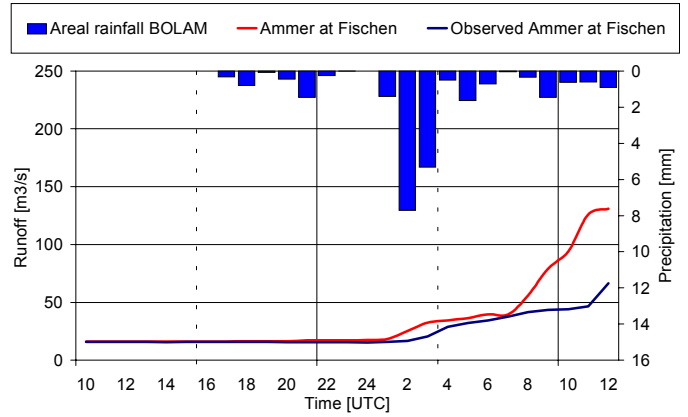
c) Meso-NH forecast high resolution (standard)
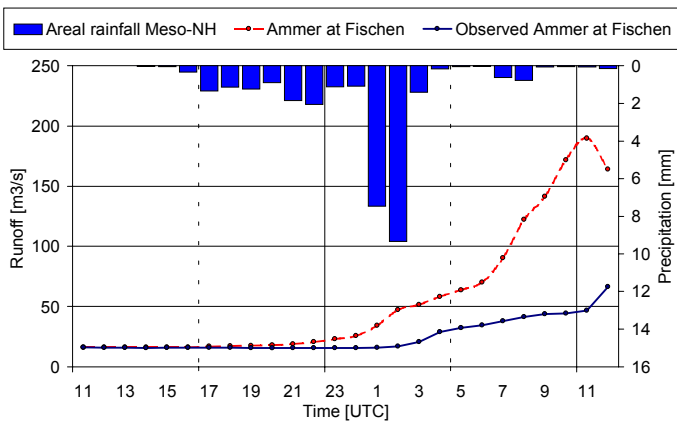
d) Meso-NH forecast high resolution (ice phase)
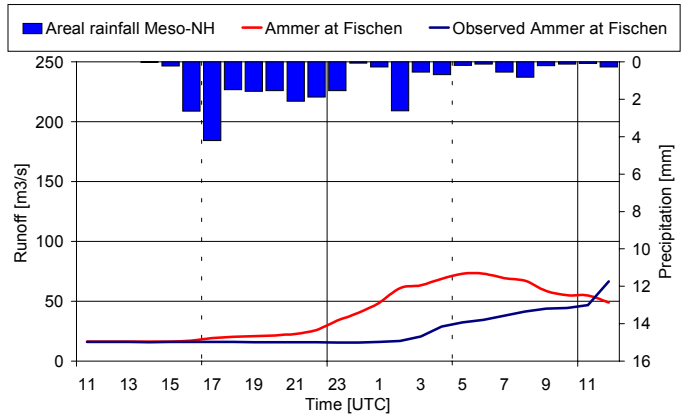
Fig. 6.7.a-d: The hydrological model results of the Christopherus Flood starting on 17 July 1997 at 10:00 respectively 11:00 UTC – forecast in the high resolution mode. In red are shown the hourly modelled runoff hydrograph applying the referring precipitation input data set (a) DWD rain gauge measurements; b) BOLAM ; c) Meso-NH standard; d) Meso-NH including ice phase algorithm) and in blue the hourly measured runoff at the stream gauge in Fischen. Also included in every diagram is the hourly areal rainfall for the Ammer catchment calculated with the referring precipitation data set

In comparison to the standard resolution mode, BOLAM surprisingly inverts the starting conditions, resulting in an increase of precipitation (Fig. 6.6.e; Fig. 6.6.f). The volume of the flood peak that might be identified at the end of the time window, would be in good agreement with the observed one although it would be anticipated by 5 hours (Fig. 6.7.b). Meso-NH standard high resolution mode predicts a very similar temporal distribution of rainfall (Fig. 6.6.b; Fig. 6.6.c), with an even higher magnitude of rainfall resulting in an overestimation of runoff (Fig. 6.7.c).

Additional to the standard high resolution mode of Meso-NH also a high resolution data set of Meso-NH was computed that includes an ice phase algorithm.

On finer scale simulations, a larger fraction of the precipitation is explicitly resolved and increased accuracy in the microphysical scheme becomes more essential. The reversible transformation between the liquid and the ice phase is accompanied by a significant heat release which can contribute to a further growth of convective clouds aloft or cooling beneath by precipitating particles falling in an unsaturated environment. An expected consequence of these different aerodynamical properties is a larger time scale for the life cycle of partially glaciated convective clouds due to the larger residence time of solid hydrometeors and a modified spatial distribution of liquid precipitation. Therefore Meso-NH has incorporated an ice phase scheme (BENOIT et al. 2000).

Applying the Meso-NH ice phase data lacks accuracy in terms of rainfall volume and its temporal distribution (Fig. 6.6.d). However much better agreement to measured conditions is achieved using the Meso-NH ice-phase data (Fig. 6.7.d). Although the modelled runoff is again overestimated during the starting hours of the event, the overall amount of rainfall is modelled to be far less than in the high-resolution standard mode and tends to furtherly decrease during the rising period of the gauged runoff.

Nevertheless, the differences in rainfall distribution compared to the standard mode application of BOLAM and Meso-NH leads to an improved approximation of observed runoff, yet a considerable displacement of the actual runoff peak time is introduced.

The conclusion can be drawn that a finer NWP resolution and accordingly the finer representation of rainfall fields improve hydrological response modelling, especially in small catchments like the Ammer.

6.1.2. Sensitivity analysis

6.1.2.1 Radial Shift

A sensitivity analysis of PROMET-D was carried out to evaluate the impact of shifted precipitation fields of the NWP model outputs on the hydrological model performance. To account for a possibly inexact spatial coverage of the meteorological model, a one-pixel (10 km for BOLAM, MC2 and Meso-NH or 14 km for SM) radial shift of the modelled precipitation field is performed.

The radial shift for the Christopherus Flood was calculated using all meteorological models in the analysis mode. The shifted rainfall fields were disaggregated applying the simple

duplication algorithm. The orientation indicates the original location of the rainfall field. The results are shown in figure 6.8.

a) BOLAM
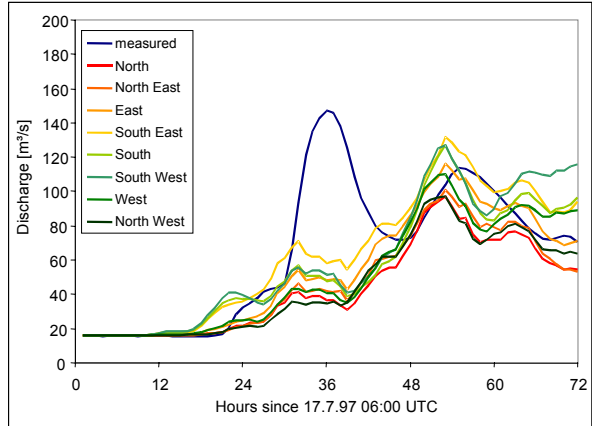
b) MC2
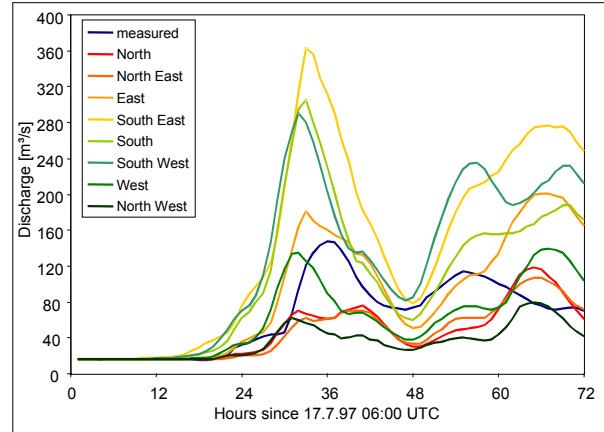
c) Meso-NH
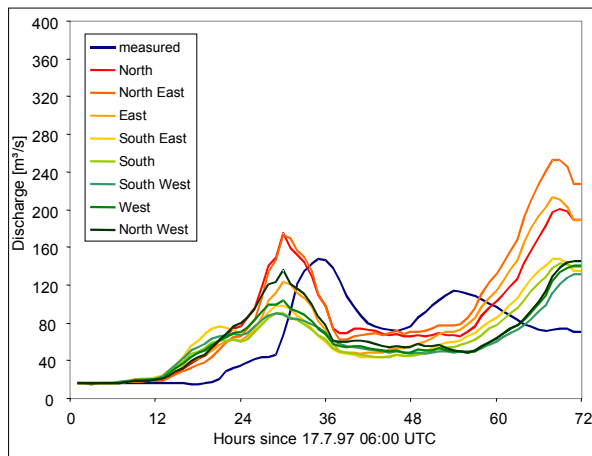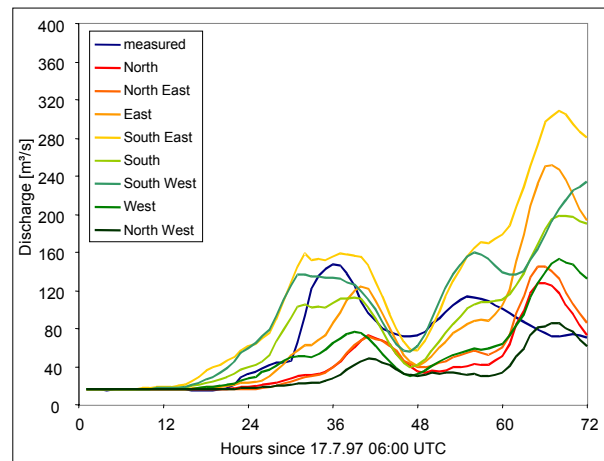
d) Swiss Model

Fig. 6.8.a-d: The hydrological model results for the Christopherus Flood applying shifted rainfall fields of a) BOLAM, b) MC2, c) Meso-NH and d) Swiss Model in the analysis mode using the simple duplicating disaggregation algorithm. In blue is indicated the hourly measured runoff at the stream gauge in Fischen

The modelled discharge applying the different shifted BOLAM rainfall fields shows only minor variations in terms of flood volume (Fig. 6.8.a). The original northerly located rainfall fields lead to the lowest runoff while highest discharge is calculated using the previous south east located one. Noticeable is the early rise in the hydrograph when utilising original southerly positioned rainfall fields. This indicates a higher rainfall intensity in these data sets at the beginning of the flood event. In the course of the flood, the hydrographs are quite

similar referring to their shape. However the model results are not improved in general. This fact is also shown by the coefficient of determination (Tab. 6.2).

A high variability in the flood volume is modelled using the MC2 shifted rainfall fields, indicating the high spatial variability of the precipitation pattern within the NWP model result (Fig. 6.8.b). A considerable surplus is calculated utilising previous southerly located rainfall fields, while the original northerly positioned ones lead to an overall discharge underestimation. Remarkable is the distinctive deviation that occurs when using the eastern and western neighbour. After 31 hours the previously easterly located rainfall field leads to a higher runoff while the original westerly located one, in general, underestimates the discharge. This shows a strong gradient of modelled rainfall not only towards the Alps (north-south) but also in longitudinal direction (west-east). However applying the shifted MC2 rainfall fields improve the model result in terms of an significantly improved coefficient of determination (Tab. 6.2).

The radial shift of the Meso-NH domain leads to opposite results compared to the other meteorological model calculations (Fig. 6.8.c). Applying previous northerly and north easterly positioned precipitation fields, the modelled discharge is overestimated; original southern and western located ones lead to lower runoffs. The variability of the calculated hydrographs is in a small range.

Like MC2 and BOLAM highest discharge is also modelled applying the previous south east positioned rainfall field of the Swiss Model (Fig. 6.8.d). The overall runoff is underestimated using the original northerly located precipitation fields. A better correspondence to measured runoff is not achieved with any of the shifted rainfall fields although the coefficient of determination is improved applying previous southerly positioned ones (Tab. 6.2). However this shows again the wide range of possible model results when usually assuming a displacement of the meteorological domain by only one grid element.

Evaluating the „spaghetti plots" of modelled runoff applying the different rainfield shifts, does not lead to a common proposition of preferred orientation and hence provides no explanation of a possible unambiguous error source. However the location of the precipitation maximum of each meteorological model can be identified. In general applying BOLAM, MC2 and Swiss Model data sets the highest discharge is calculated using the rainfall fields originally located southward in the Alps. Hydrological simulations based on MC2 and SWISS MODEL are more sensitive to the radial shift compared to the BOLAM and Meso-NH results, based on a larger spatial heterogenity of meteorological input.

Shifts in precipitation fields	Coefficient of determination			
	BOLAM	MC2	Meso-NH	Swiss Model
None	0.44	0.12	0.21	0.29
North	0.34	0.37	0.09	0.12
North-east	0.43	0.47	0.13	0.16
East	0.46	0.60	0.02	0.24
South-east	0.48	0.71	0.13	0.38
South	0.31	0.63	0.16	0.38
South-west	0.28	0.64	0.18	0.50
West	0.31	0.37	0.17	0.19
North-west	0.32	0.16	0.19	0.19

Tab. 6.2: Coefficient of determination of the different shifted rainfall fields calculated by the indicated NWP models referring to the measured runoff at the stream gauge located in Fischen.

6.2. The Whitsun flood 1999

The second flood event that is investigated in this study occurred during whitsun of 1999 (20.5 – 23.5.1999) and is furtherly referred to as the "Whitsun flood". As described in chapter 4.1 it is the most hazardous flood ever recorded in the Ammer watershed. 48-hours of excessive rainfall north of the Alps led to a devastating flood causing extensive damage. The recorded stages along the Ammer correspond to a bicentennial flood (FUCHS et al. 1999). However, measured water level data can only serve as an estimate for the calculation of the actual runoff. Due to the extreme extent of the Whitsun flood the stage-discharge relationship along the river was no longer within the valid range. An extrapolation had to be performed, estimating runoff from the recorded stages. On account of upstream levee breaks, ungauged runoff occurred to an unpredictable extent. It must be assumed that the measured actual runoff peak and volume was higher than the available recordings (Hannweber 2000). However for the validation of the modelled runoff the official runoff estimation published by the Bavarian Water Authority for the gauge Weilheim is used since it is the only available data source (Fig. 6.9).
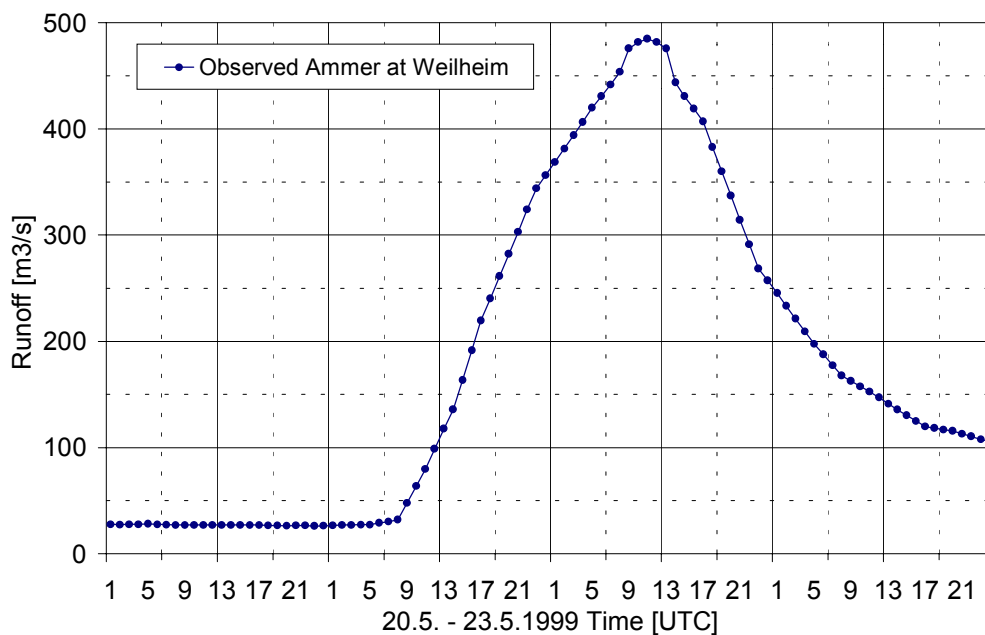
Fig. 6.9: Discharge hydrograph of the Whitsun Flood measured at the gauge Weilheim

Since the extremity of this event was partly induced by snowmelt and pre-event saturated soils, specific attention is drawn to these influencing factors. Therefore the two input fields, provided by PROMET, are discussed in the following, before the runoff model results are presented.

6.2.1. Snow modelling

During the snow melt season of 1999 an intense snow campaign was carried out in the Ammer catchment. At nine test sites the snow height, snow density and snow water equivalent was measured in order to verify the snow model results of PROMET. Measurements however were only collected at these sites for the period between the 3.2.1999 and 9.4.1999. The test sites were selected under consideration of the following aspects:

- Systematical spatial distribution within the catchment with respect to the north-south gradient.

- A minimum of influence from topography, landuse (e.g. forest) or man made artificial objects (e.g. buildings).

Additional to these test site measurements, snow water equivalent data were available from the DWD station Hohenpeissenberg. This test site is continuously operated by the DWD and contains therefore snow water equivalent measurements for the whole winter of 1998/99.

From the spatial distribution of snow test sites illustrated in table 6.3 and figure 6.10 three altitudinal classes are distinguished:

- 500 – 600 m asl.: Fischen, Wielenbach, Rettenbach

- 600 – 800 m asl.: St. Andrä, Bad Kohlgrub

- 800 – 1000m asl.: Baiersoien, Hohenpeissenberg, Unternogg, Unterammergau, Graswang.

The results of the measured and modelled snow water equivalent are presented on the basis of this division.

Testsite	Altitude asl. [m]	UTM 32 N (WGS84)	
		Longitude	Latitude
Fischen	540	660373	5310290
Wielenbach	550	661763	5303500
Rettenbach	560	660104	5296262
St. Andrä	620	662820	5295497
Kohlgrub	740	656652	5281167
Bayersoien	860	651338	5282698
Unternogg	810	650341	5279392
U-Ammergau	835	652556	5274912
Graswang	870	652661	5270538
Hohenpeissenberg	977	650689	5296226

Tab. 6.3: Geographic co-ordinates (UTM 32N) and altitude of the snow test sites
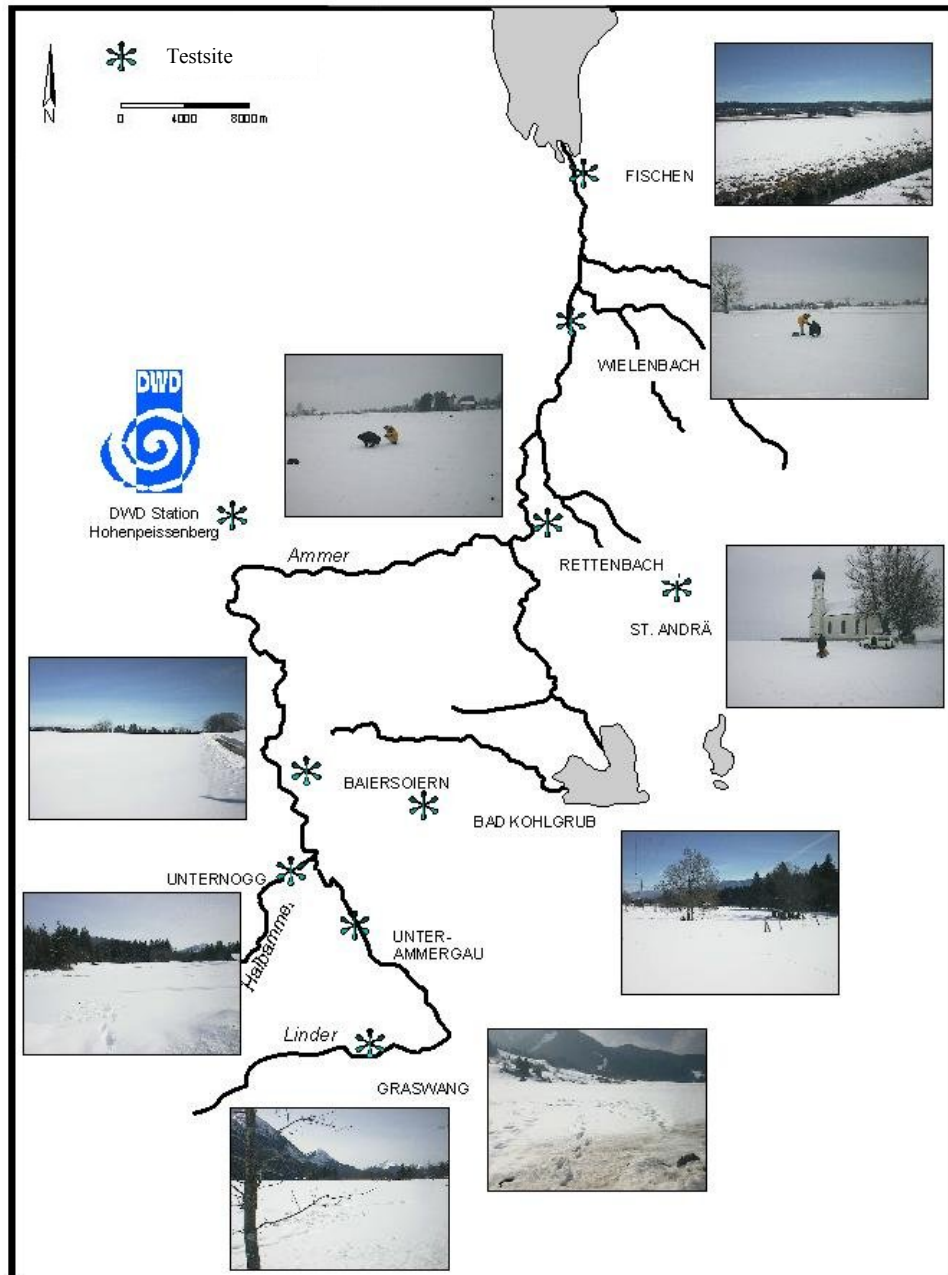
Fig. 6.10: Snow test sites in the Ammer catchment (Photos taken at 3.2.1999)

500 – 600 m asl.

The temporal course of the snow cover period, computed by PROMET for this altitude class is shown in figure 6.11. For the time between 3.2.1999 and 9.4.1999 a comparison with snow water equivalent measurements can be carried out. Snow accumulation and ablation as well as small intermediate snow melt periods, monitored at the test sites are reflected in the model results. However the absolute value of snow water equivalent is sometimes considerably over- respectively underestimated. One explanation for this miscalculation might be found in an incorrect spatial and temporal interpolation of the meteorological input data. Only at the

DWD test site Hohenpeissenberg meteorological measurements are recorded at the snow measurement test site. The snow water equivalent maximum modelled for the test sites Fischen and Rettenbach is in accordance with the referring measurements as well as the final snow ablation in February/March. While the snow cover remains fairly shallow during the winter season, the dynamics of snowpack is well represented by the snow module in PROMET-D.
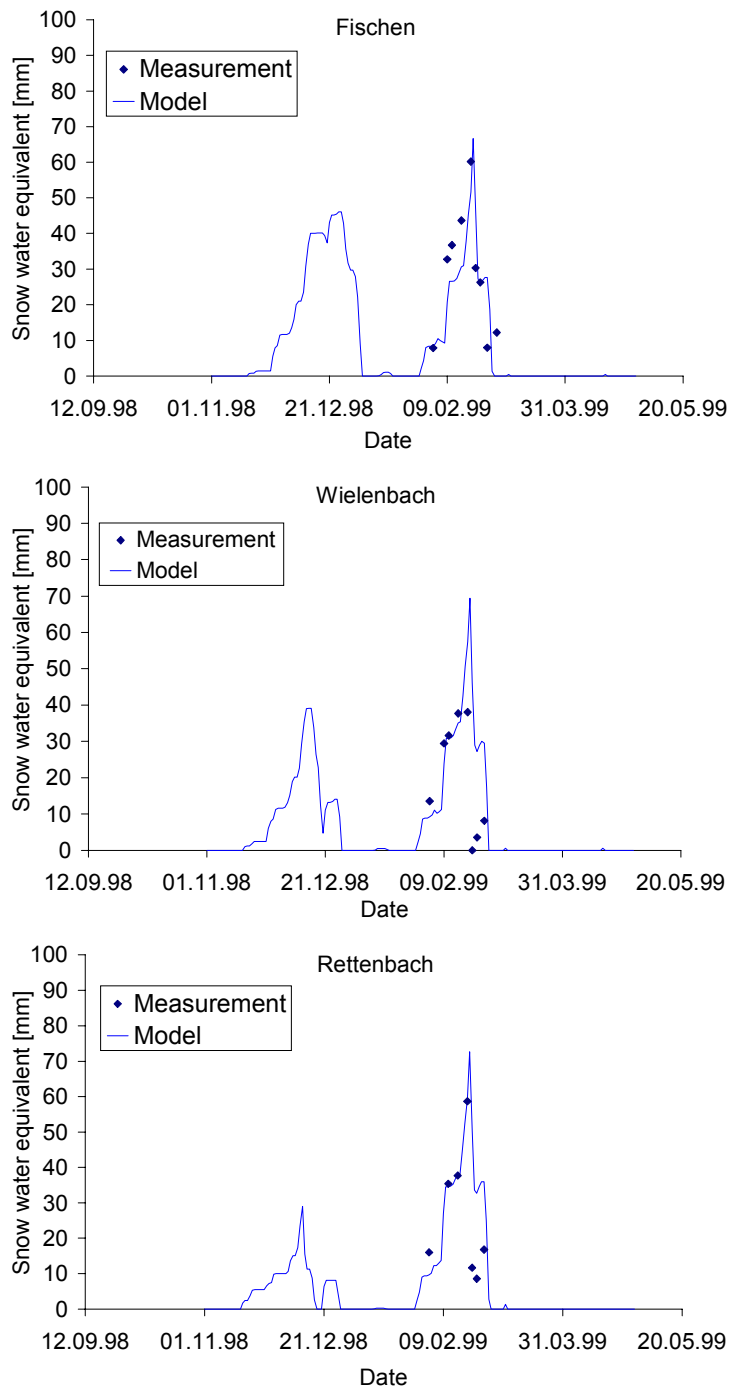
Fig. 6.11: Modelled snow water equivalent compared to measurements at the referring snow test sites (available only for the period between 9.2.1999 and 9.4.1999) in the 500 –600 m asl. zone

600 – 800 m asl.

The snow model results are significantly less accurate in this altitudinal class. At both test sites the modelled snow water equivalent is overestimated (Fig. 6.12). Especially for the test site Bad Kohlgrub the calculation result is poor. Besides the overestimated snow water equivalent, also the snow cover period is miscalculated. However the temporal distribution of the snow water equivalent is in agreement in terms of a good correspondence between periodical snow accumulation and snow ablation.
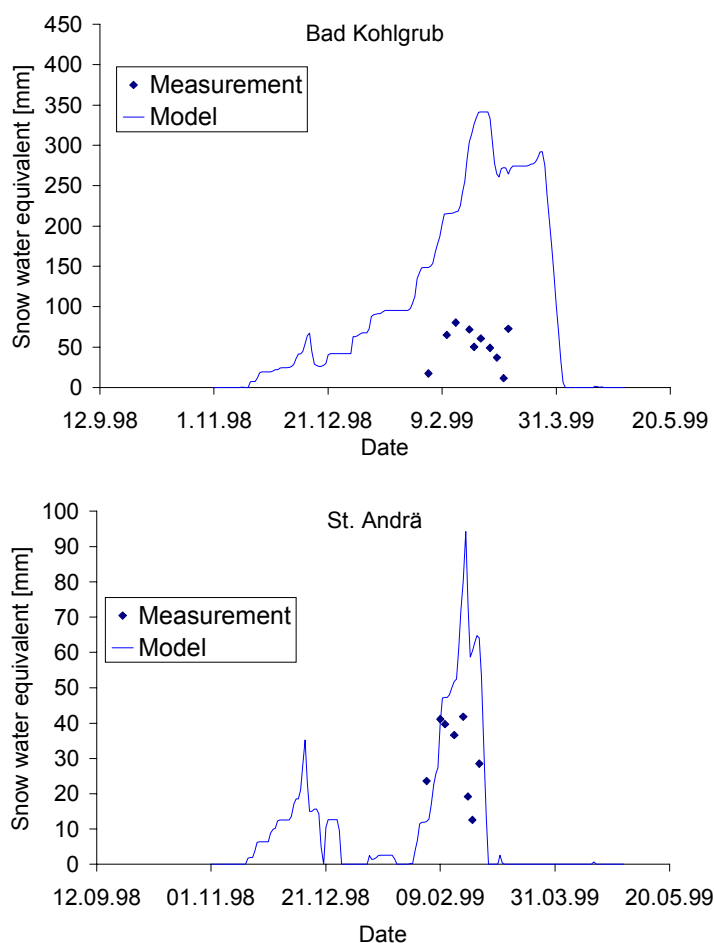
Fig. 6.12: Modelled snow water equivalent compared to measurements at the referring snow test sites (available only for the period between 9.2.1999 and 9.4.1999) in the 600 –800 m asl. zone

An explanation for the difference of computed and measured snow water equivalent can be assumed in an incorrect spatial and temporal meteorological data interpolation. However especially at Bad Kohlgrub a DWD synoptic climatic station is nearby, minimising this effect. Since however this station is not situated in an optimum location (in a steep valley, nearby a building) the meteorological measurements possibly contain errors. Since the snow module of PROMET is sensitive to the air temperature, that determinates whether a precipitation is snow

or rain, such errors have an influence on the model results. A further possible error source can be found in the test site itself, that in spring turned out to be a rough undulated field where several measurement errors can occur.

800 – 1000 m asl.

This group of test sites is located, besides the Hohenpeissenberg, in the southern part of the catchment and shows the longest uninterrupted snow cover period with the highest snow water equivalent values. Due to logistic problems, only valley testsites were in reach for consecutive measurements. Therefore no data were available to validate the computed altitudinal gradient along the steep mountain slopes.

The temporal course of snow water equivalent is generally represented by the model (Fig. 6.13). While underestimation of snow water equivalent can be observed in some parts, agreement between modelled and measured snow water equivalent is achieved especially for the snow melt period. In general a good correspondence of measurements and model results is detected for all test sites beside Baiersoien.

Of particular interest are the measurements of the Hohenpeissenberg carried out by the DWD. Data for the whole winter season of 1998/1999 were available. Also all for the model performance needed meteorological input parameters are recorded by the DWD at the same site. This enables to carry out a model verification at this location for the whole winter of 1998/99.

Due to the snow measurements the computed snow cover period is in agreement (Fig. 6.14). The calculated snow water equivalent shows a good correspondence between modelled and measured snow water equivalent. Also short snow free periods during the winter are shown by the model. However during the snow water equivalent maximum period the model results differ from the measurements. Small snow ablation periods are not modelled in this time period, e.g. the divergence of measured snow accumulation and modelled melt on March 12th. However this fact possibly can be traced back to an error in the temporal air temperature interpolation. At the synoptic climate station of the DWD at the Hohenpeissenberg, measurements of meteorological parameters are performed only three times a day and consequently a temporal interpolation has to be carried out for the hourly model step of PROMET. In this case the temporal interpolation might compute an air temperature which is too warm. Hence the model interprets the recorded precipitation as rain (instead of snow). That leads instead of a measured snow accumulation to a modelled melt (PENNDORF 2000).
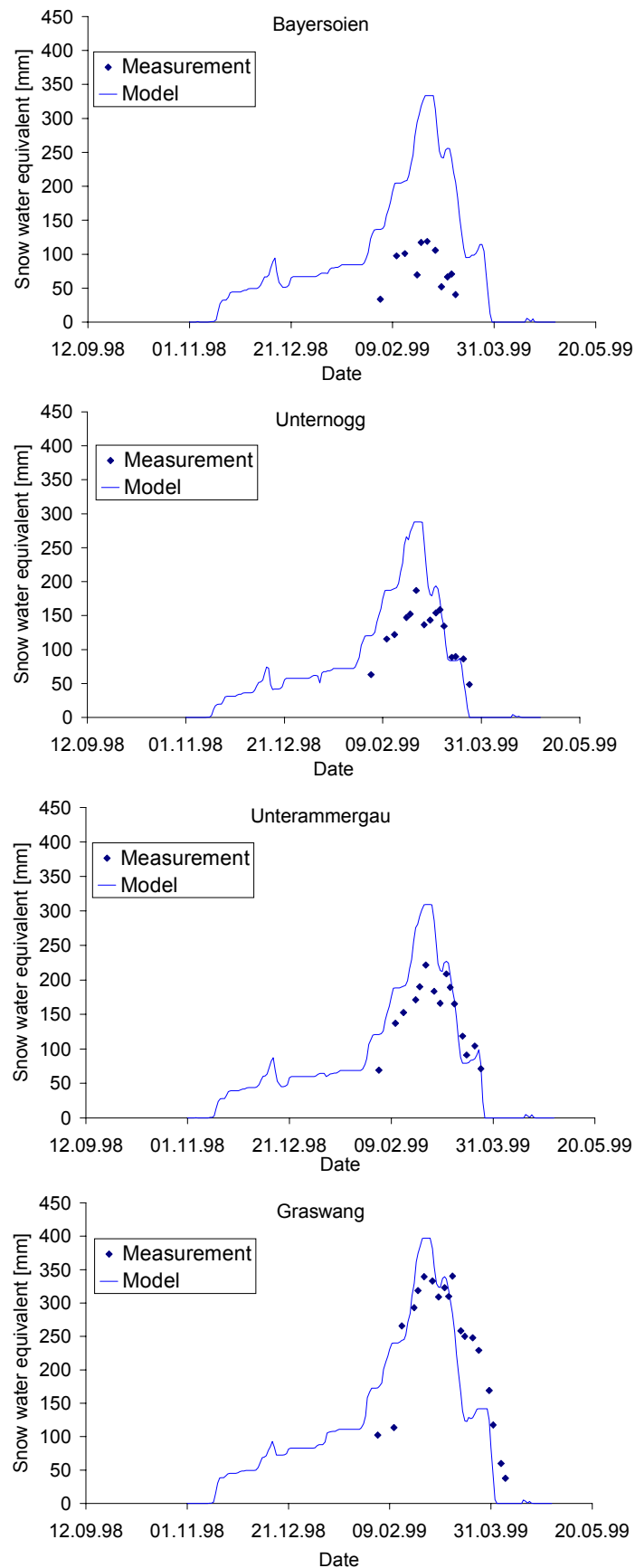
Fig. 6.13: Modelled snow water equivalent compared to measurements at the referring snow test sites (available only for the period between 9.2.1999 and 9.4.1999) in the 800 –1000 m asl. zone
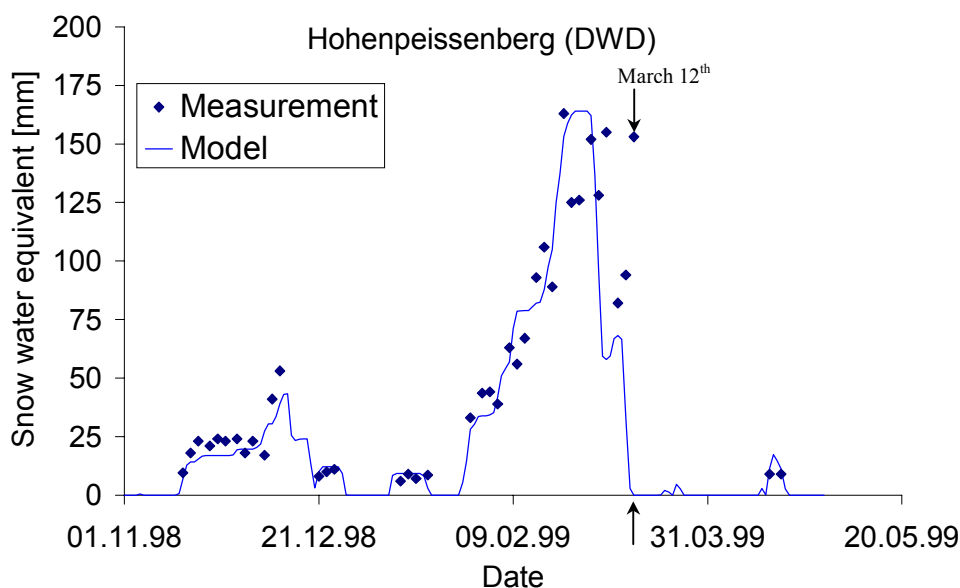
Fig. 6.14: Modelled snow water equivalent compared to measurements at the DWD station Hohenpeissenberg

Summarising the snow model results of the winter season 1998/99, PROMET proved its applicability to simulate snow dynamics with reasonable accuracy. Except for Bad Kohlgrub and Baiersoien, a good correspondence with point measurements, well distributed in the Ammer catchment, is computed. For the whole winter season 1998/1999 the model results were independently verified at the DWD station Hohenpeissenberg. A statistical regression analysis leads to a coefficient of determination of 0.55 and an overestimation of the snow water equivalent by the model of 14%.

Since the test sites Bad Kohlgrub and Baiersoien have shown an extraordinary deviation from the rest of the comparison both test site were omitted from further analysis.

The recalculated coefficient of determination increases to 0.89, while overestimation decreases to 4%. Whether the reason of the deviations at the test sites Bad Kohlgrub and Baiersoien can be found will have to be shown in further snow campaigns. Investigations of the meteorological conditions however have shown no significant result (PENNDORF 2000).

Unfortunately no measurements are available to validate the modelled snow water equivalent during the Whitsun flood period. As demonstrated by the field measurements (Fig. 6.11- 6.14) several weeks prior to the flood event, in the lower altitudes of the catchment as well as in the alpine valleys no snow cover was recorded. This fact leads to the conclusion that the basin was only partly snow covered.

The only available information about the snow cover extent during the Whitsun flood period is derived from the Lech catchment which is adjacent to the Ammer basin. As recorded by the Water Authority in Kempten snowmelt was enforced up to altitudes of 1800 m asl.

The snow model performance in the Ammer basin is in accordance to this record. As shown in figure 6.15 snowmelt is calculated by PROMET for altitudes up to 1800 m asl whereas at higher altitudes snow is accumulated.
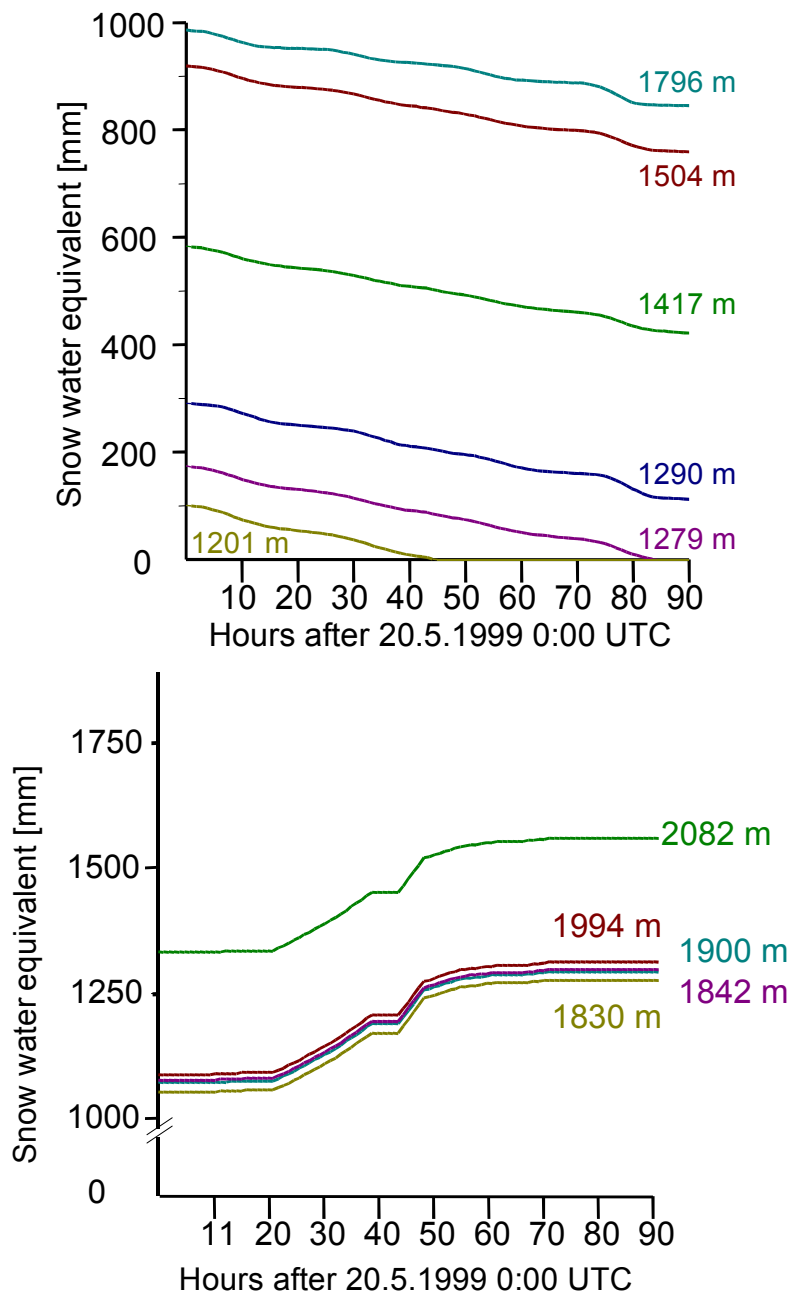
Fig. 6.15: Modelled snow water equivalent at selected locations in the Ammer catchment during the Whitsun flood period

Calculating the difference of modelled snow water equivalent at the beginning and at the end of the Whitsun flood leads to a spatial information of snow accumulation areas and areas

where snow melt occurred. Figure 6.16 (a) shows that only the alpine ridges in the basin were modelled snow covered. Most of this snow melted during the flood event and contributed to the runoff generation. However figure 6.16 (b) demonstrates that also snow accumulation was computed by the model. These areas are mainly above an altitude of 1800 m asl. and non below 1600 m asl..

(a)

(b)
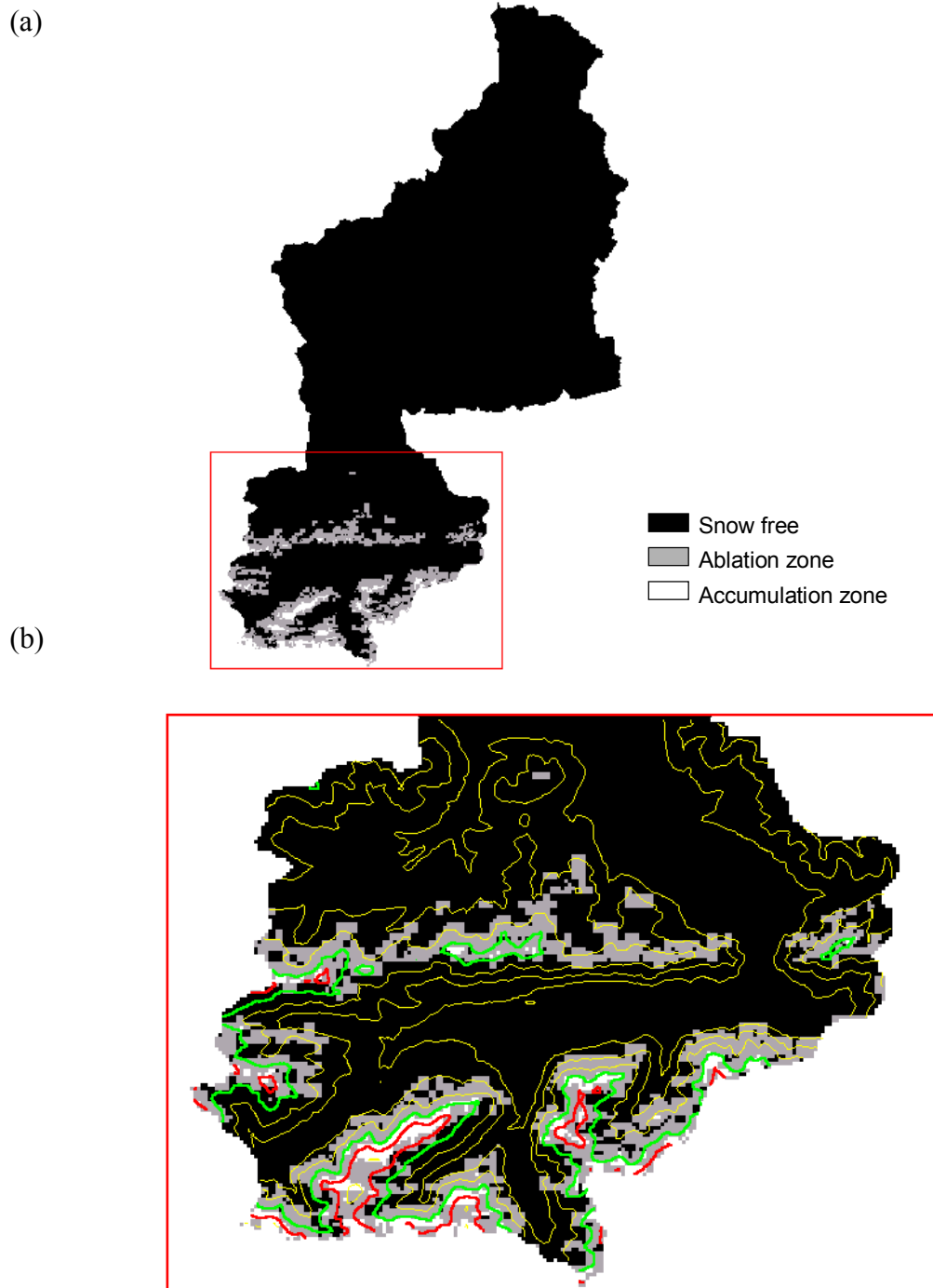
Fig. 6.16: Difference of modelled snow water equivalent in the Ammer catchment at the beginning and at the end of the Whitsun flood. (b) shows a zoom in of the Alpine region superimposed by the contour lines calculated from the DEM (in yellow: contour line with an equidistance of 200 m, in green the 1600 m contour line, in red the 1800 m contour line)

In conclusion, the snow water equivalent is computed accurately by PROMET. Also for the Whitsun flood it can be assumed that the overall amount of snow melted direct runoff is balanced by PROMET in a valid range.

6.2.2. Soil moisture modelling

Also of particular interest is the soil moisture situation prior to the flood event because it determines the capacity for further infiltration.

As described in Chapter 4.1, a small flood event (13.-15.5.1999) occurred a few days before the Whitsun flood. Therefore the soils are assumed to be almost saturated before the occurrence of the Whitsun flood event when almost all precipitation was transferred into direct runoff.

Since there are no particular soil moisture measurements available to verify or validate the PROMET soil moisture results, only a relative analysis can be carried out.

A spatial distribution of modelled soil moisture just before the Whitsun flood event is given in figure 6.17. Depending on soil type and landuse the soils were almost saturated in the whole Ammer catchment.

Figure 6.17 also illustrates the modelled temporal distribution of soil moisture for the main soil type (loam) under the most frequent landuse types in the Ammer catchment: meadow, forest and agriculture. The course of modelled soil moisture shows an increase referring to the pre Whitsun flood event. During the period between the two floods the soil moisture decreased to a relative minimum at high level. With the onset of the Whitsun precipitation the soil moisture increased.
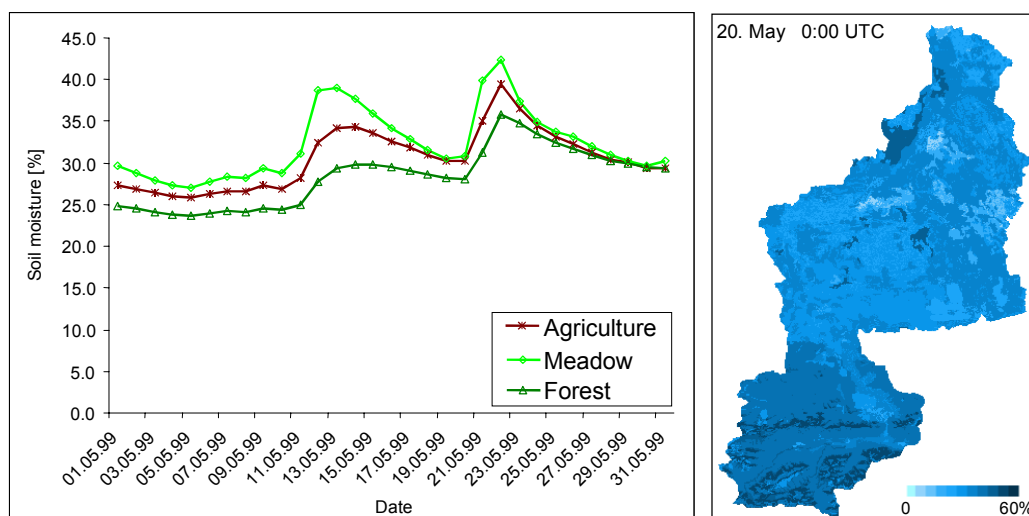
Fig. 6.17: Modelled soil moisture in May 1999 for loam under forest, agriculture and meadow locations (left) and spatially distributed modelled soil moisture previous to the Whitsun flood (right)

This is also reflected in the runoff model results. The calculated development of the saturated areas in the Ammer catchment during the Whitsun flood is animated in the enclosed film in appendix E (saturated areas.avi). For this simulation the Swiss Model forecast, disaggregated by the inverse distance algorithm is opposed to the compared saturation areas. Clearly detectable is that the first rainfall simultaneously produces the first saturated areas. With ongoing precipitation the saturated area extends over the whole catchment.

Two examples for the relation between precipitation and saturated area are given in figure 6.18. On the left side the quick saturation of the soils in accordance to the rainfall intensity at the beginning of the flood event is demonstrated while on the right side the maximum extent of the saturated area is shown.

The also enclosed 3-D spatial animation of the saturated areas (3D saturated areas.avi) illustrates the spatial distribution of the saturated areas within the catchment modelled by the topographic index approach. The film shows that besides the moors, the northern region of the basin, especially the area around Weilheim shows the largest extent of saturated areas. Especially this region was mostly affected by the Whitsun Flood.
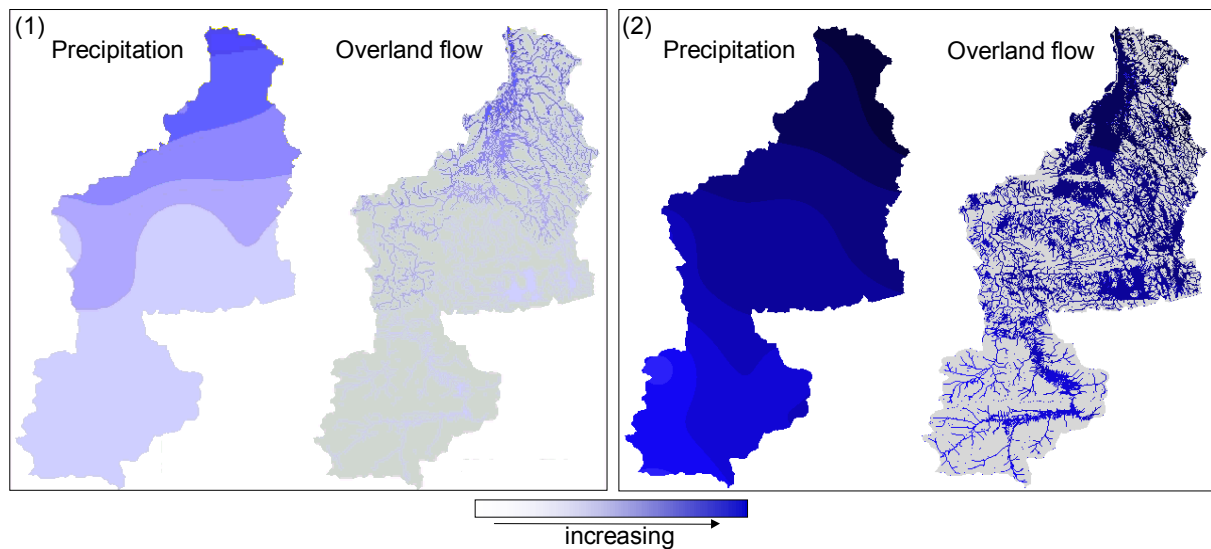
Fig. 6.18: Modelled precipitation (Swiss Model) and saturated areas (PROMET-D) for the beginning of the Whitsun flood (1) and for the maximum extent of the saturated areas (2)

The PROMET modelled soil moisture distribution was used as the boundary condition for the TOPMODEL application.

6.2.3. Flood modelling

As precipitation input data for the calculation of the Whitsun flood, the Swiss Model (SM) operational meteorological forecasts, rain radar data from the DWD rain radar Fürholzen as well as DWD rain gauge data and METEOSAT derived precipitation were used for the flood modelling.

Swiss Model results, initialised by the boundary conditions of DWD's Europa Model, are downscaled to a 100 m grid by applying three different interpolation schemes (as described in chapter 5.2.1): duplicating (SM-d), bilinear interpolation (SM-i) res. a quadratic inverse distance algorithm (SM-id) assuming that the modelled rainfall represents the centre of the 14 km pixel.

Rain radar measurements was corrected by the German Aerospace Centre (DLR), accounting for beam blockage, ground clutter and non-standard drop size distribution. The METEOSAT derived precipitation was computed applying the MSM technique described in chapter 3.3.2.2.1. Both data sets were disaggregated by the duplicating scheme.

No further hydrological model calibration was carried out for this flood event. All necessary parameters were taken from LUDWIG (2000). The specific values of the different runoff simulations are summarised in appendix A respectively in appendix C.

In a first step, a pixel-wise analysis of precipitation data was performed, comparing extracted rainfall intensities of the various data sources to the measurements at rain gauge Weilheim for a 96h-period (Fig. 6.19). The METEOSAT derived precipitation data set is not listed since the algorithm uses the station measurement which is in turn included in the data as the original recordings (see chapter 3.3.2.2).
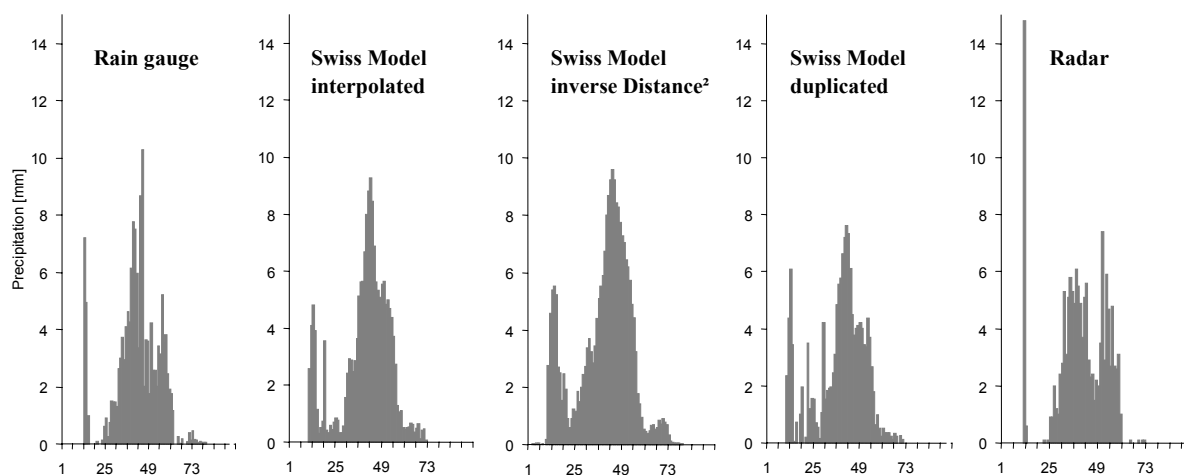
Fig. 6.19: Pixel-wise comparison of rainfall data taken from NWP and rain radar to measured data at the rain gauge Weilheim

Reasonable agreement can be detected in temporal sequence for all precipitation data sets, whereas the intensities vary considerably depending on the chosen data set and disaggregation scheme.

A significant feature can be detected in figure 6.19. Although good agreement with measured data can be delineated for the NWP data, a general overestimation of precipitation can be identified at the beginning of the event, which will consequently lead to an unrealistic filling of the soil storage and will hence reduce its storage capacity resulting in a quicker catchment response in surface runoff. Radar data has the poorest correlation ($R^2 = 0.28$) to measurements and shows a second distinct rainfall maximum towards the end of the event, which is not present in any other data source.

Table 6.4 summarises the statistical result of the pixel-wise data comparison. The coefficient of determination R^2 and the Root Mean Square Error RMS are used as the objective functions to describe the data correlation:

Recorded precipitation at Weilheim $\sum$ = 147.5 mm				
	Swiss Model interpolated	Swiss Model inv. Distance	Swiss Model duplicated	DWD Rain Radar
R^2	0.64	0.69	0.65	0.28
RMS (mm)	1.96	1.40	1.37	2.28
$\sum$ (mm)	222.4	172.2	147.9	142.2

Tab. 6.4: Pixel-wise comparison of precipitation

The spatial distribution of aggregated rainfall over a 96h period shows specific deviations between measured and modelled data (Fig. 6.20) although not as drastic as during the Christopherus flood.
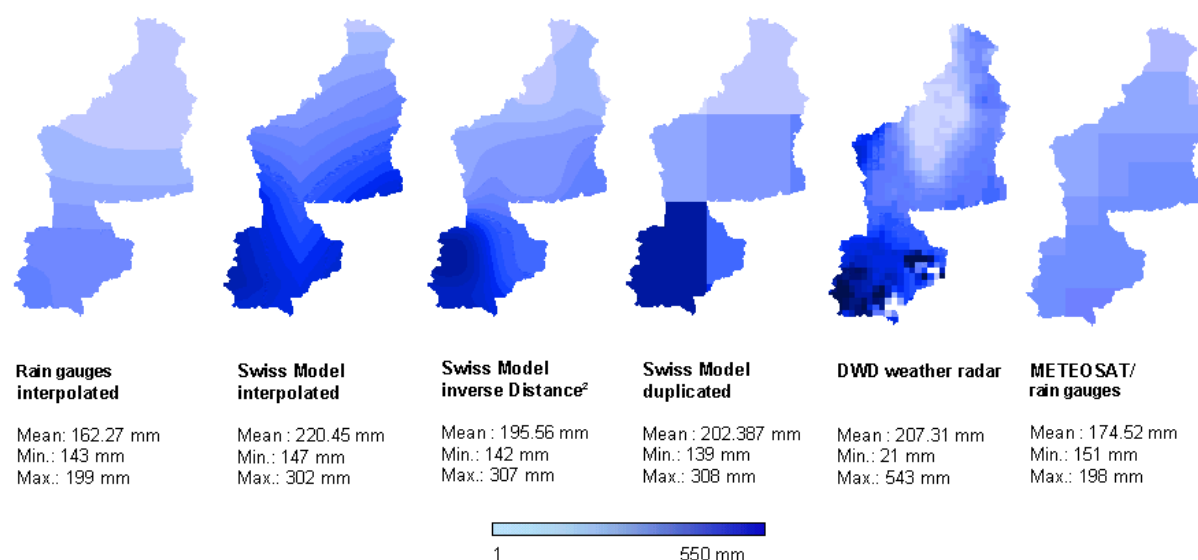
Fig. 6.20: The spatial distribution of aggregated rainfall for the Whitsun flood over a period of 96 hours

While all of the data sets show a positive southbound gradient of areal precipitation, remarkable differences in its intensity become evident. The rain gauges and the METEOSAT derived rainfall report only a low gradient towards the south while Swiss Model and rain radar measurement indicate distinct maxima in the Alps. In particular, the rain radar provides an extremely high variance, which can be explained by effects of ground clutter and beam blockage at the alpine ridges (maximum of 543 mm; minimum 21 mm). The statistical values included in figure 6.20 show that SM-i calculates the highest mean areal rainfall with 220 mm. Besides the rain radar data all other data sets demonstrate a low variance in the minimum precipitation while Swiss Model computes a much higher maxima (about 30 – 60 mm more than the rain gauge data set). The different disaggregated Swiss Model data show the most significant difference in the mean areal precipitation, demonstrating the effect of the selected interpolation algorithm on the original Swiss Model data set. The best quantitative agreement is achieved with SM-id (+ 20.5 %).

The modelled runoff using METEOSAT derived rainfall data delivers the best approximation of the recorded hydrograph at stream gauge Weilheim ($R^2 = 0.94$) though the coefficient of determination is not the highest one (Fig. 6.21.f and Tab. 6.5). The integrated 96 h runoff volume is underestimated by only 3%, while the simulated peak discharge is reduced by 2.5%. The runoff hydrograph shows two peaks with the second one slightly higher and five hours later than the measured one.

a) DWD Rain Gauges
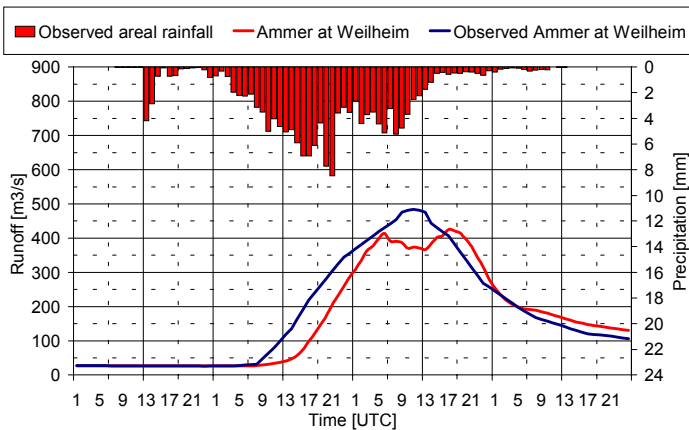
b) Swiss Model bilinear interpolated
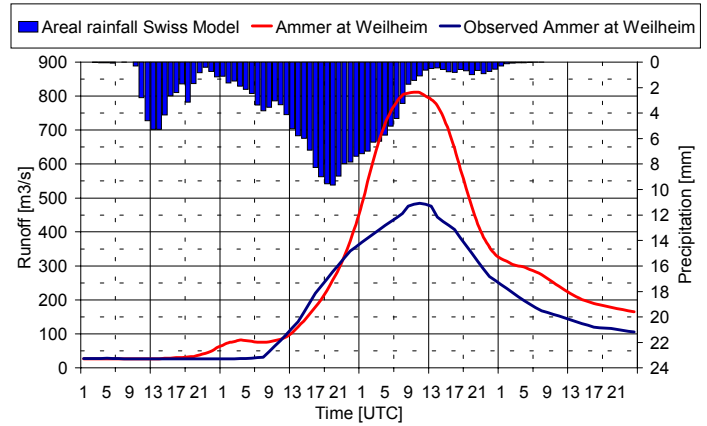
c) Swiss Model inverse distance
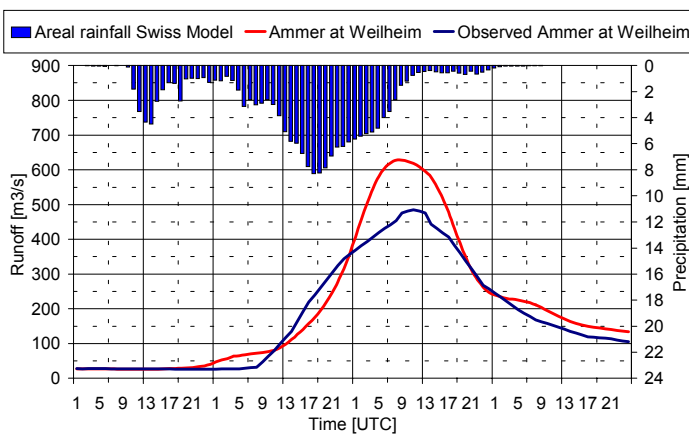
d) Swiss Model duplicated
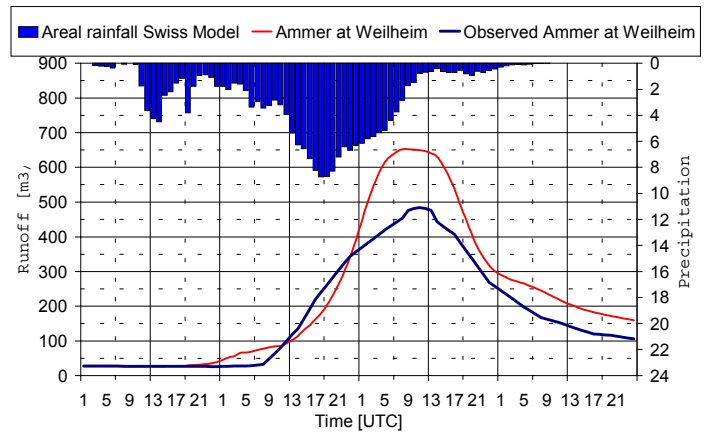
e) rain radar Fürholzen
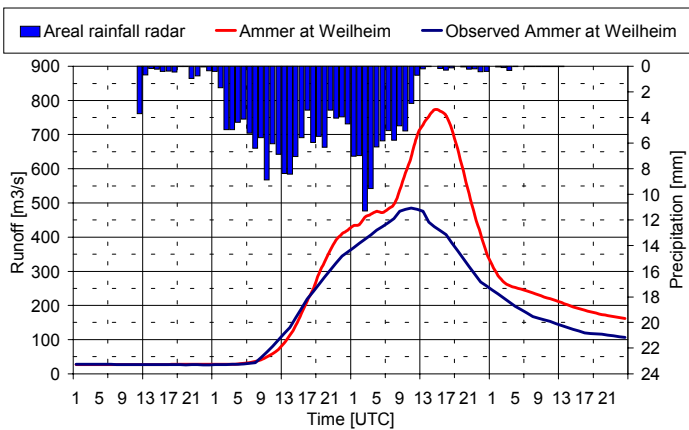
f) MSM
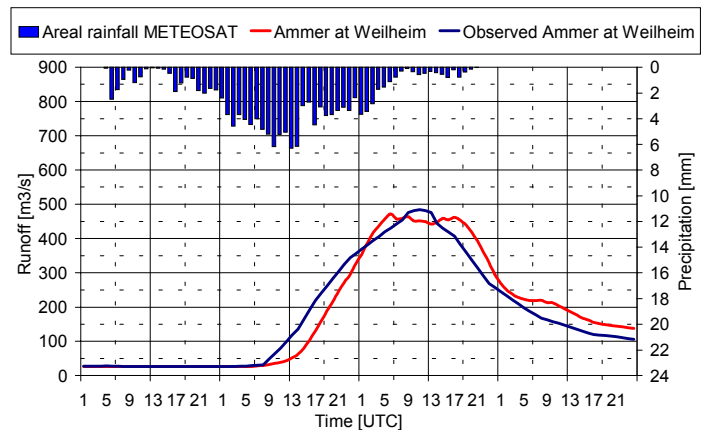
Fig. 6.21.a-f: The hydrological model results of the Whitsun Flood starting on 20 May 1999 at 00:00 UTC. In red are shown the hourly modelled runoff hydrograph applying the referring precipitation input data set (a) DWD rain gauge measurements; b) Swiss Model bilinear interpolated; c) Swiss Model inverse distance; d) Swiss Model duplicated; e) rain radar Fürholzen; f) MSM) and in blue the hourly measured runoff at the stream gauge in Weilheim. Also included in every diagram is the hourly areal rainfall for the Ammer catchment calculated with the referring precipitation data set

	Rain gauge	Swiss Model interpolated	Swiss Model inverse Distance²	Swiss Model duplicated	Radar	METEOSAT MSM
Peak [%]	- 12	+ 67	+ 30	+ 35	+ 59	- 2.5
Volume[%]	- 9	+ 46	+ 15	+ 27	+ 33	+3
Peak Time[h]	- 5, + 6	- 1	- 3	- 2	+ 4	- 5
R²	0.91	0.94	0.95	0.95	0.91	0.94

Tab. 6.5: Statistical key values of flood modelling results. All values are referred to the stream gauge measurements at Weilheim

The results are slightly less accurate when applying the interpolated rain gauge measurements (Fig.6.21.a). The runoff volume is underestimated by 9%, the related peak discharge by 12%. However, compared to measured runoff, this result is still in a reasonable range.

In addition to the systematic errors of rain gauges the underestimation of the calculated runoff applying the rain gauge data set is assumed to be caused by missing spatial precipitation information in the Linder valley. The rain gauge at Linderhof, located in the Linder valley, was not operational during the Whitsun flood period. No measured information is available from this part of the catchment. This fact is also reflected in the aggregated rainfall for the Whitsun flood. Only a slight increasing southward gradient is detectable in the aggregated spatial rainfall image for the rain gauge data set (Fig. 6.20). On the other side a much larger gradient is computed by Swiss Model. A study was carried out dealing with runoff simulations in the Linder valley also for the Whitsun flood (LINDENAU 2000). Also here the applied rain gauge data led to a runoff underestimation compared to the measured runoff at the stream gauge Oberammergau. This underlines the assumption that the precipitation in the southern part of the catchment is underestimated in the rain gauge data set.

The model runs applying the Swiss Model results show a general overestimation of runoff volume (Fig.6.21.b-d). The highest peak runoff is computed applying the bilinear interpolated data set (Fig.6.21.b). The overestimation amounts 67% while using the inverse distance respectively the duplicated data set leads to a 30 % (SM-id) respectively 35 % (SM-d) higher peak runoff. The flood volume is best estimated with Swiss Model data applying the inverse distance data set (15 %). The time displacement of the runoff peak varies from one to three hours depending on the applied data set.

The overestimation of simulated runoff using Swiss Model data can be related to an overestimation of precipitation amount for 20 May 1999, leading to an unrealistic decrease of

soil water deficit advancing the flood event. These divergent initial conditions result in an early rise and a general surplus of modelled flood discharge. The temporally delayed maximum in discharge simulated using the rain radar data is caused by an extreme overestimation of precipitation in the southernmost alpine region, related to difficulties in ground clutter-corrections (TASCHNER et al. 2001).

The modelled runoff results applying the rain radar data leads to good approximation of the rise of the hydrograph (Fig. 6.21.e). This can be traced back to a similar temporal mean areal precipitation distribution for the first 24 hours of the flood event compared to the rain gauge data set (Fig. 6.21.a res. Fig 6.21.e). However in the following the peak runoff is overestimated by 59%. The temporally delayed (4 hours) maximum in discharge simulated using the rain radar data is caused by an extreme overestimation of precipitation in the southernmost alpine region, related to difficulties in ground clutter-corrections (see. Fig 6.20). The coefficients of determination applying the described data sets range from 0.91 for the rain radar and the rain gauge data set to 0.95 for the Swiss model rainfields (Tab. 6.5).

In co-operation with Prof. Bendix from the University of Marburg and Dr. Reudenbach from the University of Bonn an additional study was carried out investigating another meteorological model that derives precipitation from METEOSAT (BENDIX et. al. 2000). The algorithm of the ECST, described in chapter 3.3.2.2. was applied for the Whitsun Flood.

The parameterization of the ECST was adapted to the specific meteorological situation of the Whitsun flood period. The rain rate determination was modelled for a highly convective situation near the Alps under consideration of flow blockage at the alpine ridges. For the weather development radiosoundings of Udine (20.5.) and Payenne (21-23.5) were available. In comparison to the MSM technique this METEOSAT derived precipitation is not based on any ground precipitation measurements. The result applying this precipitation data set is presented in figure 6.22.
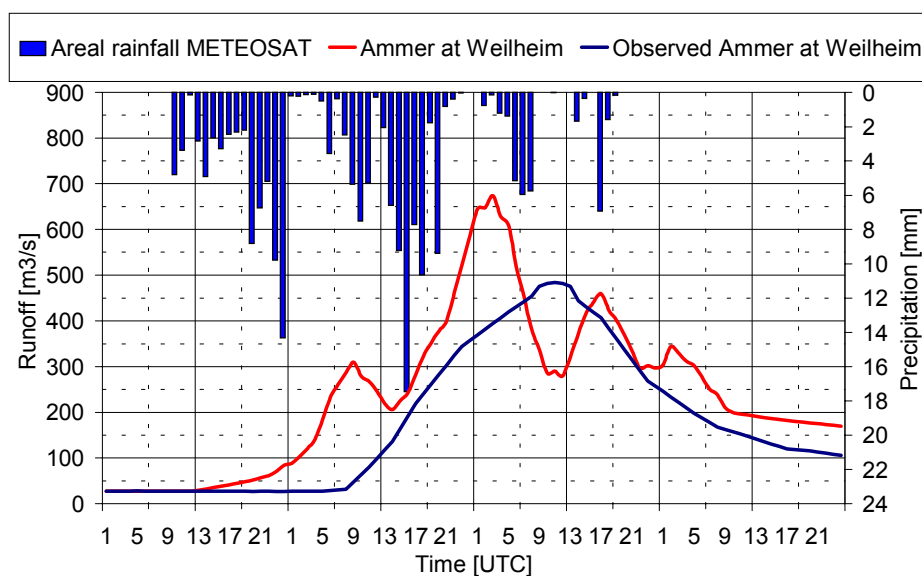
Fig. 6.22: The hydrological model results of the Whitsun Flood applying the ECST data set (starting on 20. May 1999 at 00:00 UTC). In red is shown the hourly modelled runoff hydrograph applying the ECST METEOSAT data set and in blue the hourly measured runoff at the stream gauge in Weilheim. Also included is the hourly areal rainfall for the Ammer catchment calculated with the precipitation data set

The runoff peak volume (39%) and the discharge volume (33%) are clearly overestimated Instead of a more homogeneous temporal rainfall distribution, the calculated precipitation is characterised by several distinctive peaks with high precipitation rates. The modelled hydrograph shows two major peaks which are in accordance to the model results computed with the rain gauge data set in terms of temporal distribution. Like in the model run applying the Swiss Model results an early rise in the hydrograph is dedectable due to an overestimation of precipitation at the beginning of the event. The coefficient of determination however shows the lowest value (0.69) for this applied data set.

6.2.4. Sensitivity analysis

6.2.4.1 Radial Shift

As for the Christopherus Flood also for the Whitsun flood the radial shift of the precipitation fields was carried out applying Swiss Model results disaggregated by duplicating. Areal precipitation and aggregated rainfall along with the related hydrograph simulations were calculated, using the eight differently shifted rainfall fields referring to the adjacent cells (further details are described in chapter 6.1.2.1)

Surveying a larger domain of NWP model data, a significant precipitation gradient can be detected approaching the Alps (Fig. 6.23.g-i). Consequently, shifting the rain field north

results in a basin-wide increase of areal precipitation, while shifting south provides greater similarity to the interpolated rain gauge data (Fig. 6.23.a-i; Tab. 6.6). Best agreement is achieved with rainfall fields original located north-east.

This is also reflected in the hydrographs (Fig. 6.24.a-i). An obvious overestimation of the flood is modelled applying the previously southerly located rainfall fields (Fig. 6.24.g-i), while the use of the originally northerly positioned ones show the best correspondence of modelled and measured runoff (Fig. 6.24.a-c; Tab. 6.6). Also the use of the previously westerly located rainfall field is in accordance to the measured runoff (Fig. 6.24.d). The originally easterly located rainfall field has less effect compared to the result computed with the original data set (Fig. 6.24.f).

This procedure of rain field shifting may not be scientifically correct in terms of a mathematical or statistical description, but can generally be applied to define the sensitivity of the hydrological response to errors in the spatial localisation of rainfall predictions.
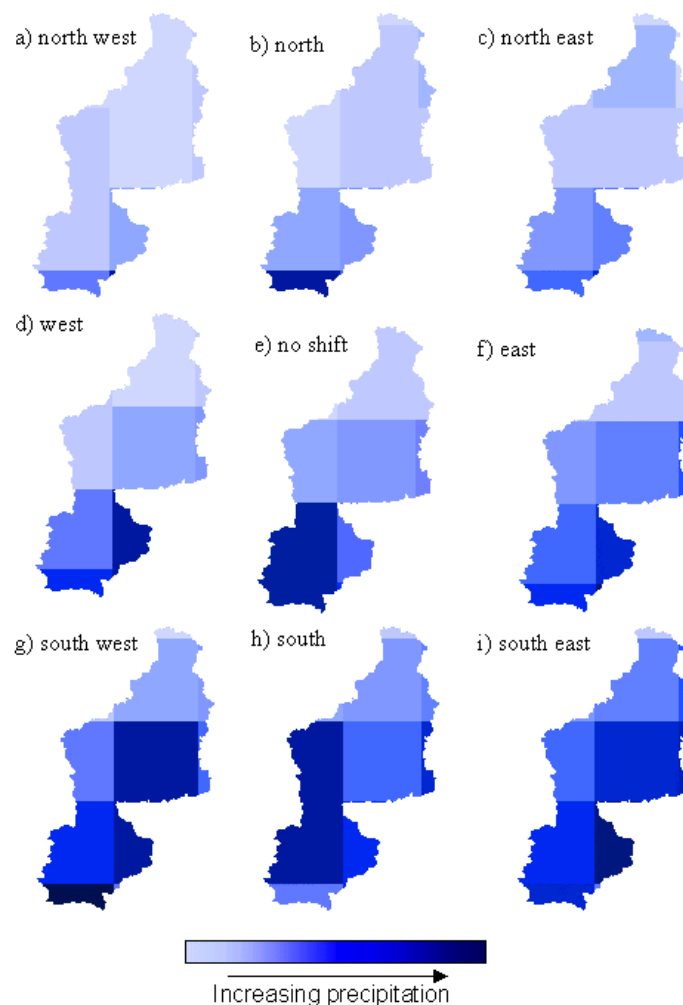
Fig. 6.23.a-i: Radial shift: Aggregated rainfall for the Whitsun flood event applying duplicated Swiss Model forecast
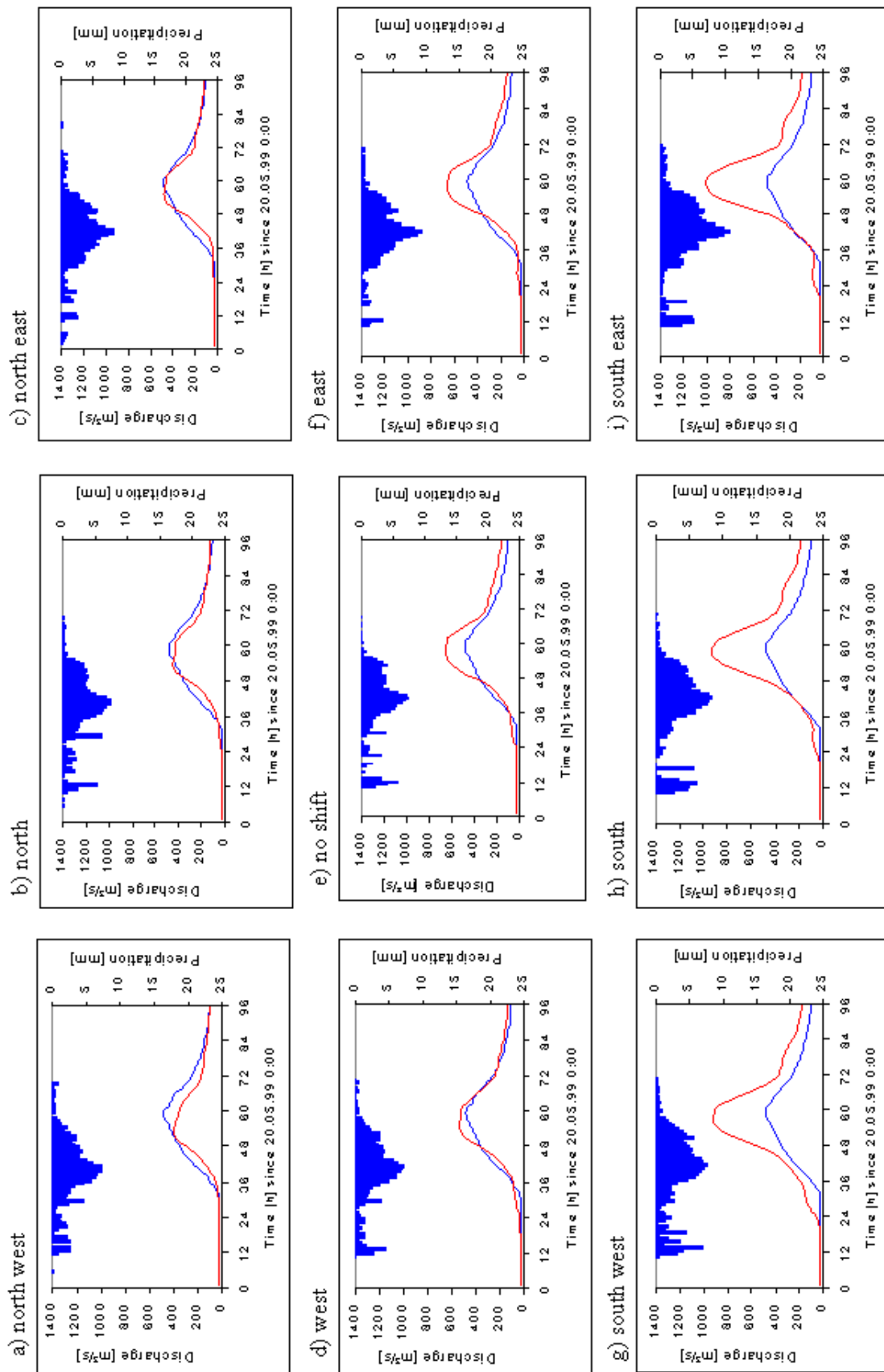
Fig. 6.24.a-i: Radial shift: Modelled runoff hydrograph (in red) for the Whitsun flood event applying shifted duplicated Swiss Model forecast precipitation fields compared to measured runoff (in blue) at the gauge Weilheim

Original located precipitation fields	Areal Precipitation [%]	Flood peak entry time [h]	Flood peak discharge [%]	Flood volume [%]	Coefficient of determination
None	24.7	-2	35	27	0.95
North	-10.5	-6	-8.3	-10.2	0.96
North-east	-1.0	-4	-1.4	-8.0	0.94
East	20.3	-1	36.1	22.0	0.93
South-east	52.3	-1	108.5	72.5	0.93
South	49.3	-1	91.9	66.0	0.94
South-west	53.6	-2	91.3	75.3	0.96
West	10.3	-4	10.7	8.1	0.96
North-west	-10.5	-6	-16.6	-19.7	0.95

Tab. 6.6: Statistical key values of the different shifted rainfall fields calculated by applying duplicated Swiss Model forecast referring to the measured runoff at the stream gauge in Weilheim respectively to aggregated rainfall fields of the rain gauge data set

6.2.4.2. Combined Precipitation Data Set

Another study was carried out accounting for the obvious overestimation of Swiss Model precipitation during the first 24 hours of the Whitsun Flood event as compared to the Weilheim rain gauge recordings (Fig. 6.19). This overestimation of precipitation at 20 May 1999 has the consequence of an overestimated simulated runoff using Swiss Model data due to early soil saturation.

To estimate the effect of data fusion the first 24 hours of Swiss Model forecast are substituted with the data from the spatially interpolated rain gauge data set. This procedure assumes that the rain gauge measurements are available as quasi online data and the forecast would still remain the same for the following 72 hours.

Combining rain gauge data with different disaggregated Swiss Model rainfields shows a higher similarity between measured and modelled hydrograph which is related to the more realistic initial conditions of the model run (Fig. 6.24). The computed beginning rise of the hydrograph is of a higher accuracy, however the ongoing course of the hydrograph rise is less steep than the measured one. The overestimation of the peak and runoff volume still remains for all different disaggregated data sets but is drastically reduced especially for the interpolated Swiss Model data (Table 6.7). This effect can be related to an overall reduction of the areal precipitation. However the coefficient of determination has decreased slightly.
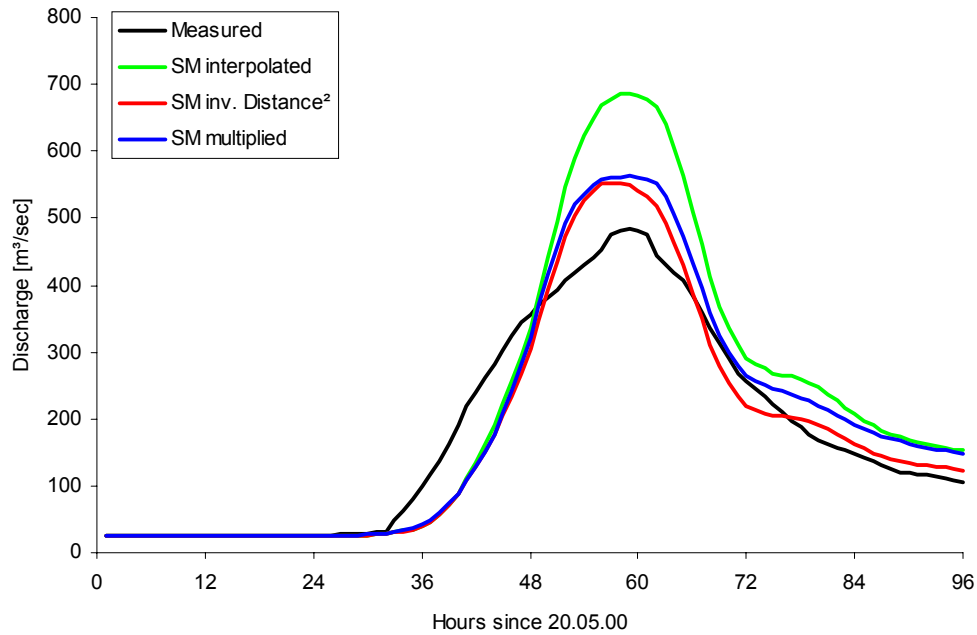
Fig. 6.25: Hydrological model results of the Whitsun flood event using the combined precipitation data set (first 24 hours with rain gauge data, following 72 hours Swiss Model)

Nevertheless the presented approach of combined precipitation data sets (online measurements and meteorological model results) shows promising results and offers perspectives for future applications in real time flood forecasting applying meteorological data fusion.

Data Set	Mode	Mean areal rainfall [mm]	Peak Volume [m³/s]	Flood Volume [m³/s]	R²
Measured	-	162.3	484.6	17409	-
Combined	Measurements + Swiss Model dupl.	162.1	559.9	18694	0.93
Combined	Measurements + Swiss Model interpolated	198.4	687.5	20980	0.91
Combined	Measurements + Swiss Model. distance	136.4	548.2	17208	0.93
Swiss Model	duplicated	202.4	652.2	22150	0.95
Swiss Model	interpolated	220.5	811.2	25429	0.94
Swiss Model	inv. Distance²	195.6	628.1	20086	0.95

Tab. 6.7: Comparison of statistical key values of the flood model runs for the Whitsun flood applying different disaggregated Swiss Model forecast and data fusion rainfields

7. Summary and Conclusion

The remarkable increase of extreme flood events in the last years has lead to an urgent social and economic demand for improved prediction and sustainable prevention. Counteracting measures require reliable information on the characteristic features of floods, the temporal evolution and spatial extent of runoff volume and peak, which can be investigated by means of sophisticated simulation techniques.

One of the major tasks in hydrology is to link recent progress in atmospherical and hydrological sciences to improve flood forecasting and control. The main objective of the EU-funded project RAPHAEL was to investigate the current potential and the possibilities of flood forecasting in terms of a synergetic use of meteorological and hydrological models in selected alpine testsites and testcases. The presented study, prepared within the RAPHAEL project, focused this issue on two selected flood events in one of the project target areas, namely the Ammer catchment.

The Ammer catchment is located south-west of Munich in the Bavarian Alps and prealpine foreland covering an area of 709 km² to the catchment outlet at gauge Fischen. It is characterised by physiographic heterogeneity in terms of morphology, pedology and climatology. From the steep mountainous regions of the Bavarian Alps (> 2100 m asl) the Ammer river heads north through the smoothly reliefed molassic structures of the alpine foreland, before entering Lake Ammer (533 m asl). The mean annual streamflow in the Ammer river of 16.6 m³/s at the gauge Fischen averages a pluvio-nival runoff regime, in which maximum flow rates result from a transition of snow melt periods in spring and summerly precipitation maxima. Meteorological measurements indicate a N – S gradient of decreasing temperature and increasing precipitation. The mean annual amount of precipitation is 1200 mm, ranging from 900 mm in the north to over 1800 mm in the mountains. About 50 % of the catchment is forested, while the rest is mainly in agricultural use (90 % pasture, 10 % crop).

Flood modelling in the Ammer watershed was performed in this study applying the hydrological model PROMET-D. It is characterised by a model link established between the physically based SVAT model PROMET (MAUSER and SCHÄDLICH 1998) and an enhanced distributed GIS-version of the conceptual rainfall-runoff model TOPMODEL (BEVEN and KIRKBY 1979; LUDWIG 2000).

The physically based SVAT-model PROMET is based on the Penman-Monteith equation (MONTEITH 1978), which calculates the actual evapotranspiration as a function of water availability, radiation balance and the physiological regulation mechanisms of heterogeneous plant stands. The multi-layer soil water module of PROMET computes the soil water content, as a function of infiltration, exfiltration and capillary rise, applying a simplified solution of the Richards equation (EAGLESON 1978 a-g) while a two-layer snow module describes the accumulation and melting processes according to energy balance terms and calculating the melt water runoff (TODINI 1996, TASCHNER et al. 1998).

The TOPMODEL-PROMET interface is characterised by assessing outputs of PROMET (evapotranspiration, snowmelt, soil moisture to initialise the flood event) to hourly update the water balance terms of the runoff model in a distributed sense.

The TOPMODEL approach within PROMET-D calculates runoff formation and stream discharge in hourly resolution. The basic assumptions of the TOPMODEL concept are adopted and in parts extended by LUDWIG (2000).

Runoff generation is computed for each pixel taking into account local variations of meteorology, evapotranspiration, snow cover, soil texture and landuse. Herefore evapotranspiration and snow melt calculated by PROMET are applied. Landuse information is used to estimate the soil root depth while from the soil texture map the field capacity can be derived. Both are applied to balance the soil root zone at every time step and each pixel. Infiltration excess for each pixel is calculated applying the GREEN and AMPT approach (1911).

One of the major extensions of the TOPMODEL approach within PROMET-D is the evapotranspiration-soil-topographic index introduced by LUDWIG (2000). The formerly used static distribution of index-values is replaced by a dynamic course of distributed index values representing the seasonal course of saturation excess runoff potential in the catchment. It takes into account the variability of plant activity by means of transpiration, rooting and surface roughness and its influence on the variable contributing area to surface runoff. This enhancement consequently leads to a more dynamic description of runoff formation, allowing not only for spatial changes in the location of the variable source-areas contributing to surface runoff, but also creating a temporal course in the separation of runoff components. Saturation probability hence decreases during the growing season but increases in the winter months.

Infiltration and saturation excess are added and undergo an overland flow algorithm based on the application of time-area functions. The time of concentration is calculated by employing

the SCS-method (SOIL CONSERVATION SERVICE 1983). The flow velocity in the channel is computed using the Manning-Strickler equation.

The model was performed in hourly time steps on a 100 m grid resolution. No special event calibration was carried out. All necessary model parameters were derived from a previous study (LUDWIG 2000).

Various rainfall input data sources were available to perform flood forecasting in the Ammer catchment:

- observation data from DWD rain gauges and climatic stations,

- NWP simulated precipitation in forecast mode, hourly time steps and a spatial resolution of 10 -14 km,

- NWP simulated precipitation in analysis mode, hourly time steps and a spatial resolution of 10 -14 km,

- rain radar observations of precipitation provided by the DWD rain radar in Fürholzen in a grid resolution of 1 by 1 km (sampled to a 1-hour time step) and

- METEOSAT derived rainfall fields with a spatial resolution of 5 km.

Since the hydrological model is performed on a 100 m grid and an hourly time step, all precipitation data have to be processed to these application scales.

The DWD climatic station measurements are recorded three times a day (7:30, 14:30, 21:30). In order to generate the meteorological input parameter fields for hourly modelling, these measurements have to be temporally and spatially interpolated. This is performed within the spatial modeller of PROMET.

DWDs rain gauge measurements were made available as continuous records. They were sampled to an hourly resolution and spatially interpolated. To all measured precipitation a correction procedure was applied (SCHULLA 1997).

Several disaggregation schemes were applied to overcome the resolution gap between NWP results, rain radar data, METEOSAT derived precipitation and the hydrological model.

NWP data are downscaled to a 100 m grid by applying different interpolation schemes, such as simple disaggregation of the original resolution assuming a constant distribution over the pixel area, linear and squared inverse distance interpolation.

The downscaling of the rain radar and METEOSAT derived precipitation data sets was performed by using a simple disaggregation of equal distribution onto the 100 m model grid.

Two selected flood events were analysed in the presented study:

- the Christopherus flood (July 17th – 20th 1997) and

- the Whitsun flood (May 20th – 23rd 1999) being the most hazardous flood event ever recorded in the Ammer basin, for which Swiss Model forecast, rain radar interpreted precipitation and METEOSAT derived precipitation were available.

These two events represent very different storms, both in terms of quantities and origin and are therefore considered as suitable examples to interpret the effectiveness of the meteo-hydro model synergy.

For the computation of the Christopherus flood (17.-20.7.1997) DWD rain gauge measurements, climatic station recordings and rainfall fields of four NWP models in analysis mode and forecast mode were available. The disaggregation of the NWP outputs to the grid resolution of PROMET-D was performed applying the duplicating method.

Applying the DWD rain gauge data set leads to the most accurate hydrograph simulation. The peak runoff volume difference is –1.5 % and the overall discharge volume is underestimated by 10.8 %. The resulting coefficient of determination reaches 0.65. The model calculation using the DWD climatic station data set leads to similar results in terms of the shape of the hydrograph. It is closely approximated but shows a time shift of 9 hours. This possibly can be traced back to the temporal interpolation of the climatic station measurements.

The results applying the meteorological data are widespread in both the analysis and forecast mode, with a general incapacity to accurately represent the first measured peak. The runoff volume is over- but also underestimated (+10.2% to –24.5%) depending on the applied data set. The same can be observed for the peak runoff volume (+16.1% to -68.6%). The peak entry time is in general too early (up to 5 hours). Only the runoff computations using Swiss Model results in the analysis mode lead to a four hours delayed peak.

Comparing runoff results of analysis and forecast mode data show only minor deviations in the hydrograph shape applying BOLAM and Meso-NH data. An improvement can be observed due to the runoff course using MC2 and Swiss Model data in the forecast mode.

High resolution NWP model data were made available from BOLAM (3.5 km) and Meso-NH (2 km), with Meso-NH additionally providing a data set descending from a model run implementing an ice-phase algorithm. However these NWP data cover only the starting hours of the flood event. In comparison to the standard resolution mode applying BOLAM in the high resolution mode improves the modeled runoff. Much better agreement to measured conditions is achieved only using the Meso-NH ice-phase data.

A sensitivity analysis was carried out to evaluate the impact of shifted precipitation fields of the NWP model outputs on the hydrological model performance. To account for a possibly inexact spatial coverage of the meteorological model, a one-pixel (10 km for BOLAM, MC2 and Meso-NH or 14 km for Swiss Model) radial shift of the modelled precipitation field in analysis mode was performed for 8 directions. The computed runoff results are widespread within each NWP data set of shifted rainfall fields. The biggest difference of calculated runoff is achieved applying the MC2 and Swiss Model data sets.

For the computation of the Whitsun flood rain gauge measurements, Swiss Model forecast, rain radar data and two data sets of METEOSAT derived precipitation were available.
The Swiss Model forecast was disaggregated to the hydrological model resolution of 100 m by applying three different schemes: duplicating the original 14 km pixel, linear interpolation and a quadratic inverse distance algorithm. Rain radar data and METEOSAT derived precipitation were downscaled by using the method of duplicating.

The modelled runoff at the Weilheim stream gauge, using the rain gauge data set, represents well the measured runoff ($R^2 = 0.91$). The calculated 96 h runoff volume is underestimated by only 9%, while the simulated peak discharge is reduced by 12 %.
The model runs applying the Swiss Model results show a general overestimation of runoff volume (15- 46%) and peak discharge (30 - 67%) with a corresponding time displacement of only one to three hours. The overestimation of simulated runoff using Swiss Model data is related to an overestimation of precipitation amount for 20 May 1999. This leads to an unrealistic decrease of soil water deficit advancing the flood event.
The temporally delayed (4 hours) overestimated maximum in discharge (59%) simulated using the rain radar data is caused by an extreme overestimation of precipitation in the southernmost alpine region, related to difficulties in ground clutter-corrections.
Similar results in runoff modelling compared to the rain gauge data set are obtained by applying the METEOSAT derived precipitation data that takes into account the rain gauge measurements. Using the precipitation fields calculated by the ECST approach (BENDIX et al. 2000) leads to an overestimation of the peak runoff volume by 39% and the discharge volume by 33 %. The peak entry time is 9 hours too early.
Two sensitivity analyses were conducted for the Whitsun flood.

On the one hand the first 24 hours of the Swiss Model forecast were replaced by rain gauge measurements. This leads to an improved runoff calculation which is related to the more realistic decrease of soil water deficit advancing the flood event.

To account for a possibly inexact spatial basin coverage of the meteorological domain, a radial shift of the modelled mesoscale precipitation field by one NWP cell was performed for 8 directions. The results show a large variety of possible runoff results that are caused by a slight deviation in the spatial location of rainfall fields computed by NWP model.

Different hydrological models like e.g. PROMET-D, have shown their fundamental capability to simulate floods up to a reasonable degree of certainty in numerous applications. But no matter how good physically based and spatially distributed hydrological models are in terms of process description, they still depend on the accuracy of their input data. Until now, all of the available data sources are only applicable for flood modelling at the catchment scale with a number of limitations.

Conventional rain gauging lacks accuracy on account of several well-known, but hardly quantifiable error-sources, such as wind turbulence, evapotranspiration or wetting. Correction-algorithms can only counteract these systematical errors based on empirically determined coefficients, which are generally not transferable in time and space.

Rain radars provide images of spatially distributed rainfall intensities at a high temporal and for flood modelling at the scale of the Ammer basin, reasonable spatial resolution. However, these intensities are provided in coarse intervals, due to high uncertainties in the reflectivity equations. The exact knowledge about the actual drop size distribution or even the phase of precipitation is generally not available and hence requires complex correction procedures. In the present study, additional problems emerge from the relatively far distance (~ 80 km) of the radar, and the beam blockage and ground clutter. Due to this the application of rain radar data is critical in Alpine catchments, since radar beam obstruction and ground clutter cannot be prevented in rugged terrain. An increase of radar beam angle would introduce additional problems in terms of phase interpretation or precipitation displacement and would consequently lead to even greater uncertainties.

METEOSAT derived precipitation is another source to derive rainfall in a distributed sense. Though several studies deal with image analysis of geostationary data for the determination of spatially distributed rainfall fields, most of them were developed for convective precipitation in the tropics and are not generally transferable to the mid-latitudes. This indirect method of

precipitation measurement furthermore contains error sources being dependent on an unambiguous parameterisation of the current weather situation and the cloud type.

The mesoscale meteorological models are basically the only data source to provide short-term rainfall forecasts in full spatial coverage and high temporal resolution over a large domain. Disadvantages for flood forecasting at a catchment size like the Ammer basin descend from the very coarse spatial resolution (10-14 km), which makes disaggregating and downscaling of data necessary and hence introduces an additional error source. The model accuracy largely depends on the initialising boundary conditions of models working at even larger scales like e.g. the Europa Modell of the German Weather Service or the ECMWF.

The coarse spatial resolution of NWP models cannot represent the high resolution structures of rainfields in complex convective meteorological situations in terms of an adequate localisation in time and space. While the meteorological models proved their potential to accurately determine precipitation sums over a larger array of time and space, subscale applications still require a more accurate temporal and spatial distribution of rainfall in order to provide reliable runoff simulations.

Even minor deviations in NWP results are crucial for flood modelling at the catchment scale. They largely affect the basinwide availability of water for flood generation, which consequently leads to major uncertainties in flood simulations.

Furtherly, the complex physics, simulated in the meteorological models, require sophisticated algorithms and high computer-power, which only few institutions are capable of providing.

As shown for the selected flood events, at the current stage of research a high variability in flood modelling results still has to be accepted, leading to the conclusion that the probability for reliable flood forecasting in the Ammer catchment based on NWP model outputs is low at present. Nevertheless, as demonstrated for the Whitsun Flood, good results can be obtained under certain circumstances, i.e. foreseeable and stable meteorological situations.

The procedure of rainfield shifting can be generally applied upon NWP data when used for flood modelling, to provide flood forecasting information within a certain range of reliability, defining the minimum and maximum boundary runoff values of possible predictions.

For future applications in practice an assimilation of online-connected rain gauges, rain radar and remote sensing measurements within the meteorological models will be an important step towards more accurate rainfall predictions. Coupled meteo-hydro-models will then be an useful tool for flood warning services.

References

ABBOT, M. B., BATHURST, J. C., CUNGE, J. A., O'CONNELL, P. E. (1986a): An Introduction to the European Hydrological System – Système Hydrologique Européen "SHE". In: J. Hydrol., Vol. 87 (1/2), pp. 45-59.

ABBOT, M. B., BATHURST, J. C., CUNGE, J. A., O'CONNELL, P.E. (1986b): An Introduction to the European Hydrological System – Système Hydrologique Européen "SHE". In: J. Hydrol., Vol. 87 (1/2), pp. 61-77.

ADLER, R. F., NEGRI, A. J. (1988): A satellite infrared technique to estimate tropical convective and stratiform rainfall. In: J. Appl. Meteorol., Vol. 27, pp. 30-51.

ALLEY, W. M., SMITH, P. E. (1982):Distributed Rainfall Runoff Model – Version II. In: Geological Survey open file report, pp. 82-344.

ANIOL, R., RIEDL, J., DIERINGER, M. (1980): Über kleinräumige und zeitliche Variationen der Niederschlagsintensität. In: Meteorol. Rdsch., Vol. 33, pp. 50-56.

ARKIN, P. A. (1979): The relationship between fractional coverage of high cloud and rainfall accumulations during GATE over B-scale array. In: Mon. Wea. Rev., Vol. 107, pp. 1382-1387.

ARKIN, P. A., MEISNER, B. (1987). The relationship between large-scale convective rainfall and cold cloud over the Western Hemisphere during 1982-1984. In: Mon. Wea. Rev., Vol.115, pp. 51-74.

ASENCIO, N., BOUGEAULT, P., CAILLY, C., CUXART, J., DUCROCQ, V., FISCHER, C., HEREIL, P., LAFORE, J. P., MASCART, P., PINTY, J. P., REDELSPERGER, J. L., RICHARD, E., STEIN, J. (1994): Le projet de modèle non-hydrostatique commun CNRM - Laboratoire d'Aérologie: Spécifications Techniques. Laboratoire d'Aérologie. Toulouse.

BACCHI, B., RANZI, R. (Eds.) (2000): RAPHAEL – runoff and atmospheric processes for flood hazard forecasting and control. Final report. University of Brescia. Brescia.

BACH, H., LAMPART G., RIEGLER G., MAUSER W. (1998): First Results of an Integrated Flood Forecast System based on Remote Sensing Data. In: Proceedings of the Second International Workshop on Retrieval of Bio- and Geo-physical Parameters from SAR Data for Land Applications, ESTEC, Noordwijk. ESA-SP-441, pp.463-469.

BACH, H., BRAUN, M., LAMPART, G., RANZI, R. (2000): Estimates of surface parameters via remote sensing for the Toce watershed, In: BACCHI, B., RANZI, R. (Eds.) (2000): RAPHAEL – runoff and atmospheric processes for flood hazard forecasting and control. Final report, University of Brescia. Brescia.

BALDOCCHI, D. D., HICKS, B. B., CAMARA, P. (1987): A canopy stomatal resistance model for gaseous depositions to vegetated surfaces. In: Atm. Environm., Vol. 21, pp. 91-101.

BARDOSSY, A., CASPARY, H. J. (1990): Detection of climate change in Europe by analyzing European atmospheric circulation patterns from 1981 to 1989. In: Theoretical and Applied Climatology, Vol. 42, pp. 155-167.

BARNES, H. H. Jr. (1967): Roughness characteristics of natural channels. In: U.S. Geol. Surv. Water Supply Paper, No. 1849.

BARRETT, E. C. (1970): The estimation of monthly rainfall from satellite data. In: Mon. Wea. Rev., Vol. 98, pp. 322-327.

BAUMGARTNER, A., LIEBSCHER, H.-J. (1990): Lehrbuch der Hydrologie, Band 1 Allgemeine Hydrologie. Gebrüder Bornträger Verlag. Berlin.

BAYERISCHER KLIMAFORSCHUNGSVERBUND (Ed.) (1996): Klimaatlas von Bayern. Bay.Forklim, Meteorologisches Institut, University of Munich, München.

BAYERISCHES GEOLOGISCHES LANDESAMT (Ed.) (1976): Bericht über hydrogeologische Untersuchungen im Schotterfeld zwischen Murnau und Weilheim. München, unpublished.

BAYERISCHES LANDESAMT FÜR STATISTIK UND DATENVERARBEITUNG (1991/1995): Ergebnisse der Flächenerhebung in Bayern. In: Statistisches Jahrbuch für Bayern.

BAYERISCHES LANDESAMT FÜR WASSERWIRTSCHAFT (1978): Verzeichnis der Bach- und Flußgebiete in Bayern, mit einem Gewässeratlas 1:200000. München.

BAYERISCHES LANDESAMT FÜR WASSERWIRTSCHAFT (Ed.) (1997): Deutsches Gewässerkundliches Jahrbuch – Donaugebiet 1991, 1992. München.

BAYERISCHES LANDESAMT FÜR WASSERWIRTSCHAFT (Ed.) (1998): Spektrum Wasser 1: Hochwasser. München.

BAYERISCHES LANDESVERMESSUNGSAMT (Ed.) (1997): Amtliche topographische Karten CD, Bayern (Süd).München.

BECKER, A. (1975): The integrated hydrological catchment model EGMO. Int. Symposium and Workshop Appl. Math. Models in Hydrology and Water Res. Systems, Bratislava. In: Hydrol. Sci. Bull., Vol. 21, No. 1.

BECKER, A., SERBAN, P. (1990): Hydrological Models for Water Resources Systems Design and Operation. Operational Hydrology Report No. 34, World Meteorological Organisation, Geneva.

BELL, F.G. (1983): Engineering properties of soils and rocks, 2. Edition, Butterworths, London.

BENDIX, J (1997): Adjustment of the convective stratiform technique (CST) to estimate 1991/93 El Niño rainfall distribution in Ecuador and Peru by means of Meteosat-3 IR data. In: Int. J. Remote Sensing, Vol. 18, pp. 1387-1394 & 2707.

BENDIX, J., REUDENBACH, C., TASCHNER, S., LUDWIG, R., MAUSER, W. (2000): Retrieval konvektiver Niederschläge in Mitteleuropa mit Fernerkundung und Modellen, In: DLR Mitteilungen 2001-02; pp. 69-78.

BENOIT, R., DESGAGNÉ, M. (1996): Explicit condensation and Foehn modelling for the Brig 1993 flash flood case of MAP. In: Proceedings of 7th Mesoscale Conference of the AMS, Reading, UK, pp. 252-254.

BENOIT, R., DESGAGNÉ, M., PELLERIN, P., PELLERIN, S., DESJARDINS, S., CHARTIER, Y. (1997): The Canadian MC2: a semi-lagrangian, semi-implicit wide-band atmospheric model suited for fine-scale process studies and simulation. In: Mon. Wea. Rev., Vol. 125, pp. 2382-2415.

BENOIT, R., BUZZI, A., BINDER, P., COSMA, S., KAUFMANN, P., RICHARD, E. (2000): Meteorological simulations of some heavy precipitation events. In: BACCHI, B., RANZI, R. (Eds.) (2000): RAPHAEL – runoff and atmospheric processes for flood hazard forecasting and control. Final report. University of Brescia. Brescia.

BERGSTRÖM, S. (1976): Development and application of a conceptual runoff model for Scandinavian catchments. In: SMHI Report RHO, No. 7.

BERZ, G. (1999): Naturkatastrophen und Klimaänderung - Befürchtungen und Handlungsoptionen der Versicherungswirtschaft. In: DEUTSCHER WETTERDIENST (Ed.): Klimastatusbericht 1999. Offenbach.

BEVEN, K J. (1984): Infiltration into a class of vertically non-uniform soils. In: Hydrol. Sci. J., Vol. 29, pp. 425-434.

BEVEN, K. J. (1989): Changing ideas in hydrology: The case of physically-based models. In: J. Hydrol., Vol. 105, pp. 157-172.

BEVEN, K. J., KIRKBY, M. J. (1979): A physically based variable contributing area model of basin hydrology. In: Hydrol. Sci. Bull, Vol. 24(1), pp. 43-69.

BEVEN, K. J., WOOD, E. F. (1983): Catchment geomorphology and the dynamics of runoff contributing areas. In: J. Hydrol., Vol. 65, pp. 139-158.

BEVEN, K. J., WOOD, E. F. (1993): Flow routing and the hydrological response of channel networks. In: BEVEN, K. J, KIRKBY, M.J. (Ed), Channel Network Hydrology, Wiley, Chichester, Chapter 5.

BEVEN, K. J., QUINN, P., ROMANOWICZ, R.,FREER, J., FISHER, J., LAMB, R. (1994): TOPMODEL and GRIDATB: A users guide to the distribution versions. CRES Technical Report TR110 (2nd Edition), Lancaster University, Lancaster.

BEVEN, K. J., LAMB, R., QUINN, P., ROMANOWICZ, R., FREER, J. (1995): TOPMODEL. In: SINGH, V.P. (Ed): Models of watershed hydrology. Water Resources Publications. Highlands Ranch (Colorado). Chapter 18.

BISCOE, P. V., COHEN, Y., WALLACE, J. S. (1976): Community Water Relations. Daily and Seasonal Changes of Water Potential in Cereals. In: Phil. Trans. Royal Soc. London, Ser. B, No. 273, pp. 565-580.

BISMUTH, C., GARBER, W-D., MERZ, R. (Eds.) (1998): Ursachen der Hochwasserentstehung und ihre anthropogene Beeinflussung. In: Texte des Umweltbundesamtes, No 18/98. Berlin.

BOLZ, H. M. (1949a): Die Abhängigkeit der infraroten Gegenstrahlung von der Bewölkung. Teil I. In: Z. Meteorologie, Vol. 3, pp. 201-203.

BOLZ, H. M. (1949b): Die Abhängigkeit der infraroten Gegenstrahlung von der Bewölkung. Teil II. In: Z. Meteorologie, Vol. 4 , pp. 314-317.

BOUGEAULT, P., BINDER, P., KUETTNER, J. (1998): MAP Science Plan. Zürich. http://www.map.ethz.ch/splan/spindex.htm.

BRONDSTERT, A. (Ed.) (1996): Hochwasser in Deutschland unter Aspekten globaler Veränderung – Bericht über das DFG-Rundgespräch am 9. Oktober 1995 in Potsdam. In: PIK Report No.17. Postdam.

BROOKS, R. H., COREY, A. T. (1964): Properties of Porous Media Affecting Fluid Flow. In: Journ. Irr. Drain. Div., Am. Soc. Civil Engin. IR2, pp. 61-88.

BRUDSAERT, W. (1982): Evaporation into the Atmosphere - Theory, History and Application. D. Reidel pub. Comp, Dordrecht-Boston-London.

BRUNEAU, P., BEVEN, K. J. (1995): Sensitivity to time and space resolution of a hydrological model using digital elevation data. In: Hydrological Processes, Vol. 9, pp. 69-81.

BUDYNCUK, S. (1996): Aufbau und Nutzung eines Geographischen Informationssystems für die Hochwassermodellierung im Einzugsgebiet der Ammer, unpublished Diploma thesis, University of Munich. München.

BUZZI, A., FANTINI, M., MALGUZZI, P., NEROZZI, F. (1994): Validation of a limited area model in cases of Mediterranean cyclogenesis: surface fields and precipitation scores. In: Meteorol. Atmos. Phys., Vol. 53, pp. 137-153.

CARDINALI, C., CAIAN, M., PAILLEAUX, J., TARTAGLIONE, N., BUZZI, A., LAVAGNINI, A. (1998): An intercomparison between a global variable mesh and two limited area models on a case of rapid cyclogenesis. In: Meteorology and Atmospheric Physics, Vol. 65, pp. 93-111.

CARMAN, P. C. (1937): Fluid Flow through Granular Beds. In: Trans. Inst. Chem. Eng., No. 15, pp. 150-166.

CASPARY, H. J. (1998): Markieren die Winterhochwasser 1990 und 1993 das Ende der Stationarität in der Hochwasserhydrologie infolge von Klimaänderung?. In: Wasser und Boden, Vol. 47 (3), pp. 18-24.

CHEN, H. (1996): Object Watershed Link Simulation (OWLS). PhD Thesis. Oregon State University. Corvallis (Oregon).

CIARAPICA, L., TODINI, E. (2002): TOPKAPI: a model for the representation of the rainfall-runoff process at different scales. In: Hydrological Processes, Vol. 16, pp.207-230.

CLARK, C. O. (1945): Storage and unit hydrograph. In: Trans. Am. Soc. Civil Eng., Vol. 110, pp. 1419-1488.

CRAWFORD, N. H. and LINSLEY, R. K. Jr. (1966): Digital simulation in hydrology: Stanford Watershed Model IV. In: Technical Report No. 39. Department of Civil Engineering, Stanford University. Stanford (California).

De ROO, A.P.J., WESSELING, C. G. and VAN DEURSEN, W. P. A. (2000): Physically Based River Basin Modelling within a GIS: the LISFLOOD Model. In: Hydrological Processes, Vol. 14, pp. 1981-1992.

DOBEN, K., FRANK, H. (1983): Erläuterungen zur Geologischen Karte von Bayern 1:25000, Blatt Nr. 8333 Murnau. Bayerisches Geologisches Landesamt, München.

DYCK, S., PESCHKE, G. (1995): Grundlagen der Hydrologie, 3. Edition, Verlag für Bauwesen, Berlin.

EAGLESON, P. S. (1978 a): Climate, Soil and Vegetation, 1. Introduction to Water Balance Dynamics. In: Water Resour. Res., Vol. 14, pp. 705-712.

EAGLESON, P. S. (1978 b).: Climate, Soil and Vegetation, 2. The Distribution of Annual Precipitation Derived from Observed Storm Sequences. In: Water Resour. Res., Vol. 14, pp. 713-721.

EAGLESON, P. S. (1978 c): Climate, Soil and Vegetation, 3. A Simplified Model of Soil Movement in the Liquid Phase. In: Water Resour. Res., Vol. 14, pp. 722-730.

EAGLESON, P. S. (1978 d): Climate, Soil and Vegetation, 4. The Expected Value of Annual Evapotranspiration. In: Water Resour. Res., Vol. 14, pp. 731-739.

EAGLESON, P. S. (1978 e): Climate, Soil and Vegetation, 5. A Derived Distribution of Storm Surface Runoff. In: Water Resour. Res., Vol. 14, pp. 741-748.

EAGLESON, P. S. (1978 f): Climate, Soil and Vegetation, 6. Dynamics of the Annual Water Balance. In: Water Resour. Res., Vol. 14, pp. 749-764.

EAGLESON, P. S. (1978 g): Climate, Soil and Vegetation, 7. A Derived Distribution of Annual Water Yield. In: Water Resour. Res., Vol. 14, pp. 765-776.

EWEN, J. (1995): Contaminant transport component of the catchment modelling system SHETRAN. In: TRUDGILL, S. T. (Ed.): Solute Modelling in Catchment Systems, Wiley, Chichester, UK. pp. 417-441.

FABRY, F., BELLON, A., DUNCAN, M. R., AUSTIN, G. L. (1994): High resolution rainfall measurements by radar for very small basins: the sampling problem reeaxamined. In: J. of Hydrol., Vol. 161, pp. 415-428.

FELDMANN, L. (1990): Jungquartäre Gletscher- und Flußgeschichte im Bereich der Münchener Schotterebene. PhD thesis University Düsseldorf. Düsseldorf.

FETZER, K. D. (1986): Erläuterungen zur Standortkundlichen Bodenkarte von Bayern, München-Augsburg und Umgebung. Bayerisches Geologisches Landesamt, München.

FISHER, N. I., T. LEWIS, EMBLETON, B. J. J. (1987): Statistical Analysis of Spherical Data, Cambridge University Press. Cambridge.

FOLLANSBEE, W. A. (1973). Estimation of Average Daily Rainfall from Satellite Cloud Photographs. In: NOAA Tech. Memo. NESS 44, Washington, DC.

FRANCHINI, M., WENDLING, J., OBLED, C., TODINI, E. (1996): Physical interpretation and sensitivity analysis of the TOPMODEL. In: Journal of Hydrol., Vol. 175, pp. 293-338.

FRANKE, W. (1987): Meteorologisch-statistische Verfahren zur verbesserten Verwendung von BKF-Niederschlagsvorhersage für Hydrologie und Wasserwirtschaft. In: Mitteilung VIII der Senatskommission für Wasserforschung der DFG. Wiley-VCH. Weinheim. pp. 131-141.

FUCHS, T., RAPP, J. (1997): Zwei außergewöhnliche starke Regenepisoden als Ursache des Oderhochwassers im Juli 1997. In: DEUTSCHER WETTERDIENST (Ed.): Klimastatusbericht 1997. Offenbach.

FUCHS, T., RAPP, J., RUDOLF, B. (1999): Niederschlagsanalyse zum Pfingsthochwasser 1999 in Einzugsgebiet von Donau und Bodensee. In: DEUTSCHER WETTERDIENST (Ed.): Klimastatusbericht 1999. Offenbach.

GABELLA, M., JOSS, J., PERONA, P. (2000): Optimizing quantitative precipitation estimates using a non-coherent and coherent radar operating on the same area. In: J. Geophys. Res. - Atmos., Vol. 105 D2, pp. 2237-2245.

GARBRECHT, J., MARTZ, L. (1993): DEDNM - A software system for the automated extraction of channel network and watershed data from raster digital elevation models. In: HARLIN, J. M. and LANFEAR, K. J. (Eds.): Proceedings of the Symposium on Geographic Information Systems in Water Resources. American Water Resources Association, Mobile, Alabama, pp. 211-220.

GEORGELIN M., RICHARD, E., PETITDIDIER, M., DRUILHET, A. (1994): Impact of subgrid scale orography parameterization on the simulation of orographic flows. In: Mon. Wea. Rev., Vol. 122, pp. 1509-1522.

GEYER, B., JARVIS, P. (1991): A review of models of soil-vegetation-atmosphere-transfer-schemes (SVATS). Report to the TIGER III Committee, Institute of Ecology and Resource Management, University of Edinburgh, Edinburgh.

GLAHN, H. P., LOWRY, D. A. (1972): The use of model output statistics (MOS) in objective weather forecasting. In: J. Appl. Meteor., Vol. 11, pp. 1203-1211.

GOLLVIK, S. (1997):The Teleflood project, estimation of precipitation over drainage basins. In: SMHI Reports Meteorology and Climatology, RMK No. 77. Sveriges meteorologiska och hydrologiska institut. Stockholm.

GRAY, M., PROWSE, T. D. (1993): Snow and Floating Ice. In: MAIDMENT, D. R. (Ed.): Handbook of Hydrology. McGraw-Hill, New York. Chapter 7.

GREEN, W. H., AMPT, G. A. (1911): Studies on Soil Physics: 1. The flow of air and water through soils. In: Journal of Agricultural Sciences, Vol. 4, pp. 1-24.

GRIFFITH, C. G., WOODLEY, W. L., GRUBE, P. G., MARTIN, D. W., STOUT, J, SIKDAR, D. N. (1978): Rain estimation from geosynchronous satellite imagery-visible and infraed studies. In: Mon. Wea. Rev., Vol. 106, pp. 1153-1171.

GRUBER, A. (1973): Estimating rainfall in regions of active convection. In: J. Appl. Meteor., Vol. 12, pp. 110-118.

GRÜNEWALD, U. (1996): Rapporteursbericht zum Themenbereich Landnutzung & Versiegelung. In: BRONDSTERT, A. (Ed.) (1996): Hochwasser in Deutschland unter Aspekten globaler Veränderung – Bericht über das DFG-Rundgespräch am 9. Oktober 1995 in Potsdam. In: PIK Report No.17. Postdam.

GYAKUM, J.R., CARRERA, M., ZHANG, D.-L, MILLER, S., CAVEEN, J., BENOIT, R., BLACK, T., BUZZI, A., CHOUINARD, C., FANTINI, M., FOLLONI, C., KATZFEI, J.J., KUO, Y.-H, LALAURETTE, F., LOW-NAM, S., MAILHOT, J., MALGUZZI, P., MCGREGOR, J.M., NAKAMURA, M., TRIPOLI, G., WILSON, C. (1996): A regional model intercomparison using a case of explosive oceanic cyclogenesis. In: Weather and Forecasting, Vol.11 (4), pp. 521-543.

HAAN, C. T., BARFIELD, B. J., HAYES, J. C. (1994): Design Hydrology and Sedimentology for Small Catchments. Academic Press. San Diego.

HAGEN, M. (1997): Identification of ground clutter by polarimetric radar. In: Proc. 28th Conf. Radar Meteorology in Austin. Amer. Meteorol. Soc., Boston, pp. 67-68.

HAGEN, M., HACKER, S., MEISCHNER, P. (1998): Estimation of rainfall rate from measurements of polarimetric radar parameters by the C-band multiparameter radar POLDIRAD. In: Preprints COST 75 Final International Seminar, Advanced Weather Radar Systems, Locarno, European Communities, Luxembourg, Publication EUR 18567 EN, pp.710-716.

HAGEN, M., MEISCHNER, P. (2000): Precipitation Measurements with Doppler Radars. In: BACCHI, B., RANZI, R. (Eds.) (2000): RAPHAEL – runoff and atmospheric processes for flood hazard forecasting and control. Final report. University of Brescia. Brescia.

HANNWEBER, M. (2000): personnel communication. Wasserwirtschaftsamt ,Weilheim.

HOTTEL, H. C. (1976): A simple model for estimating the transmittance of direct solar radiation through clear atmospheres. In: Solar Energy, Vol. 18, pp. 129-134.

JARRETT, R. D. (1984). Hydraulics of high gradient streams. In: J. Hydraul. Eng., Vol. 110, pp. 1519-1539.

JARVIS, P. G. (1976): The Interpretation of Variations of Leaf Water Potential and Stomatal Conductance Found in Canopies in the Field. In: Phil. Trans. Royal Soc. London, Ser. B, Vol. 273, pp. 593-610.

JERZ, H. (1993a): Geologie von Bayern Band II. Das Eiszeitalter in Bayern. E. Schweizerbart'sche Verlagsbuchhandlung, Stuttgart.

JERZ, H. (1993b): Erläuterungen zur Geologischen Karte von Bayern 1:25 000. Blatt Nr. 8132 Weilheim. Bayerisches Geologisches Landesamt, München.

JONES, J. A. A. (1997): Global hydrology : processes, resources and environmental management.1. Edition. Longman. Harlow.

JOSS, J., WALDVOGEL, A. (1990): Precipitation measurements and hydrology. In: ATLAS, D. (Ed.): Radar in Meteorology, Amer. Meteor. Soc., pp. 577-606.

JOSS, J., SCHÄDLER, B., GALLI, G., CAVALLI, R., BOSCACCI, M., HELD, E., DELLA BRUNA, G., KAPPENBERGER, G., NESPOR, V., SPIESS, R. (1997): Operational Use of Radar for Precipitation Measurements in Switzerland. Nationales Forschungsprogramm "Klimaänderungen und Naturkatastrophen" (NFP 31), Schlussbericht. vdf Hochschulverlag. Zürich.

KAUFMANN, P. (1999): personnel communication. MeteoSchweiz, Zürich.

KIDDER, S. Q., VANDER HAAR, T. H. (1995): Satellite Meteorology. Academic Press. San Diego.

KILONSKY, B. J., RAMAGE, C. S. (1976): A technique for estimating tropical open-ocean rainfall from satellite observations. In: J. Appl. Meteor., Vol. 15, pp. 972-975.

KLEIN, W. H., LEWIS, B. M., ENGER, I. (1959): Objective prediction of five-day mean temperature during winter. In: J. Meteor., Vol. 16, pp. 672-682.

KÖRNER, C., SCHEEL, J. A., BAUER, H. (1979): Maximum Leaf Diffusive Conductance of Vascular Plants. In: In. Photosynthetica, Vol. 13, pp. 45-82.

KOUWEN, N., SOULIS, E. D. (1990): WATFLOOD – a fully integrated data management system for flood forecasting. In: Proceedings Flood Plain Management Conference Toronto, 10pp..

KOUWEN, N., SEGLENIEKS, F., SOULIS, E. D., BENOIT, R., MAILHOT, J., PELLERIN, P., LEE, V., DANARD, M., CHIN, W. C. (1996): Modelling Large Watersheds with Numerical Weather Data. In: Scientific Meeting of the Canadian Geophysical Meeting, Banff, Alberta, May 5-9, 1996. No. 26.

KRZYSZTOFOWICZ, R., DRZAL, W., DRAKE, T., WEYMAN, J., GIORDANO, L., (1993): Probabilistic quantitative precipitation forecasts for river basins. In: Weather and Forecasting, Vol. 8, pp. 424-439.

KUHNERT, C. (1967): Erläuterungen zur Geologischen Karte von Bayern 1:25 000, Blatt Nr. 8432 Oberammergau. Bayerisches Geologisches Landesamt, München.

KUSCH, W., PANDER, R., PEYINGHAUS, W. (1985): MOS: statistisch-numerische Modellinterpretation im DWD. In: Promet, Vol. 4, pp. 29-31.

LANGHOLZ, H., HÄCKEL, H. (1985): Messungen der photosynthetisch aktiven Strahlung und Korrelationen mit der Globalstrahlung. In: Meteorol. Rdsch., 38, No. 3, pp. 75-82.

LAURENSEN, E. M., MEIN, R. G. (1988): RORB – Version 4, Runoff Routing Program, User Manual. Department of Civil Engineering. Monash University. Clayton (Victoria).

LEAVESLEY, G. H., LICHTY, R. W., TROUTMAN, B. M., SAINDON, L. G. (1983): Precipitation-Runoff Modeling System: Users Manual. U.S. Geological Survey, Water Resources Investigation Report, Washington, DC, pp. 83-4238.

LETHBRIDGE, M. (1967): Precipitation probability and satellite radiation data. In: Mon. Wea. Rev., Vol. 95, pp. 487-490.

LIEDTKE, H., MARCINEK, J. (Eds.) (1995): Physische Geographie Deutschlands. Justus Perthes Verlag. Gotha.

LILJEQUIST, G. H., CEHAK, K. (1994): Allgemeine Meteorologie, 3. Edition. Friedrich Viehweg & Sohn. Braunschweig.

LINDENAU, D. (2000): Hochwassermodellierung im Lindertal. Unpublished Diploma thesis, University of Munich. München.

LIU, B. Y. H., JORDAN, R. C. (1960): The interrelationship and characteristic distribution of direct, diffuse and total solar radiation. In: Solar Engineering, Vol. 4(3), pp. 1-19.

LOVEJOY, S., AUSTIN, G. L. (1979): The sources of error in rain amount estimating schemes for GOES visible and IR satellite data, In: Mon. Wea. Rev., Vol. 107, pp. 77-92.

LUDWIG, R (2000): Die flächenverteilte Modellierung von Wasserhaushalt und Abflußbildung im Einzugsgebiet der Ammer, In: Münchener Geographische Abhandlungen. Bd. B 32.

LUDWIG, R., MAUSER, W. (2000): Modelling the water-balance within a GIS-based SVAT-model framework. In: Hydrology and Earth System Sciences, HESS, Vol. 4(2), pp. 239-249.

MAIDMENT, D. R. (Ed.) (1993): Handbook of Hydrology. Mc Graw-Hill, New York.

MALITZ, G., SCHMIDT, T. (1997): Hydrometeorologische Aspekte des Sommerhochwassers der Oder 1997. In: DEUTSCHER WETTERDIENST (Ed.): Klimastatusbericht 1997. Offenbach.

MAUSER, W. (1985): Prognose von Hochwässern mit LANDSAT-Daten. Verlag Beiträge zur Hydrologie. Kirchzarten.

MAUSER, W. (1989): Die Verwendung hochauflösender Satellitendaten in einem Geographischen Informationssystem zur Modellierung von Flächenverdunstung und Bodenfeuchte. Habilitationsschrift, Albert-Ludwigs-Universität, Freiburg i. Br..

MAUSER, W. (1999): personnel communication. Department für Geo- und Umweltwissenschaften, Sektion Geographie, Universität München.

MAUSER, W., BACH, H. (1993): FAP Flächendaten-Analyseprogramm. Ein interaktives Programm zur Bearbeitung von Vektor- und Rasterdaten (unpublished). University of Munich. München.

MAUSER, W., BACH, H. (1994): Bericht zur Studie: Untersuchung der Eignung von kombinierten METEOSAT und UMEG-Daten und Modellrechnungen des DWD zur Bestimmung von Niederschlagsfeldern bei extremen Hochwasserereignissen. Auftraggeber LFU Baden-Würthenberg.

MAUSER, W., BACH, H. (1995): Bericht zur Studie: Integration der METEOSAT-Daten in die Datenströme der Hochwasservorhersagezentrale der LFU zur Bestimmung der Niederschlagsverteilung. Auftraggeber LFU Baden-Würthenberg.

MAUSER, W., SCHÄDLICH, S. (1998): Modelling the Spatial Distribution of Evapotranspiration Using Remote Sensing Data and PROMET. In: J. of Hydrol. Vol. 213, p. 250-267.

MCCLATCHEY, R. A. (1972): Optical properties of the atmosphere. In: Air-Force Cambridge Research Laboratories, Environmental Research Paper, No. 411 (AFCRL-72-0497), Third Edition.

MEISCHNER, P. F., BRINGI, V. N., HEIMANN, D., HÖLLER, H. (1991). A squall line in Southern Germany; Kinematics and precipitation formation as deduced by advances polarimetric and doppler radar measurements. In: Mon. Wea. Rev., Vol. 19, pp. 678-701.

MERZ, R., PIOCK-ELLENA, P., BLÖSCHL, G., GUTKNECHT, D. (1999): Seasonality of flood processes in Austria. In: IAHS Pub., Vol. 255, pp. 273-278.

MEYNEN, E., SCHMITHÜSEN, J., G ELLERT, J., NEEF, E., MÜLLER-MINY, H., SCHULTZE, H. J. (1962): Handbuch der naturräumlichen Gliederung Deutschlands. Verlag der Bundesanstalt für Landeskunde und Raumforschung. Bad Godesberg.

MÖBUS, G. (1997): Geologie der Alpen: eine Einführung in die regional-geologischen Einheiten zwischen Genf und Wien. Loga Verlag. Köln.

MÖSER, W., RASCHKE, E. (1983): Mapping of Global Radiation and of Cloudiness from METEOSAT Image Data. In: Meteorologische Randschau, Bd. 36, Heft 2.

MONTEITH, J. L. (1965): Evaporation and the environment. In: Symp. Soc. Expl. Biol., Vol. 19, pp. 205-234.

MONTEITH, J. L. (1978): Grundzüge der Umweltphysik. Dr. Dietrich Steinkopf Verlag, Darmstadt.

MUNICH RE (1999): Ein Jahr, ein Jahrhundert und ein Jahrtausend der Naturkatastrophen gehen zu Ende - 1999 liegt voll im Katastrophentrend. Pressemitteilung vom 20. Dezember 1999, München.

NEGRI, A. J., ADLER R. F. (1987a): Infrared and visible satellite rain estimation Part I: A cell grid approach. In: Journal of Climate and Applied Meteorology, Vol. 26, pp. 1553-1564.

NEGRI, A. J., ADLER R. F. (1987b): Infrared and visible satellite rain estimation Part II: A cloud definition approach. In: Journal of Climate and Applied Meteorology, Vol. 26, pp. 1565-1576.

NEGRI, A. J., NELKIN, E. J., ADLER, R. F., HUFFMAN, G. J., KUMMEROV, C. (1995): Evaluation of passive microwave precipitation algorithms in wintertime midlatitudes situations. In: J. Atmos. Ocean Technol., Vol. 12, pp. 20-32.

NORMAN, J. M. (1979): Modeling the complete plant canopy. In: Modification of the Areal Environment of Plants. In: Am. Soc. Agric. Engr. pp. 248-277.

OBLED, C., WENDLING, J., BEVEN, K. J. (1994): The sensitivity of hydrological models to spatial rainfall patterns: an evaluation using observed data. In: Journal of Hydrol., Vol.159, pp. 305-333.

PARDE, M. (1960): Les facteurs des règimes fluviaux. In: Revue Norois Poitiers (France), No. 27.

PENNDORF, A. (2000): Entwicklung eines Verfahrens zur Ableitung subskaliger Schneeflächenparameter aus NOAA-AVHR- Daten für die hydrologische Modellierung. Unpublished Diploma thesis, University of Munich. München.

PHILIP, J. R. (1960): General Method of Extract Solution of the Concentration-Dependent Diffusion Equation. In: Aust. J. Phys., No. 13, pp. 1-12.

PILGRIM, D. H., HUFF, . D., STEELE, T. D. (1978): A field evaluation of subsurface and surface runoff, II, Runoff processes. In: J. of. Hydrol., Vol. 38., pp. 319-341.

PILGRIM, D. H., CORDERY, I. (1993): Flood runoff. In: MAIDMENT, D. R. (Ed.): Handbook of Hydrology. McGraw-Hill, New York. Chapter 9.

POSPISILOVA, J., SOLAROVA, J. (1980): Environmental and biological control of diffusive conductance of adaxial and abaxial leaf epidermis. In: Photosynthetica, Vol. 14, pp. 90-127.

QUINN, P., BEVEN, K. J., CHEVALIER, P., PLANCHON, O. (1993): The Prediction of Hillslope Flow Paths for Distributed Hydrological Modelling Using Digital Terrain Models. In: BEVEN, K.J., MOORE, L.D. (Eds.): Terrain Analysis and Distributed Modelling in Hydrology. Wiley. Chichester.

RAKHMANOV, V. V. (1958): Forest-cover effects on snowpack accumulation and snow melting in relation to meteorological conditions. IAHS pub., Vol. 46, pp. 210-221.

RANZI, R. (1994): The wavelet transform as a new technique for analysing spatial scales of rainfall fields, In: Proc. Int. Meeting on "Atmospheric Physics and Dynamics in the Analysis and Prognosis of Precipitation Fields", Rome, 15-18 Nov. pp. 211-214.

RANZI, R. (1997): The RAPHAEL Project. In: MAP Newsletters, Vol. 7, pp. 9-11.

RANZI, R. (2000): Disaggregation of the precipitation forecasts. In: BACCHI, B., RANZI, R. (Eds.) (2000): RAPHAEL – runoff and atmospheric processes for flood hazard forecasting and control. Final report. University of Brescia. Brescia.

RANZI, R., BACCHI, B., GROSSI, G., BUZZI, A., MALGUZZI, P., RATTO, C., CORAZZA, M., (2001): Previsioni di piena mediante un modello idrologico e un modello meteorologico ad area limitata: alcune esperienze applicative durante l'esperimento M.A.P.-S.O.P.. In: Proc.XXVII Convegno di Idraulica e Costruzioni Idrauliche, Genova 12-15 september 2000. Vol. II, pp.385-392.

RAPP, J., SCHÖNWIESE, C. (1995): Atlas der Niederschlags- und Temperaturtrends in Deutschland 1891-1990. Frankfurter Geowissenschaftliche Arbeiten, Serie B, Bd. 5. Institut für Meteorologie und Geophysik, Johann Wolfgang Goethe-Universität, Frankfurt am Main.

RAWLS, W. J., AHUJA, L. R., BRAKENSIEK, D. L., SHIROHAMMADI, A. (1993): Infiltration and Soil Water Management. In: MAIDMENT, D. R. (Ed.): Handbook of Hydrology. McGraw-Hill, New York. Chapter 5.

REUDENBACH, C., HEINEMANN, G., HEUEL, E., BENDIX, J., WINIGER, M. (2001): Investigation of summertime convective rainfall in Western Europe based on a synergy of remote sensing data and numerical models. In: Meteorol. Atmos. Phys. Vol.76 (1-2), pp. 23-41.

RICHARD, E., CHARNEY, J., COSMA, S., BENOIT, R., CHAMBERLAND, S., BUZZI, A., FOSCHINI, L., FERRETTI, R., STEIN, J. (1998): Intercomparison of simulated precipitation fields for some MAP episodes. In: Map Newsletter, Vol. 9, pp. 19-21.

RICHARDS, L.A. (1931): Capillary Conduction of Liquids through Porous Mediums. In: Physics, Vol. 1, pp. 318-333.

RIEKEL, T. (1983): Hydrogeologische und hydrochemische Untersuchungen im Flußgebiet der Ammer. PhD Thesis, Lehrstuhl für Hydrogeologie and Hydrochemie der TU München, München.

ROHRER, M. B. (1992): Die Schneedecke im Schweizer Alpenraum und ihre Modellierung. Züricher Geographische Schriften, H. 49, Zürich.

SACHIDANANDA, M., ZRNIC, D.S. (1987): Rain rate estimated from differential polarization measurements. In: J. Atmos. Oceanic Technol., Vol. 4, pp. 588-598.

SAUVAGEOT, H. (1992) : Radar Meteorology. Artech House. Boston.

SCHÄDLICH, S. (1998): Regionalisierung von aktueller Verdunstung mit Flächenparametern aus Fernerkandungsdaten. In: Münchner Geographische Abhandlungen, München, Bd. B27.

SCHULLA, J. (1997): Hydrologische Modellierung von Flußgebieten zur Abschätzung der Folgen von Klimaänderungen. In: Züricher Geographische Schriften, No. 69, 161 pp., Zürich.

SCOTT, H. D. (2000): Soil Physics: Agricultural and Environmental Applications. Iowa State University Press. Ames.

SHERMAN, L. K. (1932): Streamflow from rainfall by the unit-graph method. In: Eng. News-Rec., Vol. 108, pp. 501-505.

SNYDER, F. F. (1938): Synthetic unit hydrographs. In: Trans. Am. Geophys. Union, Vol. 19, pp. 447-454.

SOIL CONSERVATION SERVICE (Ed.) (1975): Urban hydrology for small watersheds. Technical Release 55. U.S. Department of Agriculture, Washington, DC.

SOIL CONSERVATION SERVICE (Ed.) (1983): Computer Program for Project Formulation Hydrology. Technical Release 20. U.S. Department of Agriculture, Washington, DC.

SOIL CONSERVATION SERVICE (Ed.) (1985): Hydrology. Engineering Handbook, Section 4. U.S. Department of Agriculture, Washington, DC.

STOLZ, R. (1998): Die Verwendung der Fuzzy Logic Theorie zur wissensbasierten Klassifikation von Fernerkundungsdaten. In: Münchner Geographische Abhandlungen, München, Bd. B26.

STRAHLER, A. N. (1957): Quantitative analysis of watershed geomorphology. In: Trans. Amer. Geophys. Union, Vol. 38, pp. 913-920.

STRASSER, U. (1998): Regionalisierung des Wasserhaushalts mit einem SVAT-Modell am Beispiel des Weser-Einzugsgebiets. In: Münchner Geographische Abhandlungen, München, Bd. B28.

SWISS RE (1998): Floods – an insurable risk?. Swiss Reinsurance Company. Zürich

TASCHNER, S., STRASSER, U., MAUSER, W. (1998): Modelling the spatial snow water equivalent using NOAA-AVHRR data for mesoscale catchments. In: Proc. of the EUROPTO Conference Barcelona. SPIE Proceeding Series, No.3499 Remote Sensing for Agriculture, Ecosystems, and Hydrology, pp. 69-79.

TASCHNER, S., LUDWIG, R., MAUSER, W. (2001): Flood Modelling in a mountain watershed using inputs from rain-radar and mesoscale meteorological models, In: IAHS Pub., Vol. 267, pp. 586-588.

TODINI, E. (1995): AFORISM - A Comprehensive Forecasting System for Flood Risk Mitigation and Control. Final Report. University of Bologna, Bologna.

TODINI, E. (1996): The ARNO rainfall-runoff model. In: J. of Hydrol., Vol. 175, pp. 339-382.

TODINI, E. (1997): The Role of Rainfall Measurement and Forecasts in Real-Time Flood Forecasting and Management. In: BRAGA, B. Jr., MASSAMBANI, O. (Eds.): Weather Radar Technology for Water Resources Management. IRTCUD/ University of Sao Paulo, Brazil and IHP-UNESCO. Sao Paulo.

TSONIS, A. A., ISAAC, G. A. (1985): On a new approach for instantaneous rain area delineation in the midlatitudes using GOES data. In: J. Climate Appl. Meteor., Vol. 24, pp. 1208-1218.

UHLENBROOK S., STEINBRICH, A., TETZLAFF, D., LEIBUNDGUT, Ch. (2001): Zusammenhang zwischen extremen Hochwassern und ihren Einflussgrößen In: Arbeitskreis KLIWA (Klimaveränderung und Konsequenzen für die Wasserwirtschaft, Herausgeber), KLIWA-Symposium, 29.-30.11.2000, Karlsruhe, KLIWA-Berichte, Vol. 1, pp. 187-204.

U. S. ARMY CORPS OF ENGINEERS (1981): HEC-1, Flood hydrograph package, Users Manual. Hydrologic Engineering Centre. Davis (California).

VERTESSY, R., O'LOUGHLIN, E., BEVERLY, E., BUTT, T. (1994): Australian experiences with the CSIRO Topog model in land and water resources management. In: Proceedings of UNESCO International Symposium on Water Resources Planning in a Changing World, Karlsruhe, Germany, June 28-30, Vol. III, pp. 135-144.

VIESSMAN, W. Jr., LEWIS, G. L., KNAPP, J. W. (1989): Introduction to hydrology. 3. edition., Harper and Row. New York.

VOLKERT, H., BINDER, P., BENOIT, R., BOUGEAULT, P., BUZZI, A., MAYR, G., SCHŠR, C., STEINACKER, R. (1996): The Mesoscale Alpine Programme (MAP): An international research initiative in Alpine meteorology. In: Interprevent 1996, International Symposium. Garmisch-Partenkirchen. Vol. 1, pp. 55-63.

WASSERWIRTSCHAFTSAMT WEILHEIM (Ed.) (2001): Aufzeichnung des Pegels Peissenberg. Weilheim. unpublished.

WESTRICK, K. J., STORCH, P., MASS, C. F. (2000): Evaluation of the MM5-DHSVM Streamflow forecast system in the Pacific Northwest. In: Proceedings of the Western Snow Conference – Poster Presentation. Port Angeles.

WILHELM, F. (1997): Hydrogeographie. Grundlagen der Allgemeinen Hydrogeographie. Das Geographische Seminar. 3. stark veränderte Auflage. Höller and Zwick. Braunschweig.

WITTMANN, O. (1991): Standortkundliche Landesgliederung von Bayern. GLA Fachberichte 5, Bayerisches Geologisches Landesamt. München.

WMO (1986): Manual for estimation of probable maximum precipitation, Operational Hydrology Report No. 1, 2. Edition, WMO- No.332, Geneva.

WMO (1993): Meteorologische Systeme für hydrologische Anwendungen. IHP/OHP-Berichte, Vol. 9., Koblenz.

WMO (1996): Numerical weather prediction progress report for 1995, NWPP report series No. 22. Geneva.

WOOD, E. F., SIVAPALAN, M., BEVEN, K. J.(1990): Scale and similarity in catchment storm response. In: Reviews of Geophysics, Vol. 28 (1), pp. 1-18.

WOODLEY, W. L., GRIFFITH, C. G., GRIFFIN, J. S., STROMATT, S. C. (1980): The inference of GATE convective rainfall from SMS-1 imagery. In: J. Appl. Meteor., Vol. 19, pp. 388-408.

WU, R., WEINMANN, J., CHI, R. (1985): Determination of rainfall patterns from GOES satellite images by a pattern recognition technique. In: J. of Atmos. And Ocean Tech., Vol. 2, pp. 314-330.

WYLIE, D. P. (1979): An application of a geostationary satellite rain estimation technique to an extratropical area. In: J. Appl. Meteor., Vol. 18, pp. 1640-1648.

Appendix

Appendix A:
Specific values of the runoff model results applying PROMET-D for the Christopherus Flood and the Whitsun Flood
(dupl. = duplicated, interp. = linear interpolated, inv. dis. = inverse distance², ice = with ice phase)

| Name of flood event | Duration of flood [h] | Meteorological model | | | Precipitation sum in the basin | | | | Flood peak | | | | | | | | | | | Hydro |
		Name	Mode	Grid size Km²	simulated mm	observed mm	difference (sim. - obs) mm	%	Entry time simulated h	observed h	difference h	Discharge simulated m³/s	observed m³/s	difference (sim. - obs) m³/s	%	Flood volume simulated m³/s	observed m³/s	difference (sim. - obs) m³/s	%	R²
Christopherus	72	BOLAM	AN	10	56.58	53.37	3.21	6.0	32	36	-4	46.3	147.6	-101.3	-68.6	3538.4	4684.4	-1146.0	-24.5	0.44
Christopherus	72	BOLAM	FC	10	56.29	53.37	2.92	5.5	32	36	-4	55.7	147.6	-91.9	-62.3	3641.5	4684.4	-1042.9	-22.3	0.39
Christopherus	27	BOLAM	FC	3.5	24.60	35.85	-11.25	-31.4	-	-	-	-	-	-	-	960.9	665.3	295.6	44.4	0.87
Christopherus	72	MC 2	AN	10	87.98	53.37	34.61	64.8	33	36	-3	58.7	147.6	-88.9	-60.2	4657.4	4684.4	-27.0	-0.6	0.12
Christopherus	72	MC 2	FC	10	88.68	53.37	35.31	66.2	35	36	-1	108.2	147.6	-39.4	-26.7	4961.9	4684.4	277.5	5.9	0.48
Christopherus	72	Meso-NH	AN	10	74.57	53.37	21.20	39.7	31	36	-5	124.9	147.6	-22.7	-15.4	5164.4	4684.4	480.0	10.2	0.21
Christopherus	72	Meso-NH	FC	10	68.18	53.37	14.81	27.7	32	36	-4	125.6	147.6	-22.0	-14.9	4561.2	4684.4	-123.2	-2.6	0.30
Christopherus	26	Meso-NH	FC	2	31.23	35.85	-4.62	-12.9	-	-	-	-	-	-	-	1459.0	649.4	809.6	124.7	0.88
Christopherus	26	Meso-NH	FC ice	2	23.70	35.85	-12.15	-33.9	-	-	-	-	-	-	-	1043.9	649.4	394.5	60.7	0.40
Christopherus	72	SM	AN	14	69.08	53.37	15.71	29.4	40	36	4	97.8	147.6	-49.8	-33.7	4331.3	4684.4	-353.1	-7.5	0.29
Christopherus	72	SM	FC	14	79.19	53.37	25.82	48.4	32	36	-4	171.4	147.6	23.8	16.1	5437.2	4684.4	752.8	16.1	0.56
Christopherus	65	DWD	-	0.1	69.49	52.93	16.56	31.3	27	36	-9	141.0	147.6	-6.6	-4.5	3875.5	4172.4	-296.9	-7.1	0.04
Christopherus	72	Raingauge	-	0.1	53.37	53.37	0.00	0.0	33	36	-3	145.4	147.6	-2.2	-1.5	4177.6	4684.4	-506.8	-10.8	0.65
Whitsun	96	SM	FC dupl.	14	202.38	162.27	40.12	24.7	57	59	-2	652.2	484.6	167.6	34.6	22150.4	17409.1	4741.3	27.2	0.95
Whitsun	96	SM	FC interp	14	220.45	162.27	58.18	35.9	58	59	-1	811.2	484.6	326.6	67.4	25428.5	17409.1	8019.4	46.1	0.94
Whitsun	96	SM	FC inv. dis.	14	195.56	162.27	33.29	20.5	56	59	-3	628.1	484.6	143.5	29.6	20086.1	17409.1	2677	15.4	0.95
Whitsun	96	Radar	-	1	207.31	162.27	45.04	27.8	63	59	4	772.3	484.6	287.7	59.4	23152.9	17409.1	5743.8	33.0	0.91
Whitsun	96	MSM	-	5	174.52	162.27	12.25	7.5	54	59	-5	472.4	484.6	-12.2	-2.5	17903.1	17409.1	493.9	2.8	0.94
Whitsun	96	ECST	-	5	197.06	162.27	34.79	21.4	51	59	-8	673.6	484.6	189.0	39.0	23118.2	17409.1	5709.1	32.8	0.69
Whitsun	96	Raingauge	-	0.1	162.27	162.27	0	0	65	59	6	424.8	484.6	-59.8	-12.3	15877.9	17409.1	-1531.2	-8.8	0.91

Appendix B:
Specific values of the runoff model results applying PROMET-D for the Christopherus Flood in the sensitivity mode

(rad = radial shift, n = north, ne = north east, e = east, se = south east, s = south, sw = south west, w = west, nw = north west)

Name Of Flood Event	Duration of flood [h]	Meteorological model Name	Mode	Grid size Km²	Precipitation sum in the basin simulated mm	observed mm	difference (sim. - obs) mm	%	Flood peak Entry time simulated h	observed h	difference h	Discharge simulated m³/s	observed m³/s	difference (sim. - obs) m³/s	%	Flood volume simulated m³/s	observed m³/s	difference (sim. - obs) m³/s	%	Hydro R²
Christopherus	72	BOLAM	AN rad n	10	34.60	53.37	-18.77	-35.2	32	36	-4	41.0	147.6	-106.6	-72.2	3156.3	4684.4	-1528.1	-32.6	0.34
Christopherus	72	BOLAM	AN rad ne	10	46.33	53.37	-7.04	-13.2	32	36	-4	46.2	147.6	-101.4	-68.7	3360.8	4684.4	-1323.6	-28.3	0.43
Christopherus	72	BOLAM	AN rad e	10	63.66	53.37	10.29	19.3	32	36	-4	54.2	147.6	-93.4	-63.3	3886.6	4684.4	-797.8	-17.0	0.46
Christopherus	72	BOLAM	AN rad se	10	65.14	53.37	11.77	22.1	32	36	-4	71.2	147.6	-76.4	-51.8	4570.5	4684.4	-113.9	-2.4	0.48
Christopherus	72	BOLAM	AN rad s	10	49.78	53.37	-3.59	-6.7	32	36	-4	57.2	147.6	-90.4	-61.2	4054.5	4684.4	-629.9	-13.4	0.31
Christopherus	72	BOLAM	AN rad sw	10	53.99	53.37	0.62	1.2	32	36	-4	55.8	147.6	-91.8	-62.2	4342.7	4684.4	-341.7	-7.3	0.28
Christopherus	72	BOLAM	AN rad w	10	46.69	53.37	-6.68	-12.5	32	36	-4	43.6	147.6	-104.0	-70.5	3695.0	4684.4	-989.4	-21.1	0.31
Christopherus	72	BOLAM	AN rad nw	10	37.77	53.37	-15.60	-29.2	31	36	-5	35.8	147.6	-111.8	-75.7	3265.9	4684.4	-1418.5	-30.3	0.32
Christopherus	72	MC 2	AN rad n	10	42.94	53.37	-10.43	-19.5	41	36	5	76.3	147.6	-71.3	-48.3	3421.9	4684.4	-1262.5	-27.0	0.37
Christopherus	72	MC 2	AN rad ne	10	28.73	53.37	-24.64	-46.2	41	36	5	70.9	147.6	-76.7	-52.0	3381.1	4684.4	-1303.3	-27.8	0.47
Christopherus	72	MC 2	AN rad e	10	35.51	53.37	-17.86	-33.5	33	36	-3	181.0	147.6	33.4	22.6	6436.0	4684.4	1751.6	37.4	0.60
Christopherus	72	MC 2	AN rad se	10	111.25	53.37	57.88	108.5	33	36	-3	362.7	147.6	215.1	145.7	10535.5	4684.4	5851.1	124.9	0.71
Christopherus	72	MC 2	AN rad s	10	66.61	53.37	13.24	24.8	33	36	-3	305.5	147.6	157.9	107.0	7796.6	4684.4	3112.2	66.4	0.63
Christopherus	72	MC 2	AN rad sw	10	59.83	53.37	6.46	12.1	32	36	-4	290.3	147.6	142.7	96.7	9226.0	4684.4	4541.6	97.0	0.64
Christopherus	72	MC 2	AN rad w	10	20.23	53.37	-33.14	-62.1	32	36	-4	134.6	147.6	-13.0	-8.8	4470.7	4684.4	-213.7	-4.6	0.37
Christopherus	72	MC 2	AN rad nw	10	29.31	53.37	-24.06	-45.1	31	36	-5	62.8	147.6	-84.8	-57.5	2587.3	4684.4	-2097.1	-44.8	0.16
Christopherus	72	Meso-NH	AN rad n	10	128.87	53.37	75.50	141.5	30	36	-6	175.1	147.6	27.5	18.6	5847.6	4684.4	1163.2	24.8	0.09
Christopherus	72	Meso-NH	AN rad ne	10	106.07	53.37	52.70	98.7	30	36	-6	173.3	147.6	25.7	17.4	6425.0	4684.4	1740.6	37.2	0.13
Christopherus	72	Meso-NH	AN rad e	10	125.38	53.37	72.01	134.9	30	36	-6	123.2	147.6	-24.4	-16.5	5403.8	4684.4	719.4	15.4	0.02
Christopherus	72	Meso-NH	AN rad se	10	100.59	53.37	47.22	88.5	30	36	-6	98.0	147.6	-49.6	-33.6	4570.8	4684.4	-113.6	-2.4	0.13
Christopherus	72	Meso-NH	AN rad s	10	107.87	53.37	54.50	102.1	30	36	-6	90.3	147.6	-57.3	-38.8	4267.1	4684.4	-417.3	-8.9	0.16
Christopherus	72	Meso-NH	AN rad sw	10	76.20	53.37	22.83	42.8	30	36	-6	88.5	147.6	-59.1	-40.0	4094.6	4684.4	-589.8	-12.6	0.18
Christopherus	72	Meso-NH	AN rad w	10	53.00	53.37	-0.37	-0.7	30	36	-6	103.7	147.6	-43.9	-29.7	4240.6	4684.4	-443.8	-9.5	0.17
Christopherus	72	Meso-NH	AN rad nw	10	81.79	53.37	28.42	53.3	30	36	-6	136.3	147.6	-11.3	-7.7	4579.5	4684.4	-104.9	-2.2	0.19
Christopherus	72	SM	AN rad n	14	43.22	53.37	-10.15	-19.0	41	36	5	72.8	147.6	-74.8	-50.7	3106.7	4684.4	-1577.7	-33.7	0.12
Christopherus	72	SM	AN rad ne	14	38.51	53.37	-14.86	-27.8	41	36	5	71.8	147.6	-75.8	-51.4	3369.3	4684.4	-1315.1	-28.1	0.16
Christopherus	72	SM	AN rad e	14	41.03	53.37	-12.34	-23.1	40	36	4	123.8	147.6	-23.8	-16.1	5525.5	4684.4	841.1	18.0	0.24
Christopherus	72	SM	AN rad se	14	117.88	53.37	64.51	120.9	37	36	1	158.4	147.6	10.8	7.3	8332.8	4684.4	3648.4	77.9	0.38
Christopherus	72	SM	AN rad s	14	64.60	53.37	11.23	21.0	39	36	3	112.7	147.6	-34.9	-23.6	5578.3	4684.4	893.9	19.1	0.38
Christopherus	72	SM	AN rad sw	14	57.61	53.37	4.24	7.9	32	36	-4	137.1	147.6	-10.5	-7.1	6844.4	4684.4	2160.0	46.1	0.50
Christopherus	72	SM	AN rad w	14	14.88	53.37	-38.49	-72.1	39	36	3	76.4	147.6	-71.2	-48.2	3787.4	4684.4	-897.0	-19.1	0.19
Christopherus	72	SM	AN rad nw	14	28.42	53.37	-24.95	-46.7	41	36	5	48.2	147.6	-99.4	-67.3	2347.4	4684.4	-2337.0	-49.9	0.19

Appendix C:

Specific values of the runoff model results applying PROMET-D for the Whitsun Flood in the sensitivity mode

(rad = radial shift, n = north, ne = north east, e = east, se = south east, s = south, sw = south west, w = west, nw = north west, Rg = raingauges)

Name Of Flood Event	Duration of flood [h]	Meteorological model		Grid size	Precipitation sum in the basin				Flood peak							Flood volume				Hydro
		Name	Mode		simulated	observed	difference (sim. - obs)		Entry time			Discharge				simulated	observed	difference (sim. - obs)		
									simulated	observed	difference	simulated	observed	difference (sim. - obs)						
	[h]			Km²	mm	mm	mm	%	h	h	h	m³/s	m³/s	m³/s	%	m³/s	m³/s	m³/s	%	R²
Whitsun	96	SM	FC rad n	14	145.29	162.27	-16.98	-10.5	53	59	-6	444.6	484.6	-40.0	-8.3	15629.8	17409.1	-1779.3	-10.2	0.96
Whitsun	96	SM	FC rad ne	14	160.72	162.27	-1.55	-1.0	55	59	-4	478.0	484.6	-6.6	-1.4	16016.9	17409.1	-1392.2	-8.0	0.94
Whitsun	96	SM	FC rad e	14	195.22	162.27	32.95	20.3	58	59	-1	659.3	484.6	174.7	36.1	21230.8	17409.1	3821.7	22.0	0.93
Whitsun	96	SM	FC rad se	14	247.12	162.27	84.85	52.3	58	59	-1	1010.5	484.6	525.9	108.5	30042.5	17409.1	12633.4	72.5	0.93
Whitsun	96	SM	FC rad s	14	242.20	162.27	79.93	49.3	58	59	-1	929.8	484.6	445.2	91.9	28897.1	17409.1	11488	66.0	0.94
Whitsun	96	SM	FC rad sw	14	249.18	162.27	86.91	53.6	57	59	-2	926.8	484.6	442.2	91.3	30510.5	17409.1	13101.4	75.3	0.96
Whitsun	96	SM	FC rad w	14	179.06	162.27	16.79	10.3	55	59	-4	536.5	484.6	51.9	10.7	18820.7	17409.1	1411.6	8.1	0.96
Whitsun	96	SM	FC rad nw	14	145.29	162.27	-16.98	-10.5	53	59	-6	404.0	484.6	-80.6	-16.6	13977.1	17409.1	-3421	-19.7	0.95
Whitsun	96	Combined	Rg + FC dupl.	14	162.10	162.27	-0.17	-0.1	47	59	-2	559.9	484.6	75.3	15.5	18694.5	17409.1	1285.4	7.4	0.93
Whitsun	96	Combined	Rg + FC int.	14	198.40	162.27	36.13	22.3	59	59	0	687.5	484.6	202.9	41.9	20980.9	17409.1	3571.8	20.5	0.91
Whitsun	96	Combined	Rg + FC inv dis	14	136.40	162.27	-25.87	-15.9	59	59	0	548.2	484.6	63.6	13.1	17208.2	17409.1	-200.8	-1.1	0.93

Appendix D:
Recordings of the stream gauge Peissenberg (1962-2000)
(WASSERWIRTSCHAFTSAMT WEILHEIM 2001)

Maximum monthly runoff in m³/s

Hydrol. Year	Nov	Dec	Jan	Feb	Mar	Apr	May	Jun	Jul	Aug	Sep	Oct
2000	11.9	27.0	19.3	40.3	62.1	35.6	78.8	147.0	41.5	201.0	103.0	29.7
1999	65.1	36.4	11.2	51.3	25.2	57.1	365.0	68.2	39.7	22.1	24.7	27.4
1998	5.8	37.0	12.1	6.6	23.8	22.5	23.1	64.6	36.1	57.4	48.2	31.1
1997	24.3	15.4	5.6	24.0	28.6	53.3	30.2	27.2	117.0	16.9	13.7	31.3
1996	33.3	44.9	12.2	4.2	39.1	15.5	65.3	53.5	89.1	80.3	87.7	53.5
1995	20.6	33.3	25.9	13.6	18.2	56.5	54.4	106.0	85.6	109.0	36.4	11.8
1994	6.1	20.9	20.6	10.2	35.3	49.4	30.8	38.3	19.7	47.4	21.8	15.0
1993	94.0	28.6	31.3	6.6	20.5	31.2	21.2	33.9	192.0	48.7	45.5	16.2
1992	8.8	105.0	7.6	33.4	40.1	38.8	15.8	78.3	76.2	37.5	23.1	13.4
1991	19.8	14.7	25.3	7.4	47.9	21.3	69.5	62.9	28.2	45.8	12.6	7.1
1990	22.1	26.2	13.6	94.0	16.3	14.1	43.3	72.4	144.0	63.1	35.8	35.8
1989	58.7	22.8	22.6	22.6	9.7	29.6	14.9	25.6	74.2	47.7	62.9	28.6
1988	14.2	108.0	7.6	5.3	51.8	47.8	19.6	55.4	42.6	93.9	32.9	13.9
1987	6.5	14.3	37.6	33.0	63.5	39.2	25.3	45.5	62.8	41.3	29.2	7.0
1986	11.0	10.9	26.2	6.8	22.6	27.2	52.7	31.2	76.6	21.5	7.7	11.7
1985	8.1	20.6	25.7	48.0	8.7	22.6	53.3	34.6	65.8	121.0	16.3	5.2
1984	18.6	55.7	19.6	11.6	12.4	17.7	18.0	51.0	52.1	62.8	60.9	21.7
1983	13.0	13.1	23.0	22.0	29.3	17.0	34.4	83.6	55.6	58.2	27.4	11.5
1982	28.4	20.8	43.7	21.3	20.0	29.8	33.0	99.8	33.5	38.6	37.3	18.7
1981	7.0	13.4	11.0	14.8	71.5	31.7	24.5	24.8	177.0	33.0	75.3	84.0
1980	95.5	15.7	10.8	39.4	11.3	33.3	30.8	26.1	54.9	9.2	19.9	17.9
1979	7.7	13.1	17.0	14.5	65.3	19.9	84.7	156.0	76.0	46.6	39.4	6.5
1978	25.5	50.3	10.1	12.8	74.9	29.8	41.1	19.0	67.4	111.0	47.5	65.0
1977	5.2	12.9	9.7	23.8	33.3	71.8	23.0	38.8	169.0	132.0	30.9	11.5
1976	12.8	15.3	6.4	5.2	8.1	8.2	26.5	157.0	25.9	16.1	11.6	4.8
1975	20.6	40.0	15.8	10.1	5.8	15.0	25.4	46.6	100.0	54.0	15.1	8.7
1974	65.6	17.4	22.1	10.5	16.0	9.4	18.5	44.9	70.0	77.0	94.6	24.4
1973	30.4	8.1	8.8	3.9	11.7	20.0	37.4	59.7	31.3	26.7	16.9	53.3
1972	7.8	8.9	5.3	2.8	3.2	12.7	11.7	28.8	33.7	23.0	14.1	9.5
1971	14.9	11.2	8.1	4.3	15.3	14.0	22.3	73.4	24.0	32.1	14.1	7.8
1970	8.9	9.2	10.1	45.9	19.8	48.3	36.2	34.2	25.8	286.0	37.4	34.7
1969	5.5	7.7	45.9	5.3	13.0	24.6	15.3	35.5	42.0	93.1	94.9	6.8
1968	9.2	21.8	37.7	11.2	20.3	22.3	30.8	75.1	76.0	68.2	24.0	118.0
1967	13.0	13.0	21.8	39.8	32.8	36.2	81.4	145.0	104.0	34.8	63.1	14.9
1966	9.5	24.6	8.9	59.7	24.0	52.3	49.1	52.3	179.0	76.0	16.6	15.8
1965	68.4	9.8	8.3	8.7	41.7	58.0	73.8	182.0	34.8	15.3	13.7	5.5
1964	11.0	6.3	3.7	10.3	16.4	13.6	138.0	23.5	27.9	48.3	17.6	23.5
1963	3.7	30.3	4.7	3.7	18.6	18.6	69.2	43.9	22.0	22.0	36.5	39.7
1962	7.3	38.3	28.1	24.6	28.1	29.7	74.7	19.9	58.5	8.7	11.7	3.0

Mean runoff, mean flood flow and flood flow for specified annualtity

MQ (m³/s)	MHQ (m³/s)	HQ1 (m³/s)	HQ2 (m³/s)	HQ5 (m³/s)	HQ10 (m³/s)	HQ20 (m³/s)	HQ50 (m³/s)	HQ100 (m³/s)
8.0	115	90	120	152	185	220	270	310

Appendix E:
Animated graphics (enclosed CD-ROM)

- The meteorological situation of the Whitsun Flood period 1999 documented by METEOSAT images (meteosat.avi)

- Development of the saturated areas in the Ammer basin during the Whitsun flood 1999 (saturated_areas.avi)

- 3-D spatial animation of the saturated areas in the Ammer basin during the Whitsun flood 1999 (3D_saturated_areas.avi)

Files can be shown with several multimedia players like e.g. Real Player© (free software download under : http://www.real.com)

Curriculum Vitae

Personal

Name:	Stefan Taschner
Date of birth:	02. December 1969
Place of birth:	Bamberg
Nationality:	German
Contact:	Via Branze 38,
	25123 Brescia, Italy
E-mail:	s.taschner@gmx.de

School Education and Military Service

09/1976 – 08/1982	Primary school, Munich
09/1982 – 08/1989	High school, Munich
	Graduation: Abitur (certification for University entry)
09/1989 - 09/1990	basic military service

Scientific Career

09/1990 – 03/1997	Study of Physical Geography, Ludwig-Maximilians-Universität, Munich Subsidiary subjects: Bioclimatology and Zoology Diploma thesis supervisor Professor Dr. W. Mauser Title: „Sensitivity analysis of the SVAT Model PROMET" Graduation: Diplom-Geograph
04/1997 – 11/2000	Scientific researcher and PhD student at the Chair of Geography and Geographical Remote Sensing at the Institute of Geography, Ludwig-Maximilians-Universität, Munich.

Collaboration in the projects:
- Regionalization in Hydrology
- RAPHAEL (Runoff and Atmospheric Processes for Flood Hazard Forecasting and Control)

Since 11/2000	Scientific assistant at the Department of Civil Engineering at the University of Brescia, Italy.

Collaboration in the projects:
- Monitoring the snow cover with satellite data
- GLIMS*it* (Global Landice Monitoring from Space, *Italian Alps*)